Coordination Chemistry Reviews 441 (2021) 213927

Contents lists available at ScienceDirect

Coordination Chemistry Reviews

journal homepage: www.elsevier.com/locate/ccr

Review

Coordination chemistry of elemental phosphorus

Leonardo Giusti [a,1], Vanessa R. Landaeta [b,1], Matteo Vanni [a], John A. Kelly [b], Robert Wolf [b,*], Maria Caporali [a,*]

[a] Istituto di Chimica dei Composti Oganometallici, Consiglio Nazionale delle Ricerche (ICCOM CNR), Via Madonna del Piano 10, 50019 Sesto Fiorentino, Italy
[b] University of Regensburg, Institute of Inorganic Chemistry, 93040 Regensburg, Germany

ARTICLE INFO

Article history:
Received 4 December 2020
Received in revised form 9 March 2021
Accepted 14 March 2021

This contribution is dedicated to our mentor and friend Maurizio Peruzzini on the occasion of his retirement.

ABSTRACT

This review comprehensively covers the coordination chemistry of elemental phosphorus during the years 2011–2020. The main part is dedicated to the activation of white phosphorus mediated by early and late transition metals and its subsequent reactivity once in the coordination sphere of a metal. The burgeoning interest towards early TMs has opened the way to new coordination topologies and types of reactivity. Meanwhile, the coordination chemistry of P_4 towards late transition metal elements has also attracted significant attention. Numerous studies have targeted transformations of P_4-derived phosphorus ligands and the subsequent release of said ligand fragments. The final part of this review focuses on the black allotrope of phosphorus, which offers a polydentate phosphorus surface able to interact with transition metals forming new functionalized 2D materials.

Contents

* Corresponding authors.
E-mail addresses: robert.wolf@ur.de (R. Wolf), maria.caporali@iccom.cnr.it (M. Caporali).

[1] These authors contributed equally to the work.

https://doi.org/10.1016/j.ccr.2021.213927
0010-8545/

1. Introduction

Phosphorus (element 15 in the periodic table) is essential to life and human society [1,2]. It is one of the six "biogenic elements", which are needed in large quantities to create life [3]. Inorganic and organic phosphorus-containing molecules are ubiquitous in living organisms and nature. With that said, the industrial utilization of phosphorus for synthetic materials has prospered for over a century. A multitude of phosphorus compounds are produced by industry and have important commercial applications in agriculture, chemistry, and pharmaceuticals [4].

The high fundamental and industrial significance of elemental phosphorus has inspired extensive studies of its reactivity and its structural features. A range of different allotropes of phosphorus are known, among which, the three most common are white, red, and black phosphorus (Scheme 1). White phosphorus is the most reactive allotrope and, undoubtedly, the most industrially relevant form of elemental phosphorus [5]. Its structure consists of discrete tetrahedral P_4 molecules, with single P-P bonds. It is produced commercially by heating phosphate rock in an electric furnace in the presence of silica and suitable reducing agents, mainly coke [6,7].

The production of organophosphorus compounds generally relies on the white allotrope as a starting material. This is disadvantageous as the process is energy intensive, requires highly corrosive/hazardous reagents, proceeds *via* harmful intermediates and generates large amounts of chemical waste. Consequently, it has been a goal in contemporary research to find methods for P_4 transformations that replace this unsustainable and environmentally harmful process. Such efforts towards a comprehensive, efficient, and less-polluting transformation of P_4 have been matter of interest for over four decades, being extensively studied by many research groups. On an academic level, alternatives such as the direct reaction of P_4 with main group elements [8–14] have been envisaged, but these processes usually suffer from low selectivity and low efficiency, thus their transfer to an industrial level looks doubtful. Other P-sources [15,16], such as phosphoric acid [17], traditionally utilized to produce phosphate fertilizers, could be

Abbreviations: Acac, acetylacetonate; $BAr^F{}_4$, tetrakis[3,5-bis(trifluoromethyl)phenyl]borate; BDI, *NN′*-bis(2,6-diisopropylphenyl)-3,5-dimethyl-β-diketiminate; ^{dipp}BIAN, 1,2-bis(2,6-diisopropylphenylimino)acenaphthene; ^{Mes}BIAN, bis(mesitylimino)acenaphthenediimine; *t*Bu, *tert*-butyl; *t*BuXPhos, P*t*Bu_2(2′,4′,6′-triisopropylbiphenyl); Bu, butyl; BP, black phosphorus; BPQD, black phosphorus quantum dots; bpy, 2,2′-bipyridine; Bz, benzyl; CHD, cyclohexadiene; CHT, cycloheptatriene; $CNAr^{Dipp2}$, 2,6-Bis(2,6-diisopropylphenyl)phenyl isocyanide; $CNAr^{Mes2}$, 2,6-Bis(2,4,6-trimethyl)phenyl isocyanide; $CNAr^{Tripp2}$, 2,4,6-tris(2,6-diisopropylphenyl)phenyl isocyanide; Cot, cyclooctatetraene; Cod, cyclooctadiene; Cp, cyclopentadienyl; Cp*, pentamethylcyclopentadienyl; Cp′′, 1,3-di-*tert*-butylcyclopentadienyl or 1,3-di-(trimethylsilyl)cyclopentadienyl; Cp′′′ or Cp^R, 1,2,4-tris-*tert*-butylcyclopentadienyl; Cp^{BIG}, *pentakis*(4-*n*-butylphenyl)cyclopentadienyl; Cp^{Bn5}, Pentabenzylcyclopentadienyl; Cp^{4iPr}, C_5HiPr_4; Cy, cyclohexyl; D-A, Diels-Alder; DB18C6, dibenzo-18-crown-6 ether; DCM, dichloromethane; DFT, density functional theory; DIB, 1,3-diisopropylbenzene; DMAP, 4-*N,N′*-dimethylaminopyridine; DMB, 2,3-dimethyl-1,3-butadiene; DME, dimethoxyethane; DMF, dimethylformamide; Dmp, 2,6-(2,6-di-isopropyl)phenyl; Dipp, 2,6-diisopropylphenyl; DippForm, *N,N′*-bis(2,6-diisopropylphenyl)formamidinate; DIP_2pyr, 2,5-bis{N-(2,6-diisopropylphenyl)iminomethyl}pyrrolyl; dppe, 1,2-bis(diphenylphosphino)ethane; dppm, 1,1-bis(diphenylphosphino)methane; dppp, 1,3-bis(diphenylphosphanyl)propane; dtbbpy, 4,4′-di-*tert*-butyl-2,2′-bipyridine; ENDOR, Electron-Nuclear Double Resonance Spectroscopy; EPR, electron paramagnetic resonance; ESI, electrospray ionization; Et, ethyl; ETM, early transition metal; EXSY, exchange spectroscopy; FAI, $[FAl\{OC_6F_{10}(C_6F_5)\}_3]^-$; Fc, ferrocenyl; HMPA, hexamethylphosphoramide; HOMO, highest occupied molecular orbital; HSAB, Hard and Soft (Lewis) Acid and Base; IDipp, 1,3-bis(2,6-diisopropylphenyl)imidazolin-2-ylidene; IMes, [1,3-bis(2,4,6-trimethylphenyl)imidazolin-2-ylidene; IPh, 1,3-diphenylimidazolin-2-ylidene; JohnPhos, P*t*Bu_2(*o*-biphenyl); LA, Lewis acid; LMCT, ligand to metal charge transfer; LTM, late transition metal; LUMO, lowest unoccupied molecular orbital; MALDI, matrix-assisted laser desorption/ionization; MAS, magic-angle spinning; Me, methyl; Mes, Mesityl, 1,3,5-trimethylbenzene; MO, molecular orbital; MRI, magnetic resonance imaging; MS, mass spectroscopy; nacnac, $HC(C(Me)NC_6H_3iPr_2)_2$; NBO, natural bond orbital; NHC, *N*-heterocyclic carbine; ^{Me}NHC, 1,3,4,5-tetramethylimidazolin-2-ylidene; NMP, *N*-methyl-2-pyrrolidone; NMR, Nuclear Magnetic Resonance; NN^{fc}, $[(\eta^5\text{-}C_5H_4SiMetBu_2)_2Fe$; Np, neopentyl; NPA, natural population analysis; *n*-Pr, normal propyl; iPr_2Im, 1,3-di-isopropylimidazolin-2-ylidene; *i*Pr, isopropyl; Ph, phenyl; PHDI, bis(2,6-diisopropylphenyl)phenanthrene-9,10-diimine; $^{Ph}PP_2{}^{Cy}$, $PhP(CH_2CH_2PCy_2)_2$; Ppy, 2-(2-pyridyl)phenyl; rt, room temperature; SQUID, superconducting quantum interference device; TEF, $[Al\{OC(CF_3)_3\}_4]$; TEM, transmission electron microscopy; Tf, trifluoromethanesulfonate; THF, tetrahydrofuran; Tipp, 2,4,6-triisopropylphenyl; TM, transition metal; TMDPDD, 3,4,8,9-tetramethyl-1,6-diphosphabicyclo(4.4.0)deca-3,8-diene; TMS, trimethylsilyl; Tol, toluene; tppme, 1,1,1-tris(diphenylphosphinomethyl)ethane1; TPPMS, sodium salt of *m*-monosulfonated triphenylphosphine; $Tren^{TIPS}$, $N(CH_2CH_2NSiiPr_3)_3$; Triphos, 1,1,1-tris(diphenylphosphinomethyl)ethane; Ts^{Tol}, $HC(SiMe_2NAr)_3$; UV, ultraviolet light; Vis, visible light; vtms, $Me_3SiCH{=}CH_2$; WCA, weakly coordinating anions; XAS, X-ray absorption spectroscopy; XPS, *X-ray photoelectron spectroscopy*; XRD, X-ray diffraction analysis.

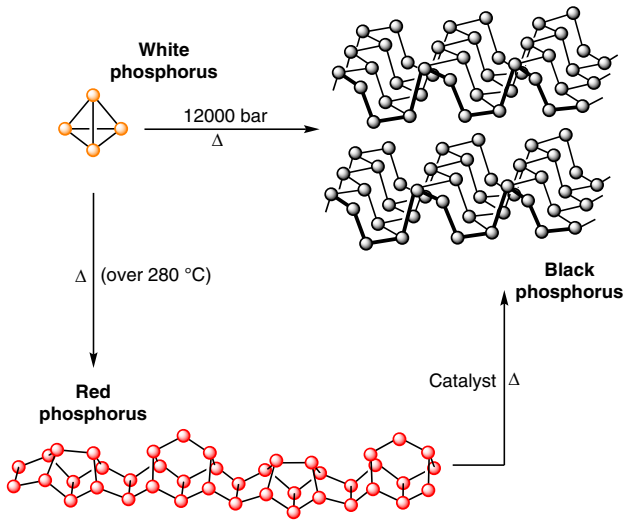

Scheme 1. Structures of the most common allotropic forms of elemental phosphorus. Focus of this work are white and black phosphorus.

considered, but this field is still in its infancy for the synthesis of organophosphorus species. Therefore, in the current research climate, the degradation of P_4 into P_1-P_4 fragments still constitutes the most important pathway towards the synthesis of organophosphorus compounds [2,11,18]. Also, its aggregation into P_n ($P_n \geq 5$) frameworks could provide further insights into the understanding of the structure and bonding in metal phosphides [19–21]. In this scenario, an eco-benign functionalization of P_4 emerges as a challenging task to afford the desired P-derivatives selectively. Accordingly, the development of such protocols, and comprehension of the mechanisms involved in the reactions [22] is an important goal in both academia and industry.

To achieve such a goal, one of the strategies has been to study the coordination of white phosphorus towards transition metals (TMs). By incorporating the P_4 molecule into the coordination sphere of a TM, an activated [M]-$(P)_x$ species can be obtained, hence facilitating the transformation of the phosphorus motifs formed. This could lead to new reaction pathways to circumvent the use of hazardous/corrosive phosphorus halides in the synthesis of organophosphorus compounds. Alternatively, such activation could be a straightforward route to access polyphosphorus cages/frameworks [19,23], obtaining building blocks for coordination polymers and supramolecular chemistry (*e.g.* the family of pentaphosphaferrocenes) [24], or synthesizing P-containing inorganic derivatives/phosphide materials [19,20].

When white phosphorus is heated or irradiated with UV light, the polymeric red allotrope is formed (Scheme 1) [12]. The precise structure of red phosphorus is unknown, although it is commonly thought to be an amorphous arrangement of different building units. By heating the amorphous red allotrope, other forms of elemental phosphorus can be obtained. These correspond to crystalline forms of red phosphorus, of which, for example, the structures of fibrous phosphorus and violet phosphorus are known. There are five proposed structural forms of red phosphorus, with commercially available amorphous red phosphorus being type I, fibrous phosphorus being type IV, and violet phosphorus being type V [12,25]. The molecular structures of types II and III have not been determined so far. Fibrous phosphorus, or type IV, and violet phosphorus (also known as Hittorf's phosphorus, type V) are assumed to be intermediates in the process to obtain black phosphorus from amorphous red phosphorus [26,27]. Both fibrous phosphorus and violet phosphorus share similar structural features, being composed of pentagonal P_8 and P_9 cages connected by P_2 dumbbell-like linkers [28]. The main difference between them is the crosswise linkage of the strands through the P_9 units in violet phosphorus, or their parallel arrangement under formation of double tubes in fibrous phosphorus [12,28].

The third fundamental allotrope, black phosphorus (BP, Scheme 1) [29], is the most thermodynamically stable form of the element. In fact, from white to black, the phosphorus allotropes become progressively more stable [30]. BP can be obtained either by heating red phosphorus at low pressures in the presence of a suitable catalyst (*e.g.* SnI_4) [31,32] or, alternatively, by heating white phosphorus at elevated pressures (12000 bar). Like the red allotrope, BP is polymeric, although by contrast, it has an ordered layered structure, resembling that of graphite. Weak van der Waals interactions hold together the layers. As with graphite, a monolayer of BP can be obtained by mechanical or liquid phase exfoliation [33]. This exfoliated monolayer of BP is known as phosphorene, by analogy with graphene, and is a 2D material that exhibits atypical physical, chemical, and biomedical properties [34–37]. Phosphorene [38,39] has ignited a renaissance for black phosphorus in recent times [40], giving rise to enormous scientific interest.

2D black phosphorus is now a protagonist next to silicene and germanene in the post-graphene era. The possibility to access phosphorus-containing materials by reaction of exfoliated black phosphorus has consequently gained widespread attention. However, since phosphorene is highly reactive and unstable towards light, oxygen and water (exposure to air results in facile formation of phosphates) [41], scarce information regarding its interaction with transition metals was available, until recently. Attention has been directed towards the design of efficient strategies to perform protective modification of exfoliated black phosphorus, aimed at increasing its stability. Such modifications could enable the development of black phosphorus or phosphorene-based optoelectronic devices, among other interesting applications in materials science.

Throughout the history of chemical research, a wide array of information on the chemistry of elemental phosphorus towards transition metals has appeared in the literature. In previous decades, extensive studies have been summarized in several reviews [6,7,42,43], and the field is still very much in the academic zeitgeist today. Most of those reviews explicitly focused on the coordination chemistry of white phosphorus towards early [6] or late [7,44,45] transition metals (TMs). As well, photochemical [46,47] or electrochemical [48–52] pathways for the selective transformation of P_4 have also been developed recently. In addition, strategies for the functionalization of phosphorene have also been reviewed lately [38].

Nevertheless, these published reviews are either outdated, most of them having appeared before 2011, or they focus on other aspects of P_4 chemistry neglecting its coordination chemistry, which has continued to thrive. We felt that the rapid developments in the field necessitated an update covering the period 2011–2020. Prior contributions will not be covered in this work, although some are included when relevant for a particular discussion. Most of these exciting studies make use of a stoichiometric amount of metal, affording novel and oftentimes an unpredictable variety of phosphorus-containing structural motifs. For the moment, there are very few contributions which have achieved the long sought-after catalytic functionalization of P_4 [53,54] yielding either aryl phosphines or aryl phosphates. It is also worth mentioning the emerging interest towards the coordination of white phosphorus by early transition metals, lanthanides and actinides, reactivity that previously was in the remit of late TMs. Another intriguing development is the study of P_n ligands, directly derived from P_4 and a suitable transition metal complex. It has been shown that they can be used as building blocks in the construction of either supramolecular assemblies or 1D and 2D coordination polymers

giving access to fascinating hybrid organic/organometallic frameworks [55].

To help the reader navigate this voyage through phosphorus coordination chemistry, the review has been divided into sections. Section 2 has been dedicated to the coordination chemistry of white phosphorus towards early transition metals (groups 3–7), including examples with lanthanides and actinides, while Section 3 provides an overview of the contributions with late transition metals (groups 8–11). Section 4 showcases the emerging field of surface coordination of exfoliated black phosphorus, which transcends the classical coordination chemistry of phosphorus compounds.

2. Coordination chemistry of white phosphorus by early transition metals

2.1. Group 3 metals

2.1.1. Scandium

In the last decade, activation of white phosphorus with rare earth elements and actinides has seen important breakthroughs, although the field remains less developed with respect to late transition metals. Group 3 elements, whose coordination chemistry is dominated by M(III) metal complexes (d^0), are amongst the hardest Lewis acidic metal cations. According to the HSAB theory, their matching with soft nucleophiles, such as phosphorus-containing ligands (phosphines or phosphides) is rather poor making the synthesis of rare-earth complexes bearing P-based ligands challenging [56]. However, their coordination chemistry with O-, N-, and C-based ligands is vast and well developed. Nonetheless, in 2012 Diaconescu *et al.* have disclosed the first example of the activation of white phosphorus [57] using dinuclear scandium(III) arene complexes, $[(NN^{fc})Sc]_2(\mu_2,\eta^4{:}\eta^4\text{-}C_{10}H_8)$ (**1**), and $[(NN^{fc})Sc]_2(\mu_2,\eta^6{:}\eta^6\text{-}C_{14}H_{10})$ (**2**), (NN^{fc} = 1,10-fc(NSi*t*BuMe$_2$)$_2$, and fc = ferrocenylene). As shown in Scheme 2, **1** and **2** are synthesized from the same iodide precursor **3** by reduction with KC_8 in presence of naphthalene or anthracene respectively. They feature a binuclear inverted-sandwich motif where the middle-deck is occupied by the reduced arene moiety. It was also possible for the authors to convert **1** into **2** by heating at 50 °C in the presence of anthracene.

Due to being excellent two-electron reductants, **1** and **2** reacted with P_4 giving mixtures of two different polyphosphorus clusters **4** and **5**, having either a $[P_8]^{4-}$ or a $[P_7]^{3-}$ Zintl-type anion at the core and $[(NN^{fc})Sc]^+$ units at the edges (Scheme 3) [58].

The differing solubilities of **4** and **5** allowed for facile separation and their structures were unambiguously elucidated by X-ray crystallography, see Fig. 1.

Compound **4** represents the first example of Zintl-type anion, $[P_7]^{3-}$ obtained directly from the activation of P_4, without using an alkali metal or its equivalent as a reducing agent [12]. Both the starting complexes **1**/**2** and the products **4**/**5** displayed short Fe-Sc bond (2.80 Å), evidencing a weak Fe-Sc donor–acceptor interaction which is deemed to be essential for the stability of the complexes. ^{31}P NMR analysis of **4** shows the presence of three different phosphorus atoms in 3:1:3 ratio, corresponding to three bridging atoms at the edges (P_{edge}), one phosphorus atom at the apex (P_{apex})

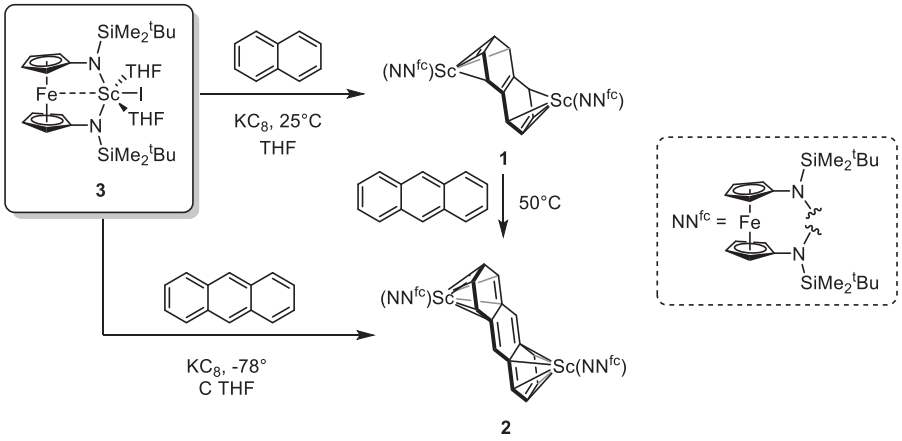

Scheme 2. Synthesis of the triple-decker complexes **1** and **2** from the common precursor **3**.

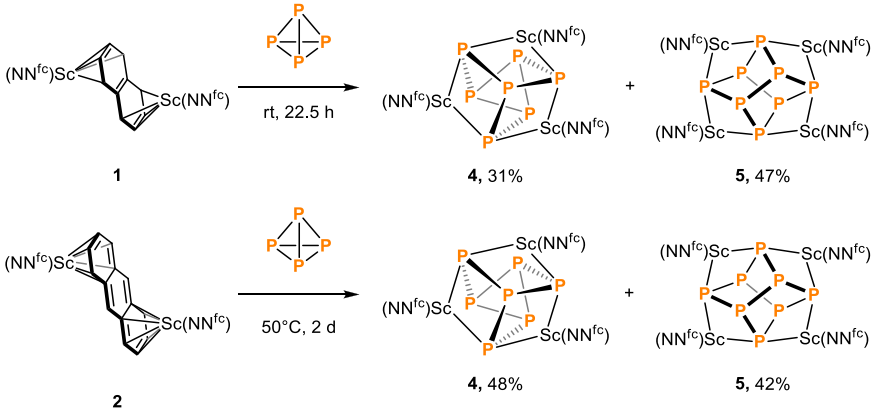

Scheme 3. Reaction of **1** and **2** with P_4.

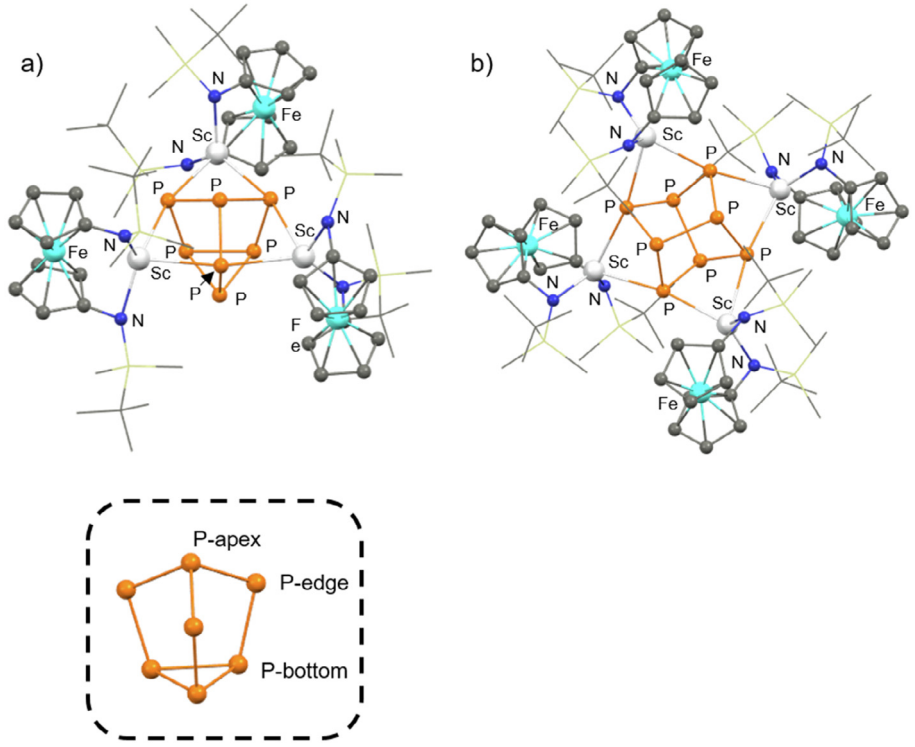

Fig. 1. X-ray crystal structure of a) **4**, b) **5**. Hydrogen atoms have been omitted for clarity; adapted from Ref. [58].

and a *cyclo*-P_3 at the bottom (P_{bottom}) forming an AA′A″MM′M″X′ spin system. This indicates that the bullvalene-type bond fluxionality, typically seen in alkaline earth polyphosphides such as Li_3P_7, is not present in **4** at room-temperature [59]. The bond distances between the phosphorus atoms are similar (P_{apex}-P_{edge} = 2.201 Å, P_{edge}-P_{bottom} = 2.197 Å, P_{bottom}-P_{bottom} = 2.201 Å) and very close to the P-P bond distance found in P_4 (2.20 Å) [60]. In addition to this, compound **4** features relatively short Sc-P_{edge} distances (2.730 and 2.747 Å), which gives the complex a prevalently covalent character. It should be noted that the formation of either P_7 or P_8 clusters by reductive coupling of white phosphorus is quite rare in early transition metal chemistry [61]. Interestingly, when using the yttrium-arene complex $[(NN^{fc})Y(THF)]_2(\mu_2,\eta^4{:}\eta^4\text{-}C_{10}H_8)$, only the Y_3P_7 species **6** is obtained. This compound shows a particularly shortened P_{edge}-P_{bottom} of 2.176 Å and longer Y-P distances (2.91 and 2.95 Å) with respect to Sc_3P_7, which can be addressed by the increased electropositivity of yttrium and therefore the complex has more ionic character. This P_4 activation protocol was extended also to analogous lanthanum and lutetium complexes such as $[(NN^{fc})La(THF)]_2(\mu_2,\eta^4{:}\eta^4\text{-}C_{10}H_8)$, and $[(NN^{fc})Lu(THF)]_2(\mu_2,\eta^4{:}\eta^4\text{-}C_{10}H_8)$, which reacted selectively with P_4 at room temperature affording the corresponding Zintl-type compounds **7** and **8** [62]. Fig. 2 shows the molecular structures of compounds **6**, **7** and **8**.

The related Zintl-type complexes **4**, **6**, **7** and **8** feature an inverse correlation between the ionic radius of the metal and the P_{edge}-P_{bottom} distance, and an increasing ionic character as the electronegativity of the metal decreases, a trend that culminates with La. The ^{31}P NMR spectrum of La_3P_7 (**7**) shows a single broad peak at room-temperature indicating the presence of the bullvalene-type tautomerization of the polyphosphide unit, which is not present in **4**, **6** and **8**.

By reacting **4** or **6** with Me_3SiI [58], the metal-free derivative $(Me_3Si)_3P_7$ was obtained and the resulting metal iodide by-product was used to prepare the starting metal-arene complexes thus opening a new way towards the metal-mediated synthesis of similar phosphorus compounds directly from P_4 (Scheme 4).

2.1.2. Yttrium

As in the case for scandium, activation of P_4 by yttrium complexes has only been achieved recently. Beside **6** described in Section 2.1.1., an analogous complex characterized with a $[P_7]^{3-}$ Zintl anion core was obtained in a two steps process from elemental phosphorus by Zhou and co-workers [63]. The reaction of P_4 with two equivalents of the metal alkyl complex LYR(THF) [**9**, L = *N,N′*-di(2,6-diisopropylphenyl)-1,4-diazabutadiene, R = 2-*N,N′*-dimetylbenzyl] followed by addition of DMAP (4-*N,N′*-dimethylaminopyridine) proceeds via the migration of the benzyl moieties from the metal centers to two adjacent phosphorus atoms of P_4, affording the rare-earth complex $(LY{\cdot}DMAP)_2$ $[\mu_2,\eta^3{:}\eta^3\text{-}1,2\text{-}R_2\text{-}cyclo\text{-}P_4]$ (**10**) (Scheme 5) where the *cyclo*-P_4 core bridges the two yttrium centers and assumes a rare twisted conformation (Fig. 3).

Interestingly, treatment with HMPA (hexamethylphosphoramide) promotes further migration of the benzylic residues affording $(LY{\cdot}HMPA)_3P_7$ [**11**, L = *N,N′*-di(2,6-diisopropylphenyl)-1,4-diazabutadiene] with concurrent loss of the tribenzylphosphine **12** (Scheme 6, Fig. 4**a**). Such a Zintl-type complex is structurally comparable to the polyphosphides described above, except that in this case the Y atoms are bound to four P atoms with distances ranging from 3.002 to 3.317 Å. After prolonged heating of **11** in toluene, a P-P migration of the benzyl residue occurs, yielding the cluster $(LY{\cdot}DMAP)_2[\mu_2,\eta^2{:}\eta^3\text{-}cyclo\text{-}P_3PR_2]$ (**13**, R = *o*-dimethylaminobenzyl), where the disubstituted phosphorus atom sits *exo* with respect to the remaining unsubstituted *cyclo*-P_3 moiety, see Fig. 4**b**. It is noteworthy to add that addition of benzylpotassium to **13** completes the extrusion of the *exo*-P atom through elimination of tribenzylphosphine. This leads to the formation of the ion-paired complex $(LY{\cdot}THF)_2$ $[(\mu_2,\eta^3{:}\eta^3\text{-}cyclo\text{-}P_3)]K$ (**14**), which possesses an unsubstituted *cyclo*-P_3 moiety and, after

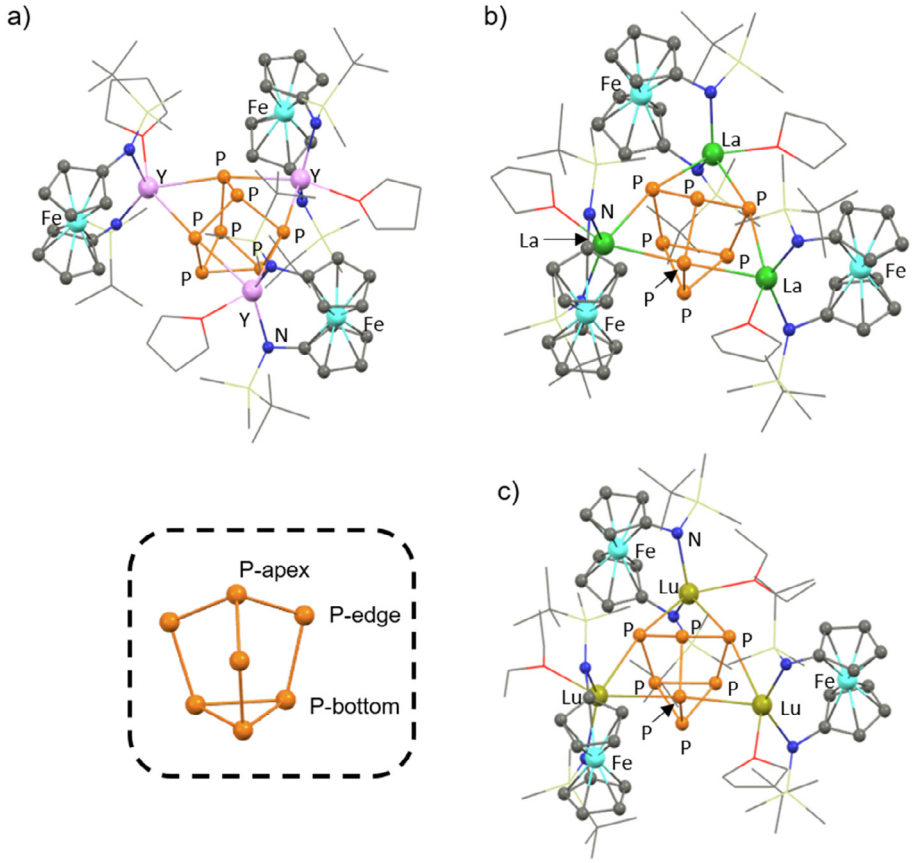

Fig. 2. Molecular structures of a) **6**, b) **7** and c) **8**. Hydrogen atoms have been omitted for clarity; adapted from Refs. [58] (**6**) and [62] (**7** and **8**).

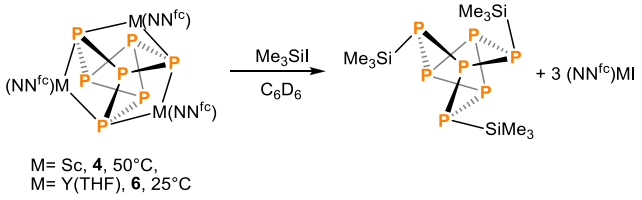

Scheme 4. Synthesis of organophosphorus derivative mediated by **4** and **6** in the presence of Me_3SiI.

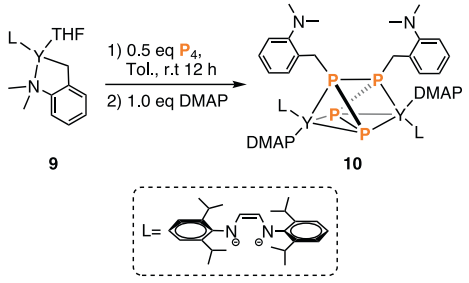

Scheme 5. Reaction of P_4 with **9**.

addition of 18-crown-6, its ion-sequestered derivative [K(18-crown-6)][LY(THF)$_2$(μ_2,η^3:η^3-*cyclo*-P$_3$)] (**15**) is formed, Fig. 4**c**. Compound **14** could also be formed by direct addition of KR (R = N,N′-dimethyl-2-benzyl) to the *cyclo*-P_4 complex **10**, indicating that the nucleophilicity of KR might promote a non-thermal benzylic migration followed by elimination of tribenzylphosphine. As such, this process represents a remarkable 2-step [3 + 1]-fragmentation process of P_4, in which one phosphorus atom is also derivatized into an organophosphine.

2.1.3. Lanthanides and actinides

2.1.3.1. Lutetium. The formation of the cyclic $[P_3]^{3-}$ anion commonly occurs via white phosphorus activation in the presence of early or late transition metal complexes. As such, P_4 follows a [3 + 1]-fragmentation pathway which usually enables the isolation of either the P_3 or the P_1 moiety. One-pot, simultaneous trapping of both fragments is much rarer and is limited to few examples, mainly with late transition metals [64–66]. That was until Zhang and co-workers achieved this by employing early transition metal (ETM) complexes such as yttrium and lutetium metallacyclopentadienes **16**, **17** and **18** (Scheme 7) [67]. These complexes react readily with 0.5 equivalents of P_4 in tetrahydrofuran at room temperature displaying dual dinucleophile/diene character. Similar to the known reactivity of 1,4-dilithium-1,3-butadienes with P_4 [68], the P_1 fragment is captured through the formation of phospholyl lithium **19**, while the remaining P_3 moiety is involved in a Diels-Alder reaction with the diene ligand. This results in the exclusive formation of the *exo*-products **20**, **21a** and **21b** (Scheme 7).

As shown in Fig. 5, the final products bear an unusual substituted bicyclo[4,1,0]triphosphaheptanide framework where the metal is *endo* with respect to the η^3-P_3 ligand and retains the M−C bonds with the terminal carbon atoms of the C_4 fragment (**20**: Y-C1 = 2.409 Å, Y-C2 = 2.402, Y-P1 = 2.711 Å; **21a**: Lu-C1 = 2.367 Å, Lu-C2 = 2.353 Å, Lu-P1 = 2.664 Å; **21b**: Lu-C1 = 2.392, Lu-C4 = 2.375 Å, Lu-P1 = 2.639 Å).

Interestingly, the Lu-P1 bond in compounds **21a** and **21b** is markedly shorter than M−P bonds commonly found in known

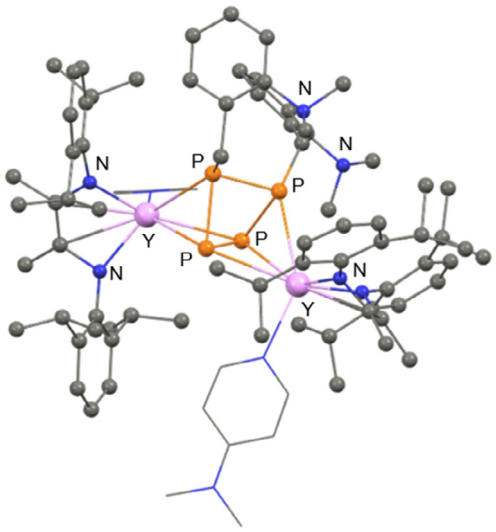

Fig. 3. Solid state structure of **10.** Hydrogen atoms have been omitted for clarity; adapted from Ref. [63].

lutetium phosphides and polyphosphides, while the Lu-P2 and Lu-P3 bond distances (**21a**: Lu-P2 = 2.976 Å, Lu-P3 = 2.992 Å; **21b**: Lu-P2 = 3.000 Å, Lu-P3 = 2.986 Å) are appreciably longer (Lu_3P_7, **8** displays average Lu-P bond = 2.893 Å). Additionally, the structural and spectroscopic features found for the *cyclo*-P_3 moiety in **20**, **21a** and **21b** are different compared to the known *cyclo*-P_3 complexes derived from the activation of white phosphorus with late-transition metals (LTM) such as Co [69], Rh, Ir [70], Ni [71], Pd and Pt [72]. In contrast with the mentioned ETM, in LTM complexes, the metal center resides opposite to the organic ligand occupying one vertex of the tetrahedron formed with the *cyclo*-P_3 fragment. In addition to this, in ETM complexes the M−P and P-P distances are averagely longer and the three P atoms are not equidistant. These features reflect in the ^{31}P NMR spectra of the complexes, which usually show two different sets of signals for the *cyclo*-P_3 fragment, while in LTM complexes only one signal was observed, usually having $^1J_{(P\text{-}P)}$ coupling constant one order of magnitude smaller. DFT calculations have confirmed the existence of a weak interaction between the newly formed π system and the 5d orbitals of the lanthanide metal center. Reminiscent of the reactivity shown by the *cyclo*-P_3 unit in LTM towards M$(CO)_5$ where M = Cr, Mo, W, Re [73,74], Zhang *et al.* investigated the behavior of **20**, **21a** and **21b** towards {$W(CO)_5$(THF)}. The coordination of the tungsten carbonyl occurred exclusively at P1 with concurrent displacement of the $Li(THF)_3$ countercation, which indicates the prevailing nucleophilic character of P1 over P2 and P3. Nevertheless, coordination to P2 was also observed when employing two equivalents of {$W(CO)_5$(THF)}. Furthermore, the oxidation of **20** with *p*-benzoquinone was studied. In this process, the P_4 molecule is released along with the formation of the aromatic phospholyl lithium.

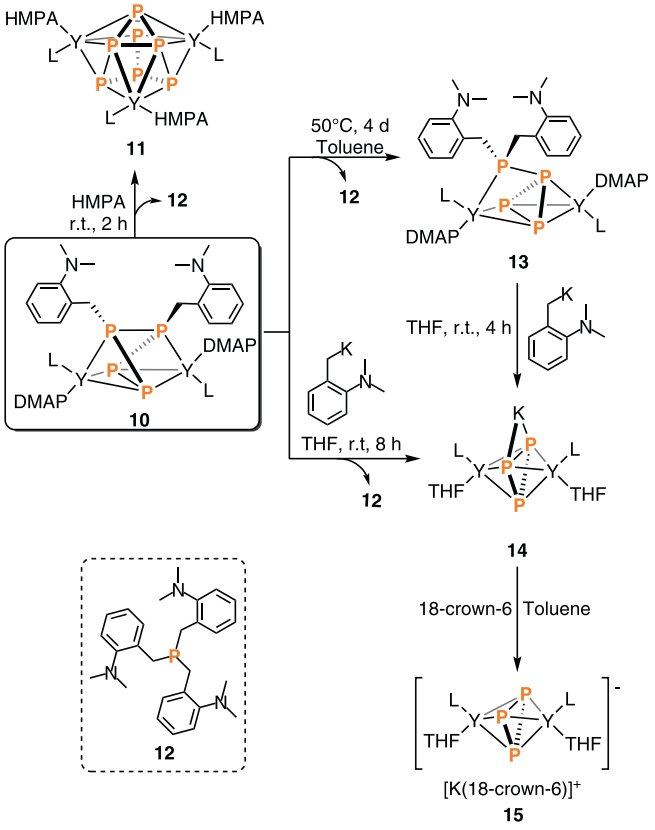

Scheme 6. Selective conversion of the *cyclo*-P_4 unit in **10** by alkyl migration.

2.1.3.2. Samarium. Low-valent samarium species have been extensively employed in the reduction of transition-metal complexes bearing phosphides or polyphosphides moieties. The first direct activation of P_4 with a samarium(II) species, not involving other transition metals, was achieved in 2009 by Roesky and coworkers. Decamethylsamarocene, Cp^*_2Sm(II), acting as a single electron donor, was shown to reductively couple two P_4 units affording the realgar-type ionic compound [{Cp^*_2Sm}$_4P_8$], the first isolated polyphosphide of the rare-earth elements [75]. To further explore how the steric demand of the reducing agent affects the activation of P_4, As_4 and As_4S_4, Roesky and coworkers employed the bulky samarium amidinate complex [$(DippForm)_2Sm(THF)_2$] (**22**, DippForm = {$(2,6\text{-}i\text{Pr}_2C_6H_3)NCN(2,6\text{-}i\text{Pr}_2C_6H_3)$}$^-$). As shown in Scheme 8, the reaction of **22** with white phosphorus afforded red crystals of the dinuclear complex [{$(DippForm)_2Sm$}$_2$(μ_2,η^4:η^4-P_4)] (**23**) in high yields (94%) [76].

The added steric hindrance of the amidinate ligands prevents the assembly of the $[P_8]^{4-}$ cage without affecting the efficiency of the reduction. Complex **23** features an inverse inorganic sandwich structure with a naked *cyclo*-P_4^{2-} moiety as the middle deck, representing the first example of an f-element to display such a structure, see Fig. 6. The *cyclo*-P_4^{2-} ligand is almost perfectly rectangular-shaped being characterized by regular P-P bonds (ranging from 2.1443 Å to 2.1618 Å) and internal P-P-P angles close to 90°. The Sm-P bonds range from 3.041 Å to 3.157 Å, which is comparable to known samarium phosphide complexes [75].

It should be mentioned that the *cyclo*-P_4^{2-} moiety, being isolobal to the cyclobutadiene dianion $[C_4H_4]^{2-}$, consists of a 6π-aromatic system. Due to its high stability, the formation of [*cyclo*-P_4]$^{2-}$ ligands occurs readily in the activation of P_4 by alkaline metals such as Cs [77], by ETM such as Zr [78], Nb [79], Ta [80] and LTM, either in monometallic complexes or by bimetallic cooperation [81,82]. In an attempt to further explore the ability of divalent samarium complexes to promote P-P bond formation, in 2013 Roesky and co-workers reacted at high temperatures the samarocenes [$Cp^*_2Sm(THF)_2$] (**24a**) and [{C_5Me_4(*n*-propyl)$_2$}Sm] **24b** with the well-known pentaphosphaferrocene [$Cp^*Fe(\eta^5\text{-}P_5)$] (**25a**) [83]. This resulted in the formation of a 2 electron-2 center P-P bond between two [$Cp^*Fe(\eta^5\text{-}P_5)$] units through a double single-electron reduction process mediated by Sm(II), which afforded the dimeric core [{$Cp^*Fe(\eta^4\text{-}P_5)$}$_2$]$^{2-}$. The latter is stabilized by two [$(C_5Me_4R_2Sm]^+$ (R = Me, *n*-Pr) cations forming the products **26a** and **26b** (Scheme 9) which constitutes the first exam-

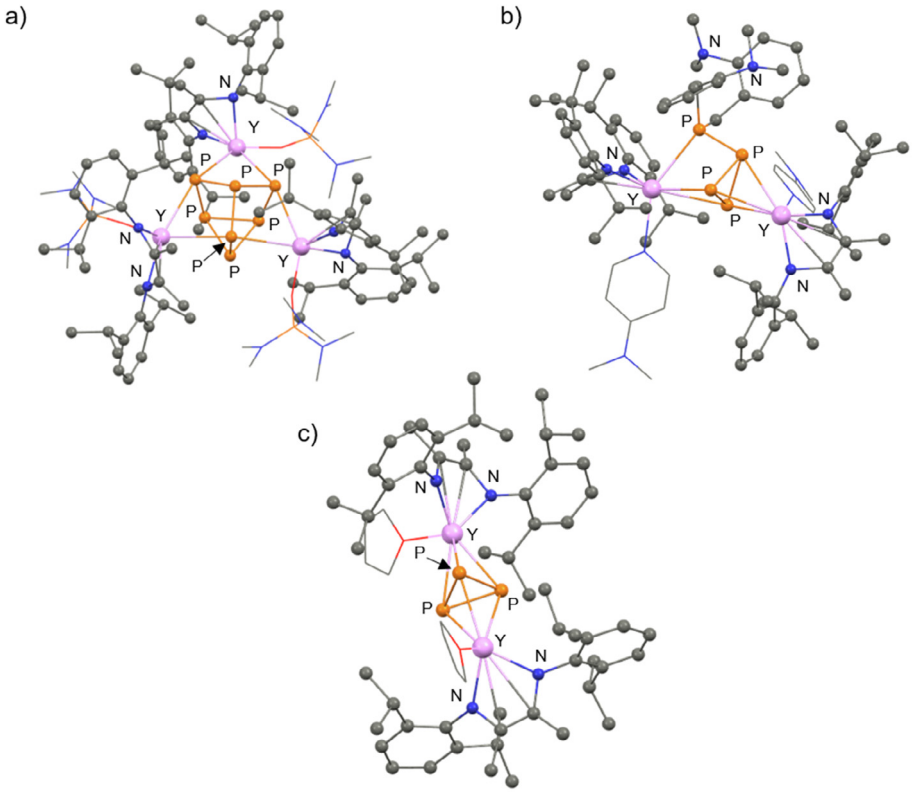

Fig. 4. Molecular structures of a) **11**, b) **13**, c) **15**. Hydrogen atoms have been omitted for clarity; adapted from Ref. [63].

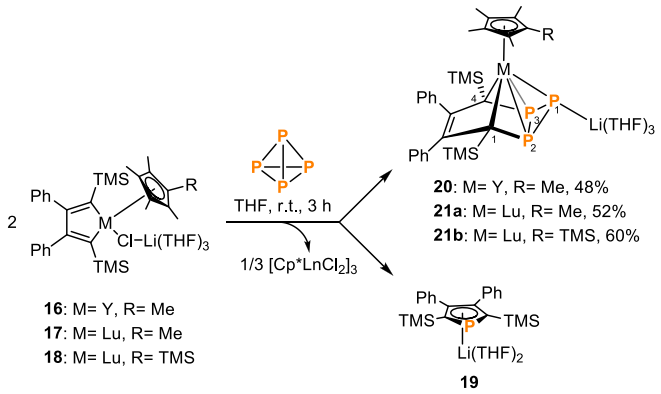

Scheme 7. Activation of P_4 with **16**, **17** and **18** by a formal [3 + 1] fragmentation process.

ple of a mixed 3d/4f polyphosphide complexes bearing a rare P_{10} bridging moiety (Scheme 9).

As shown by the molecular structure in Fig. 7, after reduction the two *cyclo*-P_5 moieties assume an envelope type conformation whereby the two off-plane P atoms are involved in a newly formed single P-P bond (P–P bond length is 2.209 Å in **26a** and 2.199 Å in **26b**). The P-P distances in the *cyclo*-P_5 ring are in the range 2.137–2.186 Å in **26a** and 2.114–2.189 Å in **26b**, suggesting partial double bond character. Considering that each iron atom is bound to the *cyclo*-P_5 in an η^4 fashion, the latter can be formally considered as a tetraphosphabutadienediide ligand formally donating six electrons.

As the Sm atom in **26a** and **26b** is in the III oxidation state, as confirmed by characteristic NIR absorption, the polyphosphide unit is one of the very few examples of a $[P_{10}]^{4-}$ anion (see Section 3.1.1). It should be mentioned that a neutral P_{10} ligand was first found in the following complexes $[(Cp''M)_4P_{10}]$ (M = Rh,

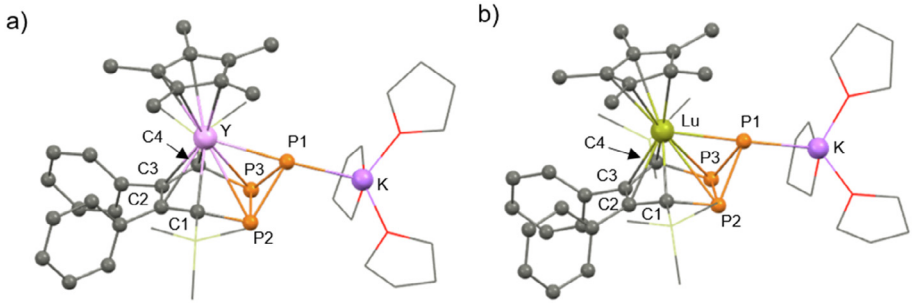

Fig. 5. Solid state structure of a) **20,** b) **21a**. Hydrogen atoms are omitted for clarity; adapted from Ref. [67].

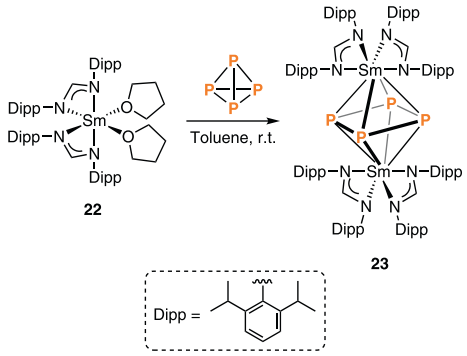

Scheme 8. Activation of P_4 with **22**.

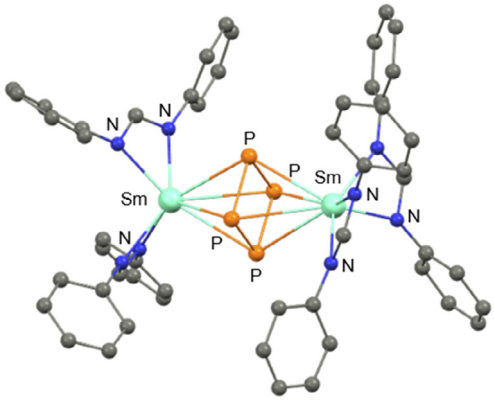

Fig. 6. Solid state structure of **23.** Hydrogen atoms and 2,6-diisopropylphenyl groups are omitted for clarity; adapted from Ref. [76].

Cp″ = 1,3-*t*Bu$_2$C$_5$H$_3$, M = Co, Cp″ = 1,3-(SiMe$_3$)$_2$C$_5$H$_3$), synthesized by Scherer in 1992 [84].

2.1.3.3. Ytterbium. The activation of P_4 with rare earth metals has been investigated by A. Trifonov *et al.* by using the reduced-arene Yb(II) complex, [Cp^{Bn5}Yb(DME)$_2$(μ_2,η^4:η^4-C$_{10}$H$_8$)] (**27**, Cp^{Bn5} = pentabenzylcyclopentadienyl), which can be conveniently synthetized by salt metathesis using [YbI(DME)$_2$]$_2$(μ_2,η^4:η^4-C$_{10}$H$_8$) and Cp^{Bn5}K [85]. Compound **27** shares similarities with other reduced-arene complexes of rare earth metals. It features an inverted sandwich motif whereby the twisted dianionic naphthalene ligand occupies the middle deck and bridges two metal centers, each one coordinated in an η^4 mode. It should be noted that the two ytterbium atoms appear in a divalent oxidation state, as confirmed by ^{1}H and ^{13}C{^{1}H} NMR analysis allowing for two potential reductive sites in addition to $(C_{10}H_8)^{2-}$. The reaction of **27** with P_4 affords the trinuclear Yb(II) complex [Cp^{Bn5}Yb(DME)]$_3$P$_7$ (**28**, Scheme 10) [86].

The molecular structure of **28** was elucidated by XRD analysis (Fig. 8). Similar to other M_3P_7 complexes (M = Sc, Y, La, Lu) described by Diaconescu [58,62] and Zhang [67], see Sections 2.1.1, 2.1.2 and 2.1.3, **28** bears a central Zintl-type $[P_7]^{3-}$ cage ligand which coordinates three Yb(II) atoms at the edges of the middle rim in an $\mu,\kappa^2{:}\kappa^2{:}\kappa^2$ mode.

The average Yb-P bond length (2.93 Å) is comparable to analogous yttrium and lutetium $[P_7]^{3-}$ polyphosphides (respectively 2.93 Å [58] and 2.89 Å) [62]. ^{1}H NMR spectroscopy showed the expected set of signals related to the organic ligands, thus confirming the diamagnetism of **28** and the divalent state of Yb ions. The ^{31}P{^{1}H} NMR spectrum collected either at room temperature and at −60 °C, displayed only a broad singlet at δ −174.2 ppm. This is possibly due to the presence of a fast bullvalene-type tautomerization typically associated to more ionic $[P_7]^{3-}$ polyphosphides.

2.1.3.4. Thorium. Following the same strategy used for the reductive activation of white phosphorus with low-valent rare earth metals, in 2016 Mills and co-workers achieved the unprecedented Th(III)-mediated activation and complexation of P_4 [87]. The reaction of complex [Th(Cp″)$_3$] (**29**, Cp″ = C$_5$H$_3$(SiMe$_3$)$_2$–1,3) with P_4 affords the binuclear derivative [{Th(Cp″)$_3$}$_2$ ($\mu,\kappa^1{:}\kappa^1$-P$_4$)] (**30**) featuring the reduced (*cyclo*-P$_4$)$^{2-}$ ligand in an unique coordination mode (Scheme 11). However, the reaction proved to be rather slow (72 h) with low yields (19%).

However, it is noteworthy to add that the analogous U complex [U(Cp″)$_3$] did not show any reactivity with elemental phosphorus even in forcing conditions (reflux, 16 h). This was attributed to the greater electropositivity of Th(III) compared to U(III). The ^{31}P{^{1}H} NMR analysis of **30** showed two low field signals at δ = 227.59 ppm (t, $^1J_{(P\text{-}P)} \approx$ 400 Hz) and δ = 328.86 ppm (t, $^1J_{(P\text{-}P)} \approx$ 400 Hz) and two unresolved broad peaks at δ = –246.55 (br m, $\Delta\nu \approx$ 2000 Hz) and 10.35 ppm (br m, $\Delta\nu \approx$ 2000 Hz). Meanwhile the low field resonances correlate well with the ionic compound $[Cs_2P_4]^{2-}$ [77], the broad signals could not be confidently assigned. The peculiar hapticity of the *cyclo*-P$_4$ moiety, attributed to the steric demand of the bulky Cp″ coordinated to the metal, predominantly involves the sp^2-hybridized lone pairs on phosphorus. This is confirmed by XRD analysis of **30** (Fig. 9), which shows P-P distances (average 2.051(9) Å) almost identical to a P=P double bond (2.04 Å) [88], whereas coordination in an η^4 fashion usually displays longer P-P bonds (2.16–2.14 Å) with greater σ-character (see for instance Section 2.1.3.2).

It is also worth mentioning that the calculated δ(P,P) delocalization index, which can be regarded as a measure of the aromaticity of the system, was found to be 1.33, close to the formal value of

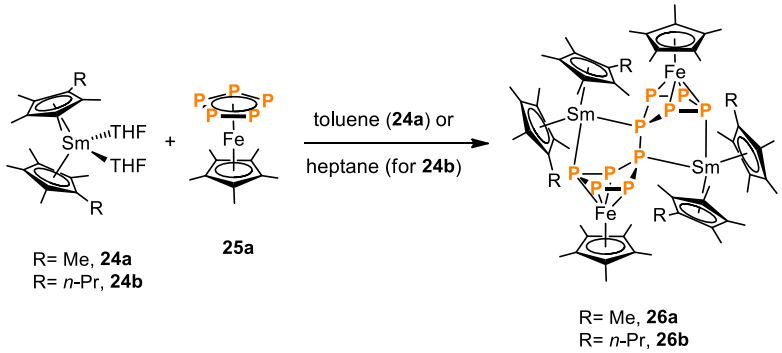

Scheme 9. Complexes **24a** and **24b** react with **25a** yielding the polyphosphides **26a** and **26b**.

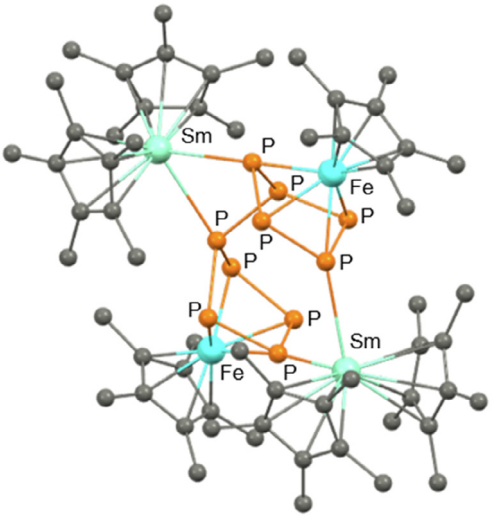

Fig. 7. Solid state structure of **26a**. Hydrogen atoms are omitted for clarity; adapted from Ref. [83].

1.50 expected for a 6π-aromatic systems. Thus, the $[cyclo\text{-}P_4]^{2-}$ moiety in **30** can be seen as a largely unperturbed, planar aromatic 6π-electron moiety. Finally, the elongation of the Th-$Cp_{centroid}$ distances going from **29** to **30** (respectively 2.519 and 2.543 Å) is in line with the formal Th(IV) assignment of **30** [89]. The Th-P distances (2.919 Å) are similar to those observed in known thorium phosphides also derived from the reaction with P_4 [90].

2.1.3.5. Uranium. Although there are only a few examples of the activation of P_4 with uranium containing complexes that have been reported in the last decade, the variety of coordination patterns in these scant examples is quite remarkable. In 2011, Green and co-workers investigated the reactivity of P_4 with the U(III) species $[U(\eta^5\text{-}C_5Me_5)\{\eta^8\text{-}C_8H_6(SiiPr_3)_2\text{-}1,4\}_2(THF)]$ (**31**, Scheme 12) [91]. This compound, upon U(III)-promoted two-fold reduction of P_4, yields the dimeric complex **32** $[U(\eta^5\text{-}C_5Me_5)\{\eta^8\text{-}C_8H_6(SiiPr_3)_2\text{-}1,4\}]_2(\mu_2,\eta^2\text{:}\eta^2\text{-}P_4)$ as black crystals, in which the bridging $[P_4]^{2-}$ unit is tilted with respect to the U-U axis as clearly shown in Fig. 10. Nonetheless, the P-P distances (2.148–2.152 Å) are almost identical and are in line with other dianionic $[P_4]^{2-}$ ligands (*vide supra*). A $^{31}P\{^1H\}$ NMR study revealed a signal at δ + 718 ppm, suggesting **32** is paramagnetic. Similarly, the $^{31}P\{^1H\}$ resonance of the $[P_4]^{2-}$ complex $[U\{N(tBu)Ar\}_3]_2(\mu2,\eta^4\text{:}\eta^4\text{-}P_4)$ was found to be +794 ppm [92].

DFT calculations were in close accordance with the observed hapticity of $[P_4]^{2-}$ in **32**, despite the absence of bulky substituents on the adopted molecular model $[U(\eta^5\text{-}C_5H_5)(\eta^8\text{-}C_8H_8)]_2(P_4)$. As suggested by the MO analysis, the singular $\mu_2,\eta^2\text{:}\eta^2$ binding mode of P_4 results from a combination of both steric (wedge-shaped nature of the UCotCp fragment) and electronic requirements (the tilting of P_4 respect to U-U vector, allows both σ and π orbitals of P_4 being involved in U-P bonding interactions).

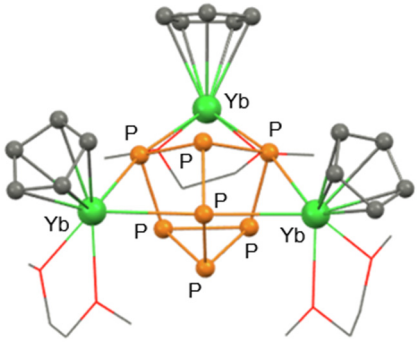

Fig. 8. Molecular structure of **28**. Hydrogen atoms and benzyl groups on the cyclopentadienyl ligands are omitted for clarity; adapted from Ref. [86].

U(III) complexes have also been involved in the formation of higher phosphides by catenation of P_4. By reacting the triamide complex $[U(Tren^{TIPS})]$ [**33**, $Tren^{TIPS}$ = $N(CH_2CH_2NSiiPr_3)_3$] with P_4, Liddle and co-workers [93] isolated the corresponding *cyclo*-P_5 dinuclear inverted-sandwich complex $[\{U(Tren^{TIPS})\}_2(\mu_2,\eta^5\text{:}\eta^5\text{-}cyclo\text{-}P_5)]$ (**34,** Scheme 13 and Fig. 11 for X-ray structure).

Compound **34** emerges as one of the few actinide complexes bearing a *cyclo*-P_5 fragment together with the two samarium complexes $[Cp^*Fe(cyclo\text{-}P_5)Sm(DIP_2pyr)]_2$ and $[Cp^*Fe(cyclo\text{-}P_5)Sm(DIP_2pyr)\text{-}(THF)_2]$ (DIP_2pyr = 2,5-bis{N-(2,6-diisopropylphenyl)iminomethyl}pyrrolyl) [94], even though in the latter complexes it assumes an envelope-like conformation. It should be mentioned that the *cyclo*-P_5 phosphide, isolobal with the cyclopentadienyl ring, is a formal mono-anionic ligand usually found in association with electron rich d-metals [7], with whom it shares σ or π bonding interactions. Nonetheless, UV–Vis and SQUID magnetometry measurements agreed with the presence of U(IV) in **34**. Accordingly, both uranium atoms display a $5f^2$ configuration, therefore suggesting a twofold reduction of the *cyclo*-P_5 moiety, making the ligand dianionic. Further investigations of the electronic structure of the complex through DFT calculations have revealed that the *cyclo*-P_5 ligand in **34** could be approximated to a dianion bridging the two metal centers via two polarized δ-bond, which are formed by the donation of uranium δ-symmetry 5f orbitals to δ-symmetry frontier molecular orbitals of the *cyclo*-P_5.

Liddle and co-workers have also investigated the behavior of reduced-arene uranium complexes towards elemental phosphorus, a strategy that has proved successful for group 3 and 4f-block metal complexes [95]. When treating the diuranium(V)-arene-tetraanion complex $[\{U(Ts^{Tol})\}_2(\mu_2,\eta^6\text{:}\eta^6\text{-}C_6H_5CH_3)]$ (**35**, Ts^{Tol} = $HC(SiMe_2NAr)_3$; Ar = 4-MeC_6H_4) with 1.1 equivalents of P_4, the corresponding Zintl-type complex $[\{U(Ts^{Tol})\}_3(\mu,\kappa^2\text{:}\kappa^2\text{:}\kappa^2\text{-}P_7)]$ (**36**) was obtained, see Scheme 14.

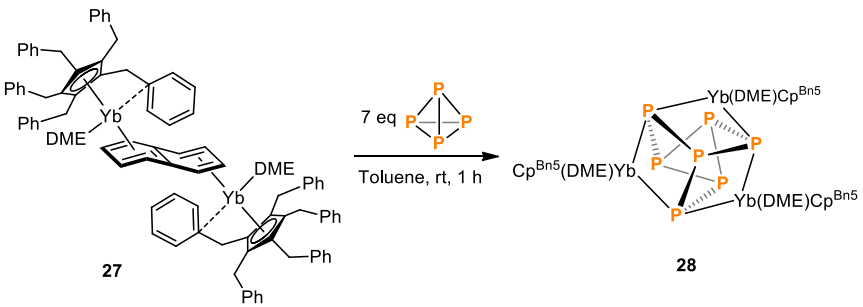

Scheme 10. Activation of P_4 by complex **27** yielding the trinuclear phosphide **28**.

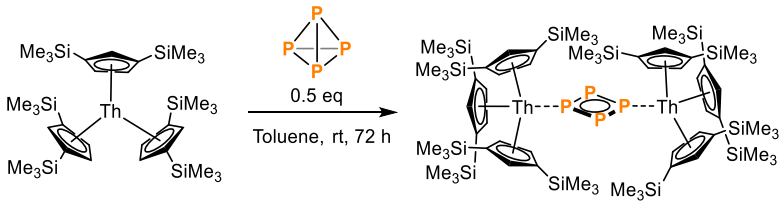

29 30

Scheme 11. Reaction of P_4 with complex **29**.

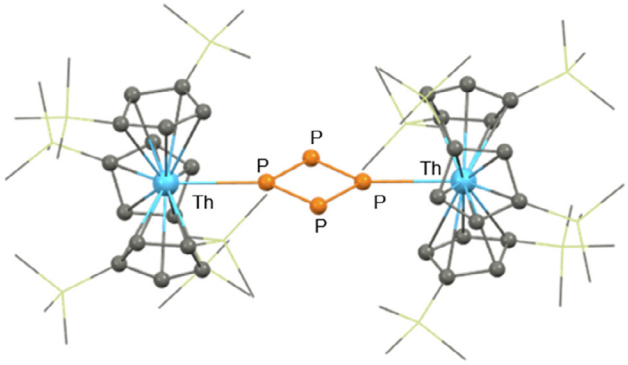

Fig. 9. Solid state structure of **30**. Hydrogen atoms are omitted for clarity; adapted from Ref. [87].

It should be mentioned that the precursor **35**, is best described as two U(III) centers bridged by a dianionic toluene moiety [96]. The magnetic moment of **36**, measured by Evans method in C_6D_6 was found to be 4.67 μ_B at 25 °C, which is a value of 2.42 μ_B per uranium atom. This is in good agreement with other U(IV) complexes [97], thus confirming a multi-electron redox process occurring between the precursor **35** and P_4. In Fig. 12 it is shown that the molecular structure of **36** features a central $[P_7]^{3-}$ trianion bridging three $[U(Ts^{Tol})]^+$ fragments, where each U center is coordinated to two P atoms on the upper rim of the Zintl-type scaffold. This represents the first example of fragmentation and catenation of P_4 promoted by uranium. U-P bond lengths in **36** are in the range of 2.948–3.031 Å, 0.1–0.2 Å longer than the sum of the covalent radii of uranium and phosphorus (2.81 Å) [58], possibly due to the steric hindrance of the $[U(Ts^{Tol})]^+$ unit and the bridging coordination mode.

A common parameter used to quantify the ionic character of heptaphosphanortricyclane cages is the Q value [98], which for ionic systems is usually in the range 1.3–1.4. XRD data allowed to determine the Q value for **36** (1.39), indicating the prevailing ionic character of the uranium cluster. As observed for other Zintl-type complexes of ETM (see Scheme 4, Section 2.1.1), the $[P_7]^{3-}$ core can be transferred to a large array of electrophiles, such as metal salts (LiCl), sp^3-C electrophiles (MeI), silyl chlorides (Me_3SiCl) and sp^2-C electrophiles (ArI), yielding the corresponding P_7R_3 substrate (R = Li, Me, Me_3Si, Ar) and the uranium halide complex.

2.2. Group 4 metals

2.2.1. Titanium

There are few examples of the titanium mediated activation of white phosphorus [6]. Nonetheless, it should be mentioned that $TiCl_4$ has been employed as a Lewis acid for the direct arylation of P_4 using ArCl, given a mixture of $PClAr_2$ and PCl_2Ar but not the desired PAr_3 [99]. In 2010, Cummins and co-workers [100] developed a protocol to synthesize aryl and alkyl tertiary phosphines, PR_3, from P_4 exploiting the known ability of P-P bonds to scavenge C-centered radical species. As showed by previous investigations, carbon radicals can be efficiently produced using the tris-amide Ti(III) complex $[Ti(N[tBu]Ar)_3]$ (**37**, Ar = 3,5-$C_6H_3Me_2$, Scheme 15), which is a potent one-electron reducing agent and halide-abstractor towards both C-sp^2 and C-sp^3 halides [101,102]. However, compound **37** does not react with P_4 directly, lowering the possibility of unwanted side reactions to occur. Reacting excess amounts of PhBr and $[Ti(N[tBu]Ar)_3]$ in presence of P_4 gives the corresponding PR_3 in good yields (72% for X = Cl and R = Ph). Interestingly, the intermediate P_2Ph_4 is selectively obtained (80% yield) by using sub-stoichiometric amounts of halide and Ti(III) complex, allowing the synthesis of mixed phosphines, PR_2R'. It should be added that, by increasing the steric demand on the organic halide, Cummins and co-workers successfully expanded the reaction scope to polyphosphorus substrates. Addition of MesBr resulted in the formation of P_3Mes_3 (61% yield), whereas when using DmpI the butterfly-type bicyclophosphine *cis*,*trans*-$DmpP_4Dmp$ was obtained in 78% isolated yield (Mes: 2,4,6-Me_3-C_6H_2, Dmp: 2,6-Mes_2-C_6H_3).

2.2.2. Zirconium

In 1988, Scherer and co-workers [103] found that zirconocene, $[Cp''_2Zr(CO)_2]$ (**38**, Cp'' = η^5-$C_5H_3tBu_2$-1,3) is able to insert into one P-P edge of the P_4 tetrahedron forming the side-on coordinated adduct $[Cp''_2Zr(\kappa^2\text{-}P_4)]$ (**39**, Scheme 16). It should be mentioned that the analogous compound $[Cp^*_2Zr(\kappa^2\text{-}P_4)]$ was only detected in solution, failing any attempt of isolation indicating the need

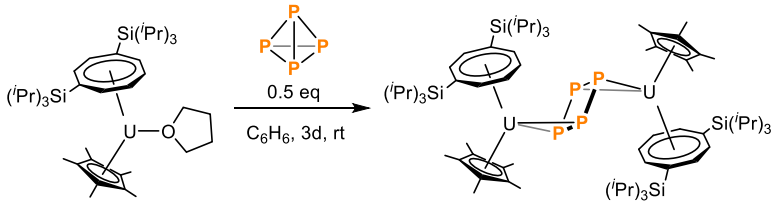

31 32

Scheme 12. Activation of P_4 with complex **31**.

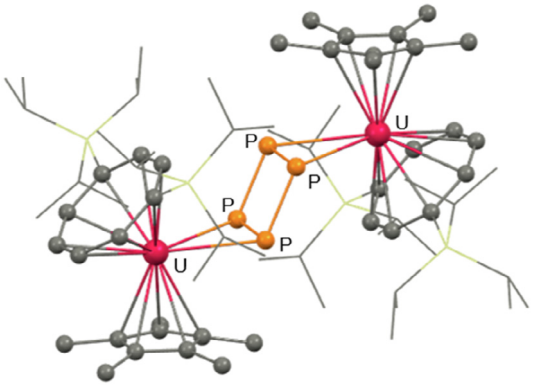

Fig. 10. Solid state structure of **32**. Hydrogen atoms are omitted for clarity; adapted from Ref. [92].

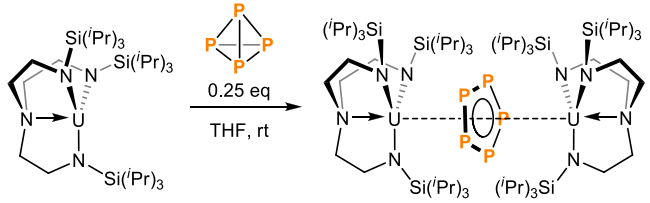

Scheme 13. Activation of P_4 by [U(Tren^{TIPS})] **33**.

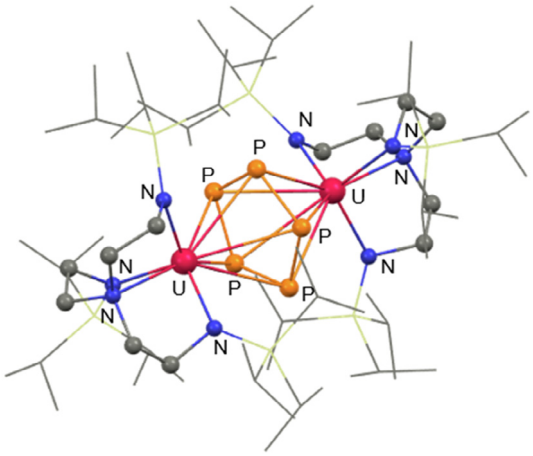

Fig. 11. Solid state structure of **34**. Hydrogen atoms are omitted for clarity; adapted from Ref. [93].

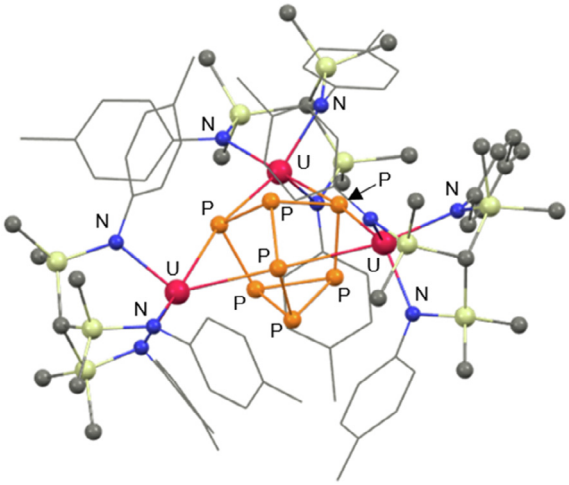

Fig. 12. Molecular structure of **36**. Hydrogen atoms are omitted for clarity; adapted from Ref. [95].

for bulkier ligands. The central tetraphosphabicyclo[1.1.0]butane motif in **39** displays P-P distances ranging from 2.178 to 2.239 Å, with the bond between the two backbone P atoms being slightly shorter (2.178 Å). As shown in Scheme 16, treating **39** with *t*BuC≡P [104] afforded complex [Cp′′$_2$Zr(κ^2-P$_3$C*t*Bu)] (**40**) as the major product among other compounds, such as [Cp′′$_2$Zr{κ^2-P$_6$(C*t*Bu)$_2$}] (**41**) displaying a ZrP_6C_2 cuneane-type framework, closely resembling the Hittorf's phosphorus allotrope [105], see Fig. 13, and the Zr-free substrate **42**.

Even though the mechanism of formation of **40** is not fully elucidated, it formally arises from the displacement of a P_2 unit in **39** with a molecule of *t*BuC≡P. In turn, **41** can be viewed as the product of double addition of *t*BuC≡P to **39**. Similarly, the polyphosphorus compound **42** can be considered as a *t*BuC≡P tetramer which is extended by a P_2 unit. DFT calculations showed that steric repulsion between Cp′′ and *t*BuC≡P plays a dominant role in directing the reaction towards the formation of the preferred regioisomer **40**, where the bulky *t*BuC fragment sits on the bridgehead position and points away from the Zr center.

DFT calculations [106] carried out on **39** show that the HOMOs are largely located on the P_4 fragment. Additionally, the P atoms directly attached to Zr are more negatively charged (−0.20) with respect to the bridgehead P atoms (+0.11) and will preferentially coordinate to Lewis acids. Steric repulsion between the LA and the hindered zirconocene moiety would in principle direct the coordination towards the bridgehead P atoms, as observed above. When [W(CO)$_5$(THF)] and **39** are mixed in equimolar amounts,

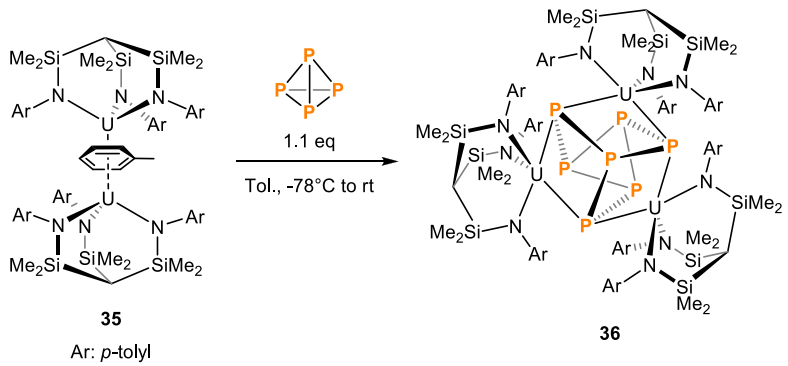

Scheme 14. Activation of P_4 by diuranium complex **35**.

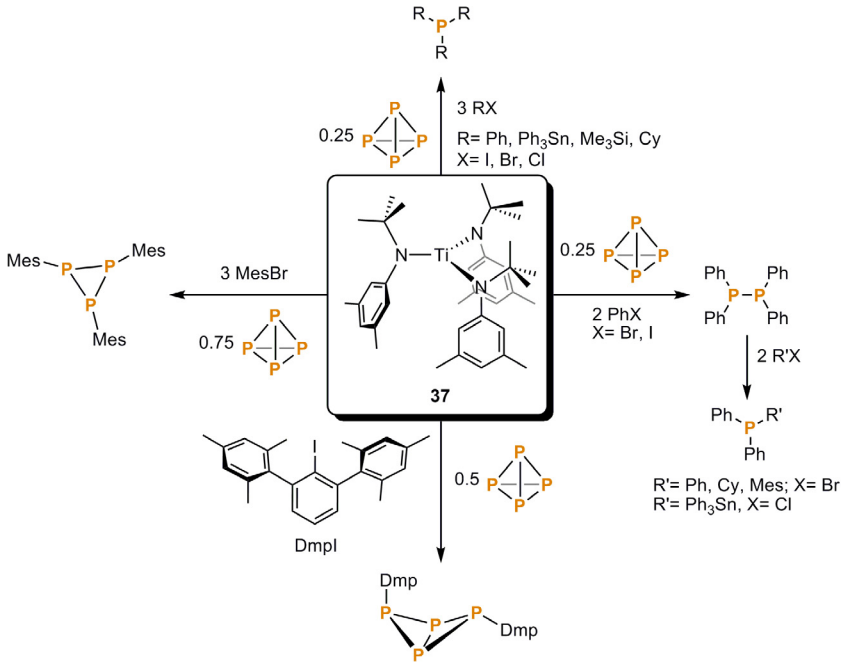

Scheme 15. [Ti(N[*t*Bu]Ar)$_3$] acts as a halide abstractor through a single electron reduction process. This allows the formation of C-radical species in-situ which react with P_4 to afford a range of phosphines or phosphides.

the [W(CO)$_5$] fragment coordinates exclusively to the Zr-attached P atoms yielding compound [Cp″$_2$Zr(μ2,κ^2:κ^1-P$_4$){W(CO)$_5$}] (**43**, see Scheme 17). Compound **43** was subsequently calculated to be 6.11 kJ/mol more stable than its bridgehead-P coordinated counterpart. Interestingly, the second equivalent of [W(CO)$_5$(THF)] still coordinates to the more electronegative P atom giving a mixture of the mono **43** and twofold coordinated adduct [Cp″$_2$Zr(μ$_3$-κ^2:κ^1:κ^1-P$_4$){W(CO)$_5$}$_2$] (**44**), in 1:4 ratio respectively (see Scheme 17 and Fig. 14 for solid-state structures of **43** and **44**). The three-fold coordinated complex [Cp″$_2$Zr(μ$_4$-κ^2:κ^1:κ^1:κ^1-P$_4$){W(CO)$_5$}$_3$] (**45**) was formed as the major product by using a large excess of LA (8 eq). It should be mentioned that these conditions did not allow for the formation of the fourfold coordinated adduct but instead the compound, [(CO)$_4$W(μ$_5$-η^4:κ^1:κ^1:κ^1:κ^1-P$_4$){W(CO)$_5$}$_4$] (**46**), arising from the detachment of the zirconocene moiety, was detected.

In contrast, the more sterically demanding [CpMn(CO)$_2$(THF)] is expected to coordinate predominantly on the bridgehead P, which was calculated to be 9.08 kJ/mol more stable than the species coordinated to the metal-bonded P atom. This was confirmed experimentally, as one equivalent of [CpMn(CO)$_2$(THF)] coordinates exclusively on the bridgehead P atoms giving complexes **47** (see Fig. 15 for X-ray structure) and **48**. Addition of two equivalents of [CpMn(CO)$_2$(THF)] gives the two mono coordinated complexes (P-backbone **47** and P-apical **49**) and the twofold coordinated complex **48** in 10:0.5:1 ratio as indicated by ^{31}P{^{1}H} NMR (Scheme 18).

In contrast with [W(CO)$_5$], the addition of one equivalent of [Fe$_2$(CO)$_9$] gives both regioisomers of [Cp″$_2$Zr(μ2,κ^2:κ^1-P$_4$)(Fe(CO)$_4$] in almost an equimolar ratio (1:1.3) as observed by ^{31}P NMR analysis (compound **50** and **51**, Scheme 19). Only **51** could be isolated after flash column chromatography and its solid-state structure is shown in Fig. 16.

After having evaluated the coordination behavior of **39** towards highly electrophilic transition metals fragments, Lewis acidic main group compounds, such as AlMe$_3$ and AlEt$_3$, were investigated (Scheme 20). In the case of AlMe$_3$, the reaction exclusively afforded the complex [Cp″$_2$Zr(μ$_3$-κ^2:κ^1:κ^1-P$_4$){AlMe$_3$}$_2$] (**52**), which bears two AlMe$_3$ molecules both bound to a P-coordinated Zr, regardless of the stoichiometry (1:1, 1:2, 1:5). The reaction employing the bulkier AlEt$_3$ gave the monocoordinated derivative [Cp″$_2$Zr(μ2,κ^2:κ^1-P$_4$){AlEt$_3$}] (**53**), where the LA is again attached to Zr bound P. The Al-P bond (2.577 Å) is shorter than in **52** (Al-P: 2.596 Å) (see Fig.17), which are both longer compared to a covalent Al-P bond (2.37 Å) indicating high dative bond character [88].

A tripodal aryloxide-coordinated zirconium hydride complex has been employed by Kawaguchi *et al.* to activate P_4 among other small molecules [107]. The reaction of complex [(O$_3$C)Zr(THF)$_3$] [**54**, (O$_3$C)$^{3-}$ = tris(2-oxy-3,5-di-*tert*-butylphenyl)methane] with NaBHEt$_3$ leads to the formation of the hydride dimer [{Na(DME)}$_2${(O$_3$C)Zr}$_2$(μ,H)$_3$] (**55**), see Scheme 21. Reacting **55** with P_4 in toluene leads to the release of one equivalent of PH_3. The remaining *cyclo*-P$_3$ fragment replaces the bridging hydrides affording the complex [(Na(THF)$_5$]-[{Na(THF)$_2$}$_2${(O$_3$C)Zr}$_2$(μ$_2$,η^3:η^3-*cyclo*-P$_3$)] (**56**), after crystallization from a THF solution (Scheme 21). Complex 56 is a contact ion-pair, where the countercation [Na(THF)$_5$]$^+$ balances the anionic complex [{Na(THF)$_2$}$_2${(O$_3$C)Zr}$_2$(μ$_2$,η^3:η^3-*cyclo*-P$_3$)]$^-$. Complex **56** features an inverse sandwich structure, where the two Zr centers are bridged by a trihapto *cyclo*-P$_3$ unit, to which a formal −3 charge is assigned.

An XRD analysis of **56** (Fig. 18) shows that each Zr center is hepta-coordinated with a distorted mono-capped octahedral geometry, with the bridgehead C atom of the [O$_3$C]$^{3-}$ ligand occupying the capped position. The *cyclo*-P$_3$ moiety displays P-P single bonds of 2.226 Å and coordinates the two staggered [(O$_3$C)Zr] units in an η^3 mode. These features are well representative of known late transition metals complexes M$_2$(μ$_2$,η^3:η^3-*cyclo*-P$_3$) with M = Ni, Co, Pd, Pt [69–74].

2.3. Group 5 metals

2.3.1. Vanadium

Low-valent vanadium species can be considered as powerful reducing agents due to their ability to undergo multiple electron processes, and therefore is an excellent candidate for the activation of white phosphorus. However, the reactivity of known V(II) complexes is often impaired by the saturation of the coordination sphere of the metal. A strategy to increase stability without imped-

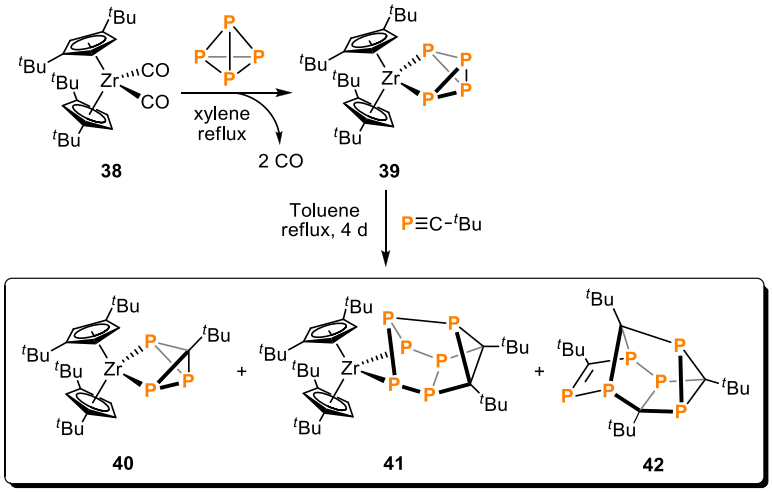

Scheme 16. Synthesis of **39** and its subsequent reactivity with the phosphalkyne.

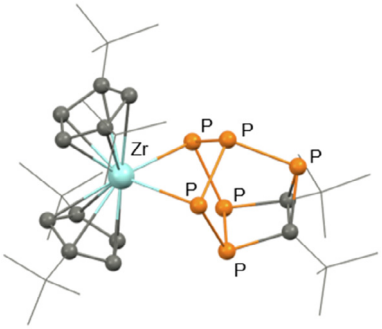

Fig. 13. Molecular structure of **41**. Hydrogen atoms are omitted for clarity; adapted from Ref. [104].

ing reactivity is to mask its coordination sites with an arene [108,109]. In 2010, Mindiola and co-workers reduced the previously synthesized [(nacnac)VCl(Ntolyl$_2$)] (**57**) [110] with KC_8 or 0.5% Na/Hg in benzene, successfully affording the arene masked V(II) complex [(nacnac)V(Ntolyl$_2$)] (**58**), see Scheme 22. XRD analysis of **58** showed unambiguously the elimination of the chloride and the presence of an η^3-coordination of Ntolyl$_2$ towards V, which is responsible of the stabilization of the highly reactive V (II) center. It should be noted that nacnac ligands generally are not effective in stabilizing electron-rich metals due to their tendency to undergo two-electron cleavage. Compound **58** is able to activate P_4 in a three electron reduction giving the diamagnetic vanadium(V) complex [(nacnac)V(η^3-*cyclo*-P_3)(Ntolyl$_2$)] (**59**), the first example of a vanadium complex bearing a [*cyclo*-P_3]$^{3-}$ ligand [111], whose solid state structure is shown in Fig. 19. The two-steps process (reduction of **57** and treatment with P_4) can be con-

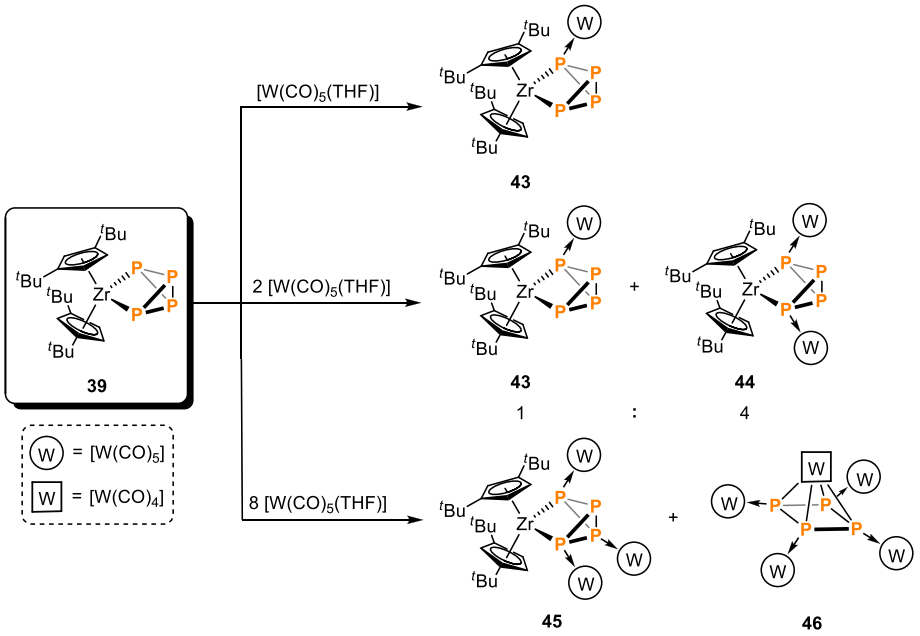

Scheme 17. Compound **39** is reacted with 1, 2 and 8 eq of [W(CO)$_5$(THF)] affording prevalently P-edge coordinated products.

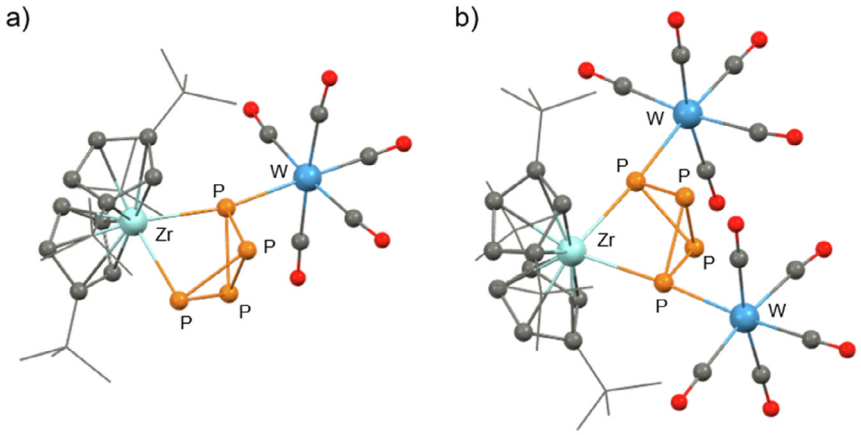

Fig. 14. Molecular structure of a) **43** and b) **44**. Hydrogen atoms are omitted for clarity; adapted from Ref. [106].

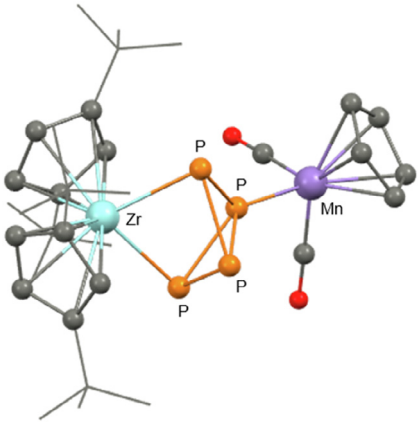

Fig. 15. Molecular structure of **47**. Hydrogen atoms are omitted for clarity; adapted from Ref. [106].

veniently performed in a one pot reaction as shown in Scheme 22. When performed with a reduced quantity of P_4 (0.25 eq of P_4), the reaction affords the dinuclear complex [(nacnac)V(Ntolyl$_2$)]$_2$(μ2, η^2:η^3-*cyclo*-P_3) (**60**) in 33% yield. The latter could be obtained in quantitative yields by reacting the mono-nuclear *cyclo*-P_3 complex **59** with one equivalent of **58**. Similarly, reduction of the starting aryloxy-coordinated complex [(nacnac)VCl(OAr)] (**61**, $^-$OAr = O{2,6-*i*Pr$_2$C$_6$H$_3$}) with 0.5% Na/Hg in presence of P_4 gave complex [(nacnac)V(η^3-*cyclo*-P_3)(OAr)] (**62**). This could also be synthesised by heating the dinitrogen complex, **63** to 90 °C for ten minutes in presence of 2 equivalents of P_4 (Scheme 22) [112].

The molecular structure of **59** (Fig. 19**a**) features V-P bond lengths between 2.443 and 2.452 Å and an average intermolecular P-P distance of 2.15 Å, which is in the range of known [*cyclo*-P_3]$^{3-}$ complexes. The *cyclo*-P_3 moiety in complex **62** has similar bond lengths. The vanadium center in **59** assumes a pseudo tetrahedral geometry having three N-atom donors and the *cyclo*-P_3 occupying the fourth position. The solid-state structure of **60** (Fig. 19**b**) displays a triple-decker geometry where the two V atoms occupy the two vertex of the trigonal bipiramidal V_2P_3 core. Consistent with the μ_2,η^2:η^3 binding mode, one V atom is η^3 coordinated to the *cyclo*-P_3 ring, having V-P distances in the range 2.472–2.50 2 Å, while the other V atom displays a remarkably elongated V-P bond (2.928 Å), in accordance with an η^2 binding. The μ_2,η^2:η^3 coordination mode is uncommon among *cyclo*-P_3 complexes; examples being [(C_5H_3tBu$_2$)$_2$Th(μ_2,η^2:η^3–*cyclo*P_3)Th(Cl)(C_5H_3-*t*Bu$_2$)$_2$], prepared by Scherer in 1991 [90] and a few d^8 metal complexes, such as [(triphos)Ni(*cyclo*-P_3)Pt(PPh_3)$_2$]$^+$ [113], and [Au{M(tppme)(*cyclo*-P_3)}$_2$]$^+$ (M = Co, Rh, Ir) [114]. Interestingly, in the case of **60**, the μ_2,η^2:η^3 binding mode seems to average out to a μ_2,η^3:η^3-*cyclo*-P_3 coordination mode in solution, as the ^{1}H NMR spectrum did not show any inequivalence between the vanadium

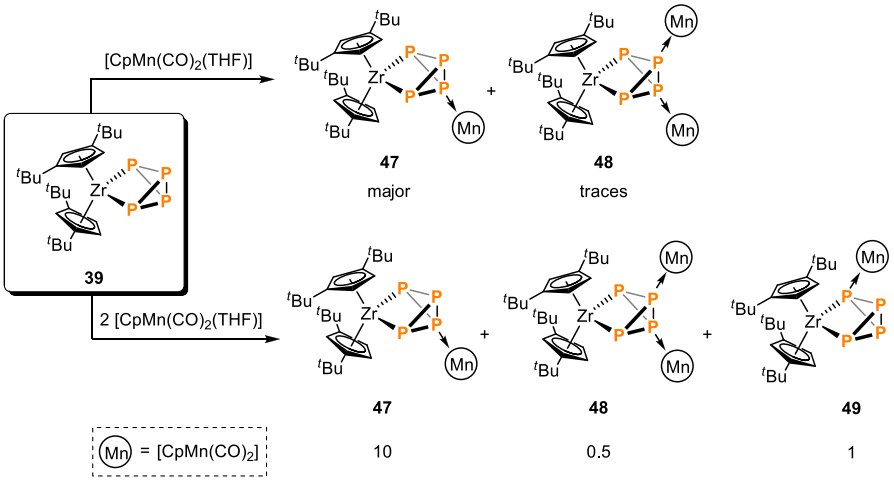

Scheme 18. [CpMn(CO)$_2$(THF)] reacting with **39** preferentially at the P-backbone.

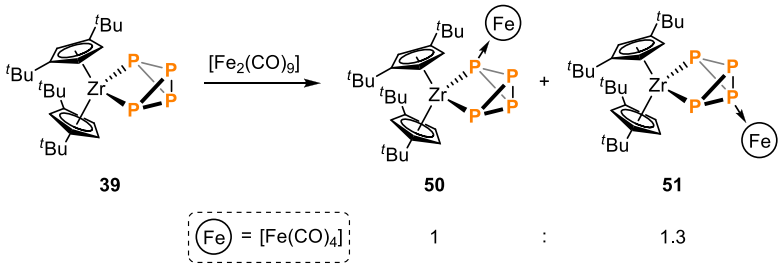

Scheme 19. Reaction of **39** with $[Fe_2(CO)_9]$ affords respectively the P-edge and P-backbone complexes **50** and **51**.

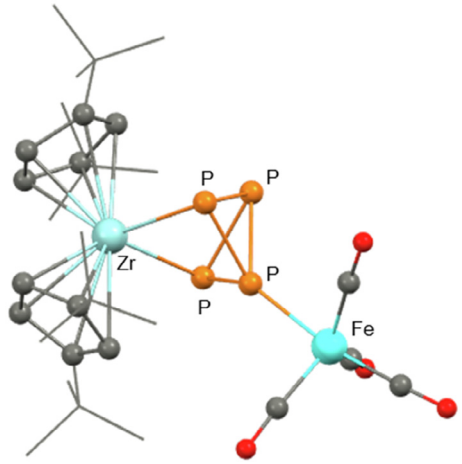

Fig. 16. Molecular structure of **51**. Hydrogen atoms are omitted for clarity; adapted from Ref. [106].

bound ligands. Compound **60** is paramagnetic as confirmed by Evans method (S = ½ at room temperature with μ_{eff} = 1.80 μ_B) and EPR gave an anisotropic *g* value ≈ 2. Unexpectedly, the solution state ^{31}P NMR spectrum of **59** and **62** showed significantly downfield signals corresponding to the P_3 moiety, with very broad resonances at δ = 85.0 and 125.0 ppm respectively, whereas the *cyclo*-P_3 motif usually displays signals within the range of −170 ppm and −220 ppm (see Section 2.1.3). This behavior was rationalized through magic-angle spinning (MAS) analysis and a detailed DFT study. It was noted that a particularly effective d(V)-p(*cyclo*-P_3) overlap in an applied external magnetic field generates a deviation to the metal-to-ligand density currents which are ultimately responsible of the deshielding phenomena.

2.3.2. Niobium

Although the selective and atom-efficient activation/functionalisation of white phosphorus remains elusive, recently great efforts have also been invested in the post-activation manipulations of polyphosphides-containing ETM complexes. For example, Cummins *et al.* reduced the niobium complex$[Cl_2Nb(ODipp)_3]$ (**64**) in the presence of white phosphorus [115] to yield $[Na(THF)_3][(\eta^3\text{-}P_3)Nb(ODipp)_3]$ (**65**) (Dipp = 2,6-diisopropylphenyl). They then demonstrated that **65** acts as a P_3 reservoir whereby the synthon $[cyclo\text{-}P_3]^-$ can be transferred to an organic fragment as well as to a different metallic complexes [116]. This can be achieved by reacting the nucleophilic complex **65** with $SnClPh_3$ (or other chlorides such as $SiMe_3Cl$, $SiPh_3Cl$ and Ph_3CCl) affording the novel neutral adduct $[(ODipp)_3Nb(\mu_2,\eta^2\text{:}\eta^1\text{-}Ph_3SnP_3)]$ (**66**) via salt metathesis. In turn, the reaction of **66** with pyridine N-oxide liberates the reactive triphosphirene intermediate Ph_3SnP_3 **67**, which can be trapped with 1,3-cyclohexadiene (CHD) to form the corresponding Diels-Alder (D-A) adduct $[Ph_3SnP_3(C_6H_8)]$ (**68**, Scheme 23, see Fig. 20**a** for solid-state structure of **68**).

As usually observed in similar cycloadditions involving P=P moieties, the *endo* product is exclusively formed due to decisive secondary orbital interactions taking place. The authors were able to observe via ^{31}P NMR spectroscopy the formation of the C_5H_5NO-coordinated complex at −10 °C prior to the release of Ph_3SnP_3. A detailed DFT study carried out by Morello and co-workers further elucidated the mechanism of this transformation [117]. The authors demonstrated that the reaction proceeds through a redox-neutral Bayer-Villiger oxygen insertion into the Nb-P bond, which is the rate-determining step of the reaction (+23.7 kcal mol^{-1}). Subsequently, the formation of the strong Nb≡O bond leads to the concomitant formation of the proposed $(\eta^1\text{-}P_3)Ph_3Sn$ intermediate (221267.7 kcal mol^{-1}), which then reacts *in situ* with CHD. The energy barrier associated with the D-A reaction is calculated to be as low as +4.8 kcal mol^{-1}. The isolable compound **68** can be considered a $[cyclo\text{-}P_3]^-$ carrier featuring a "protected" P=P bond as well as a labile Sn-P bond and can be used to deliver the *cyclo*-P_3 unit to a suitable acceptor. The reaction of **68** with the Wilkinson's catalyst $[ClRh(PPh_3)_3]$, formed the corresponding $[(\eta^3\text{-}cyclo\text{-}P_3)Rh(PPh_3)_3]$ (**69**) (Scheme 23), featuring a symmetric *cyclo*-P_3 moiety with a resonance at δ = -191 ppm and an octahedral geometry for the Rh(III) center (Fig. 20**b**), similar to the previously reported $[(\eta^3\text{-}cyclo\text{-}P_3)Rh(triphos)]$ (triphos = $CH_3C(CH_2PPh_2)_3$) [118].

More recently, Scheer *et al.* demonstrated that the anionic complex **65** can undergo ring expansion if treated with a suitable electrophilic P-atom donor, to access $[cyclo\text{-}P_4]^{3-}$ complexes [119]. The reaction of **65** with the phosphinidene complex $[Cp^*P\{W(CO)_5\}_2]$

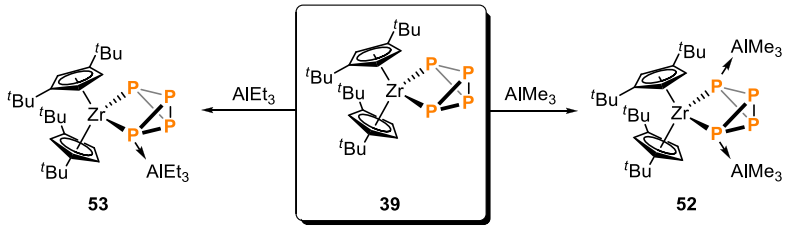

Scheme 20. Coordination behavior of **39** towards $AlMe_3$ and $AlEt_3$.

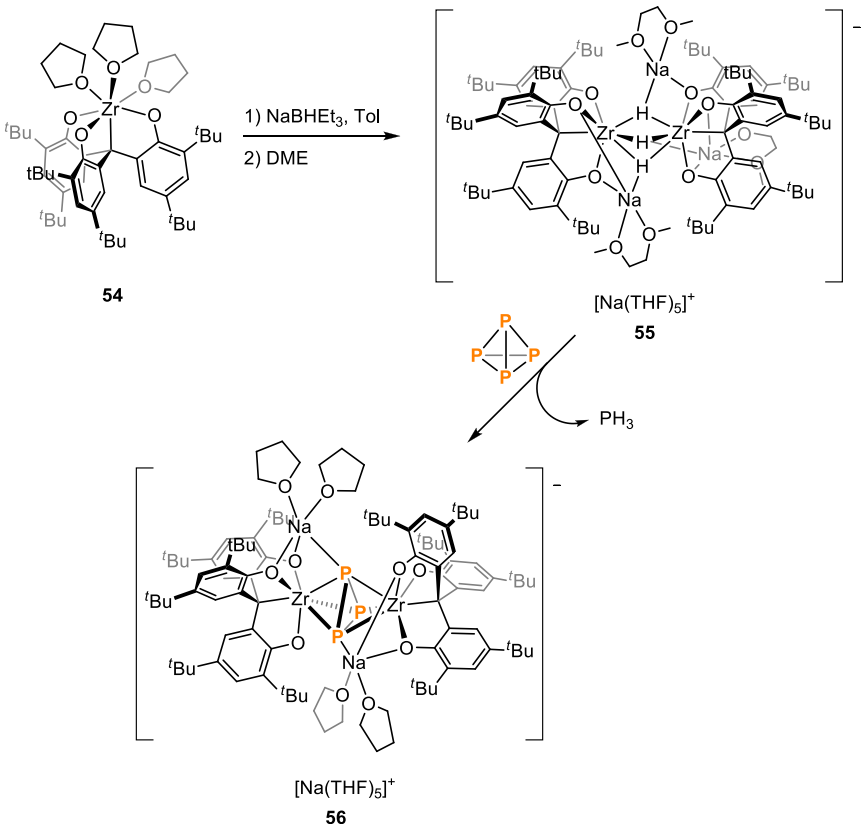

Scheme 21. Reduction of **54** with $NaBHEt_3$ affords dinuclear tri-hydride complex **55** which in turn reacts with P_4 forming the *cyclo*-P_3 complex **56** with concomitant loss of PH_3.

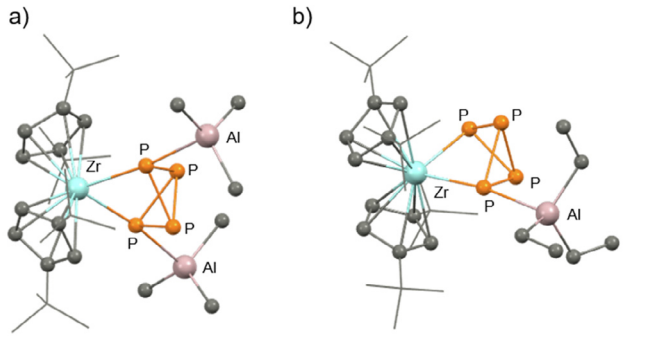

Fig. 17. Molecular structure of a) **52** and b) **53**. Hydrogen atoms are omitted for clarity; adapted from Ref. [106].

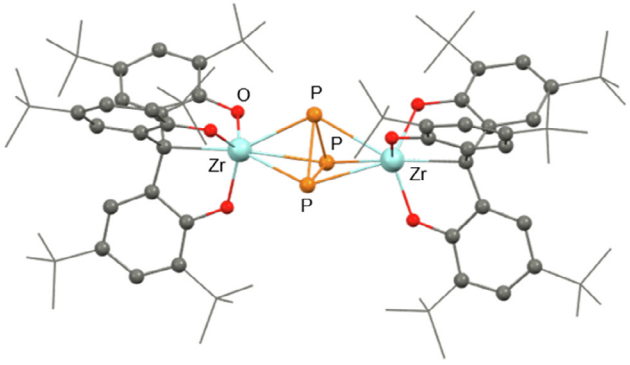

Fig. 18. Molecular structure of **56**. Hydrogen atoms and $[Na(THF)_5]^+$ are omitted for clarity; adapted from Ref. [107].

(Cp* = C_5Me_5) at −78 °C in presence of 18-crown-6 afforded [Na(18-crown-6)$(THF)_2$][{$W(CO)_5$}$_2${μ_3,η^3:κ^1:κ^1-P_4Cp*}Nb(ODipp)$_3$] (**70**) in excellent yield (Scheme 24).

As elucidated by the XRD analysis of **70** (see Fig. 21), the [*cyclo*-P_4]$^{3-}$ moiety adopts a butterfly-like conformation where the newly inserted P atom is out of the plane of the other P atoms and one of the $W(CO)_5$ fragments has migrated to the former P_3 unit. Bond lengths within the *cyclo*-P_4 range from 2.2105(15) Å to 2.2302 (14) Å, slightly longer compared to the precursor [*cyclo*-P_3]$^{3-}$ in **65** (2.194–2.205 Å).

The ^{31}P NMR spectrum of **70** reveals four different sets of signals at δ = 105.7, 73.6, 38.1 and 4.3 ppm, all downfield shifted compared to the precursor **65** that features a singlet at δ = -204.8 ppm. Additionally, the signals at δ = 38.1 and 73.6 ppm show satellites for P-W coupling with $^1J_{P\text{-}W}$ = 237 Hz and 138 Hz respectively, due to the different hybridization of the two P atoms (sp^3 and sp^2). Compound **65** not only allows access to higher congeners but also to P_2-containing complexes. Velian and Cummins showed that [IMo(N[*t*Bu]Ar)$_3$] could abstract a P^- atom from the [*cyclo*-P_3]$^-$ unit in **65** by salt metathesis [120,121]. The reaction affords [PMo(N[*t*Bu]Ar$_3$)] (**71**) in 79% yield, along with the binuclear complex **72** in 71% yield, see Scheme 25. The authors suggested that **72** could arise from the dimerization of the fragment [Nb(P_2)(ODipp)$_3$] (**73**) as the result of a 2(3–1) process which involves the starting [*cyclo*-P_3]$^-$ moiety in **65**.

XRD analysis of **72** (Fig. 22) revealed that it bears a square *cyclo*-P_4 ligand with bond lengths/angles virtually identical to the known zirconium dimer [{(L)Zr}$_2$(μ_2,η^4:η^4-P_4)] (L = PhP(CH_2SiMe_2-$NSiMe_2CH_2$)$_2$-PPh) [78]. Nonetheless the [*cyclo*-P_4]$^{4-}$ ligand in **72** occupies a disordered arrangement between the two Nb centers. The main crystalline component (75% occupancies) features an almost perfectly square planar P_4 fragment (torsion angle 0.15

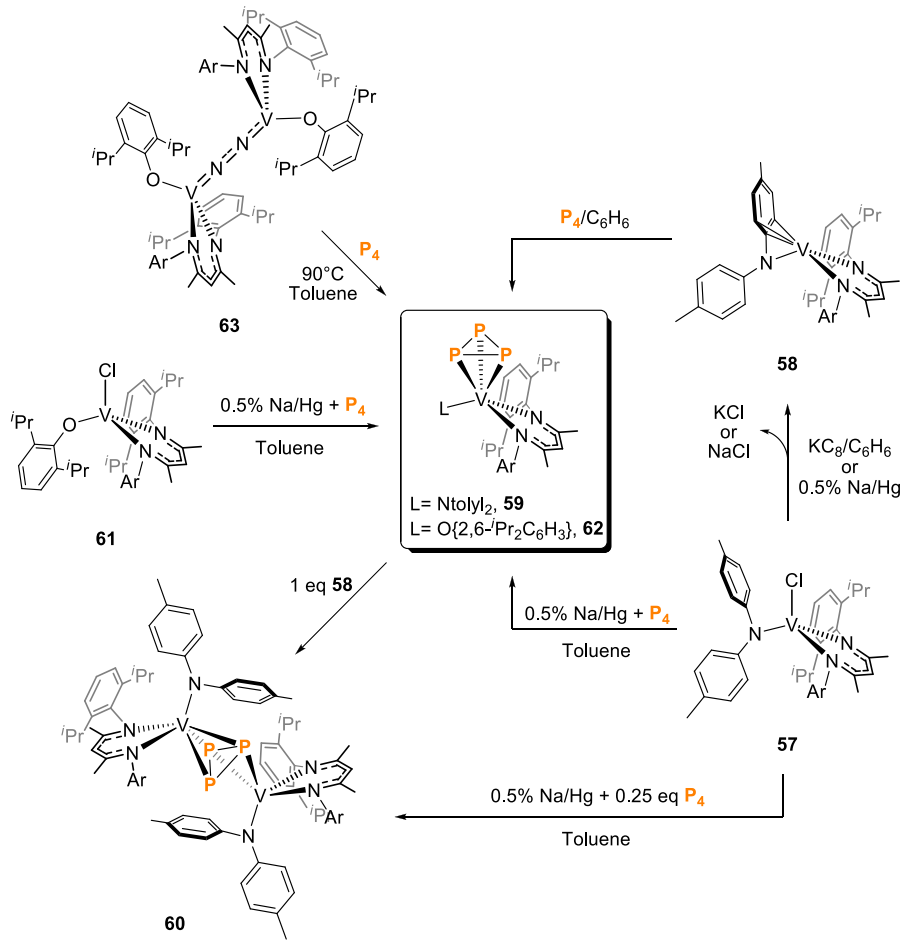

Scheme 22. Synthesis of the *cyclo*-P_3 containing complexes **59** and **62**.

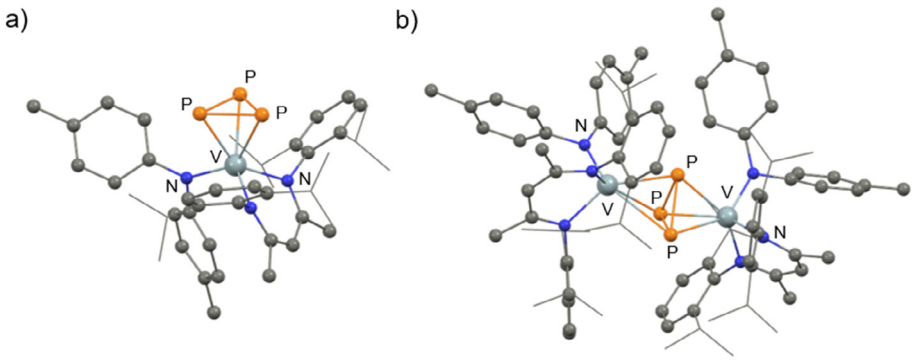

Fig. 19. Molecular structures of cycloP_3 complexes **59** and **60**. Hydrogen atoms are omitted for clarity; adapted from Ref. [112].

(9)°) which is coordinated to the metal atoms in an $\mu_2,\eta^3{:}\eta^3$ mode. Notably, the internal *cyclo*-P_4 is tilted with respect to the Nb-Nb axis as observed for [U{(η^5-C_5Me_4H)(μ^8-$C_8H_6SiiPr_3$)$_2$–1,4}(μ,η^2:η^2-P_4)] (see Section 2.1.3.5). The P-P bond lengths (ranging from 2.230 to 2.250 Å) are considerably longer compared to dianionic [*cyclo*-P_4]$^{2-}$ ligands found in the ionic salt $CsP_4{\cdot}2NH_3$, (2.146 Å, [77]), or binuclear ETM complexes. This characteristic, in conjunction with the diamagnetic nature of **72**, indicates that the P_4 deck can be formulated as a [*cyclo*-P_4]$^{4-}$ ligand. However, the structure representative at 20% occupancies shows a more rectangular shaped P_4 moiety coordinated in an $\mu_2,\eta^2{:}\eta^2$ fashion whose structure recalls the phosphide ligand in the U(III) complex **32** mentioned above (see Section 2.1.3.5).

DFT calculations indicates that the two coordination modes are separated by a small energy barrier (1.5 kcal mol^{-1}) suggesting fluxionality of the ligand. This correlates well with the $^{31}P\{^1H\}$ NMR spectrum of **72**, in which no different P atoms are detected (singlet at δ = +124 ppm). In order to intercept the reactive species **73** prior to dimerization, the reaction was repeated in the presence of a large excess of 1,3-CHD affording the corresponding D-A adduct **74**. The relative instability of **74**, due to the presence of both *retro*-Diels-Alder equilibrium and concomitant dimerization of Nb-P_2, has prevented its isolation. It is worth mentioning that the double D-A adduct **75** could be observed (45% spectroscopic yield) when using pyridine-N oxide to cleave niobium from **74**. Pursuing a complementary (2 + 1) strategy, Cummins and co-workers also

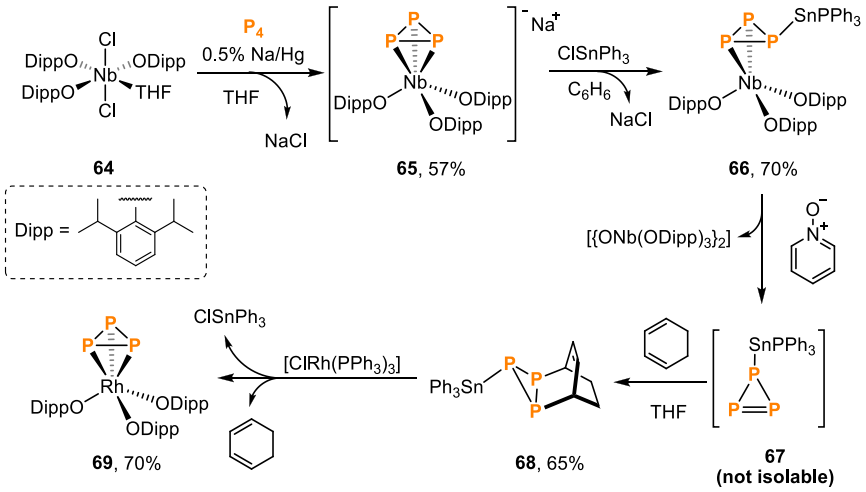

Scheme 23. Reductive activation of P_4 with Nb complex **64** and transformation in **69**.

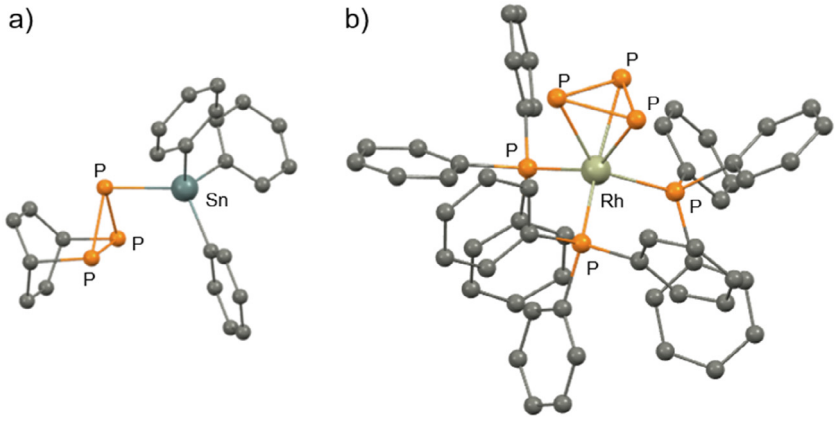

Fig. 20. Molecular structure of a) **68** and b) **69**. Hydrogen atoms are omitted for clarity; adapted from Ref. [116].

demonstrated that Nb-[*cyclo*-P_3]$^-$ complexes can be obtained by addition of the terminal phosphide complex $[Na(OEt_2)]_2\{PNb[N(Np)Ar]_3\}_2$ (**76**) to a suitable source of P_2, of which white phosphorus represents the most convenient and readily available choice [122]. When performed in a non-coordinating solvent (Et_2O), the reaction of **76** with one equivalent of P_4 led to the formation of the complex $[Na(OEt_2)][(\eta^3\text{-}P_3)Nb[N(Np)Ar]_3$ (**77**) in 56% yield (^{31}P NMR singlet at δ = –223 ppm). This process was further optimized by adding 4 equivalents of 12-crown-4 to the crude mixture, from which the monomeric cation-sequestered complex $[Na(12\text{-crown-}4)_2][(\eta^3\text{-}P_3)Nb[N(Np)Ar]_3]$ (**78**) could be obtained in an improved 83% yield (^{31}P NMR singlet at δ = -183 ppm in d_5-pyridine) (Scheme 26).

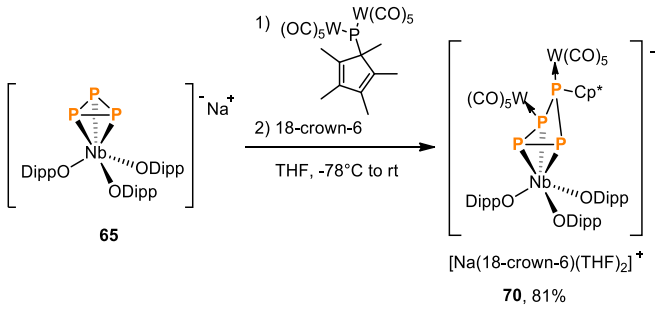

Scheme 24. Reaction of $[Cp^*P\{W(CO)_5\}_2]$ with **65** leading to **70**.

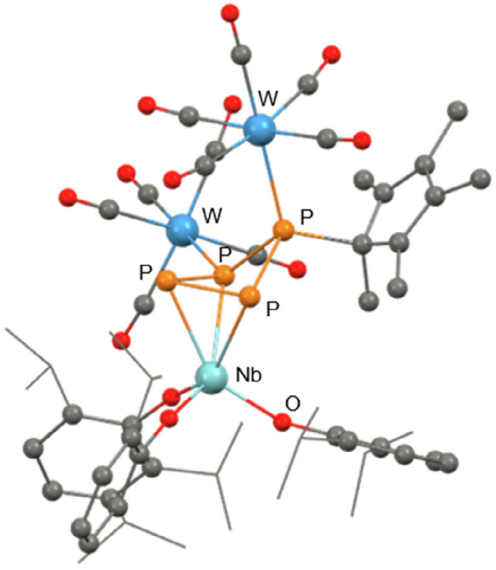

Fig. 21. Molecular structure of the monoanion in complex **70**. Hydrogen atoms are omitted for clarity; adapted from Ref. [119].

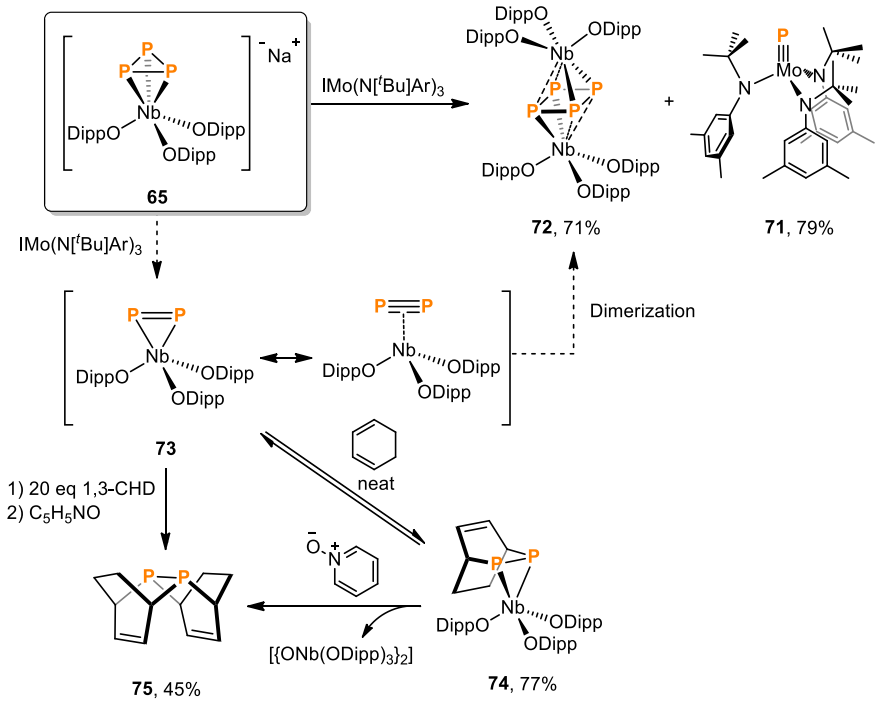

Scheme 25. Synthesis of the tetraphosphorus complex **72** and of the phosphide complex **71** via a 2(3–1) process and Diels-Alder cycloaddition product **75.**

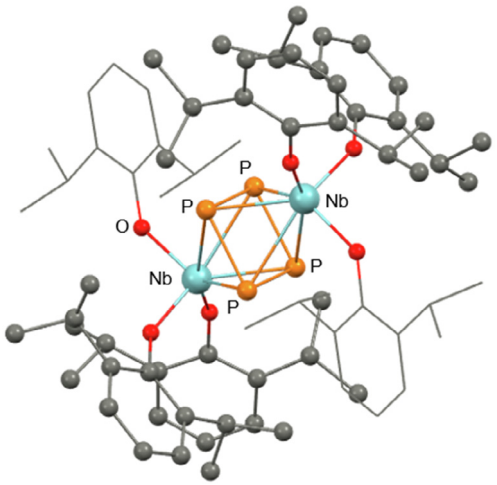

Fig. 22. Molecular structure of **72**. Hydrogen atoms are omitted for clarity; adapted from Ref. [120].

The solid-state dimeric structure of **77** reported in Fig. 23 is retained in solution as suggested by the ^{31}P NMR analysis of the complex. At room temperature **77** still possesses a pseudo three-fold symmetry due to fast scrambling of the Na-P interactions (singlet at δ = –223 ppm) which freezes out at cryogenic temperature (2:1 doublet-triplet pair at δ = -178 ppm and δ = -203 ppm respectively, showed at −80 °C).

A different product was formed when performing the reaction in THF, which furnished the formal (4 + 1) addition complex [Na(THF)$_6$]{(N[Np]Ar)(η^4-P$_5$)Nb(N[Np]Ar)$_2$} (**79**) in 71% yield with minimal observed formation of the *cyclo*-P$_3$ adduct **77** (Scheme 27).

The cyclopentaphosphane ligand [RP$_5$]$^{4-}$ in **79** possesses an envelope-like conformation with a P atom carrying the migrated anilide ligand, and the other four P atoms coordinated to the metal in an η^4 fashion (Fig. 24).

In addition to the *cyclo*-P$_5$ fragment, the remaining two anilide ligands interact with niobium in an η^3 fashion (Nb-C 2.5 Å) saturating the coordination sphere of the metal. Such interactions, although weaker than a canonical Nb-C single bond (usually below 2.3 Å), impede free rotation of the anilide fragments giving the complex an overall C_1 symmetry which translates into five different P atom environments and three different anilide ligands as observed by ^{31}P NMR and ^{1}H NMR spectroscopy, respectively. The main factor determining the observed product selectivity is the aggregation state of the phosphide source in solution. When using coordinating solvents such as THF, the starting dimeric phosphide complex **76** splits into two low-coordinate monomeric units, which add to the P$_4$ molecule to form **79**. Conversely, in non-polar solvents, **76** is believed to retain its aggregation state and reacts with P$_4$ via a twofold (2 + 1) addition to give the dimeric complex **77**. The ability of the terminal phosphide **76** to act as a single P$^-$ atom donor, has also been exploited by Krummenacher and Cummins towards the generation of the phosphaethynolate salt [NaOCP] [123]. To accomplish this, **76** was first reacted with tris(pentafluorophenyl)borane, affording the capped complex [Na(OEt)$_2$][B(C$_6$F$_5$)$_3$PNb(N[Np]Ar)$_3$] (**80**) in 87% yield, see Scheme 28 and Fig. 25.

Upon treatment with a stoichiometric amount of CO$_2$, the red solution containing **80** turned bright yellow. ^{31}P NMR analysis evidenced the consumption of **80** (δ = 514 ppm) in favor of a new product with a diagnostic resonance at δ = -393 ppm that could be attributed to the known [Na(dme)]$_2$[OCP]$_2$ (**81**). Along with **81**, the authors identified the boron-capped oxo-niobium complex [B(C$_6$F$_5$)$_3$][ONb(N[Np]Ar)$_3$] (**82**) deriving from the formal multiple bond metathesis between the two reagents (Scheme 28). As previously observed, the formation of a strong Nb≡O bond is proposed to be the thermodynamic driving force for the CO$_2$ activation. This is proposed to occur via the nucleophilic attack of the phosphide on the carbonyl, which forms the PCO$_2^-$ adduct or the cyclic Nb-P-C(O)-O intermediate [124]. The latter, previously isolated in a process involving the phosphide **76** and acylchlorides [125], undergoes [2 + 2] fragmentation to give the final products **81** and **82**.

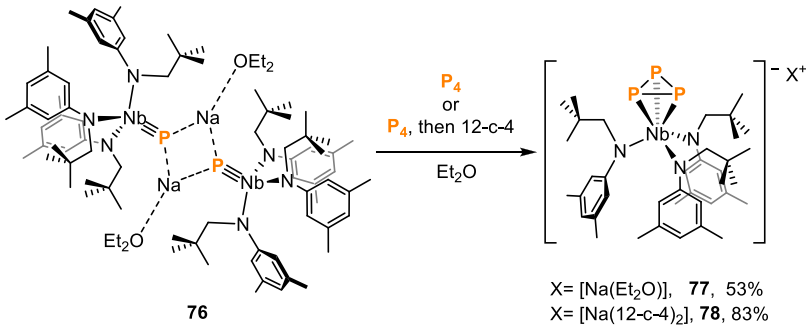

Scheme 26. Reaction of P_4 with the dimer **76** in Et_2O affords the *cyclo*-P_3 compound **77**. Yields are improved by addition of 12-crown-4 prior isolation (compound **78**).

The groups of Arnold and Maron reacted P_4 with the carbonylated precursors [(BDI)(N*t*Bu)M(CO)$_2$] [M = Nb (**83**), M = Ta (**84**), BDI = 2,6-diisopropylphenyl-*β*-diketiminate], yielding niobium and tantalum inverted sandwich complexes [(BDI)(N*t*Bu)M]$_2$(μ_2,η^3:η^3-P_4) [M = Nb (**85**), M = Ta (**86**)]. Such compounds were also obtained by hydrogenolysis of the bis-dimethyl precursor [(BDI)(N*t*Bu)Nb(Me)$_2$] in presence of P_4 [126] (Scheme 29).

The reaction proceeded much faster in the case of Nb, this is explained by the higher energy barrier for CO dissociation in the case of Ta. Interestingly, both species **85** and **86** are air-stable and were characterized in solution by ^{1}H and ^{13}C NMR spectroscopy, resulting highly symmetric diamagnetic species. The ^{31}P NMR spectra in solution did not show any signals for both complexes, thus ^{31}P MAS NMR spectroscopy was required. The niobium complex **85** displayed two sets of signals (δ_{iso} = +251(2) ppm and δ_{iso} = +84(2) ppm) in agreement with the μ_2,η^3:η^3 coordination mode adopted by the *cyclo*-P_4 ligand which was also observed in the solid-state structure (Fig. 26**a**). The ^{31}P MAS NMR spectrum of **86** was difficult to interpret because of line-broadening and only a signal at δ_{iso} = +208(8) ppm was observed. The molecular structure of **86** was elucidated by XRD, see Fig. 26**b**. The *cyclo*-P_4 core in both complexes is close to a perfect planar square, the average P-P bond lengths in **85** and **86** are 2.233 Å and 2.248 Å respectively, very similar to those reported for [{(L)Zr}$_2$(μ,η^4:η^4-P_4)] (L = PhP(CH$_2$SiMe$_2$NSiMe$_2$CH$_2$)$_2$-PPh) (2.240 Å) and [(ODipp)$_3$Nb]$_2$(μ_2,η^3:η^3-P_4) (2.232 Å, *vide supra*), formally described as containing a tetraanionic [*cyclo*-P_4]$^{4-}$ core. Complexes **85** and **86** differ from these examples as the [*cyclo*-P_4]$^{4-}$ is sandwiched between the two metals in an asymmetrical manner, as evidenced by the large difference between the M–P distances: one short (Nb-P = 2.511 Å, Ta-P = 2.500 Å), and two average bond lengths (Nb-P = 2.700 Å and 2.702 Å, Ta-P = 2.691 Å and 2.674 Å). Another route to synthesize **85** involved the hydrogenation of the dimethyl precursor [(BDI)Nb(N*t*Bu)Me$_2$] **83** in the presence of P_4. As before this protocol furnished the desired triple decker **85** as the major species but proved to be less selective. Among the by-products observed, the trinuclear niobium complex {[(BDI)NbN*t*Bu]$_3$(μ-P_{12})} (**87**), Scheme 30, was isolated bearing a rare P_{12} cluster with an unprecedented architecture of a *cyclo*-P_5 ring and a P_7 cage featuring a nortricyclane structure as shown by XRD analysis (Fig. 26**c**).

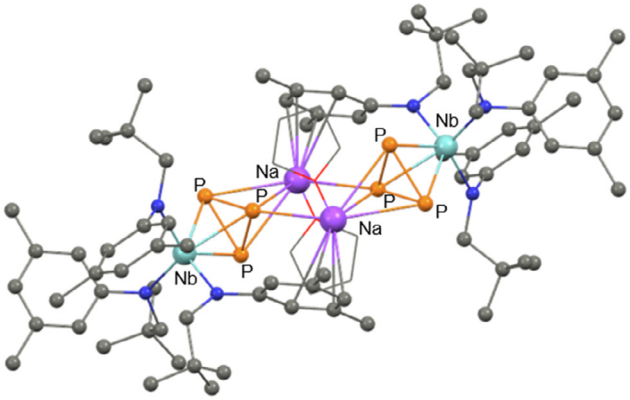

Fig. 23. Molecular structure of **77**. Hydrogen atoms are omitted for clarity; adapted from Ref. [122].

The P-P bond distances vary between 2.146 and 2.290 Å, comparable with other phosphide cages and in agreement with P-P single bonds. To date, there are only two examples of P_{12} clusters, though possessing different topology, NHC-capped P_{12} [127] and {[(Cp′)Co]$_3$(μ-P_{12})} [128]. To assess the basicity of the [*cyclo*-P_4]$^{4-}$ core in **85**, it was reacted with [HOEt$_2$][B(C$_6$F$_5$)$_4$], resulting in the

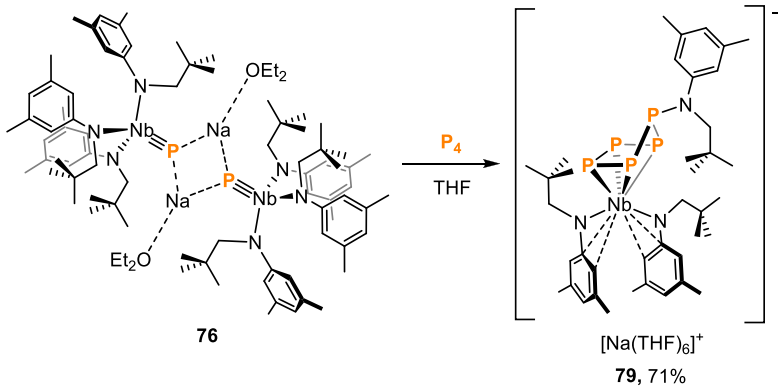

Scheme 27. Synthesis of complex **79**.

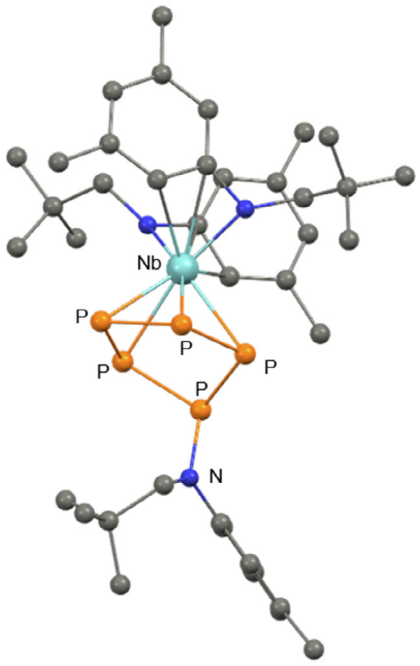

Fig. 24. Solid state structure of the monoanion in the salt complex **79**. $[Na(THF)_6]^+$ moiety and hydrogen atoms are omitted for clarity; adapted from Ref. [122].

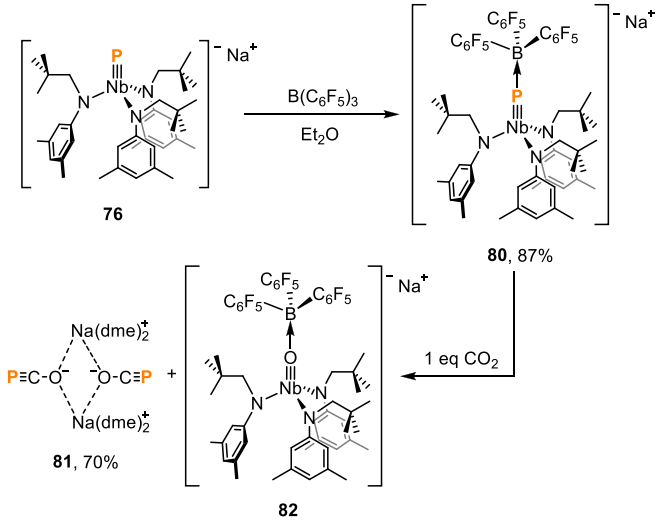

Scheme 28. Capping of **76** with $B(C_6F_5)_3$ and subsequent reaction with CO_2.

protonation of the less sterically hindered β-diketiminate backbone instead of the phosphide moiety, see Scheme 31, yielding $\{[(BDI'')(NtBu)Nb]_2(\mu 2,\eta^3{:}\eta^3\text{-}P_4)\}(BAr^F)_2$ (**88**) in 82% yield.

Oxidation with one or two equivalents of $Ag[B(Ar^F)_4]$ afforded the complexes $\{[(BDI)(NtBu)Nb]_2(\mu_2,\eta^3{:}\eta^3\text{-}P_4)\}\{B(Ar^F)_4\}$ (**89**), and $\{[(BDI)(NtBu)Nb]_2(\mu_2,\eta^3{:}\eta^3\text{-}P_4)\}\{B(Ar^F)_4\}_2$ (**90**), respectively, the latter displaying a sharp singlet at δ = +516 ppm in the ^{31}P NMR spectrum. It would seem the oxidation state of the internal *cyclo*-P_4 greatly affected the structure of the complex, particularly the interatomic P-P bond distances. The mono-oxidized form, **89**, displayed shorter P-P bonds (average, 2.209(4) Å) with respect to **85**. The P-P bond lengths are shortened further in the two-fold oxidized complex **90** (averagely 2.182(5) Å), which is consistent with known *cyclo*-P_4^{2-} complexes (Scheme 32).

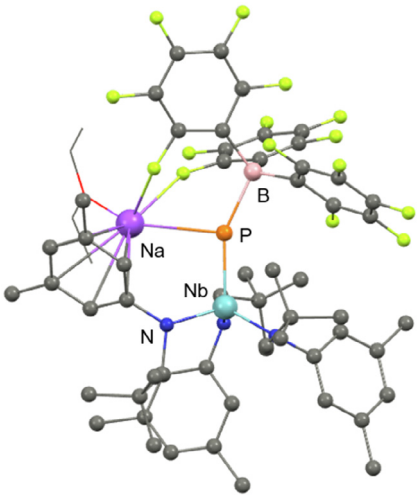

Fig. 25. Solid state structure of the anion of **80**. Hydrogen atoms are omitted for clarity; adapted from Ref. [123].

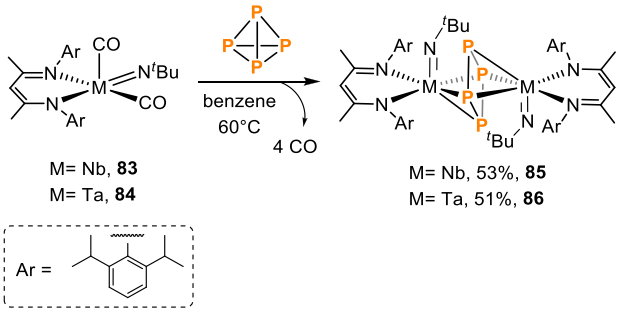

Scheme 29. Activation of P_4 with Nb and Ta complexes **83** and **84**.

2.3.3. Tantalum

The formation of inorganic fullerene-like structures, arising from the supramolecular assembly of CuX units (X = Cl, Br, I) together with $[Cp^*Fe(\eta^5\text{-}P_5)]$ (Cp^* = C_5Me_5) was established by Scheer and co-workers [129]. This approach was extended to Ta-complexes $[Cp''Ta(CO)_2(\eta^4\text{-}P_4)]$ (Cp″ = 1,3-$C_5H_3tBu_2$) containing the *cyclo*-P_4 ligand [130]. Recent studies carried out on the $[Cp^R\text{-}Ta(CO)_2(\eta^4\text{-}P_4)]$/CuX system [$Cp^R$ = 1,4-$C_5H_3tBu_2$ (**91**), or Cp^R = Cp‴ = 1,2,4-$C_5H_2tBu_3$ (**92**), X = Cl, Br) have shown that distinct non-classical fullerene structures are accessible depending on both the halide used and on the specific Cp^R ligand [55]. These supramolecular assemblies are formed upon layering a CuX solution in CH_2Cl_2/CH_3CN on a CH_2Cl_2 solution of $[Cp^RTa(CO)_2(\eta^4\text{-}P_4)]$ (see Scheme 33).

Structures ranging from **93a** to **93d** were obtained from the precursor **91** or **92** upon the addition of CuX = CuCl, CuBr. In this assembly, six *cyclo*-P_4 units are bound to eight CuX units in a 1,2,3,4-coordination mode. Each Cu atom is tetrahedrally coordinated by three P atoms and one terminal halide. The inorganic core consists of 32 atoms and features a Cu_8 cube with *cyclo*-P_4 rings above its faces. When switching to iodide, two distinct products were isolated upon layering a CH_3CN solution of CuI onto a solution of **91** in toluene, $[\{Cp''Ta(CO)_2(\eta^4\text{-}P_4)\}_{10}\{Cu_{14}I_{10}(\mu,I)_2(\mu_3,I)_2\}]$ (**94**) and $[\{Cp''Ta(CO)_2(\eta^4\text{-}P_4)\}_5\{Cu_{12}I_3(\mu,I)_8(\mu_4\text{-}I)(CH_3CN)_5\}]$ (**95**) (see Scheme 33). The molecular structure of **94**, shown in Fig. 27**a**, consists of an unprecedented nano-capsule 'peanut'-shaped motif, made up of ten *cyclo*-P_4 units bound to eight CuI units and two Cu_3I_3 units. Compound **95** also possesses a hollow structure, consisting of five *cyclo*-P_4 units bound to three neutral

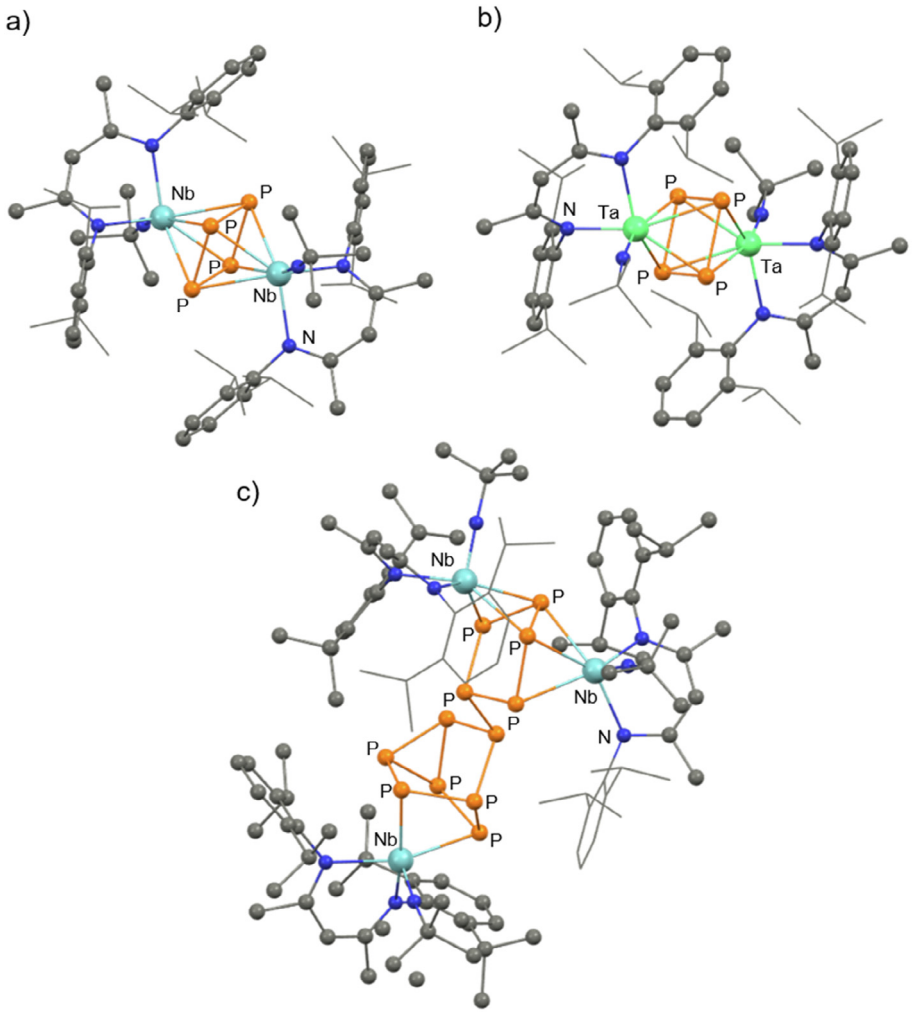

Fig. 26. Solid-state structures of a) **85** b) **86** and c) **87**. Hydrogen atoms are omitted for clarity; adapted from Ref. [126].

$\{Cu_2I_2CH_3CN\}$ units, one cationic $\{Cu_2I(CH_3CN)_2\}^+$ and one anionic $\{Cu_4I_5\}^-$ unit (Fig. 27**b**).

When an additional *tert*-butyl group is added in the Cp ring (i.e. using **92** in place of **91**), the reaction with CuI yielded a new 2D coordination polymer $[Cp'''Ta(CO)_2(\eta^4\text{-}P_4)\{Cu_4(\mu_3,I)_4\}]_n$ (**96**), in which Ta-phosphide moieties are linked to $\{Cu_4(\mu_3,I)_4\}$ heterocubane units in a 1,2,3,4-coordination mode.

2.4. Group 6 metals

2.4.1. Chromium

In 2005 the Power group reported the first stable compound featuring a quintuple Cr-Cr bond, L_2Cr_2 where L = C_6H_3-2,6(C_6H_3-2,6-*i*Pr_2)$_2$ [131]. Following this study, other examples of Cr_2 units with the same bond order have appeared in literature, such as **97** (see Scheme 34) reported by Kempe [132], where the bimetallic core, stabilized by a chelating N-ligand, displays Cr-Cr distances of 1.750 Å. In a collaboration between Scheer's and Kempe's groups [133] it was shown that Cr_2 units can be suitable platforms for the activation of P_4 as well as other pnictogens and pnictides (i.e. As_4 and AsP_3). Reacting **97** with P_4 in THF at room temperature yielded the *cyclo*-P_4^{2-} derivative (**98**) in excellent yield (97%, see Scheme 34).

The X-ray structure of **98** (Fig. 28**a**) revealed a nearly square-planar phosphorus arrangement with P-P distances ranging from 2.168 to 2.183 Å, consistent with P-P bonds of a *cyclo*-P_4^{2-} ligand.

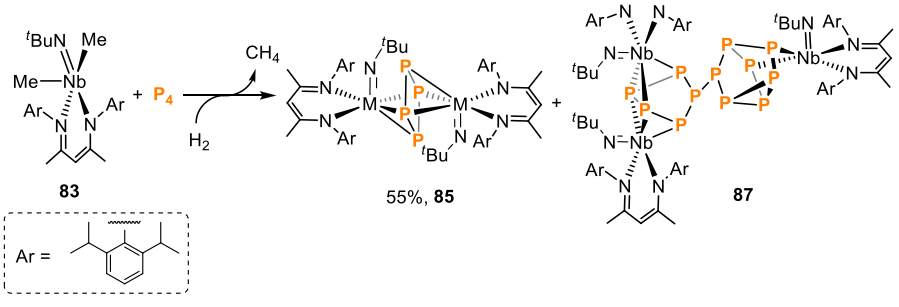

Scheme 30. Activation of P_4 with Nb and Ta complexes **83** and **84**.

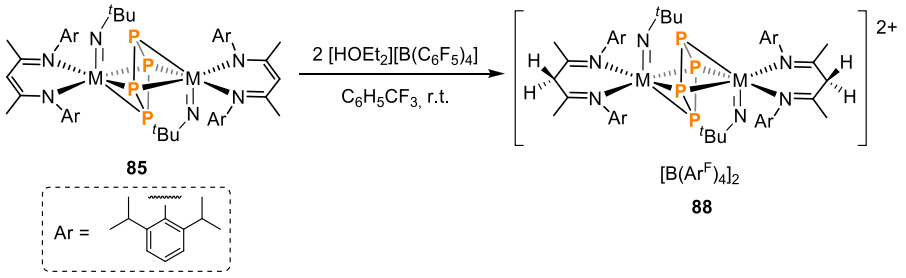

Scheme 31. Protonation of **85** occurs on the ligand backbone leaving the [*cyclo*-P_4]$^{4-}$ core unaltered.

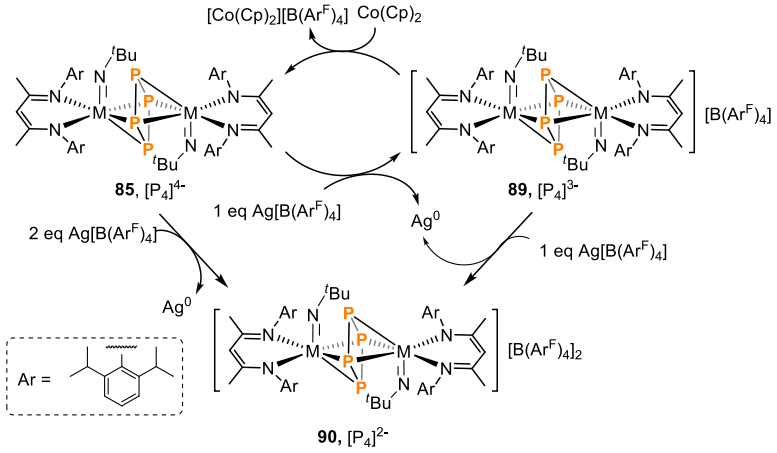

Scheme 32. Oxidation of complex **85** with Ag[$B(C_6F_5)_4$].

Opposite P1 and P3 atoms are bonded in a η^1 fashion to different Cr atoms, while P2 and P4 bridge the two Cr centers. It is worth noting that the Cr-Cr distance in **98** (1.866 Å) is indicative of quadruple bond. The elongation of the Cr-Cr distance signifies an oxidation of the Cr_2 core occurs upon reaction of **97** with P_4, which in turn is reduced to give the planar, aromatic *cyclo*-P_4^{2-} fragment in **98**. The reaction was repeated using As_4 and AsP_3, yielding the unprecedented *cyclo*-As_4^{2-} (68%) and *cyclo*-AsP_3^{2-} ligands (69%).

Aiming to investigate the reactivity of P_4^{2-} lone pairs, complex **98** was reacted with an excess of [$W(CO)_5$(THF)], which gave **99** exclusively (19%, see Scheme 34). X-ray diffraction analysis of **99** revealed the coordination of the $W(CO)_5$ fragment to a terminal phosphorus atom, see Fig. 28**b**. However, the ^{31}P NMR spectrum showed a broad pseudo triplet at δ = 250 ppm (uncoordinated P atoms) and a very broad signal between δ = 210 and δ = 230 ppm for P-W atoms, suggesting **99** possesses dynamic behavior in solution due to a switching of the {$W(CO)_5$} moiety between bridging and terminal positions on the *cyclo*-P_4^{2-} ring. This discrepancy between solid state and solution behavior was rationalized *via* DFT calculations, which indeed evidenced a relatively small energy difference existing between the two coordination modes of the {$W(CO)_5$} fragment.

2.4.2. Molybdenum

Over the past decade only a few examples of the activation of P_4 involving the use of molybdenum complexes have been reported. In 2013, Braunschweig and co-workers, reported on the reaction of Mo metallophane **100** with P_4 in toluene at 80 °C, resulting in the formation of **101** as an air and moisture-sensitive red solid in 30% yield (Scheme 35) [134].

This represents a unique mode of activation for P_4 mediated by an ansa-metallocene complex. The $^{31}P\{^1H\}$ NMR spectrum of **101** showed only one resonance at δ = -370.9 ppm, highly deshielded in comparison to other three-membered rings containing P-P bonds [135]. The solid-state structure (see Fig. 29) confirms the formation of a three-membered ring consisting of a P_2 fragment and the central molybdenum center, with concomitant cleavage of two Mo-Si bonds and formation of two Si-P bonds. This enables an appreciable release of strain as the angle between the Si-C_{ipso} axes and the C_5H_4 ligand decreases from 48.7° and 48.9° in **100** to 19.4° and 19.1° in **101**, respectively. Likewise the tilt angle between the two C_5H_4 ligands increases, from 20.48(7)° to 43.08° for **100** and **101**, respectively. The P-P bond length (2.172 Å) in **101** is shorter compared to a P-P single bond (2.21 Å) [60] but longer than a P=P double bond found in organic diphosphenes such as (tBu)$_3C_6H_2$-P=P-C_6H_2(tBu)$_3$ (2.031 Å) [136]. Wiberg bond indices and computational analysis (NBO) revealed that all the bonds involved in the three-membered cyclic core of **101** are single despite the existence of some degree of delocalization over the ring and π-π interaction between the two P atoms.

The pursuit of air-stable platforms for the safe storage, transport and controlled release of white phosphorus is a relevent challenge in contemporary research. One valuable route is the encapsulation of P_4 in supramolecular cages [137] or porous materials. In this regard, Scheer *et al.* successfully intercalated P_4 molecules in the porous structure of activated carbon [138] and the resulting P_4/C could be used as a source of P_4 either in solution or in the gas phase. In 2019, Figueroa and co-workers found that low-valent Mo complexes stabilized with bulkier isonitrile ligands could be used as a storage/release system for white phosphorus [139]. The zero-valent Mo complexes of formula [Mo(η^2-*C,H*:κ^1-*N*-(HN(*i*-Pr)$_2$)(CO)$_2$(CNAr^{Dipp2})$_2$] (**102**, Ar^{Dipp2} = 2,6-(2,6-(*i*-Pr$_2$)C_6H_3) were reacted with P_4 selectively affording the mononuclear derivative [(η^4-P_4)Mo(CO)$_2$(CNAr^{Dipp2})$_2$] (**103**) in near quantitative yield, as shown in Scheme 36. It is worth noting that **103** is kinetically stable for days upon air exposure and warming up to 90 °C.

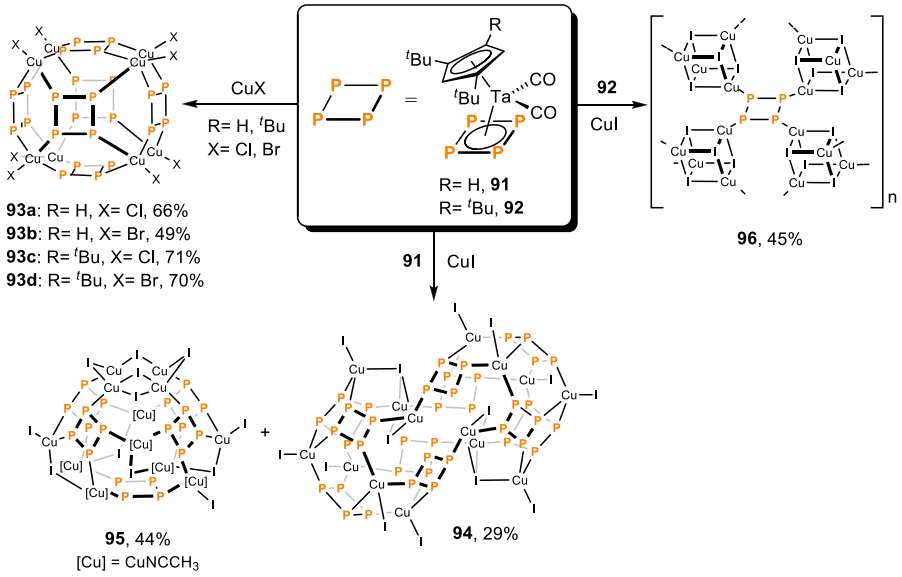

Scheme 33. Reactivity of **91** and **92** with Cu(I) halides. Each *cyclo*-P_4 unit is additionally bonded to an hexo $Cp^RTa(CO)_2$ fragment, omitted for clarity.

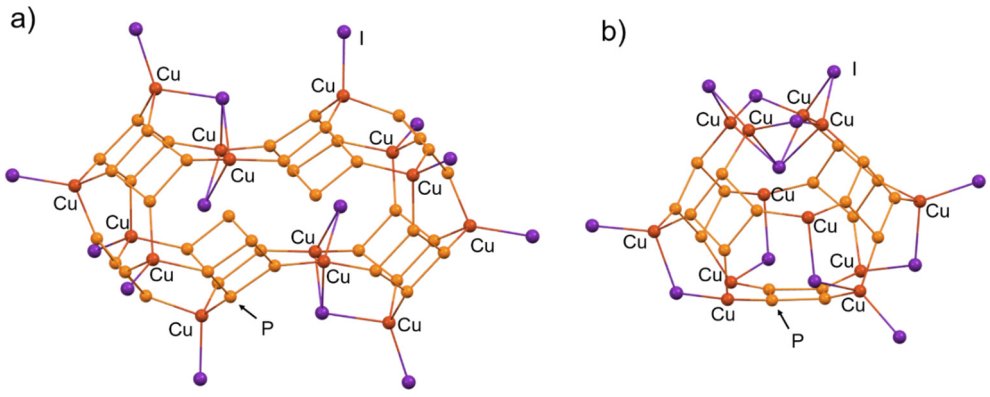

Fig. 27. Core motifs of structures a) **94** and b) **95** (b). Each *cyclo*-P_4 unit in the frame is additionally bonded to a [$Cp^RTa(CO)_2$] fragment protruding outside of the shell (omitted for clarity); adapted from Ref. [55].

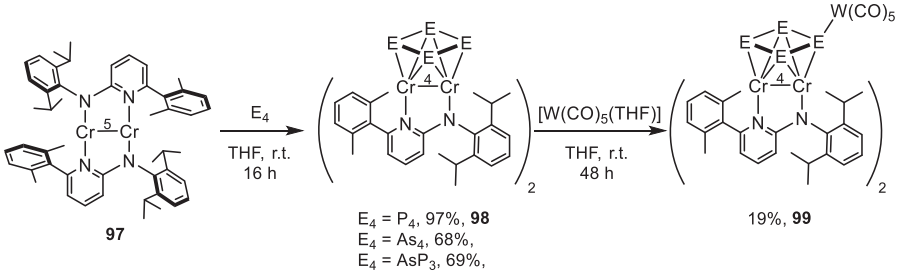

Scheme 34. Synthesis of complexes **98** and **99**. The number above the Cr-Cr bond refers to the bond order.

The solid-state structure of **103** (see Fig. 30), shows a rectangular planar *cyclo*-P_4 ligand with P-P bond lengths between 2.148(2) and 2.180(2) Å. The observation of a single NMR resonance at δ_{31P} = 113 ppm confirmed the highly symmetrical structure remains in solution. DFT calculations best formulated the *cyclo*-P_4 moiety as a six π-electron dianion ligand, indicating that a formal two-electron reduction of P_4 occurs upon reaction with **102**.

The presence of high-lying σ P-P HOMOs and low-lying P-Mo anti-bonding LUMOs suggested that release of P_4 could be achieved through light irradiation of **103** as a result of a ligand to metal charge transfer process (LMCT). However, the energy needed for this process (irradiation at λ = 284 nm), also triggers the photo degradation/polymerization of P_4 [140,141]. With the aim to reduce the energy gap involved in the LMCT transition and releasing P_4 without subsequent polymerization, the divalent complex [$MoI_2(CO)_2(CNAr^{Dipp2})_2$] (**104**, precursor of **102**) was reacted with P_4 (Scheme 37). The reaction afforded the desired P_4-adduct [(η^4-*cyclo*-P_4)$MoI_2(CO)(CNAr^{Dipp2})_2$] (**105**) in excellent yield (90%), with loss of one CO and retention of both iodide ligands, with one occupying the *trans* position respect to the centroid *cyclo*-

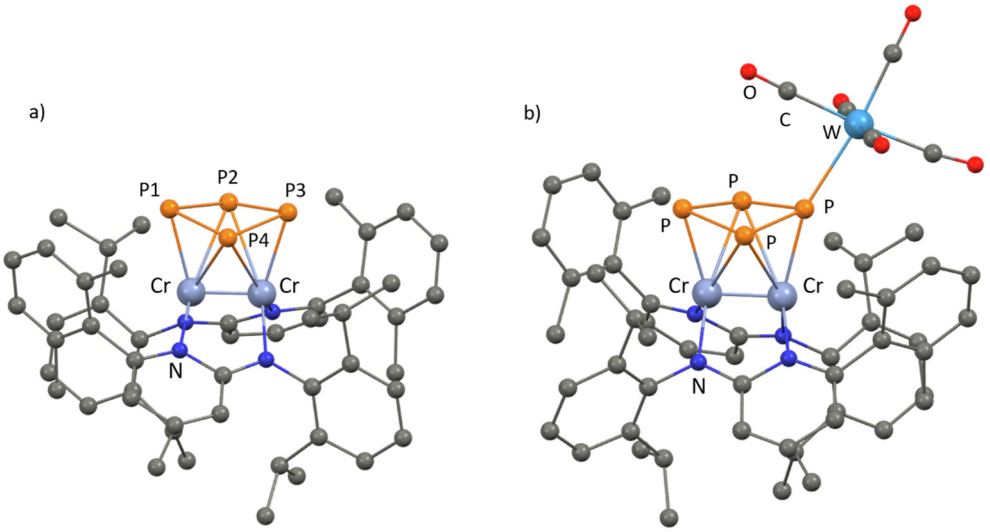

Fig. 28. Molecular structures of a) **98** and b) **99**. Hydrogen atoms are omitted for clarity; adapted from Ref. [133].

P_4, see Fig. 31. The ^{31}P NMR spectrum is desymmetrized giving an AA′BB′ spin pattern centered at δ = 75 ppm. DFT calculations on a model substrate of **105** showed that it has a smaller HOMO-LUMO gap and therefore a LMCT transition accessible at longer wavelengths. As such, irradiation of **105** in benzene together with 2% DME by a low power violet led source (18 W, λ = 385–395 nm) gave dissociation of P_4 and its replacement by a DME molecule in the coordination sphere of Mo. ^{31}P NMR spectroscopy showed the reaction was completed after only 20 min as 95% of free P_4 returned to solution. It should be added that the newly formed complex $[MoI_2(CO)(k_1\text{-O-DME})(CNAr^{Dipp2})_2]$ (**106**), coordinates the dissolved white phosphorus only when the mixture is heated at 80 °C, giving **105**, demonstrating the complete reversibility of the process (Scheme 37).

The mononuclear complexes **103** and **105** were further investigated with the aim to elucidate the aromaticity of the *cyclo*-P_4 moiety, its bonding situation towards the metal center, and how the valence of the latter influences the structural features of the complexes [142]. Thus, **105** was treated with KC_8 in THF, followed by addition of dibenzo[18-crown-6] (DB18C6), which yielded red crystal of $[K_2(\text{dibenzo-18-crown-6})][(\eta^4\text{-}P_4)Mo(CO)(CNAr^{Dipp2})_2]$ (**107**, Scheme 38).

XRD analysis (Fig. 32) revealed a three-legged piano stool geometry in which both iodide ligands are lost while one K^+ is partially sequestered and is involved in a secondary interaction with a P atom of the *cyclo*-P_4 ligand. Conversely, the second K^+ is coordinated to the C≡N and the aryl moieties of Ar^{Dipp2} and cannot be removed from the coordination sphere of the metal even using dibenzo[18-crown-6] in large excess. The ^{31}P NMR spectrum of **107** showed a singlet at δ = 112.4 ppm which is relatively close to the signals exhibited by the precursor **105** (δ = 90 ppm and δ = 60 ppm), suggesting that the dianionic nature of the [*cyclo*-

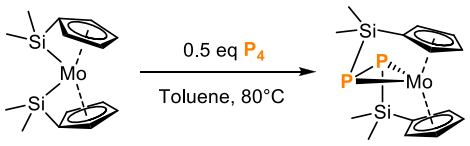

100 30%, **101**

Scheme 35. Synthesis of complex **101** by activation of P_4 mediated by the Mo complex **100**.

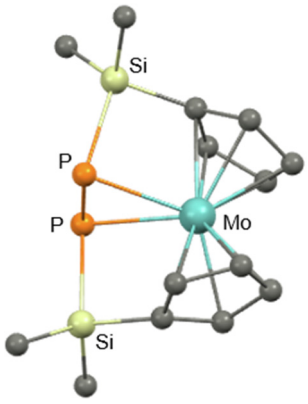

Fig. 29. Solid-state structure of **101**. Hydrogen atoms are omitted for clarity; adapted from Ref. [134].

$P_4]^{2-}$ ligand was not affected by the reduction. This is also the case for the average P-P bond length within the $[cyclo\text{-}P_4]^{2-}$, which does not appreciably change after the reaction (2.157(5) Å in **105** vs 2.160(12) Å in **107**).

Analogous results were obtained when treating **103** with KC_8. ^{31}P NMR spectroscopy evidenced the formation of two compounds, one corresponding to $K_2[(\eta^4\text{-}P_4)Mo(CO)(CNAr^{Dipp2})_2]$ (**108**), analogous to **107** without dibenzo[18-crown-6], with a resonance at δ_{31P} = 105 ppm, the other resulting from the loss of one $CNAr^{Dipp2}$ ligand, $K_2[(\eta^4\text{-}P_4)Mo(CO)_2(CNAr^{Dipp2})]$ (**109**), resonating at δ_{31P} = 121 ppm, Scheme 39. Notably, **108** could be fully converted to **109** when treated with CO.

The similar ^{31}P NMR chemical shifts found in **103**, **108** and **109**, suggested the *cyclo*-P_4 ligand remained intact upon reduction with KC_8. As with **107**, XRD analysis of **109** (see Fig. 33) showed a three-legged stool geometry with almost unchanged P-P bond lengths (2.160 Å vs 2.163 Å for **109** and **103** respectively). Conversely, a marked increase of the Mo-(η^4-P_4) distance in **108** and **109** (2.112 Å and 2.102 Å respectively) compared to **103** (2.075 Å), is representative of an increase of electron density at the metal center as confirmed also by computational analysis.

Complexes **108** and **109** possess a Mo-C bond distance for both the isocyanide and CO ligands that are 0.1 Å and 0.2 Å shorter than those for **103** and **105** respectively. This agrees with ν_{CO} and ν_{CN} IR

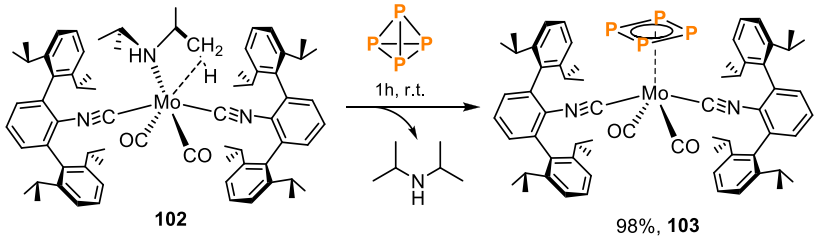

Scheme 36. Coordination of P_4 to the zero-valent Mo complex **103**.

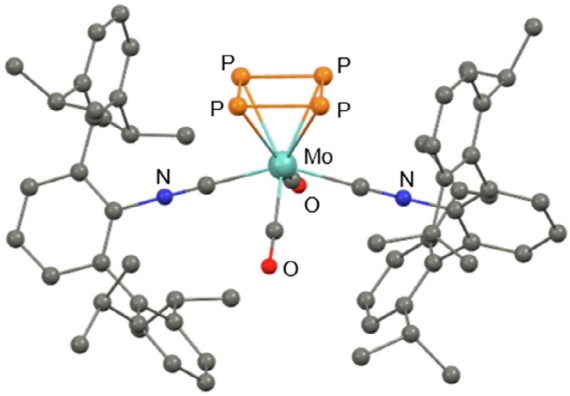

Fig. 30. X-ray structure of [(η^4-P_4) [$Mo(CO)_2(CNAr^{Dipp2})_2$] (**103**). Hydrogen atoms are omitted for clarity; adapted from Ref. [139].

bands that are lower in energy in **108** and **109** than those in **103** and **105** and support the increased π-backbonding interaction in the salts. Thus, the $(cyclo\text{-}P_4)^{2-}$ ligand can be viewed as a Hückel-type aromatic system, bound to a zero-valent Mo fragment in **108** and **109**.

Molybdenum-phosphide complexes, due to their unique coordinating properties, have also been extensively investigated in relation to the formation of 2D or 3D frameworks. In their seminal work [143], Scheer and co-workers have been committed in building up coordination polymers involving non-covalent bonding interactions between three components: 1) metal-phosphide complexes; 2) Lewis acidic metal salts coordinated to weakly coordinating anions (WCA) and 3) organic linkers. With this in mind, it was observed that the reaction of [$Cp_2Mo_2(CO)_4(\eta^2\text{-}P_2)$] (**110**) with $Ag[Al\{OC(CF_3)_3\}_4]$ forms the dimeric cluster **111** (Scheme 40), which has a dynamic coordination behavior in dichloromethane solution. It has been proposed that **111** is in equilibrium with its two monomeric forms, where a P_2 ligand can be coordinated to Ag^+ as η^1-end on (**112**) or η^2-side on (**113**). The two coordination modes are separated by a modest energetic barrier (9 kJ mol^{-1} from **113** to **112** as calculated by DFT methods) [144].

Such $\eta^2 \rightarrow \eta^1$ equilibrium opens up a free site on the Ag centers and the possibility of connecting $Ag[Cp_2Mo_2(CO)_4(\eta^2\text{-}P_2)]_2^+$ units with an appropriate linker, giving rise to new organometallic-organic hybrid materials. The reaction of **111** with the ditopic organic linker *trans*-1,2-di(pyridine-4-yl)ethene **114** in CH_2Cl_2 gives the two coordination isomers **115** and **116** shown in Scheme 41 [144].

Compound **115** is a one-dimensional chain-like polymer where the $\{Ag_2[Cp_2Mo_2(CO)_4(\eta^2\text{-}P_2)]_4\}^{2+}$ units are connected to each other through the organic linker, **114**. In particular, the six-membered Ag_2P_4 motif is retained and assumes an almost planar conformation (folding angles 2.23(7)° and 1.99(7)°) while in **111** the Ag_2P_4 units assume a chair conformation with folding angles of 20.69(2)°. The linkers are perpendicular to the plane of the Ag_2P_4 units and *trans* with respect to the Ag-Ag axis and the Ag (I) centers exhibit a distorted tetrahedral geometry (see Fig. 34 for X-ray structure of **115**). Conversely, **116** consists of a discrete molecular assembly where two Ag_2P_4 units are connected by two linker molecules which are in a *cis* arrangement (see Fig. 35 for X-ray structure of **116**) relative to the Ag-Ag axis. Compound **116**

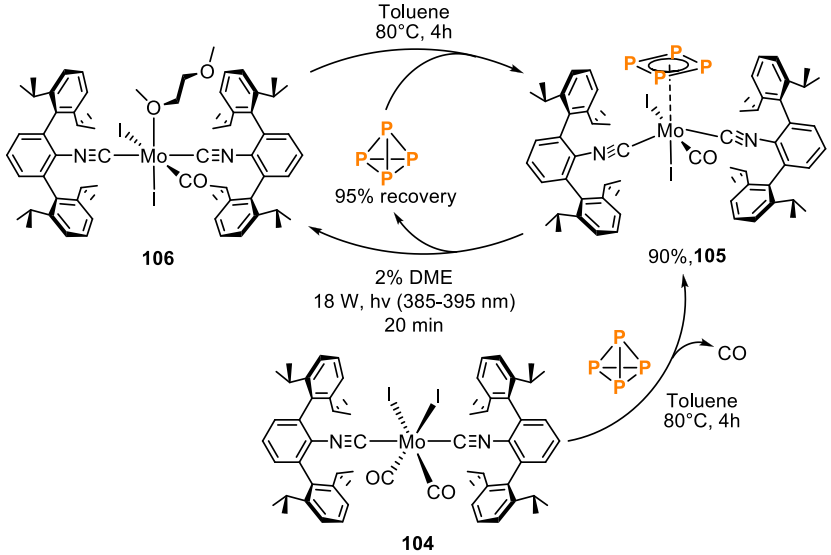

Scheme 37. Reversible process of coordination and release of P_4.

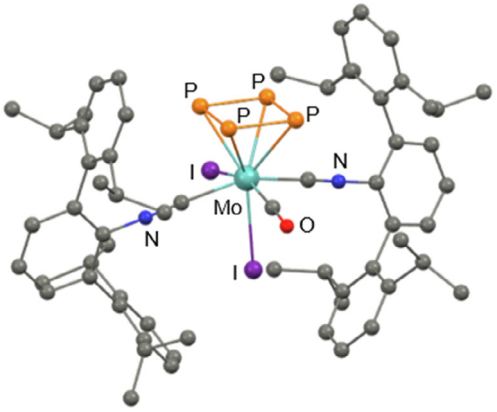

Fig. 31. X-ray structure of $[(\eta^4\text{-}cyclo\text{-}P_4)MoI_2(CO)(CNAr^{Dipp2})_2]$ (**105**). Hydrogen atoms are omitted for clarity; adapted from Ref. [139].

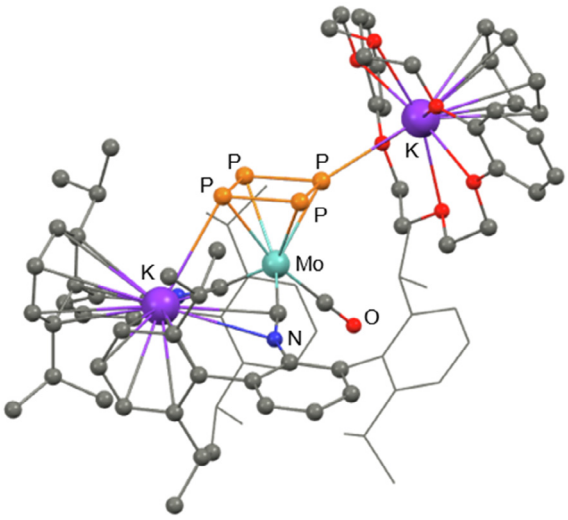

Fig. 32. X-ray structure of $[K_2(\text{dibenzo[18-crown-6]})[(\eta^4\text{-}P_4)Mo(CO)(CNAr^{Dipp2})_2]$ (**107**). Hydrogen atoms are omitted for clarity; adapted from Ref. [142].

is the first example of a metallaparacyclophane assembled using P_n ligand complexes, cationic metal salts and organic linkers [145].

It was possible to form 2D networks by replacing $Ag[Al\{OC(CF_3)_3\}_4]$ with $[Cu(CH_3CN)_4][BF_4]$. Following the same strategy as above, the reaction of $[Cu(CH_3CN)_4][BF_4]$ with the diphosphide complex ligand **110** was carried out and, independent of the stoichiometry, provided the dimeric complex $[Cu_2\{Cp_2Mo_2(CO)_4(\eta^2\text{-}P_2)\}_4][BF_4]_2$ (**117**), see Scheme 42. Compound **117** was able to coordinate the rigid *trans*-bipyridine linker **114** which replaced the η^2-side on phosphide complex ligands affording the poorly soluble coordination polymer **118**. The X-ray structure of **118** is shown in Fig. 36, and consists of a 2D network of $Cu_2[Mo]_4P_4$ nodes with [Mo] = $[CpMo(CO)_2]$ and the Cu_2P_4 six-membered ring nearly planar with a folding angle of 3.61°. The Cu(I) centers feature a distorted tetrahedral coordination geometry with N-Cu–N angles of 110.32(16)°, which creates rhomboid shaped cavities in the nanometer range with maximum diameter of 2.20 nm.

The coordination properties of dimer **117** (see Scheme 43) were further investigated by using a series of flexible linkers based on 4,4′-bipyridine (**119**, **120**) and 3,3′-bipyridine (**121**, **122**) [146]. Regardless of the length and position of the spacer between the pyridyl fragments, only 1D coordination polymers were selectively formed in moderate to high yields (65 to 94%), see compounds **123**, **124**, **125**, **126**, in Scheme 43. Two different morphologies were observed which are characterized by a different number of Cu(I) centers at the nodes of each ring of the chain: 2 Cu(I) centers for **123** and **125**, 4 Cu(I) centers for **124** and **126** (Fig. 37). Compounds **123** and **125** can be described as infinite dinuclear metallacyclic units connected to each other by Mo_2P_2 ligands, while in **124** and **126** there is a tetrametallic repeating unit, where the Mo_2P_2 ligands are part of the metallacycle. Consequently, the new one-dimensional organometallic-organic polymers possess a virtual porosity having cavities with circular (**123**–**125**) and rectangular meshes (**126**) of maximum diameter 1.47 nm.

Higher order polyphosphorus molybdenum complexes have also been considered for the formation of novel coordination polymers. The hexaphosphabenzene complex $[(Cp^*Mo)_2(\mu,\eta^6\text{:}\eta^6\text{-}P_6)]$ (**127**), (Cp^* = C_5Me_5) first isolated in 1985 by Scherer *et al.* [147], bears great potential in terms of the possible variety of coordination patterns, although the research on this field has been limited by the scarce efficiency of known protocols to obtain it. Synthesis of the triple decker complex $[(Cp^*Mo)_2(\mu_2,\eta^6\text{:}\eta^6\text{-}P_6)]$ was improved to a remarkable 64% yield by Scheer *et al.* [148] after prolonged heating of $[Cp^*Mo(CO)_{2/3}]_2$ in the presence of P_4 in refluxing diisopropylbenzene. Interestingly, the reaction also yielded trace amount of a novel binuclear complex $[(Cp^*Mo)_2(\mu_2,P_{10})]$ (**128**), displaying a folded $[P_{10}]^{2-}$ ligand with four short P-P bonds (2.140(2) Å) of double bond character. It is one of the few known P_{10} ligand derived from P_4, see Section 2.1.3.2. As shown by the solid state structure in Fig. 38, the Mo centers are coordinated to the P=P moieties in an $\eta^2\text{:}\eta^2$ mode and to the edge-P atoms in an κ^1 mode.

The coordination behavior of **127** was investigated with Ag[TEF] and Cu[TEF] (TEF = $[Al\{OC(CF_3)_3\}_4]^-$. Addition of Ag[TEF] or Cu[TEF] to a DCM solution of **127** resulted in the oxidation of the starting material to afford the paramagnetic derivative **129** (μ_{eff} = 1.67 μ_B), which was detected through ESI mass analysis (see Scheme 44). EPR analysis of **129** showed a broad signal with no hyperfine coupling at 77 K at g_{iso} = 2.024 (solid state) or g_{iso} = 2.024 (DCM solution). Suitable crystals for XRD analysis were obtained by exchanging the anion (TEF) for another WCA, $[FAl\{OC_6F_{10}(C_6F_5)\}_3]^-$ ([FAI]) affording compound **130**. According to the solid-state structure of **130**, the oxidation of the Mo center impacts the bonding situation of the *cyclo*-P_6 deck, thus it can be now regarded as

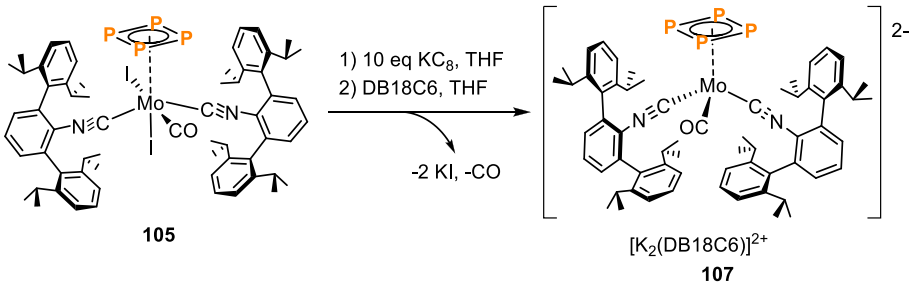

Scheme 38. Reduction of complex **79** with KC_8 affords complex $[K_2(\text{dibenzo[18-crown-6]})[(\eta^4\text{-}P_4)Mo(CO)(CNAr^{Dipp2})_2]$ (**107**).

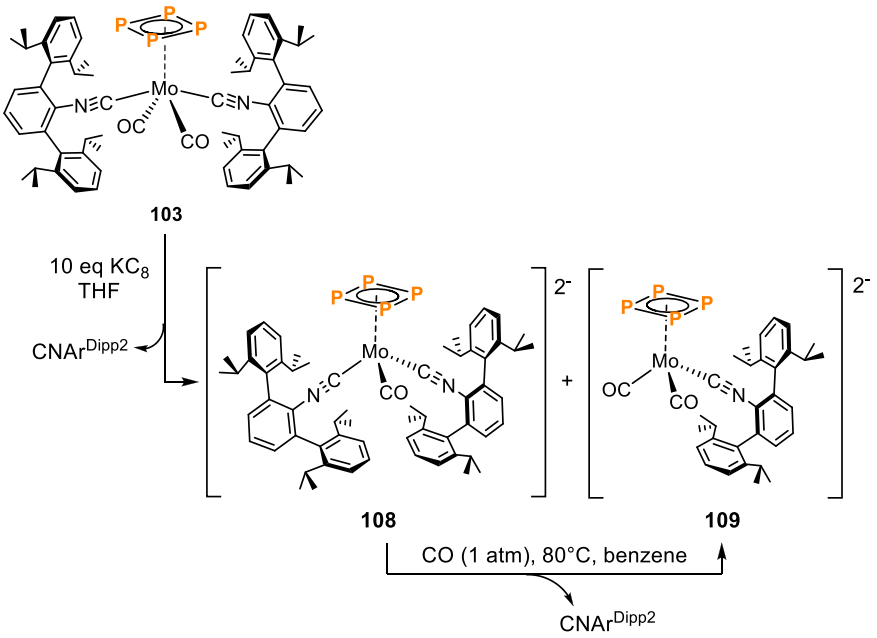

Scheme 39. Reduction of **103** with KC_8 occurs at the metal center leaving the *cyclo*-P_4 fragment intact.

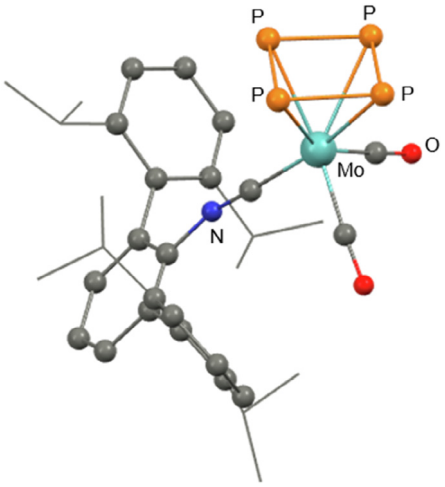

Fig. 33. X-ray structure of the dianionic portion of $[K_2(dibenzo18\text{-}crown\text{-}6)][(\eta^4\text{-}P_4)Mo(CO)_2(CNAr^{Dipp2})]$ **109**. Hydrogen atoms are omitted for clarity; adapted from Ref. [142].

two P_3 fragments joined by elongated P-P bonds (2.247 and 2.294 Å, bisallylic distortion).

The addition of Cu[TEF] and Ag[TEF] in a toluene/DCM solution of **127**, allowed for the formation of the coordination derivatives **131** and **132** respectively. The $^{31}P\{^1H\}$ NMR spectrum showed a broad singlet ($\omega_{½}$ = 126 Hz) at δ = -290.4 ppm for **131** and a broad singlet ($\omega_{½}$ = 155 Hz) at δ = -294.0 ppm for **132,** suggesting **127** possesses a highly dynamic coordination behavior towards Cu^+ and Ag^+. Single crystal X-ray analysis (Fig. 39) shows that **131** and **132** are isostructural and the central metal cation Cu(I) and Ag(I) respectively, is coordinated to two *cyclo*-P_6 moieties in an η^2 side-on mode, which results in a distorted square planar geometry.

When the reaction was performed in toluene only, the addition of Cu[TEF] to **127** provided a new coordination adduct, **133** with a distorted tetrahedral coordination geometry around the Cu(I) center and shorter Cu-P bonds with respect to **131** (Scheme 44 and Fig. 40), while the coordinating P-P bonds are longer.

Although **131** and **132** form a layered structure in the crystal lattice with alternating anionic [TEF] and cationic $\{M[(Cp^*Mo)_2(\mu,\eta^6\text{:}\eta^6\text{-}P_6)]_2\}$ (M = Ag, Cu) sheets, they do not form 2D networks. By reacting **127** with Tl[TEF], see Scheme 44 below, a 2D coordination polymer **134** was obtained and elemental analysis was consistent with a Tl^+/**127** ratio of 1:2. XRD analysis of **134**, showed that Tl^+ coordinates three *cyclo*-P_6 units in an η^2 side-on fashion displaying a bipyramidal trigonal geometry. This allows the coordination to propagate through the cationic sheets of the crystal lattice and to form a supramolecular network which can be regarded as a graphene-like structure. The $^{31}P\{^1H\}$ NMR spectrum of **134** showed no signal at room temperature, a broad peak ($\omega_{1/2}$ = 1303 Hz) at δ = -305.5 ppm was observed when cooling the solution down to 193 K. Additional studies were carried out by Scheer and coworkers using Cu(I) salts of more coordinative anions, such as halides [149]. Treatment of **127** with CuBr afforded black crystals of the polymer $[\{(CpMo)_2(\mu,\eta^{3:3:1:1:1:1}\text{-}P_3)(\mu,\eta^{3:2:1:1:1:1}\text{-}P_3)\}Cu_4(\mu,Br)_4]_n$ (**135**). This consists of a 2D network formed by four P atoms of the *cyclo*-P_6 deck, each one coordinating two copper atoms in an $\eta^1\text{:}\eta^1$ mode. The Br^- anions bridge the copper atoms completing the tetrahedral environment around Cu(I). Notably, the *cyclo*-P_6 moiety undergo not only a marked bisallylic distortion, with distances between the two P_3 fragments of 2.652(3) Å and 2.444(3) Å, but also a considerable distortion from planarity, with one P atom of the two P_3 fragments out of plane (envelope conformation). This leads the Cp ligands to be inclined by 9.26° with respect to the parallel conformation in **127**. Despite this, polymer **135** still forms layers whereby **127** units are bound together by CuBr at the level of the *cyclo*-P_6 middle-deck (see Fig. 41).

Similar results were obtained by employing CuI. Layering a CH_3CN solution of CuI on a CH_2Cl_2 solution of **127** caused the formation of black crystals of a 2D coordination polymer of formula $[\{(CpMo)_2(\mu,\eta^{3:3:1:1}\text{-}P_3)(\mu,\eta^{3:2:1:1}\text{-}P_3)\}_{0.84}\{(CpMo)_2(\mu,\eta^{6:6:1:1:1:1}\text{-}P_6)\}_{0.16}Cu_2(\mu,I)_2]_n$ (**136**)}. As with **135**, in **136** the *cyclo*-P_6 deck coordinates with Cu(I) in a 1,2,4,5 mode with only one copper atom bound to each ligating phosphorus atoms. Moreover, the *cyclo*-P_6 moiety shows some degree of disorder as

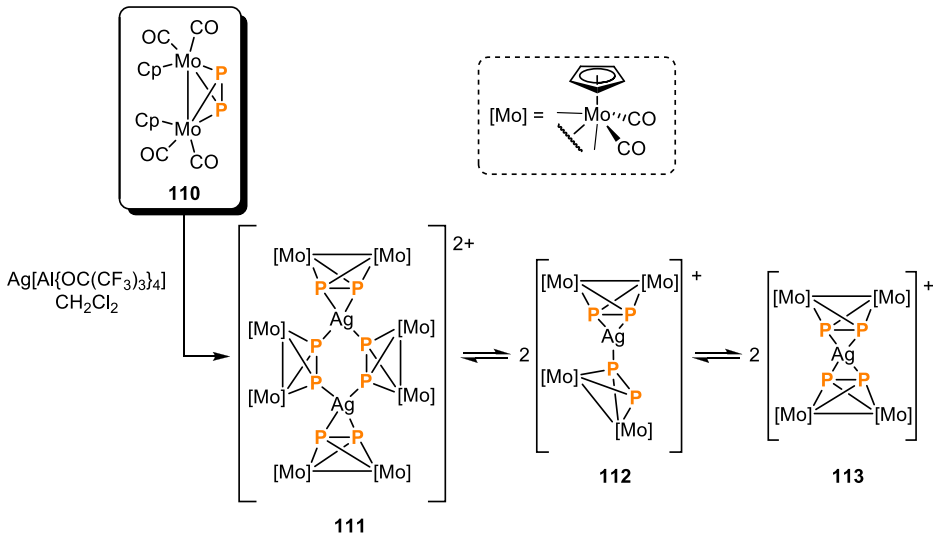

Scheme 40. Synthesis of **111** and the proposed coordination equilibrium.

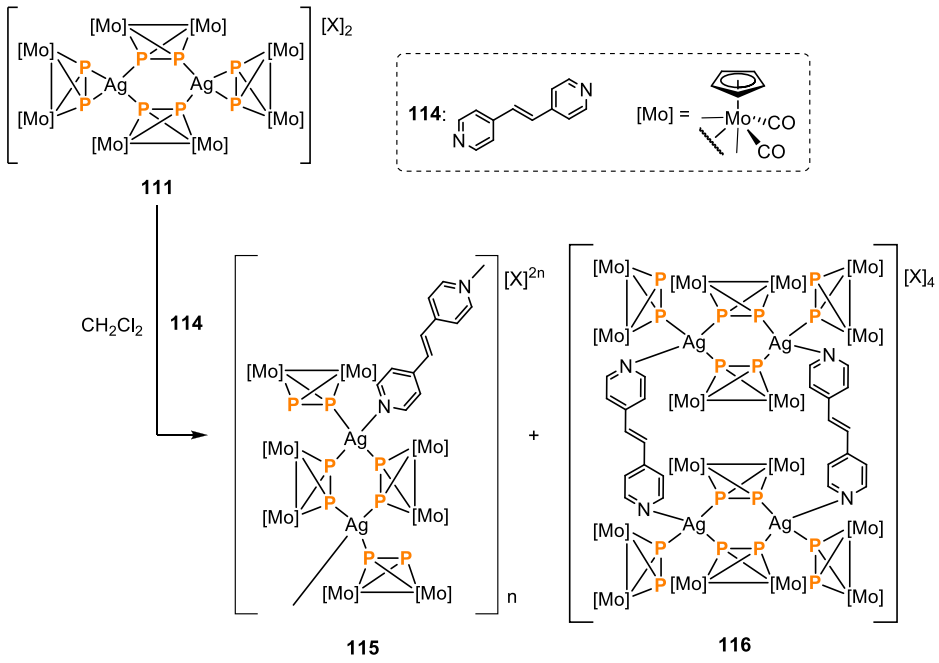

Scheme 41. Synthesis of **115** and **116** by assembly of **111** with bidentate ligand **114,** X = $[Al\{OC(CF_3)_3\}_4]^-$

it displays two different coordination patterns: $[\{(CpMo)_2(\mu,\eta^{3:3:1:1}\text{-}P_3)(\mu,\eta^{3:2:1:1}\text{-}P_3)\}Cu_2(\mu,I)_2]_n$ **136a** and $[\{(CpMo)_2(\mu,\eta^{6:6:1:1:1:1}\text{-}P_6)Cu_2(\mu,I)_2]_n$ **136b** with occupancy factors of 0.84 and 0.16 respectively. **136a** displays both bisallylic distorsion of the P_6 deck and the envelope conformation as with **135**. However, the minor component, **136b** shows a planar *cyclo*-P_6 deck with shortening of the P-P bonds upon coordination to Cu without a notable bisallylic distorsion (bond lengths in the range of 2.000–2.132 Å). Owing to their inherent insolubility, **135** and **136** were only characterized by ^{31}P MAS spectroscopy. Six different signals were observed spread over a window of 900 ppm, consistent with a distorted P_6 moiety.

Ruiz and co-workers reported the activation of P_4 by the triply bonded anion $[Mo_2Cp_2(\mu\text{-}PCy_2)(\mu\text{-}CO)_2]^-$ (**137**) under mild conditions [150], yielding the anionic diphosphorus complex $[Mo_2Cp_2(\mu2,PCy_2)(CO)_2(\mu2,\kappa^2\text{:}\kappa^2\text{-}P_2)]^-$ (**138**) (see Scheme 45).

The anionic **138** features a tetrahedral Mo_2P_2 core, where the P_2 ligand symmetrically bridges the two Mo centers. The PCy_2 ligand lies in the plane defined by a Mo_2P face, with the remaining Cp and CO ligands filling the coordination sphere of the metal. The computed P-P distance is 2.09 Å, much shorter than the value of 2.21 Å found in P_4, suggesting the presence of some additional π (P=P) character. The intrinsic nucleophilic nature of **138** translates into high reactivity towards electrophiles such as CH_3I and $ClSnPh_3$ see Scheme 45. Methylation takes place at a basal P atom, yielding the neutral diphosphenyl complex $[Mo_2Cp_2(\mu\text{-}PCy_2)(CO)_2(\mu2,\kappa^2\text{:}\kappa^2\text{-}P_2\text{-}Me)]$ (**139**), whose X-ray structure is shown in Fig. 42**a**. The P-P-C bond angle measures 122.8(1)° and is consistent with Me^+ addition to the P lone pair, as also revealed by theoretical calculation, with no effect on the P-P bond. The reaction with $SnPh_3Cl$ takes place in an analogous fashion, yielding $[Mo_2Cp_2(\mu\text{-}PCy_2)(CO)_2\{\mu2,\kappa^2\text{:}\kappa^2\text{-}P_2(SnPh_3)\}]$ (**140**) (see Fig. 42**b**). However, compared to **138**, the P-P distance in **140** is more elongated, approaching the typical value of a P-P single bond and a P-P-Sn bond angle of 80.3(1)°. As clarified by DFT calculations, interaction with $SnPh_3^+$

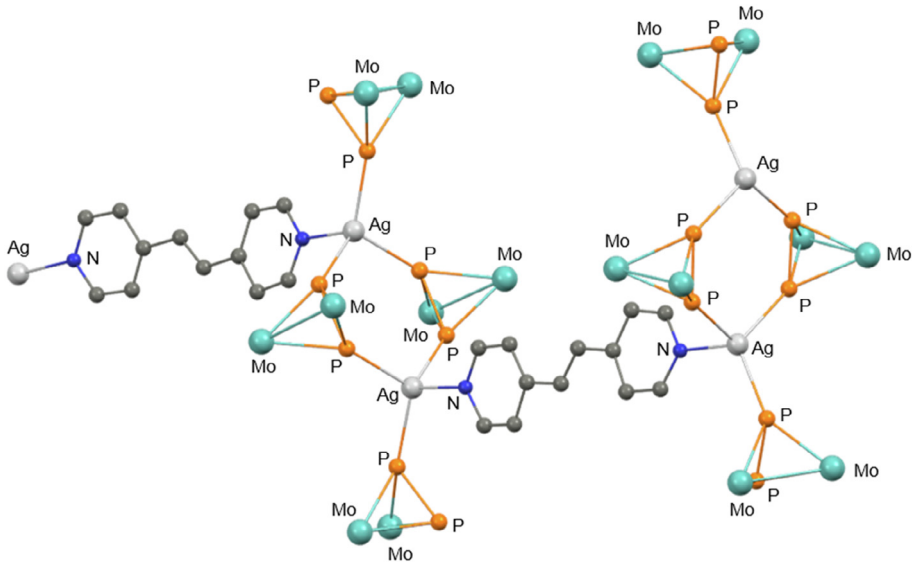

Fig. 34. Section of the cationic coordination polymer of **115** in the solid state. Hydrogen atoms, Cp and CO ligands on Mo, are omitted for clarity; adapted from Ref. [144].

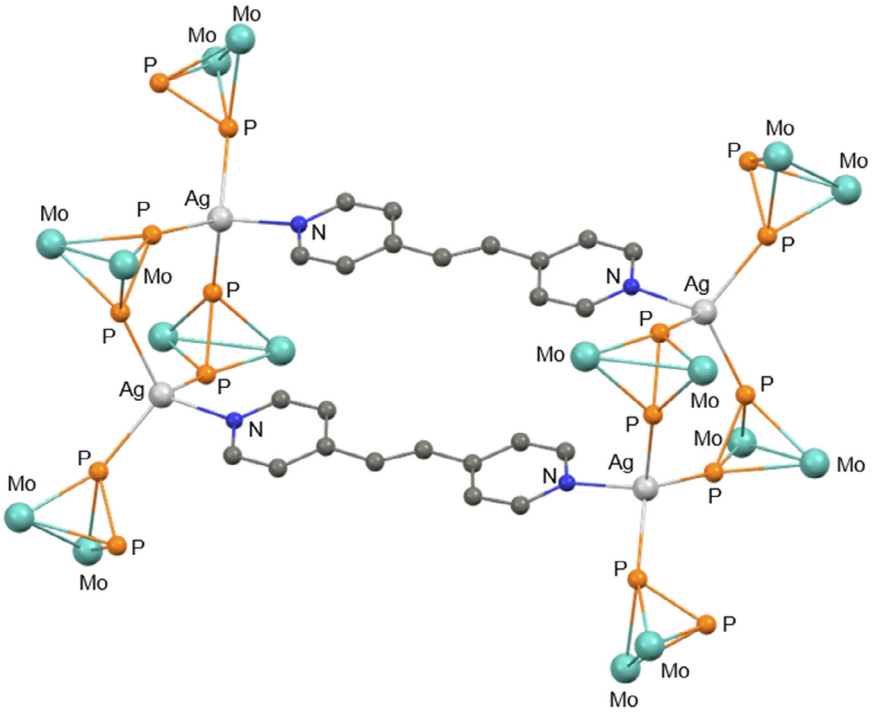

Fig. 35. Molecular structure of the tetracation of **116** in the solid state. Hydrogen atoms, Cp and CO ligands on Mo are omitted for clarity; adapted from Ref. [144].

involves filled orbitals on the anion having partial π(P=P) character, whose orientation gives the best overlap when P-P-Sn = 90°, thus explaining both the unexpectedly acute P-P-Sn bond angle and the observed P-P bond elongation. This rare coordination mode described by Ruiz *et al.*, was thoroughly explored by reacting **138** with various XER_3 electrophiles (X = halogen, E = C, Si, Ge, Sn, Pb, R = H, alkyl or aryl) [151]. In addition to this, the nuchleophilic character of the diphosphorus unit in **138**, was further investigated through the reaction with chlorophosphines $ClPR_2$ (R = Cy, Ph, *t*Bu) and transition-metal halide complexes such as $[FeClCp(CO)_2]$, $[MoCpI(CO)_3]$, $[ZrCl_2Cp_2]$, $[MnBr(CO)_5]$ and $[ReCl(CO)_5]$ [152], as well as with 16-electron metal carbonyl fragments $[ML_n(THF)]$ (ML_n = $Fe(CO)_4$, $MnCp'(CO)_2$, $Mo(CO)_5$, $W(CO)_5$) [153].

Similar studies were carried out to investigate the reactivity of **139** towards 14- and 16-electron metal carbonyl fragments [154,155], with the aim to form novel heterometallic clusters. In particular, the reaction of **139** with $[Fe_2(CO)_9]$ or $[W(CO)_4(THF)_2]$ in a 1:1 ratio yielded the stable trinuclear clusters $[Mo_2MCp_2(\mu_3\text{-}P)(\mu\text{-}PCy_2)(\mu_3\text{-}PMe)(CO)_X]$ [M = Fe, x = 5 (**141**); M = W, x = 6, **141a**], see Scheme 46 and Fig. 43**a**. Repeating the reaction with an excess of $[Fe_2(CO)_9]$, the main product was the tetranuclear phosphide- and phosphinidene-bridged derivative $[(Fe_2Mo_2Cp_2)(\mu_4\text{-}P)(\mu\text{-}PCy_2)(\mu_3\text{-}PMe)(CO)_9]$ (**142**) along with small amounts of **141**, see Scheme 46**.** In both cases, there is cleavage of the P-P bridge with a $Fe(CO)_3$ moiety sitting on the MoP_2 face of the Mo_2P_2 tetrahedral core. Additionally, in **142** a $Fe(CO)_4$ unit is coor-

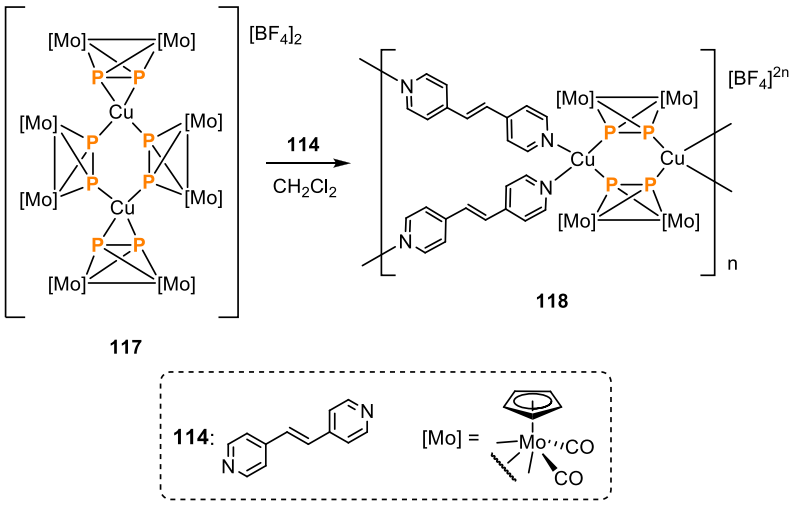

Scheme 42. Synthesis of 2D coordination polymer **118**.

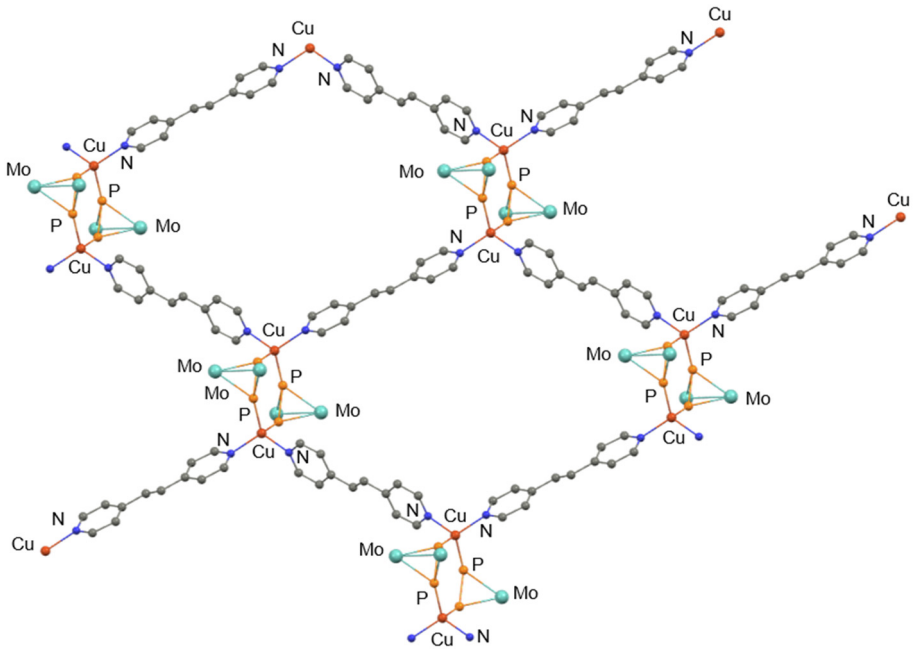

Fig. 36. Structure of the dicationic repeating unit of **118** in the solid state. Hydrogen atoms, Cp and CO ligands on Mo are omitted for clarity; adapted from ref. [144].

dinated to the naked P atom. Similarly, the reaction of **139** with an equimolar amount [MnCp′(CO$_2$)(THF)] (Cp′ = C$_5$H$_4$Me) or [W(CO)$_5$(-THF)] gave [(ML$_n$)Mo$_2$Cp$_2$(μ$_3$-P)(μ-PCy$_2$)(μ$_3$-PMe)(CO)$_x$] (ML$_n$ =-MnCp′, x = 4, **143**; ML$_n$ = W, x = 7, **143a**). These compounds were found to be unstable and decompose at room temperature or under gentle heating with loss of the methylphosphinidene (PMe) unit, yielding the corresponding trinuclear complexes [(ML$_n$)Mo$_2$Cp$_2$(-μ$_3$-P)(μ-PCy$_2$)(CO)$_x$] (ML$_n$ = MnCp′, x = 4, **144**; ML$_n$ = W, x = 7, **144a**). In turn, complexation with an excess of the 16-electron metal fragments [MnCp′(CO)$_2$(THF)] (Cp′ = C$_5$H$_4$Me) led to the formation of tetranuclear diphosphenyl-bridged [Mn$_2$Mo$_2$Cp$_2$Cp′$_2$(μ-PCy$_2$)(μ-κ^2:κ^1:κ^1:κ^1-P$_2$Me)(CO)$_6$] (**145**) along with a small amount of the trinuclear derivative **143** and the "PMe"-extruded derivative **144**. Compound **145** also proved to be unstable, forming the trinuclear complex **144** overtime. Similarly, when **139** was treated with 3.5 eq of [W(CO)$_5$(THF)], it afforded both the tetranuclear derivatives [Mo$_2$W$_2$Cp$_2$(μ-PCy$_2$)(μ,κ^2:κ^1:κ^1:κ^1-P$_2$Me)(CO)$_{12}$] (**146**) and [Mo$_2$W$_2$Cp$_2$(μ$_3$-P)(μ-PCy$_2$)(μ$_3$-PMe)(CO)$_{10}$] (**147**) in 3:2 ratio, along with small amounts of **144a** (Scheme 46). Complexes **145** and **146** feature a trigonal-planar phosphide ligand, bridging the two Mo centers in addition to the exocyclic ML$_n$ moiety. Notably, the short Mo-Mo distance (2.749(1) Å in **145** and **146** is consistent with a double Mo=Mo bond, as also confirmed by DFT calculations. Fig. 43 depicts the X-ray structures of **141**, **141a** and **144a**.

Lastly, the reaction of **139** with metal carbonyl dimers [M$_2$(CO)$_X$] where M = Mn, Re, Co; x = 10, 8, was investigated and led invariably to tetranuclear clusters, via the cleavage of the diphosphenyl moiety and incorporation of a partially decarbonylated dimetal unit. In particular, the reaction of **139** with [Co$_2$(-CO)$_8$] occurs at room temperature giving the 64-electron tetranuclear cluster [Co$_2$Mo$_2$Cp$_2$(μ-PCy$_2$)(μ$_4$-PMe)(μ-CO)(CO)$_6$] **147**, including the formation of two new Mo-Co bonds. As shown in Fig. 44, the molecular structure of **147** displays a square planar Co$_2$Mo$_2$ core symmetrically capped by a naked phosphide and a

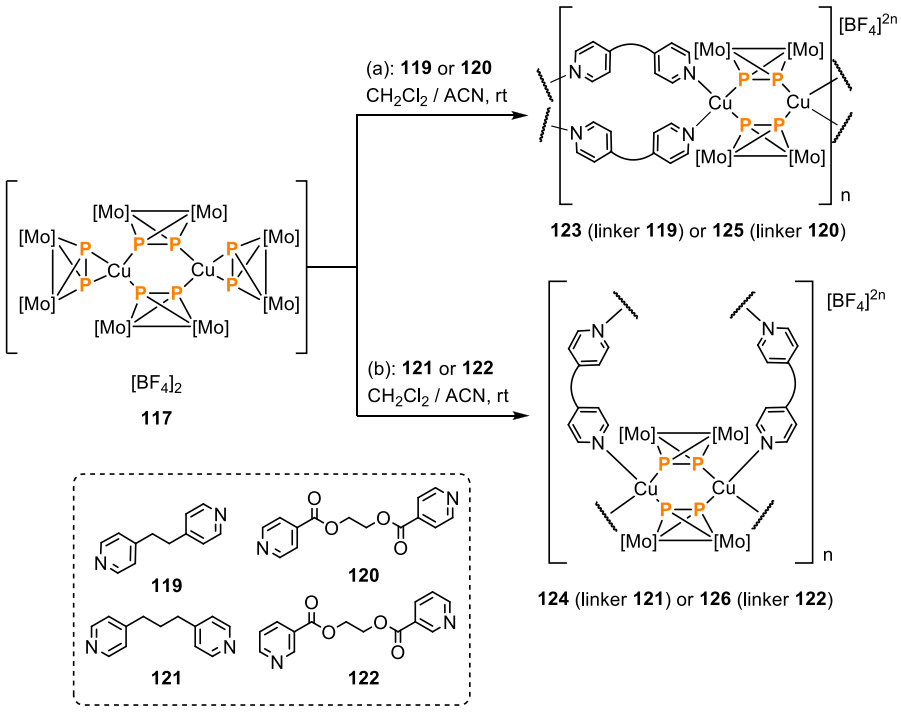

Scheme 43. Synthesis of 1D organometallic-organic polymers **123**–**126** by coordination of the flexible linkers **119**, **120**, **121** and **122** to the dimer **117.** [Mo] = [CpMo(CO)$_2$].

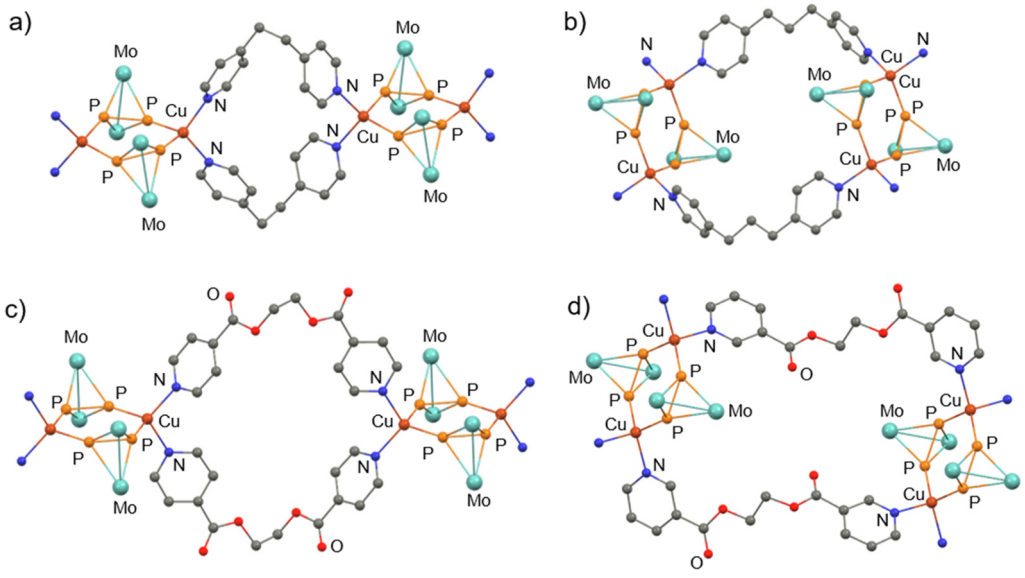

Fig. 37. Structure of the dicationic repeating unit of a) **123**, b) **124**, c) **125**, d) **126** in the solid state**.** Hydrogen atoms, Cp and CO ligands on Mo are omitted for clarity; adapted from Ref. [146].

methylphosphinidene ligand giving an overall octahedral M_4P_2 structure, with PCy_2 and CO ligands bridging two Mo centers and two Co centers, respectively.

The dimolybdenum agostic methyl-bridged complex [Mo_2Cp_2(-μ,κ^1:η^2-CH_3)(μ,P*t*Bu_2)(μ,CO)] reacts with P_4 affording the blue triphosphorus complex [Mo_2Cp_2(μ,η^3:η^3-P_3)(μ,P*t*Bu_2)] via decarbonilation and methylphosphinidene elimination [156]. XRD analysis of [Mo_2Cp_2(μ,η^3:η^3-P_3)(μ,P*t*Bu_2)]revealed that the P_3 chain is symmetrically coordinated (P-P = 2.15 Å) to the two Mo centers, which in turn are triply bound to each other (Mo-Mo = 2.622 Å). Noteworthy, the internal P atom appears to be extremely shielded as it resonates at the lowest ^{31}P chemical shift recorded to date (δ = -625.5 ppm).

Roesky and co-workers [157] investigated the reaction between the neutral complex [{CpMo(CO)$_2$}$_2$(μ$_2$,η^2-P$_2$)] (**110**) [158], and lanthanide complexes of the type [Cp*$_2$Ln(THF)$_2$] (Ln = Sm (**24a**), Yb (**148**), yielding different polyphosphide species (see Scheme 47). In particular, the reaction of **110** with **148** gave product **149**, featuring a central {P=P}$^{2-}$ ligand, end-on coordinated to two {CpMo(CO)$_2$}$_2$ fragments. The reaction of **110** with samarocene complex, **24a** led to compound **150** as the major product (see Fig. 45 for X-ray structure) in addition to small amounts of **151** and **152**, which

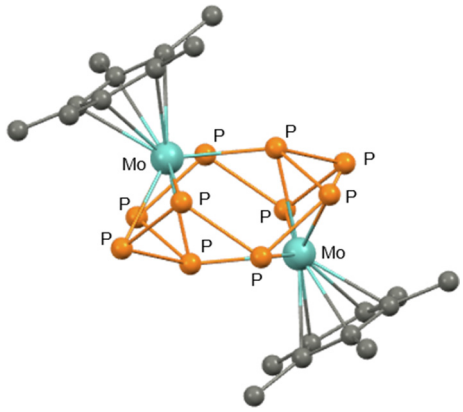

Fig. 38. X-ray structures of **128**. Hydrogen atoms are omitted for clarity; adapted from Ref. [148].

display a *cyclo*-P_4 and a *cyclo*-P_5 core units, respectively (see Scheme 47).

2.4.3. Tungsten

Ruiz and co-workers [159] applied the same functionalization strategy as seen with **137** (see Section 2.4.2) to tungsten by treating the analogous ditungsten complex $Na[W_2Cp_2(\mu,PCy_2)(\mu,CO)_2]$ (**153**) with P_4 at 60 °C in THF. The reaction afforded the novel diphosphorus-bridged ion pair $Na[W_2Cp_2(\mu,\kappa^2{:}\kappa^2\text{-}P_2)(\mu,PCy_2)(CO)_2]^-$ (**154**), although it could not be isolated. To confirm the identify of **154**, it was treated with MeI affording the more stable methyldiphosphenyl complex $[W_2Cp_2(\mu,\kappa^2{:}\kappa^2\text{-}P_2)(\mu,PCy_2)(CO)_2]^-$ (**155**, Scheme 48).

The IR spectrum of **153** revealed four C-O stretching bands deriving from an equilibrium between the contact (1824 and 1695 cm^{-1}) and solvent separated (ν = 1824 and 1757 cm^{-1}) ion-pairs at room temperature. The ^{31}P NMR analysis showed only resonances for the PCy_2 ligand and no signals were present for the $\kappa^2{:}\kappa^2$ coordinated P_2 moiety. In turn, the IR spectrum of **155** showed two C-O absorbances (ν = 1860 and 1837 cm^{-1}) which are consistent with the distorted transoid conformation of the $M_2(CO)_2$ oscillator. The bridging methyldiphosphenyl ligand displayed two multiplets at δ = -166.0 ppm for (PMe) and δ = -390.1 ppm for (P) with large mutual coupling constants ($^1J_{PP}$ = 467 Hz), which is common for κ^1 diphosphene complexes [160]. This is consistent with the short P-P bond (2.085 Å) found in the corresponding Mo complex **139**.

In an attempt to further study the reactivity of low-valent ETM-phosphide complexes and to explore the possibility of the complete functionalization of the phosphide ligand, Cummins and co-workers [161] carried out the reduction of the precursor *mer*-$Cl_3W(ODipp)_3$ (**156**) with Na/Hg amalgam in the presence of P_4 in toluene, affording the neutral aryloxide complex (η^3-P_3)W$(ODipp)_3$ (**157**) in 10% yield (Scheme 49). Compound **157** is valence-isoelectronic with $[(\eta^3\text{-}P_3)Nb(ODipp)_3]^-$ **65** (see Section 2.3.2.). The purpose was to assess the influence of the ionic charge of the complex on the transferability of the *cyclo*-P_3 ligand to main-group acceptors.

The ^{31}P NMR spectrum of **157** displayed a shielded signal at δ = -156 ppm with ^{183}W satellites ($^1J_{183W\text{-}31P}$ = 9 Hz). XRD analysis of **157** (see X-ray structure in Fig. 46**a**), showed shorter W-P and P-P distances (2.439–2.447 Å and 2.174–2.180 Å respectively) compared to **65** attributed to the smaller covalent radius of W with respect to Nb [58]. **157** proved to be remarkably less nucleophilic compared to the anionic **65**. The reaction of **157** with either PCl_3 or $AsCl_3$ in THF resulted in the displacement of the aryloxide by the chloride with no evidence of *cyclo*-P_3 transfer to the electrophile, affording (η^3-P_3)W(Cl)$(ODipp)_2$(THF) (**158**), (see Fig. 46**b** for X-ray structure). This differs significantly to the reaction of **65** with $AsCl_3$, which forms AsP_3, suggesting that salt elimination aids in the formation of EP_3 species (E = As or P).

2.5. Group 7 metals

2.5.1. Manganese

The Scheer group reported the preparation of Mn complexes bearing intact P_4 tetrahedra as ligands, in the form of both mononuclear and dinuclear complexes [162]. Remarkably, these species represent the first examples of Mn complexes bearing E_x ligands (E = pnictogen). Following some unsuccessful attempts aimed at the activation of P_4 using cymantrene-derived fragments

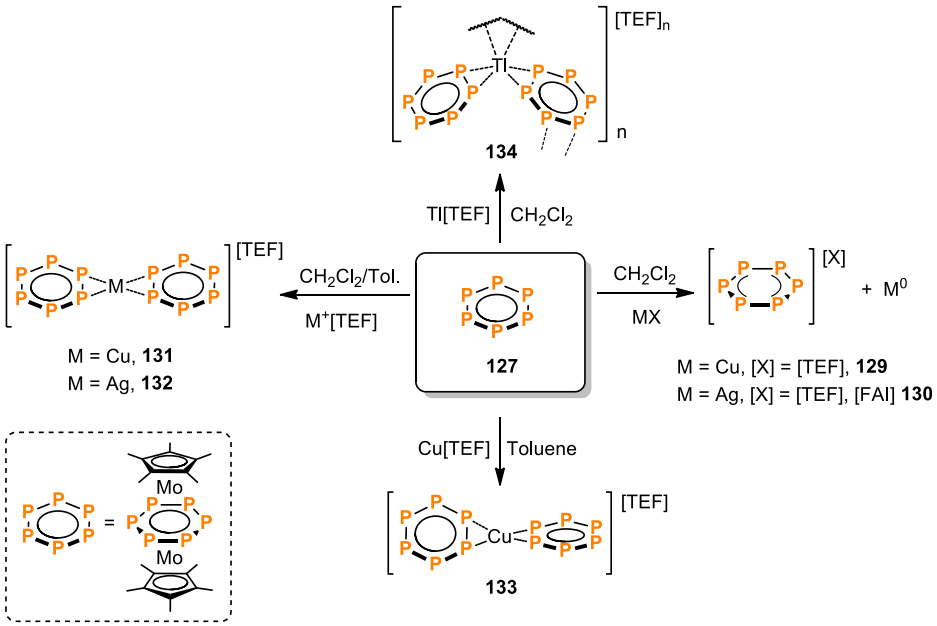

Scheme 44. Reaction of **127** with Ag(TEF), Cu(TEF) and Tl(FAl) is highly dependent on the reaction media.

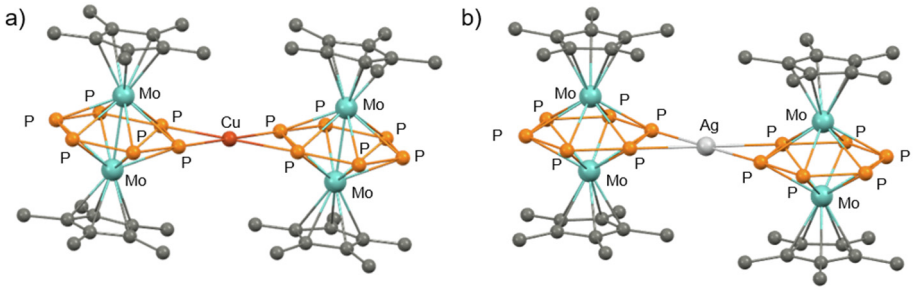

Fig. 39. Solid state structures of a) the cation of **131**, and b) the cation of **132**. Hydrogen atoms are omitted for clarity; adapted from Ref. [148].

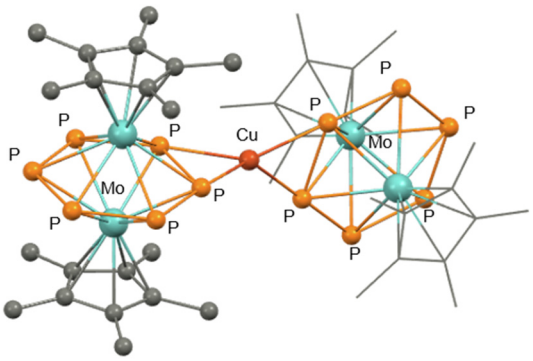

Fig. 40. Molecular structure of the cation of **133**. Hydrogen atoms are omitted for clarity; adapted from Ref. [148].

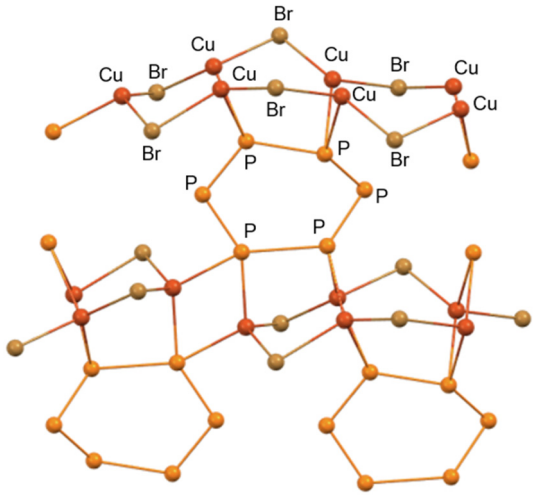

Fig. 41. Section of the 2D polymeric network **135**. [CpMo] units and hydrogen atoms are omitted for clarity; adapted from Ref. [149].

such as $[Cp^{R}Mn(CO)_3]$ (R = H, Me), $[Cp^{BIG}Mn(CO)_2(THF)]$ (**159**, $Cp^{BIG} = C_5(C_6H_4^nBu)_5$) was prepared, which possesses superior Lewis acidity and therefore is expected to react with P_4 upon displacement of the weak THF ligand. The reaction of **159** with 5 equivalents of P_4 gave the mononuclear complex $[Cp^{BIG}Mn(CO)_2(\kappa^1\text{-}P_4)]$ (**160**), which features an intact P_4 molecule end-on coordinated to Mn (see Scheme 50).

The molecular structure of complex **160** is shown in Fig. 47**a**. The bonds between the apical (P1) and the basal (P2, P3, P4) atoms (2.145–2.165 Å) are about 7 pm shorter than the basal P-P bonds (2.211–2.232 Å), as previously observed in related κ^1-P_4 complexes of Group 6 and 8 [163–169]. The $^{31}P\{^1H\}$ NMR spectrum of **160** in toluene d_8, features a quartet at δ = -305.7 ppm and a doublet at δ = -490.0 ppm with a $^1J_{PP}$ = 224 Hz, corresponding to the apical P1 atom and the three basal atoms, respectively.

When compound **159** was reacted with<5 equivalents of P_4, the dinuclear complex $[\{Cp^{BIG}Mn(CO)_2\}_2(\mu,\kappa^1\text{:}\kappa^1\text{-}P_4)]$ (**161**) was formed alongside **160**. Complex **161** can be obtained in pure form either by reacting **159** with 0.5 equivalents of P_4 or reacting **160** with 1 equivalent of **159** (see Scheme 50). A remarkable property of **160** and **161** is their stability both in the solid state and in solution at room temperature, a feature not observed before for neutral P_4 complexes. Complex **161** (see Fig. 47**b**) features an intact P_4 tetrahedron shared by two $\{Cp^{BIG}Mn(CO)_2\}$ fragments in an end-on coordination. Notably, the Mn-P distance in complexes **160** and **161** is identical within the experimental error, indicating that second coordination is as strong as the first one. In agreement with the X-ray structural analysis, $^{31}P\{^1H\}$ NMR measurements carried out at 193 K showed an A_2X_2 spin system, with two triplets at δ = -478.7 ppm and −250.2 ($^1J_{PP}$ = 159 Hz), assigned to free and Mn-coordinated P atoms respectively. Upon heating to room temperature, these signals broaden as a result of the tumbling of the P_4 unit. Thus, the P_4 tetrahedron can act as a ligand binding metal fragments either in an end-on or a side-on fashion. In both cases the P_4 molecule is kept 'intact' and its reactivity is influenced by the coordinated metal fragments.

Scheer and co-workers succeeded in the synthesis of a rare heterocubane cage $[\{CpMn\}_4(\mu_3,P)_4]$ (**162**), isolated via the thermolysis of $[CpMn(\eta^6\text{-CHT})]$ (CHT = cycloheptatriene) and P_4 at 205 °C in 1,3-diisopropylbenzene (DIB), see Scheme 51 [170]. Using a stoichiometric amount of P_4, reddish-brown needle-like crystals of **162** could be obtained with a yield of 73%. X-ray diffraction analysis revealed a highly symmetric geometry (see Fig. 48**a**), in which the Mn atoms sit at the vertices of a tetrahedron, whose faces are capped by the P atoms, resulting in a heterocubane Mn_4P_4 structure. DFT calculations revealed Mn-Mn and Mn-P bond order of 0.33 and 0.92 respectively. Considering the existence of three Mn-Mn bonds of order 1/3 for each Mn atom, the number of its valence electrons can be calculated classically to be 18. The high symmetry of **162** is also evidenced by NMR spectroscopic analysis. Both the ^1H and $^{13}C\{^1H\}$ NMR spectra of **162** show only one singlet at δ = 4.58 ppm and δ = 82.7 ppm respectively, which are typical for the cyclopentadiene ring. The $^{31}P\{^1H\}$ NMR spectrum of **162** shows an extremely low-field shifted singlet at δ = 1079.8 ppm. Bridging phosphide ligands are expected to be available for further coordination. The availability of four naked P atoms in **162** should allow for its use as a building block in coordination chemistry. Indeed, the reaction of **162** with Cu(I) salts, afforded 1D coordination polymers $[\{(CpMn)_4(\mu_3,P)_4\}(CuX)]n$ (X = Cl; Br) with a zigzag-like chain structure. As a proof of concept, complex **162** was reacted with $[CpMn(CO)_2(THF)]$, yielding $[\{(CpMn)_4(\mu_3,P)_4\}\{CpMn(CO)_2\}_n]$ species, with n = 1, 2, 3, 4 depending on the amount of $[CpMn(CO)_2(\text{-}THF)]$ used. The molecular structure of $[\{CpMn\}_4(\mu_3,P)_4\{CpMn(CO)_2\}_n]$ (**163**, n = 1) is shown in Fig. 48**b**. As revealed by X-ray

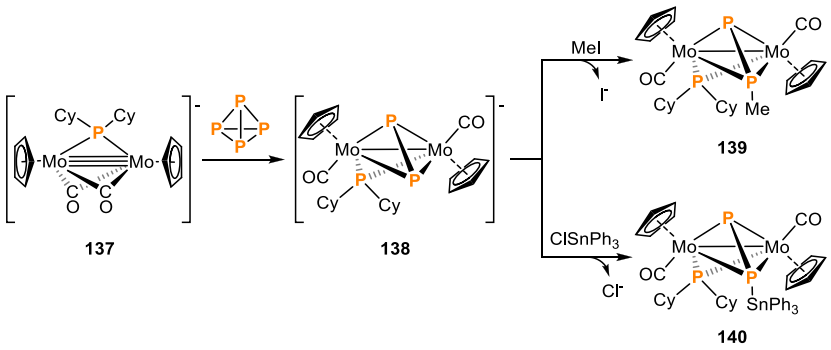

Scheme 45. Activation of P_4 by **137** affords **138** which reacts with electrophilic species, giving complexes **139** and **140**.

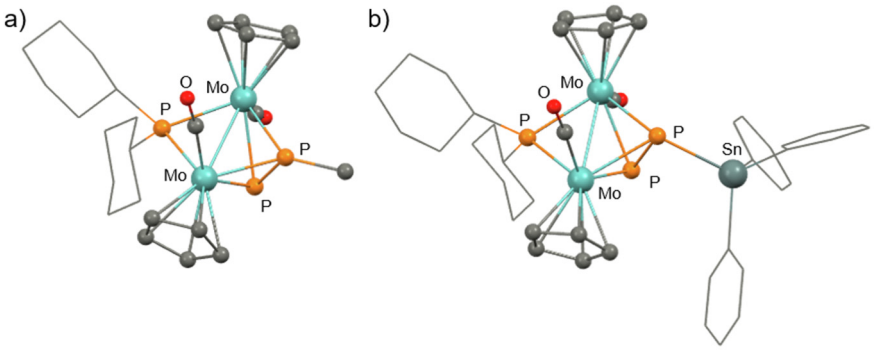

Fig. 42. X-ray structures of a) **139** and b) **140**. The different bond angle P2-P3-X (X = C, Sn) is clearly visible. Hydrogen atoms are omitted for clarity; adapted from Ref. [150].

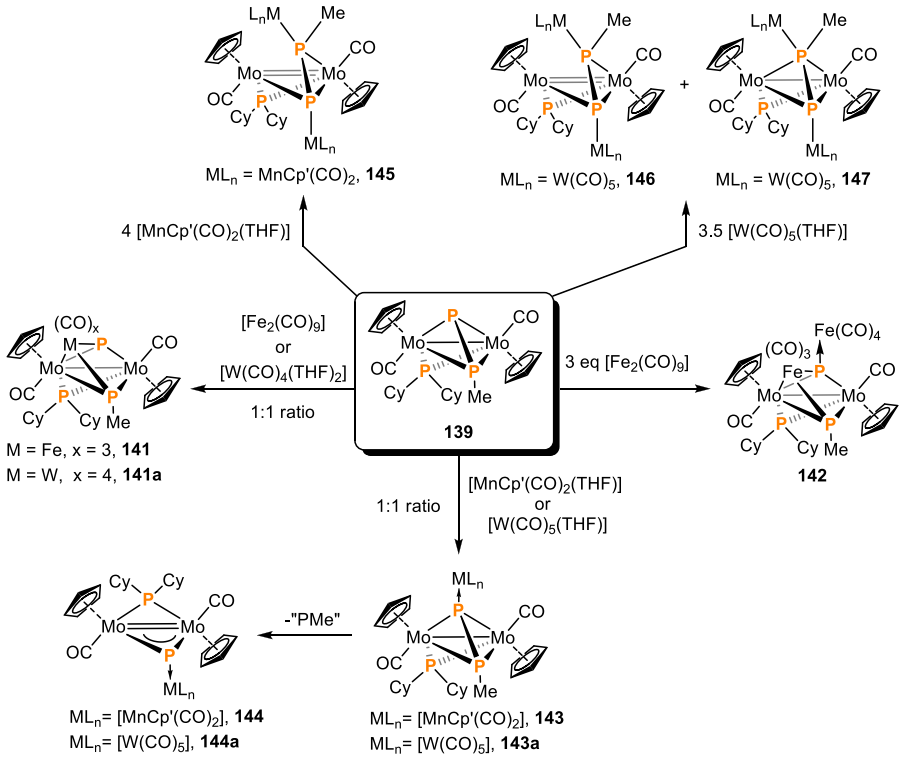

Scheme 46. Reaction of **139** with mononuclear carbonyl fragments ML_n resulting in the formation of tetra- and trinuclear complexes.

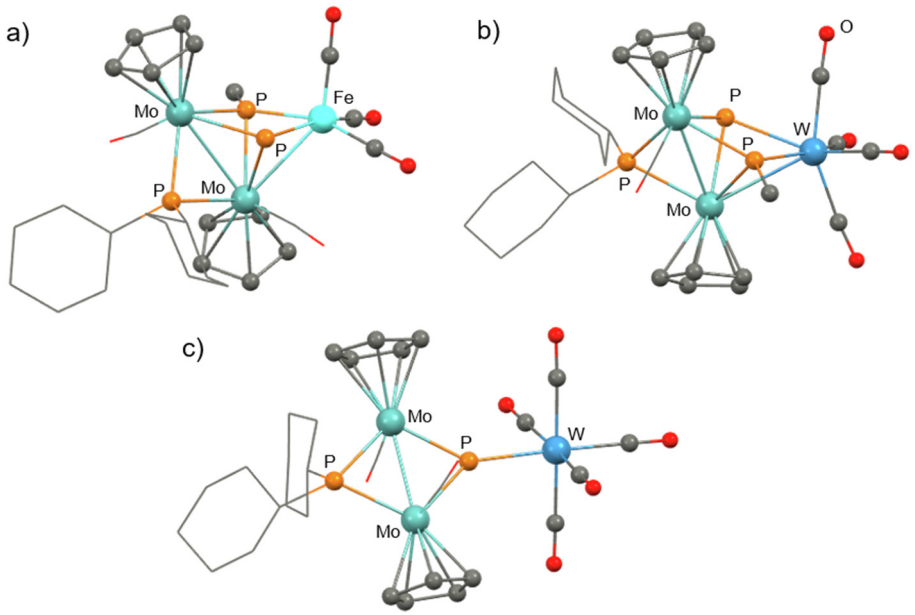

Fig. 43. X-ray structure of a) **141** and b) **141a**, featuring a cleaved diphosphorus bond. X-ray structure of complex c) **144a** reveals a [$PW(CO)_5$] ligand bridging the two Mo centers, evidencing the absence of the extruded "PMe" fragment. Hydrogen atoms are omitted for clarity; adapted from Ref. [154].

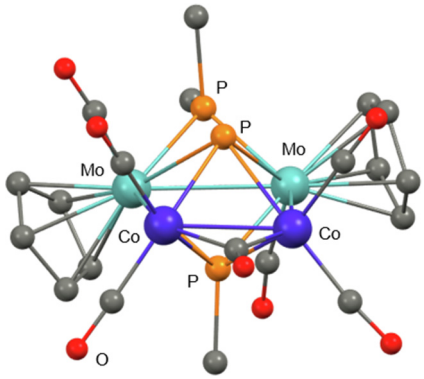

Fig. 44. Molecular structure of **147.** Hydrogen atoms and Cy groups (except the C^1 atoms) are omitted for clarity, adapted from Ref. [155].

studies, an increase in the number of attached {$CpMn(CO)_2$} fragments lead to a volume expansion of the Mn_4P_4 unit, characterized by a progressive elongation of Mn-Mn and Mn-P bonds (from av. Mn–P 2.235 Å and av. Mn–Mn 2.713 Å in **162** to av. Mn–P 2.258 Å and av. Mn–Mn 2.757 Å when n = 4).

Scheer and co-workers [171] devised the synthesis of unprecedented Mn triple decker complexes featuring central P_n ligands, using the precursor [$Cp^{BIG}Mn(CHT)$] (**164**, Cp^{BIG} = $C_5(4\text{-}n\text{BuC}_6H_4)_5$, CHT = cycloheptatriene) and reacting it with P_4. When **164** is heated in toluene with excess P_4, the CHT ligand is eliminated and complexes [{$Cp^{BIG}Mn$}$_2$($\mu2,\eta^5$:η^5-P_5)] (**165**) and [{$Cp^{BIG}Mn$}$_2$($\mu2,\eta^2$:η^2-P_2)$_2$] (**166**) are formed (see Scheme 52).

Being chemically alike, **165** and **166** could not be separated by TLC and even co-crystallize at the same crystallographic positions. This occurrence causes a triple decker complex with a disordered middle deck. Upon careful analysis of the atom occupancies in the central deck, a 7:3 mixture of **165** and **166** was ascertained. The structure of **165**, which features a *cyclo*-P_5 ligand, is shown in Fig. 49.

The P–P bond lengths in **165** have an average value of 2.20 Å, in good agreement with other known triple-decker complexes [172] containing a *cyclo*-P_5 middle-deck (typically 2.15 Å – 2.28 Å). Notably, the Mn-Mn distance is 2.795 Å, which is in the usual range for Mn-Mn single bonds. DFT calculations of **165** indicated a Mn-Mn Wiberg bond index of 0.6, confirming a bond between the two metal centers. Compound **166** features two coplanar P_2 units, each one bridging in a side-on fashion to the two Mn atoms. The $^{31}P\{^1H\}$ NMR spectrum of **165** revealed only one broad singlet at δ = 396.9 ppm. This feature was explained by DFT calculations, which showed **165** is paramagnetic with a doublet ground state. EPR measurements were then carried out at 77 K, showing a well resolved anisotropic multiplet. This arises from the coupling of the unpaired electron with two Mn centers having spin of 5/2 each. The g_{iso} value was identified to be 1.923 (simulation), slightly smaller than the value of 1.957 calculated via DFT.

2.5.2. Rhenium

Within the last decade a great deal of research related to the activation of P_4 has focused on employing reactive low-valent and coordinatively unsaturated TM complexes with the aim to promote multi-electron reductive couplings between the two species. In 2019, Arnold and co-workers [173], successfully synthesized the neutral complex Re(η^5-Cp)(BDI) (BDI = *N,N′*-bis(2,6-diisopropyl phenyl)-3,5-dimethyl-β-diketiminate) (**168**), a rare example of an isolable unsaturated Re(II)-d^5 complex, obtained in good yields (76%) from the oxidation of the anionic Re(I) precursor Na[Re(η^5-Cp)(BDI)] (**167**) with AgOTf (Scheme 53). Due to the paramagnetic and reduced nature of **168**, confirmed by the measure of its magnetic moment (μ_B = 1.67) with the Evans method, **168** was expected to be an excellent candidate for the reductive activation of P_4. Upon addition of P_4 to **168** in toluene at room temperature the novel Re(V) complex (η^3-*cyclo*-P_3)Re(η^5-Cp)(BDI) (**169**) was formed in good yield (64%) [174]. ^{31}P NMR analysis of **169** displayed two highly shielded and well resolved resonances at δ = –206.9 ppm and a δ = –297.3 ppm (a triplet and a doublet respectively with a $^1J_{PP}$ = 285 Hz), consistent with a formal trianionic [*cyclo*-P_3]$^{3-}$ ligand. The molecular structure of **169** (see Fig. 50) revealed P-P bond length in the range from 2.127 to 2.144 Å, standard for *cyclo*-P_3 moieties. The redox properties of **169** were investigated through cyclovoltammetry, which indicated an oxidation peak at –0.25 V ($E_{1/2}$ vs Fc/Fc+, THF, 0.3 M [$n\text{Bu}_4\text{N}$][PF_6]), associ-

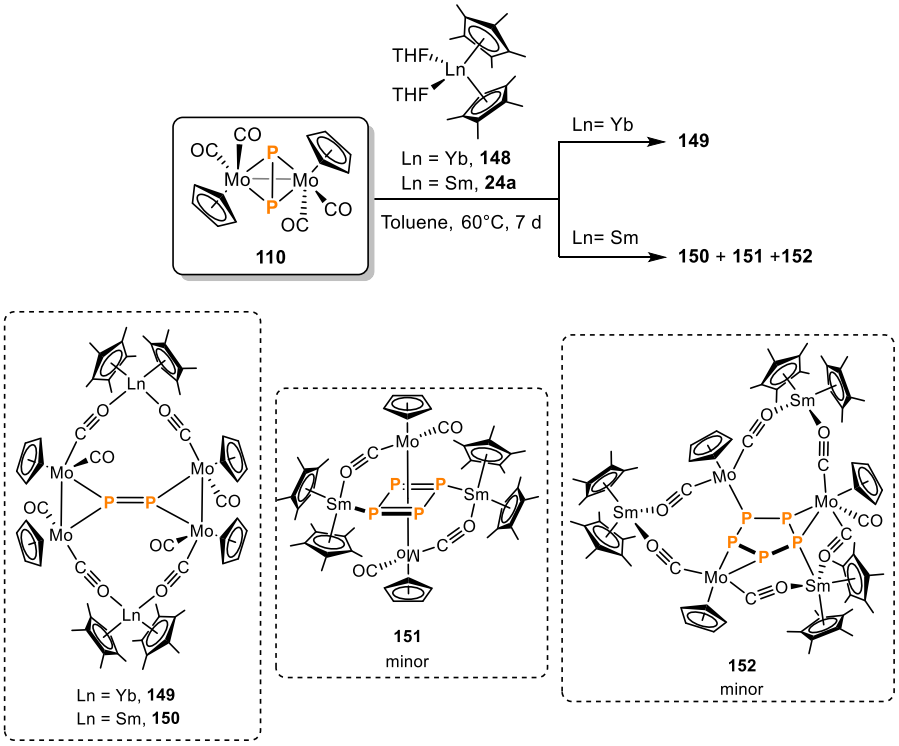

Scheme 47. Synthesis of compounds **149**, **150**, **151** and **152**.

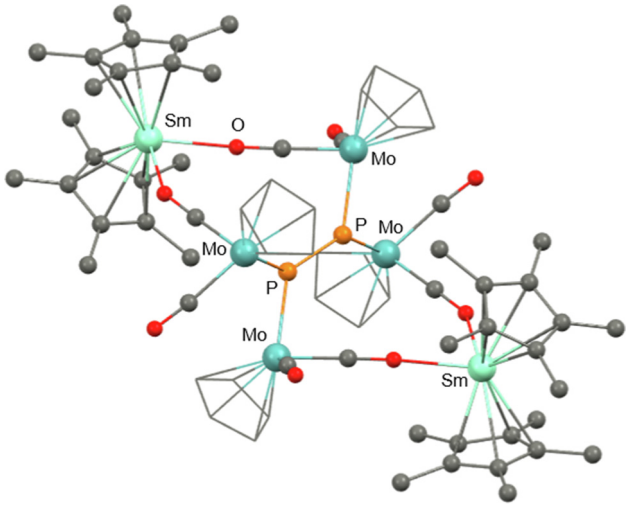

Fig. 45. X-ray structure of **150**. Hydrogen atoms are omitted for clarity; adapted from Ref. [157].

ated to the redox couple Re(V)/Re(VI). For this reason, **169** was treated with AgOTf, which afforded the Re(VI) complex [(η^3-*cyclo*-P_3)Re(η^5-Cp)(BDI)][OTf] (**170**, Scheme 53).

Interestingly, there are no remarkable differences in the Re-P and P-P bond distances between **169** and **170**. The oxidation seemed to affect only the Re-N distance of one N atom of the BDI ligand (Re-N1 gets 0.12 Å smaller going from **169** to **170**). The electronic structure of **169** was investigated by EPR and ENDOR (Electron-Nuclear Double Resonance Spectroscopy), which, in agreement with DFT calculations, indicated that the spin density of this complex is partially localized on the Re center but resides mainly on the BDI ligand, with very little spin density on the *cyclo*-P_3 fragment. This explains the observed change of Re-N distance between **169** and **170**.

3. Coordination chemistry of white phosphorus by late transition metals

The coordination chemistry of white phosphorus by late transition metals has attracted considerable attention for almost five decades now, ever since the first examples of rhodium, iridium, or nickel complexes featuring activated or intact P_4 or P_4-derived *cyclo*-P_3 ligands were reported by the groups of Ginsberg [175,176] and Sacconi [69,177] in the early seventies. The range and topology of the reported P_4-derived phosphorus moieties coordinated to late TM has, since then, grown significantly. This chemistry was comprehensively reviewed in the early 2010 by the group of Peruzzini [7], and some updates have also been included in other

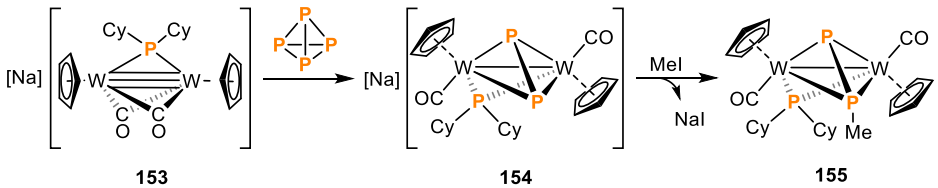

153 154 155

Scheme 48. Reaction of the dinuclear tungsten complex **153** with P_4 and subsequent alkylation with MeI yielding the complex **155**.

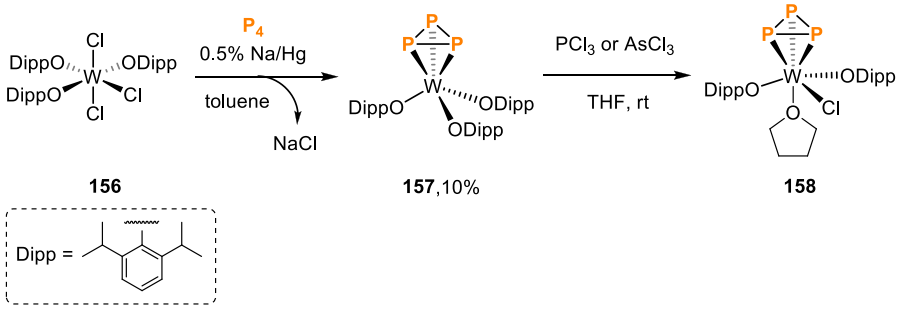

Scheme 49. Reaction of complex **156** with P_4 afforded the neutral complex **157**. Unfortunately, any attempt of further reaction with PCl_3 or $AsCl_3$ gave complex **158** bearing an intact *cyclo*-P_3 moiety.

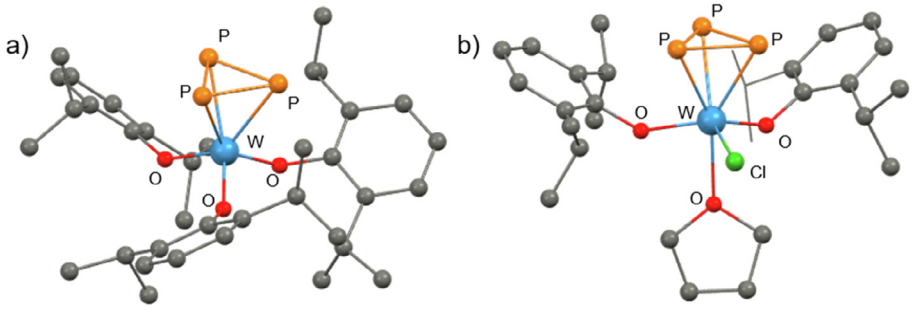

Fig. 46. X-ray structure of a) **157**, and b) **158**. Hydrogen atoms are omitted for clarity; adapted from Ref. [161].

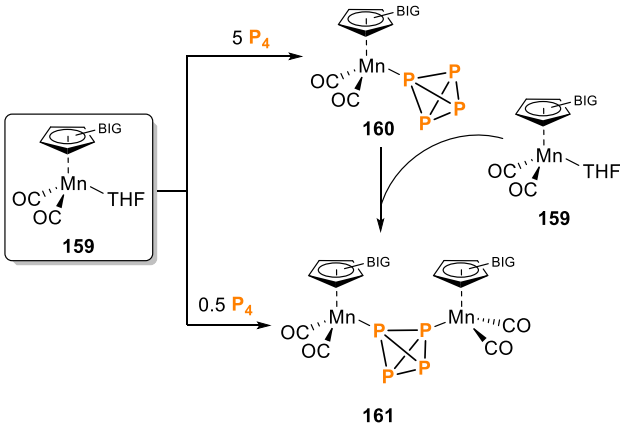

Scheme 50. Synthesis of neutral *tetrahedro*-P_4 complexes **160** and **161**.

reviews [42,43]. Further contemporary (2011–2020) insights in this field are presented herein, with subsections according to the metal groups. In the period under review, significant advances have been made on understanding the activation of the P_4 tetrahedron by late TM, and a variety of phosphorus frameworks have been reported. The reactivity of P_4 towards Earth-abundant metals, such as iron, cobalt, and nickel, has been particularly important, and striking examples have also been reported, for example, with ruthenium, copper, and gold. For the description of the transformations of white phosphorus by late transition-metal complexes, in general, the contributions have been organized according to the degree of degradation/aggregation of P_4 in each case.

3.1. Group 8 metals

Within the late transition metals, group 8 P_4-derived complexes, mainly of iron and ruthenium, account for most of the contributions in the period under review. Regarding iron, remarkable

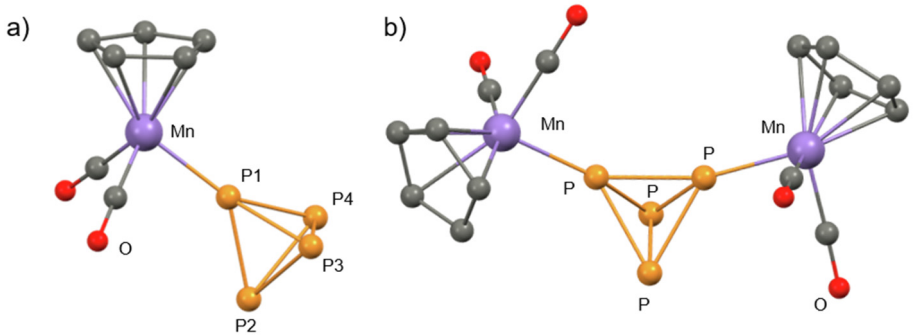

Fig. 47. Molecular structure of compounds a) **160**b) and b) **161**. 4-n-butylphenyl groups on the Cp^{BIG} ligands have been omitted for clarity; adapted from Ref. [162].

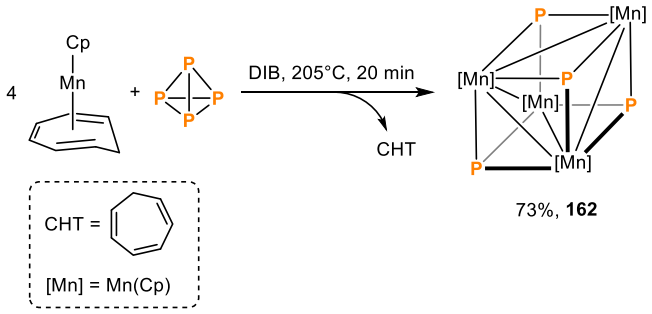

Scheme 51. Synthesis of heterocubane Mn_4P_4 (**162**).

examples include, but not limited to, the synthesis of butterfly-P_4 complexes which have been used as metalloligands to develop a rich coordination chemistry of the tetraphosphorus moiety. Furthermore, different groups have achieved the activation of white phosphorus at iron to form *cyclo*-P_4 or *catena*-P_4 motifs, as well as a variety of aggregates. Whereas the chemistry of ruthenium-P_4 complexes is largely dominated by the coordination of the intact tetrahedron and its hydrolytic functionalization, which contrasts with the stability of the free molecule in water. Osmium complexes of white phosphorus are the least represented within this group. The only example is a study of the behavior in solution, on an NMR timescale, of a compound featuring the intact P_4 tetrahedron in its coordination sphere.

3.1.1. Iron

During the period 2011–2020, an early example of the iron-mediated transformation of P_4 was the catalytic synthesis of phosphates described by Armstrong and Kilian [54]. In this system, P_4 is oxidized to PI_3 and then reacted with phenols under aerobic conditions. While a wide variety of transition-metal compounds were initially evaluated for the reaction, the use of iron(III)-diketonates (**171**, see Scheme 54, top) as catalysts were found to be more efficient, and it was determined that the addition of iodine was required, to generate substoichiometric amounts of PI_3. Remarkably, no acid waste is produced, air is used as a green oxidant, and full conversion to the phosphates with high selectivity was achieved without using chlorine. However, a minimum of 25 mol% catalyst loading was required. It was determined that this high amount of iron catalyst is necessary, since it is involved in at least two key transformations: it favors the formation of the phosphate from $O{=}PI(OPh)_2$ over the possible hydrolysis, and increases the rate of reoxidation of HI to form iodine. From the mechanistic investigations performed in the case of phenol using $Fe(acac)_3$ (**171a**, acac = 2,4-pentanedionate) as a catalyst (Scheme 54, bottom), it was concluded that initial oxidation of P_4 by iodine to form PI_3 is crucial to maintain the catalytic reaction. The nucleophilic substitution of $O{=}PI(OPh)_2$ with phenol to yield the final $O{=}P(OPh)_3$ was found to be the rate-determining step. This system represents a proof of concept of the production of phosphates from P_4 without using PCl_3 as intermediate.

In the period under revision, to the best of our knowledge, only a few examples of iron complexes featuring the intact P_4 tetrahedron as ligands were reported [178,179]. Peruzzini and co-workers have long studied the chemistry of white phosphorus towards transition metal precursors [7,42]. In 2012, this group investigated the fluxional processes in solution of $[L_nM(\eta^1\text{-}P_4)]$ complexes, featuring intact P_4 ligands [178]. Generally, the $^{31}P\{^1H\}$ NMR spectra of such compounds showcase an MQ_3 spin system, in which a doublet and a quartet are observed for the "free" and the metalated P-atoms on the coordinated P_4-tetrahedron, respectively. However, the broadened ^{31}P signals for the tetraphos-

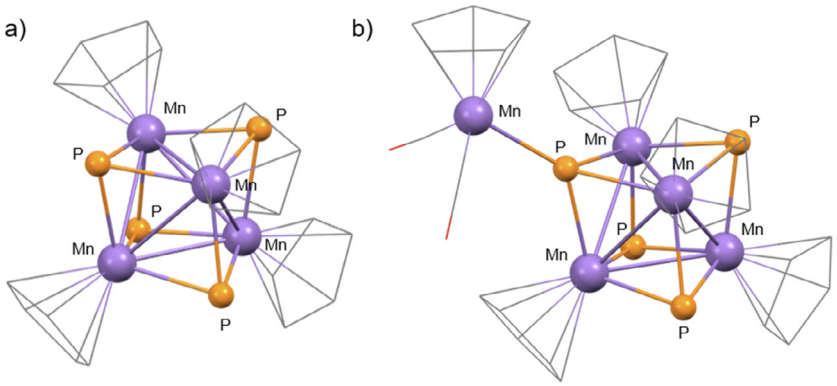

Fig. 48. Molecular structure of a) **162** and b) **163**, highlighting the Mn_4P_4 core. Hydrogen atoms are omitted for clarity; adapted from Ref. [170].

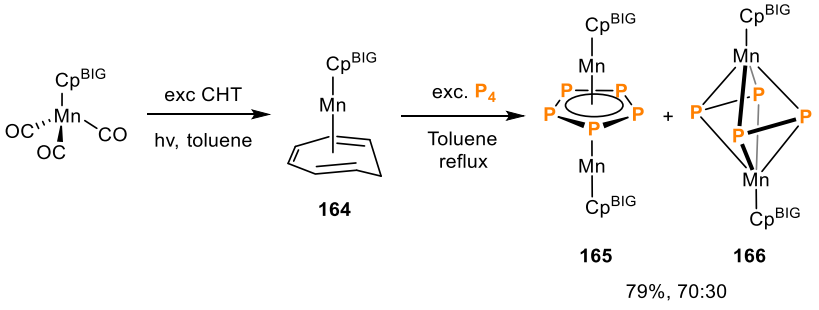

Scheme 52. Synthesis of compounds **165** and **166** from thermolytic activation of P_4 with **164**.

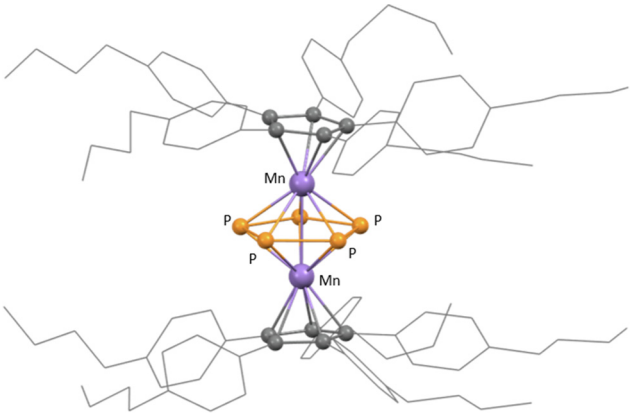

Fig. 49. Molecular structure of **165**. Hydrogen atoms are omitted for clarity; adapted from Ref. [171].

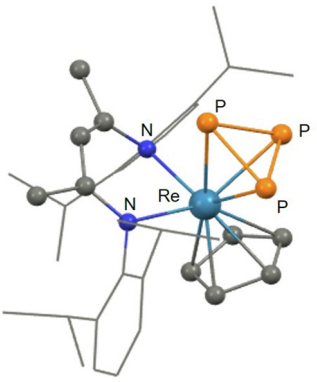

Fig. 50. X-ray structure of **169**. Hydrogen atoms are omitted for clarity; adapted from Ref. [174].

phorus ligand were indicative of fluxional processes, for which a tumbling motion of the P_4-ligand in solution, corresponding to the dynamic $\eta^1 \rightarrow \eta^2 \rightarrow \eta^1$ change in its coordination mode, was proposed. To investigate the nature of such dynamic processes, a series of rhenium [180], iron, ruthenium (see Section 3.1.2) and osmium (see Section 3.1.3) complexes featuring the intact P_4-cage, as well as three bimetallic RuPt species bearing a bridging butterfly-P_4 scaffold (*vide infra*) were studied in solution, by variable-temperature (VT) NMR and $^{31}P\{^1H\}$ exchange spectroscopy (EXSY). The iron complex $[Cp^*Fe(dppe)(\eta^1\text{-}P_4)]^+$ (**172a**, dppe = 1,2-bis(diphenylphosphino)ethane ($Ph_2PCH_2CH_2PPh_2$), Scheme 55) was obtained after reaction of $[Cp^*Fe(dppe)Cl]$ (**173**) with a chloride scavenger, followed by addition of P_4. Such species is analogous to the previously reported monometallic complex $[CpFe(dppe)(\eta^1\text{-}P_4)]^+$ (**172b**, Scheme 55), by the same group [169]. For compound **172a** in solution, the main dynamic process observed at room temperature was the dissociation of the tetraphosphorus ligand. In the $^{31}P\{^1H\}$ EXSY experiment at higher temperatures (T = 45 °C), weak exchange peaks attributed either to thermal activation of the tumbling motion of the coordinated P_4 molecule or multiple P_4 dissociation/coordination processes, were observed. Due to the decomposition of the complex at temperatures higher than 45 °C, it was not possible to determine the activation parameters of the dynamic process in solution [178].

Recently, the group of Krossing reported complexes featuring intact P_4-cages coordinated to iron centers [179]. Unlike the previous examples [169,178], in which electron-rich iron centers coordinate the tetrahedron, the work by Krossing [179] describes the use of the electron-poor fragments $[CpFe(CO)_2]^+$ and $[CpFe(CO)(PPh_3)]^+$ and the effect exerted by them on the bounded P_4-cage. Treatment of the iron precursors [CpFe(CO)(L)Br] (**174**, L = CO, PPh_3) with a strong halide scavenger in the presence of white phosphorus (2 equiv.), afforded the η^1-P_4 containing cationic complexes $[CpFe(CO)(L)(\eta^1\text{-}P_4)]^+$ (L = CO (**175**), PPh_3 (**176**), Scheme 55). An excess of P_4 (2 equiv.) was necessary to prevent the formation of the cationic dimer, $[\{CpFe(CO)_2\}_2(\mu\text{-}Br)]^+$. Their molecular structures (see Fig. 51) demonstrated an important electronic influence, evidenced by the Fe-P bond distance in both complexes: the replacement of the CO ligand with PPh_3 shortened the bond length from 2.209(2) Å in **175** to 2.178(2) Å in **176**. Furthermore, the P-P bond lengths within the cage in both compounds are remarkably shorter (2.144 Å in **175** and 2.133 Å in **176**, average values) than in the free white phosphorus molecule (2.21 Å), which is reflected also in a strong blueshift in the Raman spectra of the complexes. The phenomenon was attributed to the stronger back donation from the iron center to the P_4 ligand in **176** with respect to **175**. On the NMR timescale, a slow exchange of the phosphorus atoms for the P_4 tetrahedron in both complexes was observed, and a correlation between the electron density at the metal and the activation energy of the exchange process was established. Theoretical studies, along with the experimental results indicated that the coordination of the P_4-cage to electron-deficient iron centers, as in **175** and **176**, gives rise to an umpolung in the Fe-P_{cage} bond

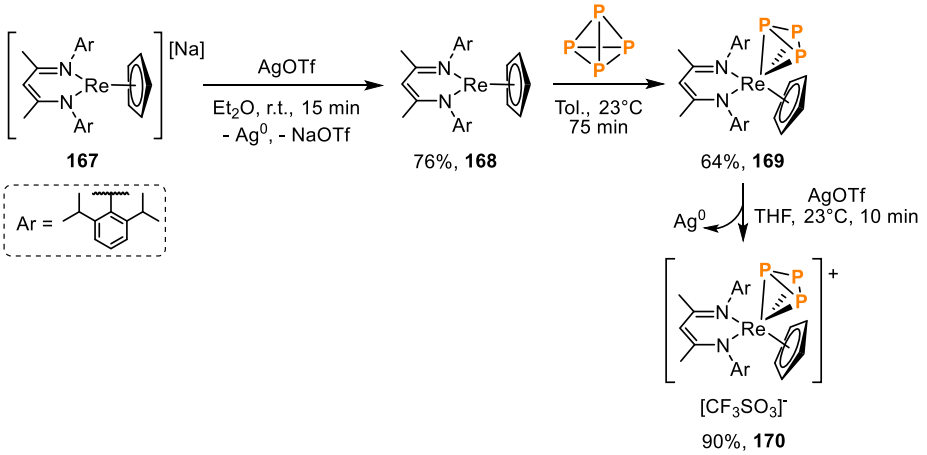

Scheme 53. Activation of P_4 with neutral Re complex **168** and subsequent oxidation with AgOTf.

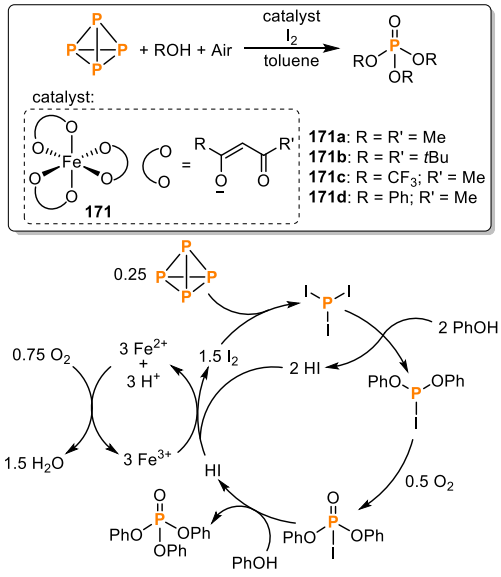

Scheme 54. General reaction for the direct synthesis of phosphates from P_4 mediated by iron(III)-diketonates (top), and proposed catalytic cycle (bottom) [54].

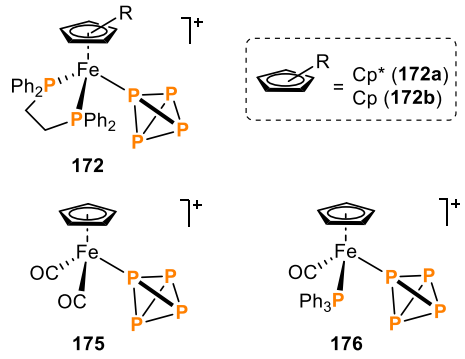

Scheme 55. Monometallic iron complexes featuring an intact P_4 ligand by the groups of Peruzzini (top) [169,178] and Krossing (bottom) [179].

and, thus, such species can be described as phosphonium complexes [179].

The activation of the white phosphorus tetrahedron can lead either to the formation of other P_4 moieties or to its fragmentation/reaggregation. Extensive studies by the group of Scheer have led to a series of P_n ligands, with the most popular being the *cyclo*-P_5 ring that replaces a Cp ligand in [$Cp^RFe(\eta^5\text{-}P_5)$] (**25**). These have been largely used as building blocks in coordination and supramolecular chemistry, in particular after P_n aggregation [129,181–187]. Several groups have agreed that, among the common P_4-activation scaffolds, the first step in the degradation at transition metals is the formation of the tetraphosphabicyclo[1.1.0]butane unit, usually known as a butterfly-P_4 ligand. This framework is obtained after cleavage of one of the P-P bonds in the P_4 tetrahedron.

The reactivity of white phosphorus with the family of iron complexes [$Cp^RFe(CO)_2]_2$ (**177**) has been a matter of interest for over two decades by different research groups [188–194]. Several P_4 activation, fragmentation and reaggregation products, obtained after photolysis, thermolysis and, more recently under ambient conditions, have been showcased. After seminal work by Scherer and co-workers [7,188,189], effort has been devoted to the study of analogous systems which could enable the activation of white

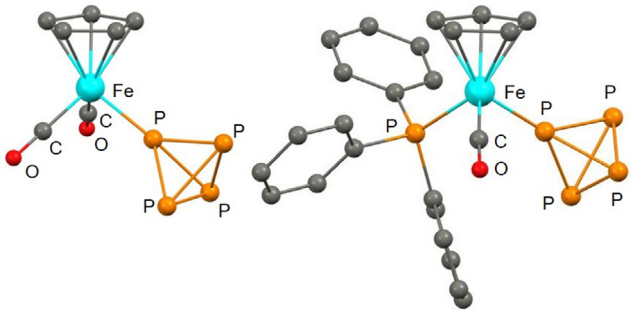

Fig. 51. X-ray structures of complexes **175** (left) and **176** (right), featuring intact P_4 tetrahedron ligands; adapted from Ref. [179].

phosphorus under milder conditions and in more selective pathways. For example, Scheer and co-workers reported the more bulky analogue, [$Cp^{BIG}Fe(CO)_2]_2$ (Cp^{BIG} = *pentakis*(4-*n*-butylphenyl)cyclopentadienyl, **177a**) which activates small molecules such as P_4, As_4, P_4S_3/P_4Se_3 and CS_2 at room temperature [190]. For the E_4 tetrahedra (E = P, As), the reaction proceeds selectively at room temperature, yielding the product of homolytic cleavage (through 17 valence electron (VE) metal-centered radicals) in almost quantitative yield (Scheme 56). The molecular structure of the iron-butterfly-P_4 complex [{$Cp^{BIG}Fe(CO)_2$}$_2$($\mu,\kappa^{1:1}$-P_4)] (**178a**) was determined (Fig. 52). The P-P bond lengths between the "wing tip" P-atoms and the bridgehead ones are within the range of single bonds (2.209 Å and 2.234 Å), and are similar to those in the P_4 tetrahedron, while the bond between the bridgehead atoms is shortened (2.172 Å). Regardless of the stoichiometry or reaction conditions used, it was not possible to further activate the P_4 unit. Heating **178a** in solution led to the formation of [$Cp^{BIG}Fe(\eta^5\text{-}P_5)$] (**25b**) and [($Cp^{BIG}Fe$)$_2$($\mu,\eta^4$:$\eta^4$-$P_4$)] (**179a**). [$Cp^RFe(\eta^5\text{-}P_5)$] (**25**) and [($Cp^{BIG}Fe$)$_2$($\mu,\eta^4$:$\eta^4$-$P_4$)] (**179**) had been previously obtained after thermolysis of **177** in the presence of P_4 at elevated temperatures (T > 190 °C) (Cp^R = Cp^{BIG} [191]; Cp‴ = 1,2,4 tris(*tert*-butyl)cyclopentadienyl (**177b**) [188]). Addition of P_4 to **178a** in solution, before heating, leads to the formation of **25b** and **179a** in the same ratio and yields as before [191]. This indicates that [{$Cp^RFe(CO)_2$}$_2$(μ,κ^1:κ^1-P_4)] (**178**) is the initial product of P_4 activation by Cp^RFe fragments. Furthermore, if **178b** is reacted with yellow arsenic (As_4), an analogous process takes place, yielding the mixed P_nAs_m ligand analogues [Cp‴Fe(η^5-P_nAs_{5-n})] (**25d**) and [{Cp‴Fe}$_2$(μ,η^4:η^4-P_nAs_{4-n})] (**179c**), which were the largest mixed E_n motifs synthesized at the time [192].

The procedure described for **178a** [190], can be extended to the synthesis of other L_nM-butterfly-E_4 [L_nM = $Cp^*Cr(CO)_3$, Cp‴Fe$(CO)_2$; E = P, As)] complexes featuring different Cp^R ligands [193], including the previously reported [{Cp‴$Fe(CO)_2$}$_2$(μ,κ^1:κ^1-P_4)] (Cp‴ = 1,2,4-tri-*tert*-butylcyclopentadienyl, **178b**, Scheme 56) [188]. Irradiation of **178a** with UV light (see Scheme 57**a**) promotes the release of two CO ligands, with selective formation of [{$Cp^{BIG}Fe$}{$Cp^{BIG}Fe(CO)_2$}(μ,η^4:η^1-P_4)] (**180**) [194]. Similar photolytic reactions were carried out on the butterfly-As_4 analogues of **178a** and **178b**, causing rearrangement or reaggregation to form a variety of structural As_n motifs (n = 4–6) in the case of the Cp^{BIG} derivatives [194], and an As_8 *cuneane* tetrametallic structure for the Cp‴ analogue [193].

Further investigations on the reactivity of the iron butterfly compound **178b** include its protonation (Scheme 57**a**) using [(Et_2-O)$_n$H]X (X = BF_4^-, n = 1; [$Al(OC(CF_3)_3)_4]^-$, n = 2) [195]. According to variable temperature (VT) ^{31}P NMR and computational studies, these reactions yielded the compounds [{Cp‴$Fe(CO)_2$}$_2$(μ,κ^1:κ^1-P_4)H]X (**181a**,**b**, X = BF_4^-; [$Al(OC(CF_3)_3)_4]^-$) in which the protonation has occurred at a wing tip P atom. The asymmetrical

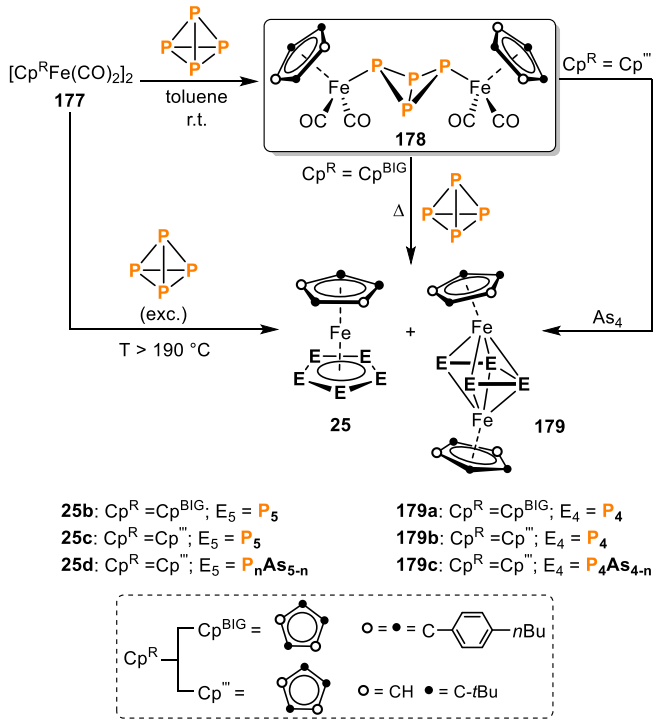

Scheme 56. Activation of P_4 at $[Cp^RFe(CO)_2]_2$ (**177**, $Cp^R = Cp^{BIG}$; Cp‴).

substitution of one P atom in the butterfly-P_4 moiety was confirmed via X-ray crystallography, although a good refinement was not possible due to the inherent poor quality of the crystals. DFT calculations also ruled out the possibility of protonation at a bridgehead P atom.

Scheer and co-workers have developed a rich array of coordination chemistry and reactivity for **178b**, taking advantage of its potential as a bidentate ligand (see Scheme 57**b**). Computational studies (DFT methods at the BP86/def-SVP level of theory) [195] performed on the model complex $[\{CpFe(CO)_2\}_2(\mu,\kappa^1{:}\kappa^1\text{-}P_4)]$ (**178c**) revealed that the position of the filled molecular orbitals should permit a substantial interaction between the wing tip P atoms on the butterfly moiety and a Lewis acid. Furthermore, the LUMO (lowest unoccupied molecular orbital) is located precisely between these wing tip P atoms and, thus, could allow back-bonding from the Lewis acid to the butterfly complex. Depending on the stoichiometry used, the reaction of **178b** with $[Cu(MeCN)_4]BF_4$ (**182**) led to the formation of two different copper complexes containing **178b** as a metalloligand (Scheme 57**b**): the monoadduct $[\{Cp'''Fe(CO)_2\}_2(\mu^3,\kappa^1{:}\kappa^1,\kappa^2\text{-}P_4)\{Cu(MeCN)\}]BF_4$ (**183**, ratio **178b**:Cu^+ = 1:1) and the spiro compound $[\{\{Cp'''Fe(CO)_2\}_2(\mu^3,\kappa^1{:}\kappa^1,\kappa^2\text{-}P_4)\}_2Cu]BF_4$ (**184**, ratio **178b**:Cu^+ = 2:1). The isolation of these complexes confirms that the butterfly-P_4 compound **178b** can coordinate unsaturated metal centers through the wing tip P atoms, and that their spatial proximity enables it to act as a bidentate ligand [195]. Such compounds were fully characterized, including single-crystal X-ray diffraction (see Fig. 53). The effect of the steric bulk of the metalloligand **178b** becomes evident when the Cu-P bond lengths in both complexes are compared. The Cu-P bond distances in these cases are 2.3224(7) Å and 2.2891(6) Å for **183** and in the range of 2.3630(8) Å to 2.4268(8) Å for **184**. Thus, in the monoadduct **183**, the ligand is more tightly bound to the copper center than in the spiro compound **184**. This is due to the reduced steric bulk in the former which enables a closer interaction with the copper metal center. Likewise, the bond distances in **184** are slightly longer than in complexes bearing bidentate phosphine ligands, such as $[(dppe)_2Cu]ClO_4$ (2.259(2) Å–2.301(2) Å; dppe = bis(diphenylphosphino)ethane) [196]. Additionally, in both complexes the Fe-P bond lengths are shorter than in the parent compound **178b** (2.2928(6) Å and 2.2845(6) Å in **183** or 2.3059(8) Å to 2.3380(8) Å in **184** *versus* 2.348(2) Å and 2.355(2) Å in **178b** [188,190]). Small bite angles towards copper were also observed in both cases in the coordinated metalloligand chelate (75.2° in **183** and 72.6° (average) in **184**) [195].

Additional coordination studies of the intact butterfly-P_4 motif were similarly carried out [197]. To investigate the outcome of the reaction with a different transition metal, a less electron rich moiety was selected (Scheme 57**b**). After reaction of **178b** with $[FeBr_2{\cdot}dme]$ (**185**, dme = dimethoxyethane), coordination of the butterfly-P_4 ligand through the wing tip P atoms to the $FeBr_2$ unit occurs, analogously to the previously observed copper(I) complexes **183** and **184**. In the compound obtained, $[\{Cp'''Fe(CO)_2\}_2(\mu_3,\kappa^1{:}\kappa^1,\kappa^2\text{-}P_4)\{FeBr_2\}]$ (**186**), according to the molecular structure determined by XRD (Fig. 54**a**), the $P_{wing\text{-}tip}$-Fe-$P_{wing\text{-}tip}$ bond angle is more acute (70.3°) in comparison to the angles observed for the copper complexes **183** and **184** (*vide infra*). Thus complex **186** is an example of the potential of metalloligand **178b** to act as a small bite angle chelate for different Lewis acids. Surprisingly, the analogous reaction of **178b** with the labile species $[Fe(MeCN)_6][PF_6]_2$

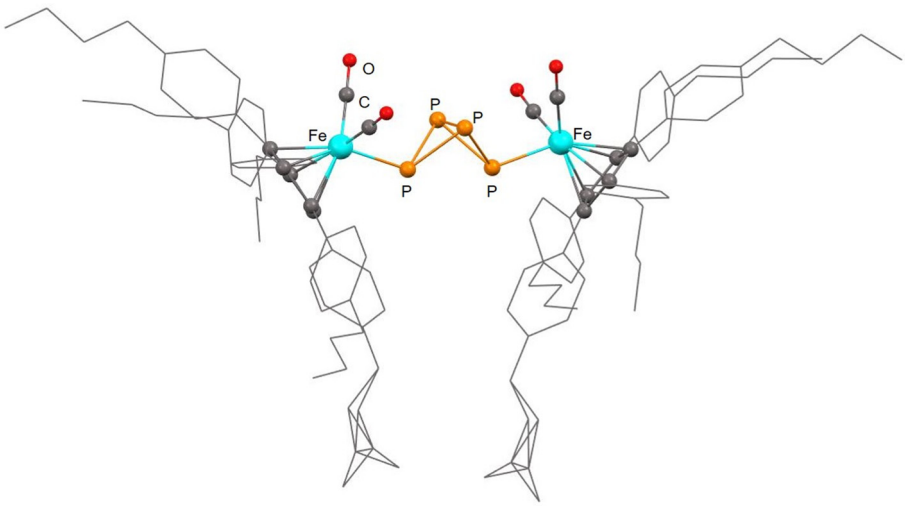

Fig. 52. Molecular structure of **178b**; adapted from Ref. [190].

(**187**) does not yield a monoadduct similar to **183**, but the unprecedented homoleptic-like sandwich complex [{(Cp‴Fe(CO)$_2$)$_2$(μ_3,η^1:η^1:η^4-P$_4$)}$_2$Fe][PF$_6$]$_2$ (**188**) featuring 6π-electrons aromatic (planar) *cyclo*-P$_4$ (P$_4$R$_2$) ligands. These *cyclo*-P$_4$R$_2$ ligands are formed by isomerization, *via* P-P bond scission between the two bridgehead phosphorus atoms of the butterfly unit in **178b**. Currently, such "carbon-free" all-phosphorus sandwich complexes are limited to a single further example: the decaphosphatitanocene dianion [Ti(η^5-*cyclo*-P$_5$)$_2$]$^{2-}$ reported by Ellis and co-workers [198]. The P-P bond distances in the *cyclo*-P$_4$R$_2$ ligands of **188** are in the range of 2.1406 Å to 2.1547 Å, which are between the values of typical P–P single (2.20–2.25 Å) and P–P double bonds (2.00–2.05 Å), as would correspond to such aromatic systems (see Fig. 54**b** for the molecular structure). Compound **188** can also be obtained upon reaction of **186** in the presence of **178b** and TlPF$_6$ (4 equivalents). However, **188** is not the sole product of the reaction. A mixture of compound **188** and the minor species [{Cp‴Fe(CO)$_2$}$_2$(μ_3,η^1:η:^{1}:η^4-P$_4$){Cp‴Fe}]PF$_6$ (**189**), [{Cp‴Fe(CO)$_2$}$_2$(μ_3,κ^1:κ^1,κ^2-P$_4$){Cp‴Fe(CO)}]PF$_6$ (**190**) (Scheme 57**b**) and other side-products, which could not be characterized, was formed. **189** corresponds to an heteroleptic *cyclo*-P$_4$R$_2$ product, while **190** still bears the intact butterfly-P$_4$ scaffold. Compounds **189** and **190** were characterized through single-crystal X ray diffraction (Fig. 54**c-d**, respectively). Complex **189** could be independently synthesized from **178b** in the presence of the dimer [Cp^{R}Fe(μ,Br)]$_2$ (**191a**, Cp^R = Cp‴) and TlPF$_6$ (3 equivalents). The authors highlighted that the stepwise transformation of the butterfly-P$_4$ motif is strongly dependent on the steric hindrance and electronic properties of the Fe-compound used [197].

An isomer of the tetraphosphabutadiene compound **179b**, [Cp‴Fe]$_2$(μ,P$_4$) (**192**), featuring a severely distorted kite-like *cyclo*-P$_4$ unit, was synthesized from the iron-hydride complex [Cp‴FeH$_2$]$_2$ (**193**) and white phosphorus when heated to 100 °C for 10 min (Scheme 58) [199]. The authors highlighted that the path of activation of white phosphorus at a transition metal center with an odd number of electrons should proceed *via* scission of two P–P bonds of the P$_4$-cage, to yield a square-planar *cyclo*-P$_4$ motif, followed by a kite-like distortion, and final disproportionation of such a unit. It was proposed that complex **192** can be considered as a "snapshot" of the disproportionation process into P$_1$ and *cyclo*-P$_3$ units after activation of P$_4$ at Fe(I). Therefore, NMR characterization of **192** showed an A$_2$MX-spin system for the *cyclo*-P$_4$ motif consistent with the mentioned distortion, which persisted in the solid state, according to XRD. Two short (2.13 Å) and two long P–

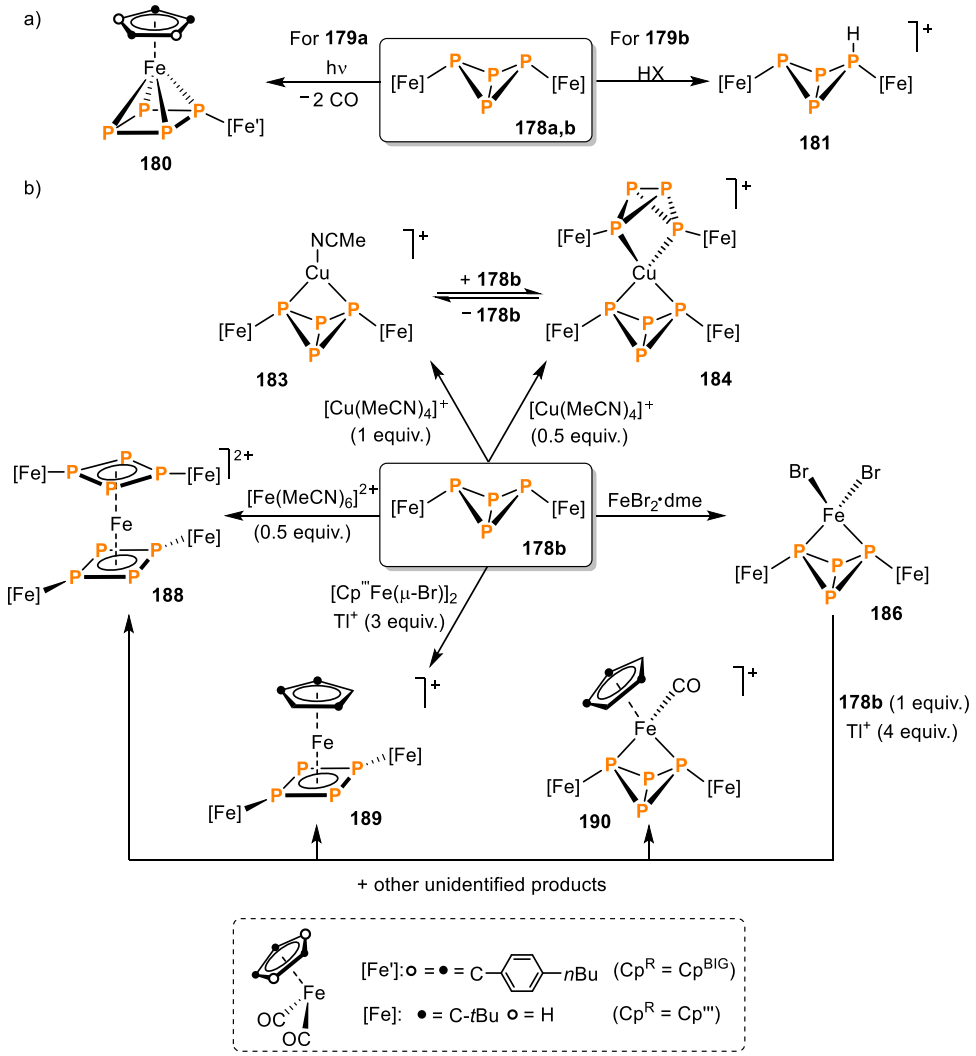

Scheme 57. Reactivity of the iron-butterfly-P$_4$ complexes **178a**,**b**. a) activation of the butterfly-P$_4$ scaffold, b) coordination chemistry of the butterfly-P$_4$ scaffold in **178b** towards Lewis acids.

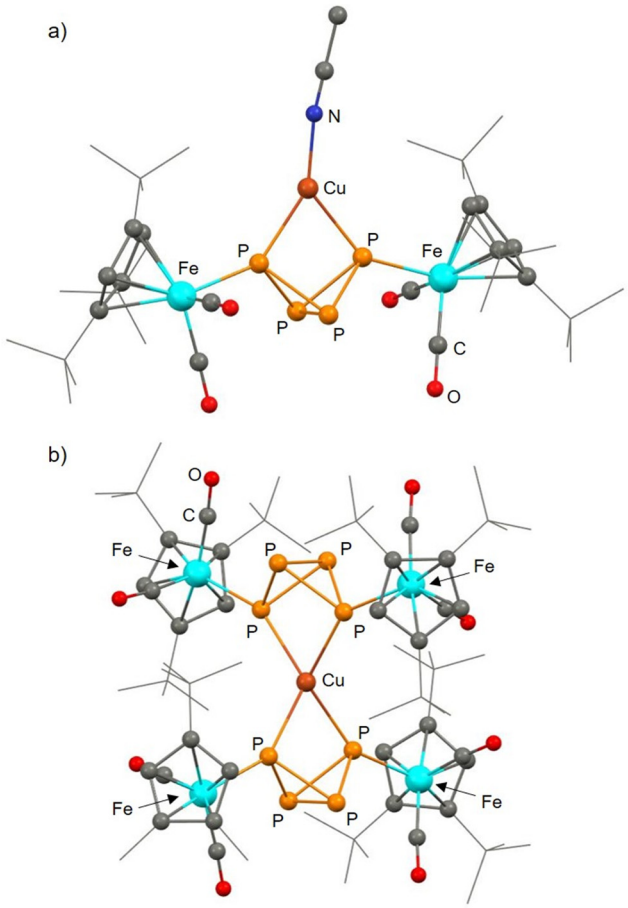

Fig. 53. X-ray structures of complexes a) **183** and b) **184**, featuring the chelating metalloligand **178b**; adapted from Ref. [195].

P distances (2.53 Å) were observed (Fig. 55 shows the molecular structure), with the longer ones in the range of values between single P–P bonds and a van-der-Waals contact. Heating a solution of **192** (75 °C, 7 days) afforded **179b** as major product, along with the phosphaallyl complex $[\{Cp'''Fe\}_2(\mu,\eta^3{:}\eta^3\text{-}P_3)]$ (**194**) and **25d**, as minor product. Thus, the kite-like distorted complex **192** can be considered an intermediate in the formation of **179b** and as a source of P_1 fragments [199].

A butterfly-P_4 scaffold was also accessed *via* the activation of P_4 by Cp^R radicals, mediated by transition-metal species [200]. The one-step synthesis was described by the group of Scheer and gives rise to a variety of $Cp^R_2P_4$ organophosphorus compounds (**195**, Cp^R: $Cp^{BIG} = C_5(4\text{-}n\text{Bu}C_6H_4)_5$, $Cp''' = 1,2,4\text{-}C_5H_2t\text{Bu}_3$, Cp^*, $Cp^{4iPr} = C_5Hi\text{Pr}_4$). While attempting to synthesize the Cp^{BIG} analogue of a species previously assigned as $[Cp^{4iPr}Cu(\kappa^2\text{-}P_4)]$ (**196**) [201], the authors obtained yellow cube-shaped crystals. XRD analysis revealed that the crystals corresponded to the metal-free compound **195a**, in which an edge of the P_4-cage has been cleaved, and two C-P bonds formed. The formation of $\{Cp^{BIG}\}^{\cdot}$ was confirmed through EPR measurements. Attempts to reproduce the reaction with other Cp^R compounds failed, this was attributed to the lack of stabilization of the alkyl substituted Cp^R radicals in comparison to those of Cp^{BIG}. The latter was posited to be a less reactive species, due to its high steric demand and mesomeric stabilization which prevents radical dimerization, allowing it to react with P_4. Since a crucial step in the formation of **195a** is the Cu(I)-mediated oxidation of $\{Cp^{BIG}\}^-$ to $\{Cp^{BIG}\}^{\cdot}$, the use of a more flexible redox system was considered. Therefore, the reaction of $[Cp'''Fe(\mu,Br)]_2$ (**191a**) with P_4 (1 equiv.; Scheme 59**a**) afforded the carbon-substituted butterfly-P_4 compound **195b**, along with the iron complex **179b** and precipitated $FeBr_2$. However, after work up product **195b** was only obtained in a low yield. The product distribution of the isomeric species, together with the presence of $FeBr_2$ provided information on the mechanistic pathway of the reaction and explains the low yield. It was proposed that in solution, **191a** disproportionates into the complex fragments $\{Cp'''Fe^I\}$ and $\{Cp'''Fe^{III}Br_2\}$. Two equivalents of the $\{Cp'''Fe^I\}$ fragment react with one P_4 molecule, thus forming **179b**, featuring a cisoid P_4^{2-} ligand. The two remaining 16 VE $\{Cp'''Fe^{III}Br_2\}$ fragments react with white phosphorus, presumably *via* initial coordination, enabling the transfer of radical $\{Cp'''\}^{\cdot}$ species onto the P_4 molecule to afford product **195b**, and reducing the Fe(III) center to Fe(II) (which precipitated as $FeBr_2$). Further modification of the system to generate the $\{Cp'''Fe^{III}Br_2\}$ fragments from $NaCp'''$ and $FeBr_3$ *in situ* and react them with P_4 (Scheme 59**b**), afforded compound **195b** in better yield without producing **179b**. The scope of this method could be extended to synthesize **195a**, as well as $Cp^*_2P_4$ (**195c**) and $Cp^{4iPr}_2P_4$ (**195d**), thus providing a general route for the transfer of carbon-centered radicals to P_4. Analysis of the molecular structures of compounds **195** revealed that all of them show an *exo-exo* configuration. Careful insight into the NMR data of **195d** also indicated that the chemical shifts observed for such compounds were nearly identical to the ones previously reported for the species assigned as $[Cp^{4iPr}Cu(\kappa^2\text{-}P_4)]$ (**196**) [201]. Furthermore, FD mass spectrometry analysis of the crude reaction mixture using the optimized method showed only the presence of the molecular ion peak of **195d** (45%) and some phosphorus-free $Cp^{4iPr}Fe$ complex fragments. It was concluded that the previous report [201] had mistakenly assigned compound **195d** as the putative copper complex **196**.

In 2017, the group of Lammertsma reported on the coordination chemistry of P_4 towards iron metalates, and their subsequent functionalization [202]. The reactivity of P_4 towards transition metal anions has been much less developed when compared with cations. To generate an anionic Fe-(η^1-P_4) adduct, a bulky nucleophilic metalate was reacted with P_4 and stabilized (trapped) by interaction with Lewis acids, in this case BAr_3 (Ar = C_6F_5, Ph) (Scheme 60). The resulting Lewis acid-stabilized iron complexes $[Cp^*Fe(CO)_2(\eta^1\text{-}P_4)]^-$ (**197**) are the first examples of transition metal generated P_4-butterfly anions and show an unprecedented metalphosphido-borane interaction. Single-crystal X-ray diffraction of complex **197a** (Fig. 56) confirmed the asymmetric substitution on the tetraphosphido moiety, caused by the coordination of the $[Cp^*Fe(CO)_2]$ ($Cp^* = C_5Me_5$) fragment on one side, and the borane on the other. The Fe-P coordination bond in **197a** is slightly shorter than for the previously observed analogous complex $[\{Cp^{BIG}Fe(CO)_2\}_2(\mu,\kappa^1{:}\kappa^1\text{-}P_4)]$ (**178a**) (2.3192 Å vs. 2.3397 Å in **178a**) [190] whilst the P-B bond is longer (2.080 Å) than for organyl-substituted $Li[Mes^*P_4{\cdot}B(C_6F_5)_3]$ (2.064 Å) butterfly-P_4 derivatives [203]. The anionic Lewis acid-stabilized butterfly-P_4 compounds **197** were reacted with $[Me_3NH][BPh_4]$ to prove their utility as nucleophilic reagents, forming initially the intermediate wing-tip protonated species **198**. Driven by the loss of the borane as the amine-borane adduct $Me_3N{\cdot}BAr_3$ (Ar = Ph, C_6F_5), the neutral bicyclo[1.1.0]tetraphosphabutane isomers *exo,endo*–**199** and *exo, exo*-**199** are formed. Calculations indicate that both isomers lie close in energy, and the evidence shows that the phosphanes decompose within 24 h, due to the lack of steric protection.

Figueroa and co-workers described the reactivity of the iron isocyanide complex $Fe(N_2)(CO)_2(CNAr^{Tripp2})_2$ (**200**, Ar^{Tripp2} = 2,6-(2,4,6-(iPr)$_3C_6H_2$)$_2C_6H_3$)) towards different substrates, including P_4 [204]. Treatment of compound **200** with 1 equivalent of white phosphorus led to the clean formation of a product, structurally characterized as the butterfly-P_4 complex $Fe(\kappa^2\text{-}P_4)(CO)_2(CNAr^{Tripp2})_2$ (**201**, Scheme 61). A similar oxidative addition was observed upon reaction, *e.g.*, with molecular hydrogen (H_2), yielding a dihydride complex.

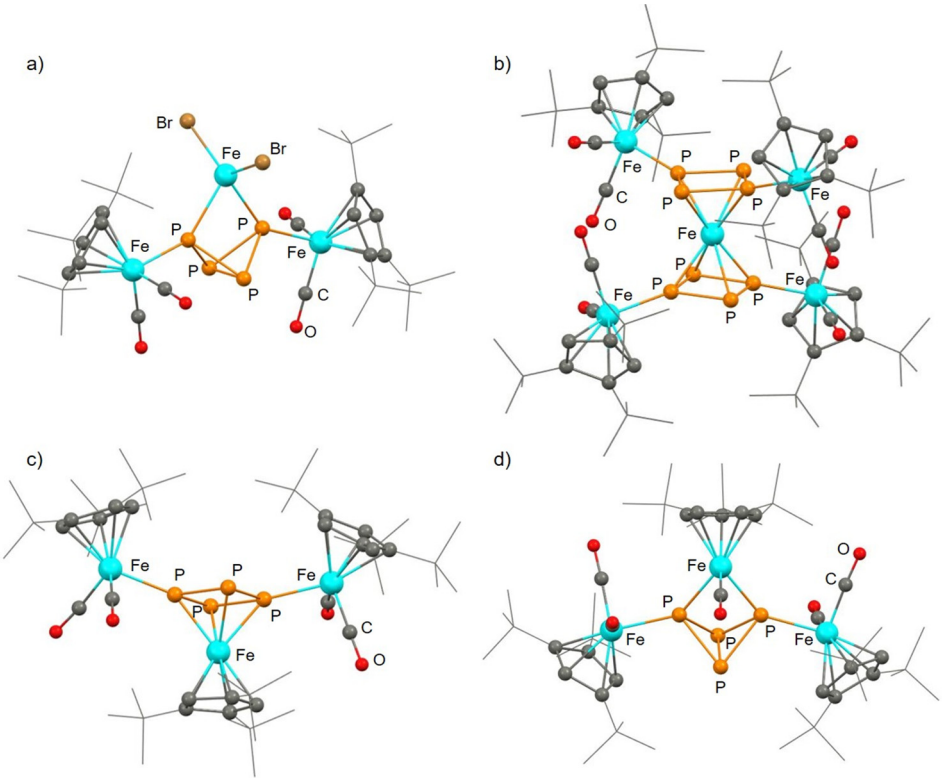

Fig. 54. X-ray structures of a) **186**, b) **188**, c) **189** and d) **190**; adapted from Ref. [197].

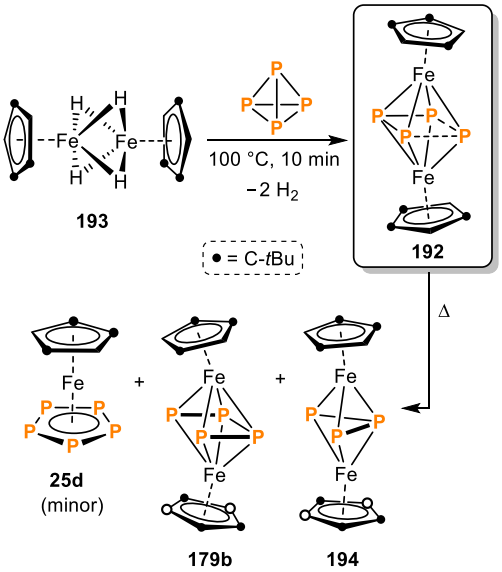

Scheme 58. Synthesis of complex $[Cp'''Fe]_2(\mu\text{-}P_4)$ (**192**), featuring a distorted kite-like *cyclo*-P_4 ligand, and its products after thermic reaction.

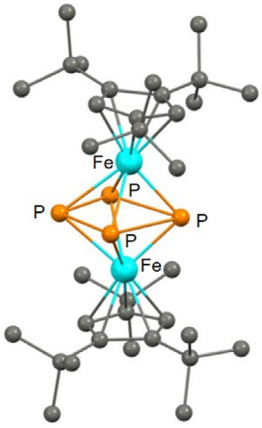

Fig. 55. X-ray structure of **192** featuring a kite-like *cyclo*-P_4 unit; adapted from Ref. [199].

As already discussed, iron complexes with *cyclo*-P_4 ligands obtained after direct activation of white phosphorus, are quite rare, with known examples reported only by the groups of Scheer [197], Mézailles [205] and Wolf [206]. Compounds **188** and **189**, by Scheer and co-workers [197] were obtained from a butterfly-P_4 iron complex, in which the butterfly-P_4 moiety underwent isomerization (*vide supra*). Later, Mézailles and co-workers [205] reported the synthesis of the first stable end-deck *cyclo*-P_4 iron complex $[(^{Ph}PP_2^{Cy})Fe(\eta^4\text{-}P_4)]$ (**202**) and investigated its reactivity towards electrophiles (Scheme 62). Complex **202** can be synthesized either in a one-pot (Scheme 62, path a) or stepwise reaction, reducing the Fe(II) precursor bearing the tridentate phosphine ligand *in situ* (**203**) to generate a coordinatively unsaturated Fe^0 fragment, which is then reacted with P_4 (Scheme 62, path b). The formation of the *cyclo*-P_4 moiety was confirmed through X-ray diffraction (Fig. 57**a**), where an almost perfect square planar configuration of the P_4^{2-} ligand was observed (sum of P-P-P angles equal to 359.99°) with bond distances (2.135(1)–2.166(1) Å) shorter than P-P single bonds (2.21 Å), but longer than typical P=P bonds (*ca.* 2.0 Å). The Mössbauer spectrum is in accordance with an Fe(II) center in a singlet state, and this evidence suggests that the reduction of white phosphorus was promoted by an Fe^0 species (two-electron transfer), thus generating the Fe(II) complex bearing a *cyclo*-P_4^{2-} ligand (**202**) [142]. Additionally, nucleus independent

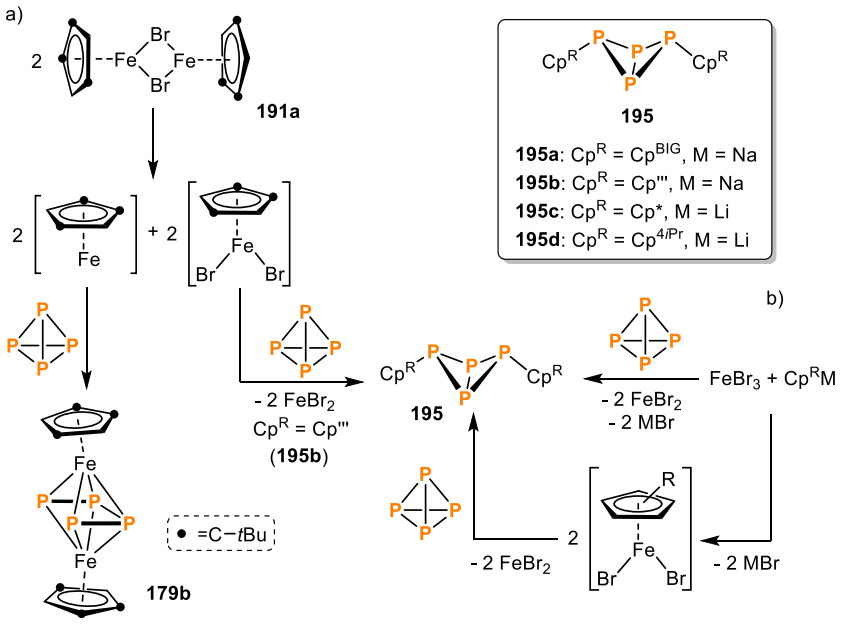

Scheme 59. Synthesis of $Cp^R_2P_4$ via one-step Fe-mediated transfer of carbon-centered radicals: a) Synthesis of **195b** mediated by $[Cp'''Fe(\mu\text{-}Br)]_2$ (**191a**) and b) Optimized synthesis using *in situ* generated $\{Cp'''Fe^{III}Br_2\}$ fragments.

chemical shift (NICS) DFT calculations confirm the aromaticity of the *cyclo*-P_4 moiety. The authors suggest that the coordination of the P_4^{2-} ligand to the Fe center results in its aromatization and constitutes the driving force for the reaction and the reason of the quantitative yield of the complex. The high stability of this species was confirmed through thermal treatment for days, making it a suitable platform for additional functionalization. Thus, the reactivity of **202** towards electrophiles was studied (Scheme 62, bottom). The reaction of **202** with $B(C_6F_5)_3$ in dichloromethane yields the P-borylated Lewis adduct **204**, in equilibrium with the end-deck *cyclo*-P_4 complex. Additionally, **202** reacts with CuCl through P-coordination on the *cyclo*-P_4 ligand, to form a tetrametallic Fe_2Cu_2 complex with two CuCl bridging moieties (**205**). The formation of both P-functionalization products was confirmed *via* X-ray diffraction (Fig. 57**b-c**). Treatment of **202** with $[H(Et_2O)_2][BAr^F_4]$ (BAr^F_4 = *tetrakis*(3,5-bis(trifluoromethyl)phenyl)borate) results in protonation at the metal center (**206**) as opposed to the *cyclo*-P_4 unit.

Wolf and co-workers reported another example of an iron complex bearing a tetraphosphacyclobutadiene (P_4^{2-}) ligand [206]. Upon reaction of $[Cp^RFe(\mu,Br)]_2$ (**191b**, $Cp^R = C_5(C_6H_4\text{-}4\text{-}Et)_5$) with potassium naphtalenide ($K(C_{10}H_8)$, 4 equiv.), followed by addition of P_4 (2 equiv.), $[\{Cp^RFe(\eta^4\text{-}cyclo\text{-}P_4)\}]^-$ (**207**, Scheme 63**a**) forms. This was isolated as a pure, crystalline solid (after addition of 2 equiv. 18-crown-6), albeit in a low yield (4%). Nonetheless, crystals suitable for X-ray diffraction were obtained, and the molecular structure of **207** determined (Fig. 58**a**). As in the example by Mézailles [205], the P-P bond distances (2.1558(6)–2.1722(6) Å) suggest that a delocalized planar P_4-square has been obtained. DFT calculations on a truncated model of **207**, $[(C_5Ph_5)Fe(\eta^4\text{-}cyclo\text{-}P_4)]^-$ (**207′**) reproduced the structure of the former, and analysis of the frontier molecular orbitals suggests a d^6 configuration for the iron center.

During these investigations, Wolf and co-workers [206] also achieved the functionalization of P_4 chains in the coordination sphere of 3d metalate anions for the first time. Reaction of $[Cp^RFe(\mu,Br)]_2$ (**191b**, $Cp^R = C_5(C_6H_4\text{-}4\text{-}Et)_5$) with Na/Hg (exc.) and P_4, instead of yielding the *cyclo*-P_4 compound **207**, led to the new diiron complex $[Na_2(THF)_5\{(Cp^RFe)_2(\mu,\eta^4{:}\eta^4\text{-}P_4)\}]$ (**208**) in moderate yield (67%) (Scheme 63**b**). Compound **208** is highly air sensi-

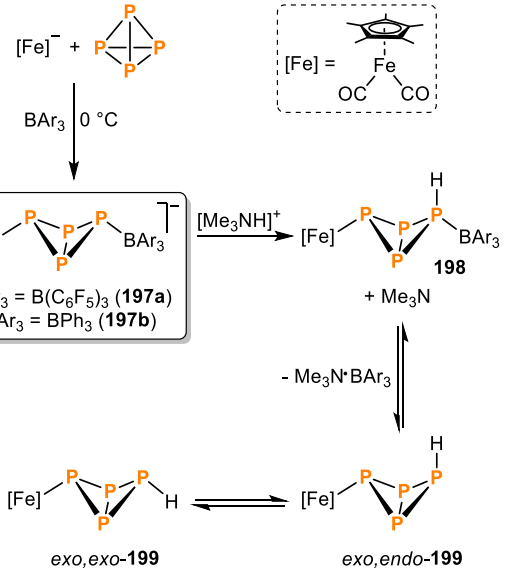

Scheme 60. Synthesis of a Lewis-acid stabilized Iron-butterfly-P_4 complex (**197**) and functionalization (protonation) of the P_4-moiety.

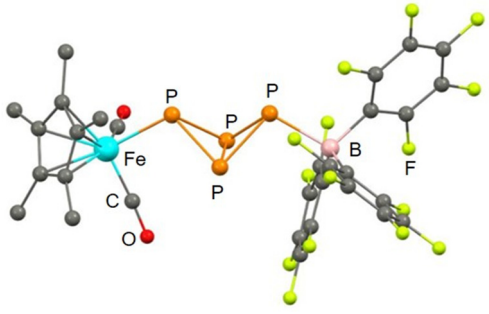

Fig. 56. X-ray structure of the Lewis-acid stabilized complex $[Cp^*Fe(CO)_2\{\eta^1\text{-}P_4\cdot[B(C_6F_5)_3]\}]^-$ (**197a**); adapted from Ref. [202].

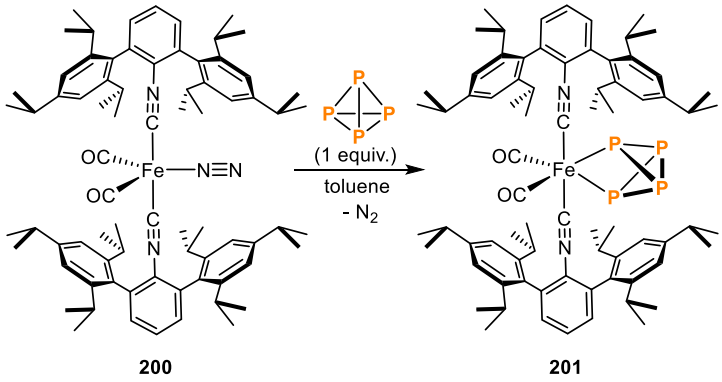

Scheme 61. Synthesis of the Fe-butterfly-P_4 complex Fe(κ^2-P_4)$(CO)_2(CNAr^{Tripp2})_2$ (**201**) by the group of Figueroa [204].

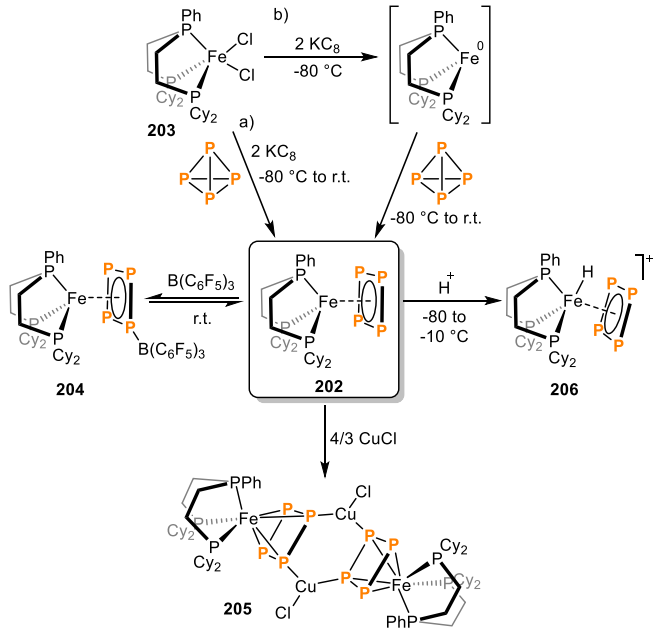

Scheme 62. Activation of P_4 at Fe, and reactivity of the *cyclo*-P_4 ligand towards electrophiles.

tive, decomposing slowly predominately to the protonated ferrate $[Na(THF)_3\{(Cp^RFe)_2(\mu,\eta^4{:}\eta^4\text{-}P_4)(H)\}]$ (**209**) when dissolved in THF. In the structure of **208** (Fig. 58**b**), two P_2 dumbbell units coordinate to the two Cp^R-iron fragments. The molecular structure reveals a weak interaction between these two units, and P-P bonds (P1–P2 = 2.0782(17) Å, P3–P4 = 2.0778(17) Å) shorter than other known compounds. The protonated ferrate **209** can be synthesized, in moderate yields, through the reaction of the diiron compound **208** with one equivalent of $Et_3N{\cdot}HCl$ or $[H(Et_2O)_2][BAr^F_4]$, or even trace amounts of water. Crystallographic (Fig. 58**c**) and spectroscopic investigations show that the proton is highly mobile. Computational optimization indicates that in both of the minimum-energy isomers, the hydride ligand is bridging the iron center and a phosphorus atom in the P_4-chain. Additionally, treatment of **208** with an excess of Me_3SiCl releases the phosphorus scaffold from the iron center and generates a mixture of $P_7(SiMe_3)_3$, $HP(SiMe_3)_2$ and $P(SiMe_3)_3$ in a ratio of 10:1:1. This proves that upon reaction with suitable electrophiles, the functionalized polyphosphido fragments can be liberated from the metal center.

Wolf, Weigand and co-workers reported on the synthesis of heterobimetallic complexes with strongly reduced P_4 ligands [207]. In their approach, a metalate was reacted with the previously reported [208] gallium tetraphosphido complex [(nacnac)Ga(κ^2-P_4)] (**210**, nacnac = CH[CMeN(2,6-*i*$Pr_2C_6H_3$)]$_2$), obtained by reaction of (nacnac)Ga^I with P_4. This methodology has proven useful for the synthesis of iron and cobalt [207,209] (see Section 3.2.1) complexes containing P_n ligands. The subsequent reactions of **210** with bis(anthracene)metalates $[M(\eta^4\text{-}C_{14}H_{10})_2]^-$ [M = Fe (**211**), Co (**212**)] were studied (Scheme 64) [207]. The ferrate [K([18]crown-6)(thf)$_2$][Fe(η^4-$C_{14}H_{10}$)$_2$] (**211**) [210,211], was reacted with **210** in a 1:1 ratio. Due to the labile anthracene ligands, **211** can be considered a source of "naked" Fe^- atoms. Dark crystals of a highly air and moisture sensitive compound were obtained although it could not be isolated in a pure form. However, its molecular structure could be determined by single-crystal X-ray diffraction analysis (Fig. 59), thus confirming the synthesis of [K([18]crown-6){(η^4-$C_{14}H_{10}$)Fe($\mu,\eta^4{:}\kappa^2$-P_4)Ga(nacnac)}] (**213**). The structure features a bridging P_4-chain in which the iron center is coordinated to the four phosphorus atoms, while the gallium center only binds to the terminal phosphorus atoms. The P-P bond distances are shorter than typical P-P single bonds, and the terminal P-P bonds (2.1166 (6) Å and 2.1131(7) Å) are shorter than the internal P-P bond (2.1801(7) Å). The long distance between the terminal atoms (3.5473(6) Å) confirms that the P_4 moiety is coordinated as an open P_4-chain.

Upon degradation of the P_4 molecule, other P_n ligands ($n < 4$) can be obtained. Such fragments can either coordinate to the metal as different structural motifs, or aggregate, giving rise to different P_n topologies. P_n frameworks with $n \geq 5$ are usually the result of the reaggregation of different P_4 degradation products. The fragmentation of P_4 at iron to yield two bridging P_2^{2-} ligands was reported by the group of M. Driess [212]. The β-diketiminato-iron(I) complex [L^0Fe·toluene] (**215a**, L^0 = CH[CHN(2,6-*i*$Pr_2C_6H_3$)]$_2$, see Scheme 65, bottom) activates white phosphorus selectively, affording the iron(III) compound $[(L^0Fe)_2(\mu_2{:}\eta^2{:}\eta^2\text{-}P_2)_2]$ (**216**), which features two dumbbell P_2^{2-} ligands (Scheme 65**a**). The P=P bond distance (2.036(2) Å) observed in the molecular structure of the complex (Fig. 60**a**), confirms the double bond on the dumbbell ligands. One-electron reduction of the dinuclear complex **216** yields the mixed-valence anion $[(L^0Fe)_2(\mu_2{:}\eta^2{:}\eta^2\text{-}P_2)_2]^-$ (**217**) without affecting the structural features of **216**. Mössbauer spectroscopic studies, as well as DFT calculations, indicate that **217** is a rare example of a delocalized mixed-valent iron(II,III) pair.

Scheer and co-workers reported very different results on the activation of P_4 using similar albeit smaller β-diketiminato-iron(I) complexes (see Scheme 65**b**) under the same reaction conditions [213]. While Driess and co-workers found that complex **215a** cleaves the P_4 molecule to form two P_2 units (Scheme 65**a**) [212], the analogous compounds **215b**-**215d** react with P_4

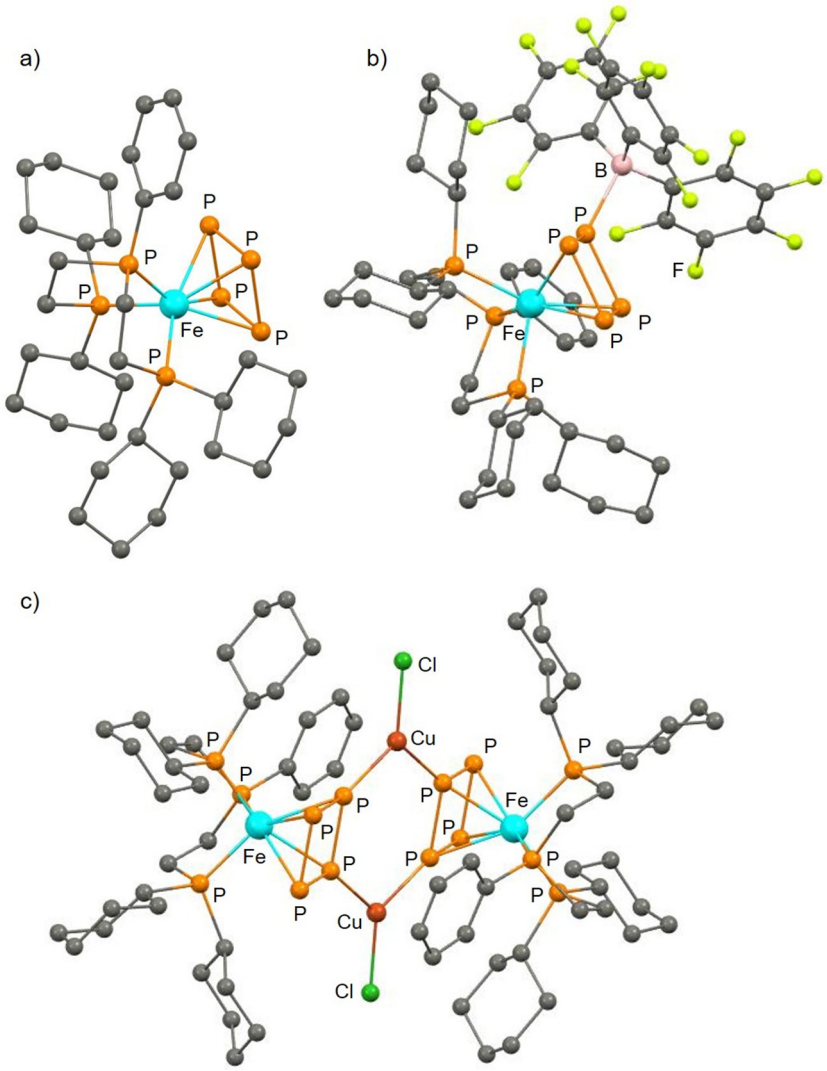

Fig. 57. X-ray structures of a) **202** and its Lewis adducts b) **204** and c) **205**; adapted from Ref. [205].

(Scheme 65**b**) to yield either tetranuclear [(LFe)$_4$(μ_4,κ^2:κ^2:κ^2:κ^2-P_8)] (L = L^1 (**218a**), L^2 (**218b**)) complexes, featuring a realgar-type P_8 structural motif or the *cyclo*-P_4 dinuclear compound [(L^3Fe)$_2$(μ,η^4:η^4-P_4)] (**219**). According to DFT calculations, the dimerization of the hypothetical species [(L^1Fe)$_2$(μ,η^4:η^4-P_4)] should be endothermic, but analysis of the stability of the spin states of the complex and dimeric product, as well as the natural population analysis (NPA), indicate the presence of Fe(II) centers and a P_8^{4-} ligand scaffold. XRD of complexes **218** (Fig. 60**b**) revealed that in the P_8^{4-} ligand the P-P bonds lie within the typical single P-P bond distances, and that the Fe(II) centers reside on a distorted tetrahedral geometry. Hence, it was found that even small changes to the nature of the flanking groups on the β-diketiminato ligands have a profound effect on the type of P_4-activation product obtained. The ligands featuring dimethylphenyl substituents afforded the tetranuclear-P_8 products, **218**, whereas complexes **216** and **219** only form when the substituent on the ligands is the more sterically demanding diisopropylphenyl (dipp). Remarkably, the effect of the α-substituents on the backbone of the β-diketiminato ligand on the activation of P_4 was also demonstrated, since **216** features two separated P_2^{2-} units [212], whilst **219** bears a planar *cyclo*-P_4 motif (Fig. 60**c**). Such an outcome was attributed to the additional steric influence of the Me groups, which tend to push the dipp substituents closer to the metal center affecting the distances between the iron(II) centers [213].

In a collaboration between the groups of Peruzzini and Scheer, the reactivity of manganese and ruthenium complexes featuring coordinated intact P_4-tetrahedra towards low-valent β-diketiminato iron and cobalt compounds was described [81]. Among these were **215c** and its cobalt congener [L^2Co·toluene] (**220a**) (L^2 = CH[CHN(2,6-$Me_2C_6H_3$)]$_2$; Scheme 66). The selective cleavage of two P-P edges from the P_4 moiety in the previously described compound [{Cp^{BIG}Mn(CO)$_2$}$_2$(μ,k^1:k^1-P_4)] [**161**, Cp^{BIG} = $C_5(C_6H_4nBu)_5$), see Section 2.5.1] by such β-diketiminato compounds, led to the formation of the π-delocalized P_4^{2-} complexes [{Cp^{BIG}Mn(CO)$_2$}$_2${ML^2}(μ,η^1:η^1:η^4-P_4)] [M = Fe (**221**), Co (**222**)] (see Fig. 61 for the molecular structures of the complexes). This study becomes particularly interesting since the differences or similarities in reactivity between the free and coordinated P_4 molecule can be examined directly. In its reactivity towards the β-diketiminato complexes, the P_4 ligand in **161** behaved analogously to the free P_4 tetrahedron, forming *cyclo*-P_4 moieties. For **221**, the effective magnetic moment (Evans method), along with EPR and ^{57}Fe Mössbauer measurements, suggested the presence of a low-spin iron(III) center with one unpaired electron. Cobalt complex **222** is diamagnetic and features an A_2X_2 spin system in the ^{31}P

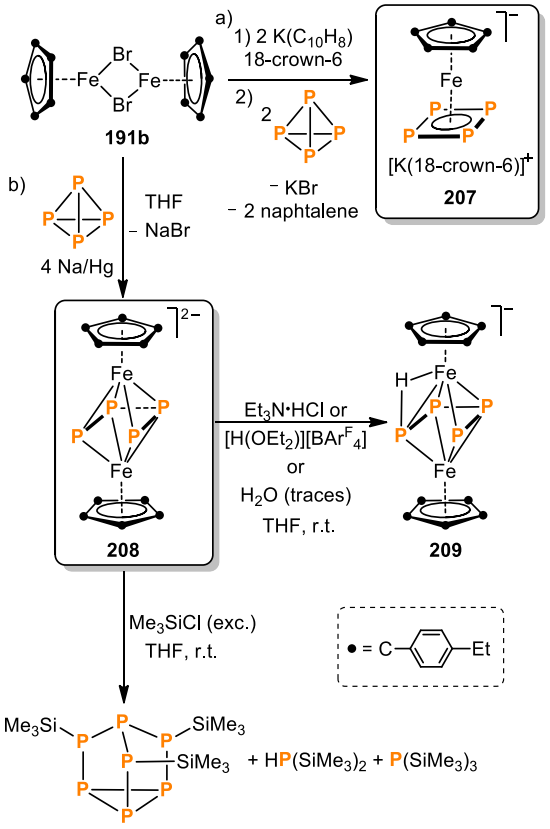

Scheme 63. Synthesis of a) $[\{Cp^{R}Fe(\eta^4\text{-}cyclo\text{-}P_4)\}]^-$ (**207**, $Cp^R = C_5(C_6H_4\text{-}4\text{-}Et)_5$) and b) a dinuclear ferrate bearing a bridging P_4 chain ligand, and its subsequent functionalization with electrophiles, by Wolf and co-workers [206].

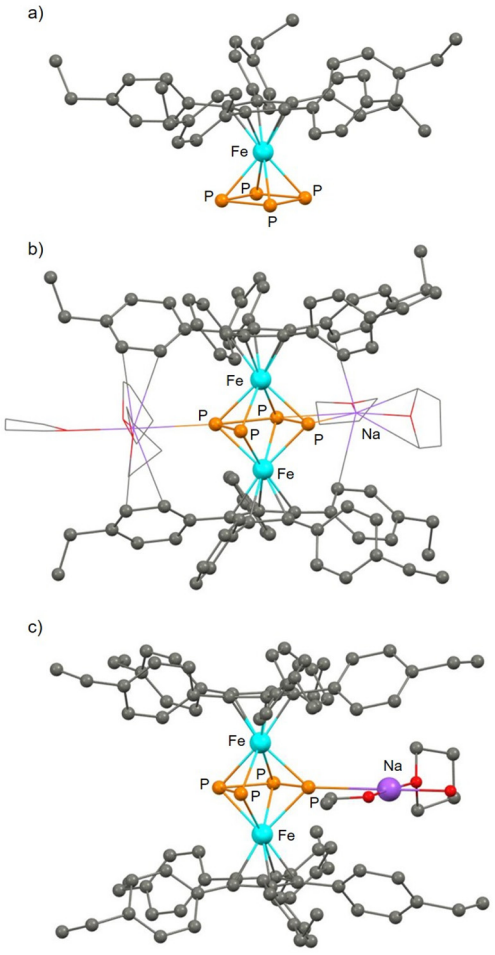

Fig. 58. X-ray structures of a) **207**, b) **208** and c) **209**; adapted from Ref. [206].

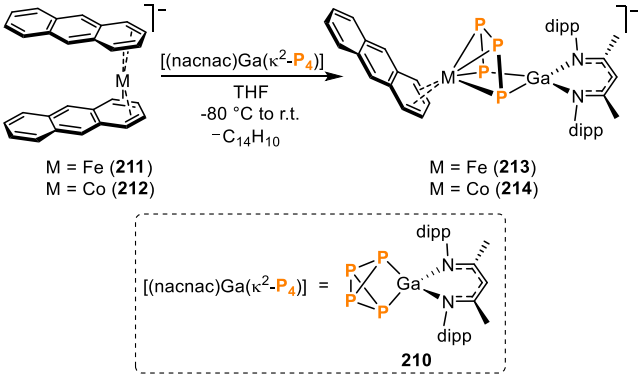

Scheme 64. Synthesis of the heterobimetallic anionic complexes $\{(\eta^4\text{-}C_{14}H_{10})M(\mu,\eta^4{:}\kappa^2\text{-}P_4)Ga(nacnac)\}^-$ [M = Fe (**213**), Co(**214**)].

{^{1}H} NMR spectrum. It was suggested that, unlike similar systems (*c.f.* complex **219**) [213], the formation of bimetallic inverted sandwich compounds with polyphosphorus middle-decks was prevented in this case by the $[Cp^{BIG}Mn(CO)_2]$ fragments bonded to the *cyclo*-P_4 ligand.

Another example of metal-mediated fragmentation-reaggregation of P_4 with anionic iron complexes, is the formation of iron polyphosphides described by the Wolf group [214]. By reacting the anionic iron complex $[K(18\text{-crown-}6)\{Cp^*Fe(\eta^4\text{-}C_{10}H_8)\}]$ (**223**) with P_4 (Scheme 67), two major products were obtained by fractional crystallization, in low to modest yield. These compounds corresponded to P_4 fragmentation and aggregation products, namely the mononuclear complex $[K\{([18]\text{-crown-}6)\}_2(Cp^*Fe(k^2\text{:}k^2\text{-}P_7)]$ (**224**) and the anionic cluster $[K([18]\text{-crown-}6)(thf)_2][(Cp^*Fe)_3(\mu,k^2\text{:}k^2\text{-}P_3)_2]$ (**225**). The molecular structures (Fig. 62) of these compounds show a P_7 norbornadiene-like framework in **224** and two *cyclo*-P_3 units in cluster **225**. Computational as well as spectroscopic studies correlate well with the findings from XRD.

Of the common P_n ligands ($n \geq 5$) formed by aggregation of different P-units, the *cyclo*-P_5 scaffold has attracted particular attention. Due to the isolobality between the C–H moiety and the phosphorus atom, the *cyclo*-P_5 motif can be viewed as an analogue of the cyclopentadienyl ligand. The coordination and supramolecular chemistry of the *cyclo*-P_5 ligand towards iron has been extensively investigated by Scheer and co-workers, particularly the family of pentaphosphaferrocene compounds [129,181–187]. However, in this review we will only summarize the reactivity of this class of compounds towards nucleophiles [215–218] and its redox chemistry [219]. For supramolecular assemblies featuring pentaphosphaferrocenes, see Refs. [129,181–187].

Scheer and co-workers studied the reactivity of the pentaphosphaferrocene compound $[Cp^RFe(\eta^5\text{–}P_5)]$ ($Cp^R = Cp^*$, **25a**) towards different main-group nucleophiles [215]. Although the reactivity was dependent on the specific nucleophile used, in general, an unprecedented functionalization of the *cyclo*-P_5 motif to generate η^4-P_5 ferrate complexes was observed. Upon reacting **25a** with $LiCH_2SiMe_3$ or $LiNMe_2$ (Scheme 68**a**), formation of the mononuclear ferrate complexes **226** was reported, whereas the analogous reaction with $NaNH_2$ yielded the dinuclear species **227** (Scheme 68**b**). A mixture of **226c** and **227b** was obtained after

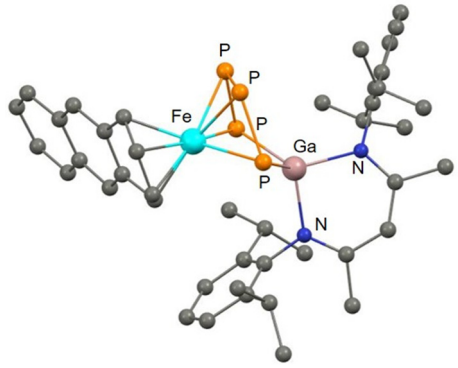

Fig. 59. X-ray structure of the anionic complex **213**; adapted from Ref. [207].

reaction with $LiPH_2$, with the latter being a by-product. The ^{31}P NMR spectra of complexes **226a** and **226b** shows an AMM′XX′ spin system for the *cyclo*-P_5 moiety. The envelope conformation of the η^4-P_5 ligand was confirmed through crystal structure analysis of **226a** (Fig. 63**a**). The four P-atoms in the η^4-P_5 unit are nearly planar, with bond distances in the order of P-P double bonds (2.130 Å–2.162 Å). The molecular structures of the dinuclear complexes **227** were also confirmed through XRD (see Fig. 63**b** for the structure of **227b**).

In a collaboration between the groups of Scheer and Roesky [216], **25a** was reacted with low-valent silicon compounds of differing steric encumbrance. Upon treatment with (N-N)SiCl (3 equiv., N-N = $PhC(NtBu)_2$, see Scheme 68**c**), selective substitution of a P-atom and insertion of the silicon fragment into the all-phosphorus ring was evidenced through the formation of [Cp*Fe{η^4–P_4Si(N-N)}] (**228**) containing the first example of a silatetraphospha-cyclopentadienyl ligand (molecular structure shown in Fig. 63**c**). This was formed alongside the functionalized phosphasilene species **229** (Fig. 63**d**). It was proposed that **228** is obtained from an intermediate [Fe](η^4-P_5)Si(N-N)(X) (**230a**, [Fe] = Cp*Fe, X = Cl) similar to **226**, which could not be isolated. $^{31}P\{^1H\}$ VT-NMR experiments indicate that the substituted *cyclo*-P_5 intermediate species **230a** is formed at −70 °C. To further investigate this species, **25a** was treated with the bulkier (N-N)Si(N$(SiMe_3)_2$) (1 equiv., N-N = $PhC(NtBu)_2$) bearing the less labile N$(SiMe_3)_2$ group, affording the Si-substituted η^4-P_5 compound **230b** as structural proof of such a reaction intermediate (Scheme 68). Crystal structure analysis of compounds **228** and **230b** confirmed the transformation of the *cyclo*-P_5 ring in both cases (Fig. 63**c,e**). Additionally, the reaction of **25a** with the Si(I) [(N-N)Si–Si(N-N)] compound (ratio **25a**:Si(I) compound = 1:1) affords complex [Cp*Fe{η^4–P_5[Si(N-N)]$_2$}] (**231**), which is the product of double ring expansion of the *cyclo*-P_5 ring, thus generating a *cyclo*-Si_2P_5 ring. The solid state structure of **231** (Fig. 63**f**) confirms the formation of this seven-membered ring. Along with **231**, complex **228** and the previously reported compound [(N-N)$_2Si_2P_2$] (**232**) [217] were detected as by-products. The authors highlighted **231** as the largest structurally characterized coordinated silicon–polyphosphorus ring. This Si_2P_5 ring is analogous to the tropylium anion [216].

Scheer and co-workers also studied the iodination of the pentaphosphametallocenes [$Cp^RM(\eta^5$–$P_5)$] [Cp^R = Cp*; M = Fe (**25a**), Ru (**233**)] as a possible method for the formation of P-I cages [218]. By reacting the corresponding pentaphosphametallocene with iodine (Scheme 69), complexes of the general formula [Cp*M(k^3-P_6I_6)]X [M = Fe, X = I (**234a**); M = Fe, X = $(I)_{0.5}(I_3)_{0.5}$ (**234b**); M = Ru, X = I (**235**)] were obtained. Each complex contained a MP_6 moiety reminiscent of the common nortricyclane anion, P_7^{3-}. The P-P bond lengths in the three compounds lie in the range of single bonds (2.160 Å–2.281 Å). When **25a** was reacted with an excess of I_2 (9 equiv.), in addition to **234b**, PI_3 is

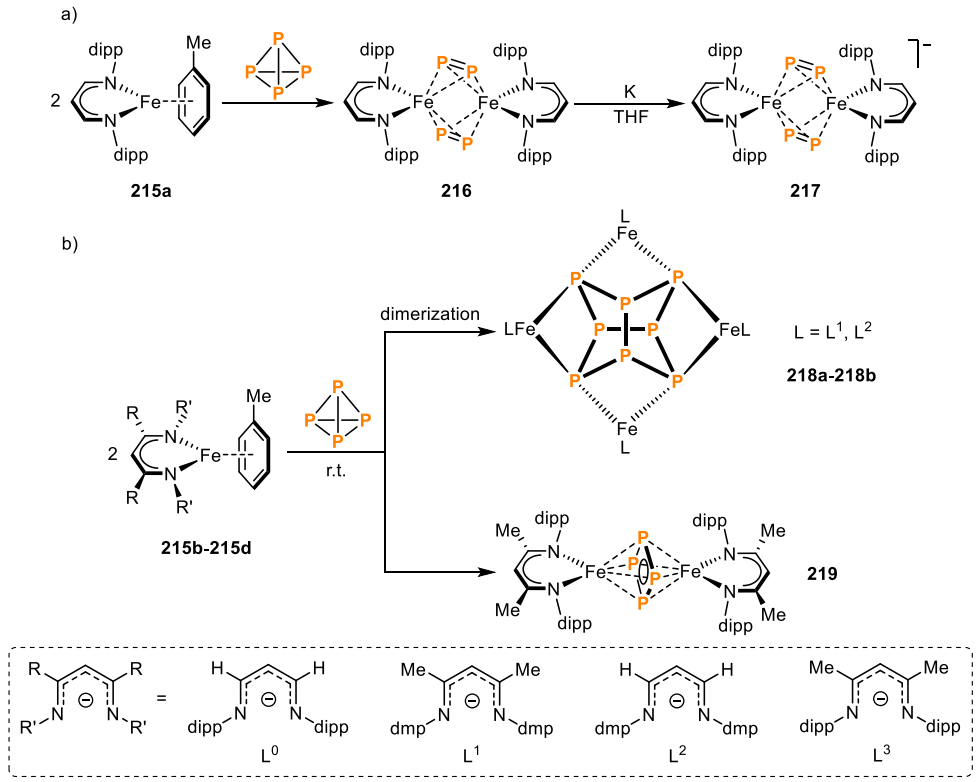

Scheme 65. Activation of P_4 at Fe(I)-β-diketiminato complexes.

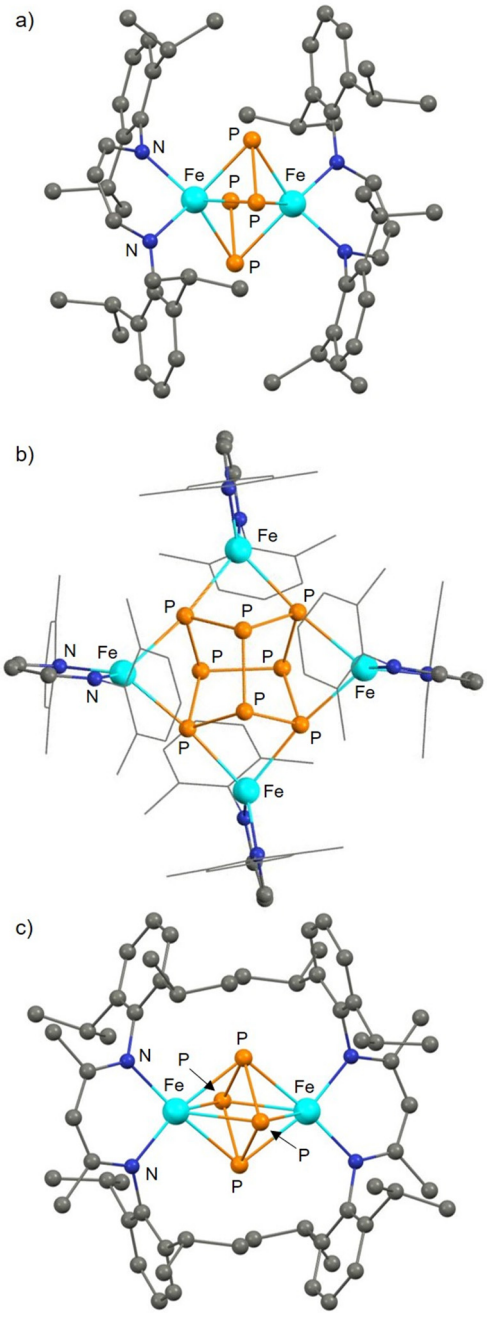

Fig. 60. X-ray structures of selected β-diketiminato-iron complexes featuring a) P_2, b) P_8 and c) *cyclo*-P_4 ligands derived from P_4, by the groups of Driess and Scheer; adapted from Refs. [212,213].

obtained. Due to the low solubility of **234a**/**b** in most conventional organic solvents, the more soluble [$Cp^{BIG}Fe(\eta^5\text{-}P_5)$] (**25b**) was screened as a starting material. However, when **25b** was treated with I_2, only the selective formation of PI_3 was observed. When **234a** was dissolved in MeOH a reaction occurred, affording [$Cp^*Fe\{k^3\text{-}P_6(OMe)_6\}$]X (**236**, Scheme 69), according to the ESI-MS and $^{31}P\{^1H\}$ NMR spectra, and MeI, as proposed by the authors. The formation of **236** is accelerated when the reaction is carried out in the presence of NaOMe, but the procedure is less selective. Attempts to react the metallo-nortricyclane complexes with a variety of nucleophiles or reducing agents were unsuccessful. The oxidation of the pentaphospharuthenocene compound **233** with iodine also resulted in an aggregation process, yielding the analogous metallo-nortricyclane complex **235** (Scheme 69).

A rich redox chemistry with pentaphosphaferrocene complexes (**25**) has also been developed [219]. A study [220] of the frontier orbitals of **25** revealed that for the pentaphosphaferrocene, strong contributions of the P atoms in the HOMOs, and metal as well as phosphorus contributions in the LUMOs are expected. This in in contrast with its carbonaceous analogue ferrocene, in which the redox chemistry is mainly metal-centered. Thus, for pentaphosphaferrocene redox reactions give rise to structural changes with participation of P atoms. Scheer and co-workers [219] were able to isolate and characterize the dicationic species [$(Cp^*Fe)_2(\mu,\eta^4\text{:}\eta^4\text{-}P_{10})]^{2+}$ (**237**), and the dianionic species [$(Cp^*Fe)_2(\mu,\eta^4\text{:}\eta^4\text{-}P_{10})]^{2-}$ (**238**) and [$Cp^*Fe(\eta^4\text{-}P_5)]^{2-}$ (**239**) after reaction of **25a** with a range of oxidizing or reducing reagents (Scheme 70). The structural features of complexes **237**–**239** were determined through XRD (see, for example, Fig. 64**a** for the structure of **237**). The results of this work highlight the differences in reactivity between ferrocene and **25a**. While ferrocene mainly shows iron-centered redox behavior, pentaphosphaferrocene exhibits an iron-centered behavior strongly coupled with the P-atoms. Thus, tilted $\eta^4\text{-}P_5$ motifs are obtained, and these can dimerize to yield P_{10} moieties, although essentially retaining the structure at the metal center upon oxidation or reduction. The anionic products **238** and **239** were reacted with P_4, yielding norbornadiene-like polyphosphorus compounds (P_7 units), including the previously reported **224** [214] and the P_{14} species **240** (Scheme 70**b**). By using this procedure, compound **224** was obtained in almost quantitative yield. Similarly, with **240** the P_{14} ligand can be described as two P_7 cages linked through the apical P-atom, as evidenced from its molecular structure (Fig. 64**b**). The $^{31}P\{^1H\}$ NMR of **240** shows signals that indicate chemical non-equivalence of the P-atoms directly coordinated to the iron centers [219].

The group of Mézailles described the synthesis of iron phosphide nanoparticles, which were obtained from *in situ* generated iron nanoparticles (using $Fe(CO)_5$ (**241**) as Fe(0) source) in the presence of white phosphorus [221]. The preferential formation of crystallized FeP (**242**) hollow nanoparticles was reported, upon heating amorphous non-hollow FeP nanoparticles at 250 °C. By using the theoretical exact stoichiometry (Fe/P = 2), or even lower amounts of white phosphorus (Fe/P = 4), either the Fe_2P (**243**) phase could not be obtained or nonpure Fe_2P hollow double-shell nanoparticles were formed, respectively. The authors indicated that the formation of Fe_2P may be possible by using an amorphous Fe–P intermediate in P-poor systems.

3.1.2. Ruthenium

The coordination of intact P_4-cage to ruthenium centers [178,222–228], as well as its subsequent functionalization via hydrolytic methods [222–227] has dominated the P_4 chemistry of this metal, during the period under review.

In 2011, Peruzzini and co-workers described the dynamic behavior of P_4 ligands coordinated to ruthenium [222]. By reacting either the Ru(II) precursor *trans*-[$Ru(dppm)_2(H)(\eta^2\text{-}H_2)]BF_4$ (**244**, dppm = $Ph_2PCH_2PPh_2$) [222] or [$Ru(dppm)_2(H)_2$] (**245a**) with $HBF_4\cdot Et_2O$ in CH_2Cl_2 in the presence of white phosphorus [178], the cationic complex *trans*-[$Ru(dppm)_2(H)(\eta^1\text{-}P_4)]^+$ (**246a**) was obtained (Scheme 71**a**). Single-crystal XRD confirmed the η^1-coordination of the P_4 tetrahedron (Fig. 65**a**), which was located *trans* to the hydride ligand in the octahedral Ru(II) center. VT $^{31}P\{^1H\}$ along with $^{31}P\{^1H\}$ EXSY NMR experiments indicated that, in solution, the P_4 ligand in complex **246a** rotates freely about the $Ru\text{-}P_{cage}$ bond. This process renders the four phosphorus atoms in the P_4 cage equivalent at room temperature. Complex **246a** reacted with [$(C_2H_4)Pt(PPh_3)_2$] (**247**) in CH_2Cl_2, affording the heterobimetallic compound [{$Ru(dppm)_2(H)$}($\mu,\kappa^1,\kappa^2\text{-}P_4$){$Pt(PPh_3)_2$}]$BF_4$ (**248a**) in quantitative yield. Complex **248a** is the product of inser-

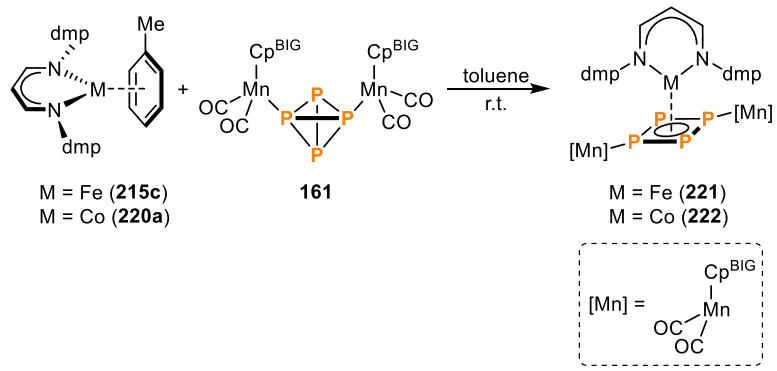

Scheme 66. Activation of P_4 at a Mn-coordinated P_4 ligand.

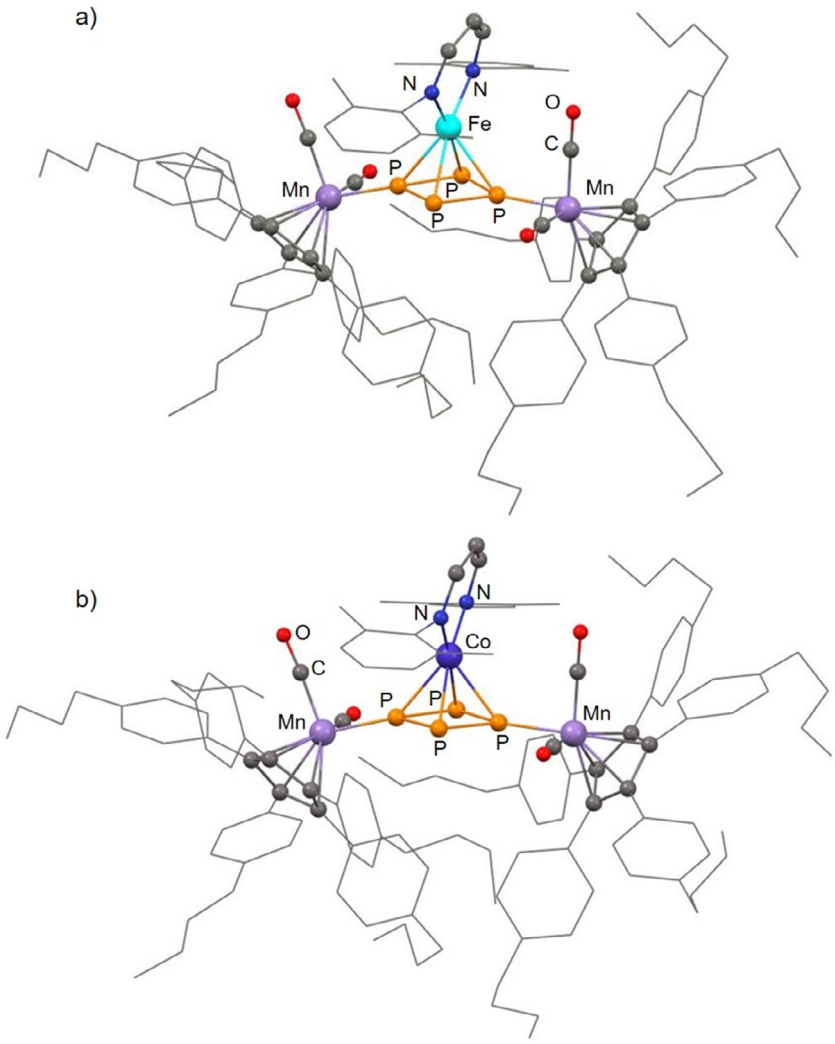

Fig. 61. Molecular structures of $[\{Cp^{BIG}Mn(CO)_2\}_2\{ML^2\}(\mu,\eta^1{:}\eta^1{:}\eta^4\text{-}P_4)]$ [a) M = Fe (**221**), b) M = Co (**222**)]; adapted from Ref. [81].

tion of the $[Pt(PPh_3)_2]$ fragment into one of the basal P-P bonds of the Ru-coordinated P_4 tetrahedron [222].

The study of the dynamic P_4 cage behavior in solution was then extended to other $Ru(\eta^1\text{-}P_4)$ complexes [178]. Compound **246b**, featuring the bidentate ligand dppe and the bimetallic RuPt complex **248b**, were synthesized by a procedure similar to the one previously described for the analogue with dppm. Moreover, treating $[Cp^RRu(PP)Cl]$ (**249**) with P_4 and a reductant forms the cationic Cp^RRu complexes $[Cp^RRu(PP)(\eta^1\text{-}P_4)]^+$ (Cp^R = Cp, PP = $(PPh_3)_2$, **250a**; Cp^R = Cp*, PP = $(PPh_3)_2$, **250b**; Cp^R = Cp*, PP = dppe, **250c**; see Scheme 71**b**). These complexes as well as the bimetallic RuPt complex $[\{CpRu(PPh_3)_2)\}(\mu,\kappa^1,\kappa^2\text{-}P_4)\{Pt(PPh_3)_2\}]^+$ (**251**) were examined in the solution phase. **246b** and complexes **250** were characterized through single-crystal X-ray diffraction (see Fig. 65-

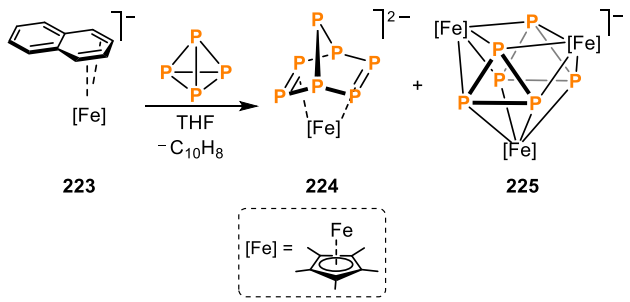

Scheme 67. Fragmentation-aggregation of P_4 mediated by Cp^*Fe^-.

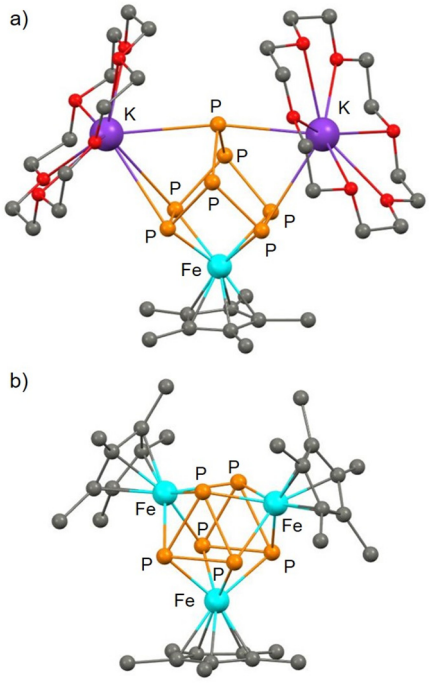

Fig. 62. X-ray structures of the iron polyphosphide complexes a) **224** and b) **225**; adapted from Ref. [214].

b-e). VT NMR and EXSY experiments revealed that the octahedral complexes **246** are considerably more fluxional in solution than the piano-stool compound **250a** or its osmium analogue [CpOs$(PPh_3)_2(\eta^1\text{-}P_4)]^+$ (**252**). Such observations were associated with the existence of a more ordered structure for the piano-stools, according to its less negative entropic term. Interestingly, by simply substituting the Cp ligand in **250a** for the more basic Cp^* in **250b**, the dynamic process in solution for the P_4-cage ligand seems to be suppressed, which was explained in terms of the electronic character of the cyclopentadienyl ligand. The different behavior of the Cp^* derivative was also evidenced by the lack of reactivity of **250b** towards hydrolysis, even at high temperatures. For **250c**, featuring a bidentate diphosphine ligand, the tumbling movement of the P_4-tetrahedron was also detected in solution, in spite of the presence of the chelating diphosphine. The activation parameters for the dynamic processes were calculated using line-shape analysis and 2D-EXSY spectra. The results showed that subtle changes at the metal center affected the activation parameters for the slow tumbling motion of the P_4-cage in the piano-stool complexes. Remarkably, for compounds **246b** and **250a**, the dynamic process was also identified in the solid state by solid state MAS ^{31}P NMR and ^{31}P MAS EXSY experiments. The results indicated that the tumbling motion of the P_4-cage is still observable in the solid state and confirm that dissociative mechanisms are not responsible for the scrambling of the four P_4 atoms in solution [178].

Additionally, Peruzzini, Yakhvarov and co-workers reported the first example of a water-soluble ruthenium complex featuring a P_4 cage, coordinated in a η^1-mode [223]. The complex [CpRu$(TPPMS)_2(\eta^1\text{-}P_4)]X$ (**250d**, TPPMS = sodium salt of *m*-monosulfonated triphenylphosphine, $Ph_2P(m\text{-}C_6H_4SO_3Na)$, X = PF_6^- or BF_4^-; Scheme 72) was obtained after reacting [CpRu$(TPPMS)_2Cl]$ (**249d**) with white phosphorus (1 equiv.) in the presence of a chloride scavenger ($TlPF_6$ or $AgBF_4$). In neat water, rapid decomposition of **250d** occurs and H_3PO_3 and H_3PO_4 were observed to form exclusively. The complex underwent mild hydrolysis with a known excess of water in DMF (25 °C) to yield $[CpRu(TPPMS)_2(PH_3)]^+$ (**253**), free phosphorous acid, H_3PO_3, phosphoric acid H_3PO_4 and molecular hydrogen. At higher temperatures (35 °C), the reaction proceeded differently since, under these conditions, **250d** afforded the complexes $[CpRu(TPPMS)_2\{\text{-}PH(OH)_2\}]^+$ (**254**) and $[CpRu(TPPMS)_2\{P(OH)_3\}]^+$ (**255**), as identified *via* $^{31}P\{^1H\}$ NMR. Kinetic measurements ($^{31}P\{^1H\}$ NMR) indicated that the hydrolysis of **250d** involves an associative mechanism, in which nucleophilic attack of water on the $\eta^1\text{-}P_4$ ligand occurs in the transition state.

Stoppioni and co-workers [224] studied the activation of coordinated P_4 by treating the cationic ruthenium complex $[\{CpRu(PPh_3)_2\}_2(\mu,\eta^1\text{:}\eta^1\text{-}P_4)](OTf)_2$ (**256**, OTf = OSO_2CF_3) with iodine (Scheme 73). Complex **256** features an intact P_4-tetrahedron as a $\eta^1\text{:}\eta^1\text{-}P_4$ bridge. In the presence of adventitious water, addition of iodine (1 equivalent) to **256** at low temperatures gives rise to the monocation $[\{CpRu(PPh_3)_2\}_2(\mu_1\text{:}\mu_3,\eta^1\text{:}\eta^1\text{-}P_4H_2I)]^+$ (**257**). This features a 1,3-dihydride-2-iodidecyclotetraphosphan-1-ide ligand, $(P_4H_2I)^-$. Facile dissociation of the iodide from the tetraphosphorus ligand in polar solvents, yielded the elusive 1,3-dihydride-2,4-bicyclotetraphosphane[1.1.0] (P_4H_2 butterfly), also stabilized by metal coordination in complex **258**. The coordinated P_4H_2 ligand is still susceptible to hydrolysis and, after addition of an excess of water, the triphosphine complex $[\{CpRu(PPh_3)_2\}_2\{\mu_1\text{:}\mu_3,\eta^1\text{:}\eta^1\text{-}PH_2PHPH_2\}](OTf)_2$ (**259**), featuring a fully hydrogenated P_3H_5 ligand, and phosphorous acid, are formed. Remarkably, at this point in time both the P_4H_2 and P_3H_5 ligands observed in the molecular structures of **258** and **259** were unknown in coordination compounds [225,226]. $^{31}P\{^1H\}$ NMR spectra of complexes **257**–**259** correlate well with the characterization in the solid state by single-crystal XRD (Fig. 66), thus concluding that the solid state structure is maintained in solution. In contrast to previous investigations by the same group [44], the iodine-mediated hydrolytic degradation of coordinated P_4 in complex **256** does not yield hydroxypolyphosphane species, suggesting that a different reaction mechanism operates in this case. The authors highlighted that stable coordination of the P_4 tetrahedron is important to achieve controlled transformations/functionalizations of white phosphorus [224].

Recently, Caporali, Peruzzini and co-workers reported on the synthesis and hydrolysis of a ruthenium-P_4 compound bearing the basic PMe_3 ligand [227]. Treatment of $[CpRu(PMe_3)_2Cl]$ (**249e**) with a chloride scavenger ($TlPF_6$ or AgOTf), followed by addition of P_4 in equimolar quantities selectively afforded the cationic compound $[\{CpRu(PMe_3)_2\}_2(\mu,\eta^1\text{:}\eta^1\text{-}P_4)]^{2+}$ (**260**, Scheme 74). Attempts to obtain the mononuclear complex $[CpRu(PMe_3)_2(\eta^1\text{-}P_4)]^+$ were unsuccessful. As with other intact P_4 complexes [222], **260** exhibits a fluxional behavior in solution. Single crystal X-ray diffraction confirmed the molecular structure of **260** and revealed a conformation in which the two cyclopentadienyl rings are eclipsed. Upon addition of water (500 equiv.), **260** hydrolyzes in solution at ambient temperature yielding a mixture of species, of which the major products correspond to [{CpRu

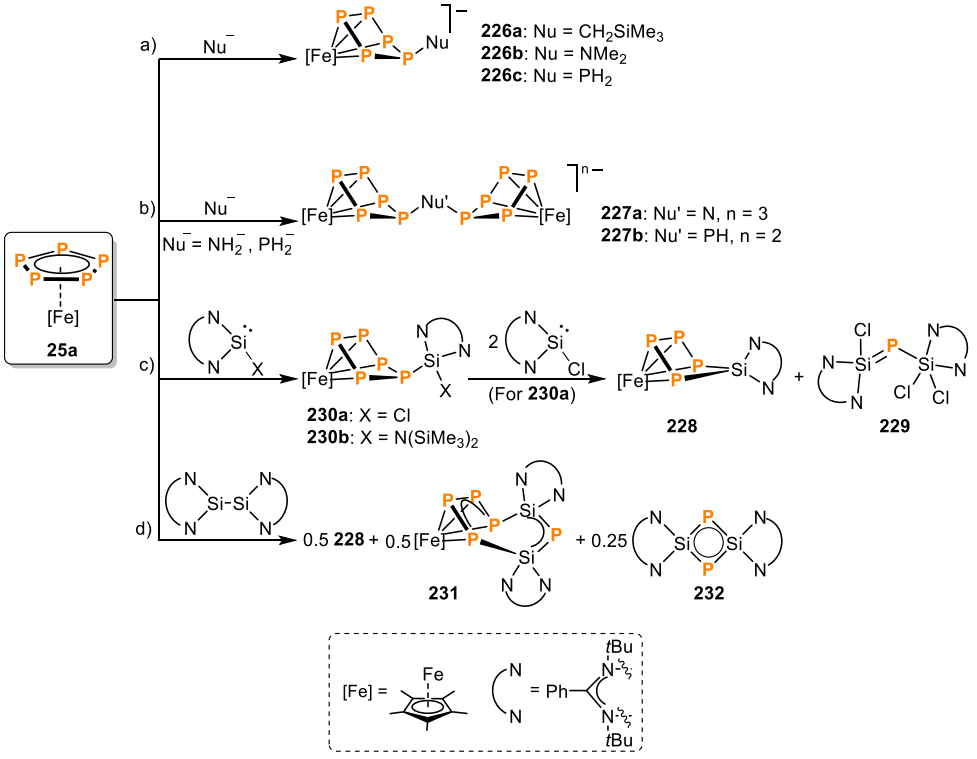

Scheme 68. Functionalization of the *cyclo*-P_5 ligand in [Cp*Fe(η^5–P_5)] (**25a**) by nucleophiles (N-N = [PhC(N*t*Bu)$_2$]).

$(PMe_3)_2\}_2(\mu,\eta^1{:}\eta^1\text{-}P_2H_4)]^{2+}$ (**261**, 75%), $[CpRu(PMe_3)_2P(OH)_3]^+$ (**262**, 18%) along with the minor species $[CpRu(PMe_3)_2(PH_3)]^+$ (**263**), $[CpRu(PMe_3)_2\{PH(OH)_2\}]^+$ (**264**) and the free phosphonic acids. Better yields of the hydrolytic products were obtained with the complex bearing the more basic phosphine ligand PMe_3, **260**, in comparison to the similar reaction with the analogous **256**. The reaction proceeds in a more selective manner by treating **260** with MeOH. In this case, only **262** and $[CpRu(PMe_3)_2\{P(OMe)_3\}]^+$ (**265**) (ratio = 2:1) were obtained, with the former resulting from the water present in the methanol.

In 2017, another example of a Ru complex showing an intact P_4 tetrahedron was reported [228]. In this case, the complex was stabilized by N-heterocyclic carbene (NHC) ligands. Treatment of a THF solution of the unsaturated hydride species $[Ru(IMe_4)_4H]^+$ (**266**) with one equivalent of P_4, afforded $[Ru(IMe_4)_4(P_4)H]BAr^F_4$ (**267**). The η^1-coordination of the P_4 cage *trans* to the hydride ligand was confirmed in the molecular structure determined by XRD (see Fig. 67). The high field ^{1}H NMR signal of the hydride ligand featured signs of fluxional behavior, showcasing a doublet at room temperature which resolved into a doublet of quartets (J_{HP} = 266.1 and 11.0 Hz) at low temperatures. The low-temperature $^{31}P\{^1H\}$ spectrum showed a pattern like that observed for other intact-P_4 complexes (quartet, δ –394.6; doublet, δ = –468.6). The chemical shifts for the hydride ligand in **267** as well as a series of other $[Ru(IMe_4)_4(L)H]^{0/+}$ species (L = vacant, H_2, N_2, CO, MeCN, O_2, SO_2, H^-, F^- and Cl^-) were modelled theoretically, finding a good correlation between experimental and computed data when a scalar relativistic correction is applied, which improves significantly after inclusion of spin–orbit effects.

In a collaboration between the groups of Caporali and Grützmacher [229], the halogenation of P_4 by the unsaturated 16 electron species [Cp*RuX(PCy_3)] [X = Cl (**268a**); X = Br (**268b**)] was investigated. When **268** was reacted with half an equivalent of P_4 (Scheme 75, featuring the X = Cl derivatives), the bimetallic complexes $[Cp^*Ru(PCy_3)(\mu_2,\eta^2{:}\eta^4\text{-}P_4X_2)RuCp^*]$ (**269**) featuring a planar P_4X_2 ligand, were obtained. It was proposed that upon interacting **268** and P_4 form an intermediate species presumably containing an intact P_4 tetrahedron in a bridging coordination mode to two Ru-centers. Subsequently, metal-promoted activation of the coordinated P_4 ligand, followed by cleavage of two P-P bonds and oxidative insertion into the Ru-X bond, gives rise to the unprecedented P_4X_2 motif, which can be described as a 1,4-dihalo tetraphosphabutadiene (X = Cl, Br). Upon reduction with magnesium, the chloro-substituents of the P_4Cl_2 ligand in complex **269a** are eliminated as chloride anions, giving rise to two weakly-interacting P_2 (dumbbell) moieties, in the triple-decker compound **270**. Likewise, selective alkylation with *n*BuLi led to the tetranuclear complex $[(Cp^*Ru)_4(\mu_3,\eta^2{:}\eta^2{:}k^4\text{-}P_4nBu_2)_2]$ (**271**), in which the P_4Cl_2 ligand has transformed into two coplanar P_4nBu_2 scaffolds. Furthermore, addition of a chloride scavenger to **269a** yielded the cationic, unstable species $[Cp^*Ru(PCy_3)(\mu_2,\eta^2{:}\kappa^4\text{-}P_4Cl)RuCp^*][GaCl_4]$ (**272**), which loses the remaining chloro-substituent to give again compound **270**. Crystal structure analyses confirmed the molecular structures of complexes **269a**-**272** (Fig. 68). DFT calculations suggest that the P_4 motif in these compounds is electronically highly flexible and behaves as a non-innocent ligand.

Fabrizi de Biani, Ienco and co-workers reported the synthesis of triple-decker *cyclo*-P_3 bimetallic Ru-Co, Ru-Ru and Os-Co complexes [230]. These were obtained either by reaction between suitable ruthenium/osmium precursors with the known [(triphos)Co(η^3-P_3)] [**273**, triphos = $CH_3C(CH_2PR_2)_3$] [231], or by direct reaction with white phosphorus. The redox properties of the triple-decker complexes, namely $[(triphos)Ru(\mu,\eta^3{:}\eta^3\text{-}P_3)Co(triphos)]^{2+}$ (**274**), $[(triphos)Ru(\mu,\eta^3{:}\eta^3\text{-}P_3)Ru(triphos)]^+$ (**275**) and $[(triphos)Os(\mu,\eta^3{:}\eta^3\text{-}P_3)Co(triphos)]^{2+}$ (**276**), were also studied and compared with analogous cobalt and nickel complexes. Of these, only **275** (Fig. 69) was obtained from direct reaction with white phosphorus, and its molecular structure was determined. Electrochemical studies of complexes **274**–**276** revealed several monoelectronic redox

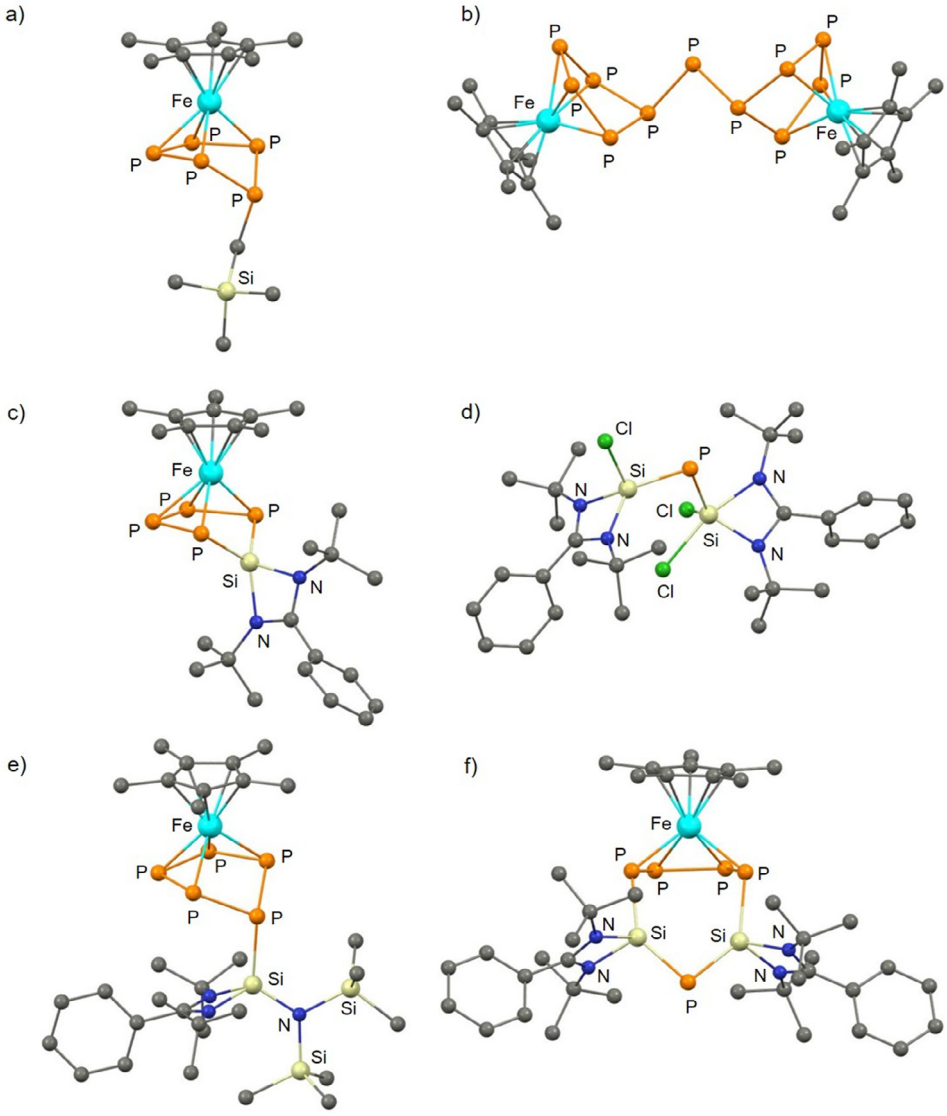

Fig. 63. X-ray structures of selected products of functionalization of the *cyclo*-P_5 ligand in $[Cp^*Fe(\eta^5\text{–}P_5)]$ (**25a**): a) $[Cp^*Fe(\eta^4\text{-}P_5CH_2SiMe_3)]^-$ (**226a**), b) $\{[Cp^*Fe(\eta^4\text{-}P_5)]_2PH\}^{2-}$ (**227b**), c) $[Cp^*Fe\{\eta^4\text{–}P_4Si(N\text{-}N)\}]$ (**228**), d) [(N-N)Si(Cl) = P-Si(N-N)$(Cl)_2$] (**229**), e) $[\{Cp^*Fe(\eta^4\text{-}P_5)\}\{(N\text{-}N)Si(N(SiMe_3)_2)\}]$ (**230b**), f) $[Cp^*Fe\{\eta^4\text{–}P_5[Si(N\text{-}N)]_2\}]$ (**231**) (N-N = PhC$(N^tBu)_2$); adapted from Ref. [215,216].

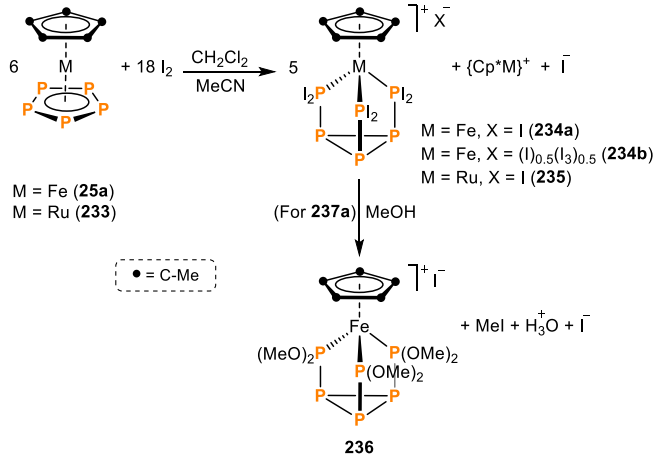

Scheme 69. Iodination of pentaphosphametallocene (M = Fe, Ru) complexes and reactivity or the iron derivative towards MeOH.

processes. These systems were compared with their dinickel and dicobalt analogues and, in general, cyclic voltammetry studies revealed that the triple-decker complexes are stable when their electronic count varies between 30 and 34 valence electrons. Interestingly, with the heavier analogue **275**, an unprecedented species with 29 VE was formed through electrochemical reactions.

3.1.3. Osmium

In the period of 2011–2020, complexes resulting from the coordination/activation of white phosphorus by osmium are the least represented among group 8 metals. As mentioned in the previous section, the triple-decker bimetallic Os-Co compound **276** was reported, and its redox properties were studied *via* cyclic voltammetry [230].

Dynamic behavior in solution was observed for the osmium(II) complex $[CpOs(PPh_3)_2(\eta^1\text{-}P_4)]^+$ (**252**), featuring an intact P_4-cage ligand [178]. This dynamic process was similar to that of its ruthenium analogue, **250a**. In both cases, they contrasted with that of the iron complex **172**, for which only the dissociation of the P_4-ligand in solution was identified. This behavior was also evidenced

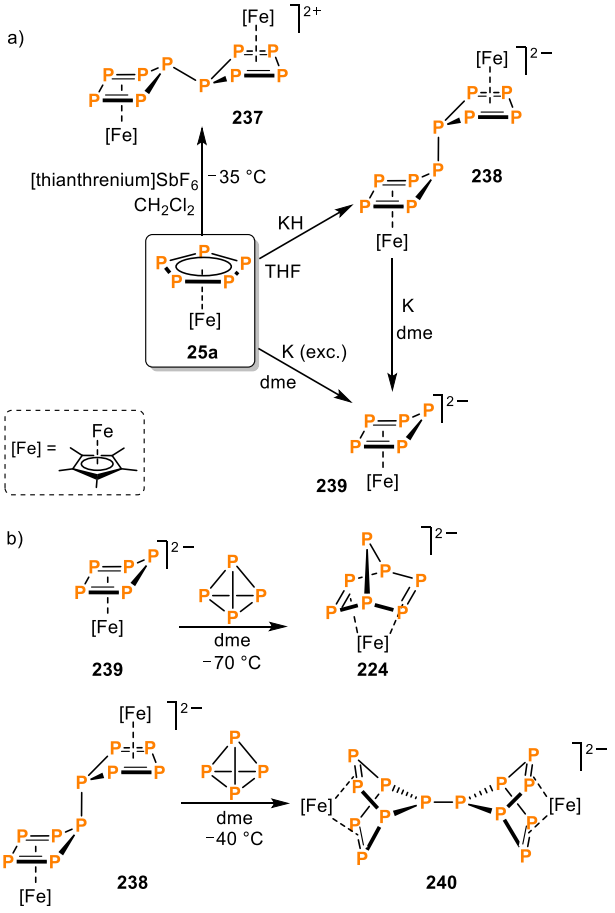

Scheme 70. a) Redox chemistry of [Cp*Fe(η^5–P_5)] (**25a**) and b) reactivity of the reduced products towards P_4.

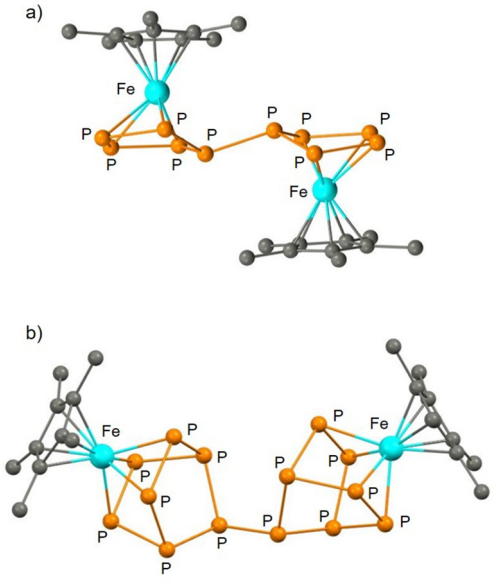

Fig. 64. X-ray structures of a) **237** and b) the P_{14}-ligand complex **240**; adapted from Ref. [219].

by the slight differences observed on the activation parameters of the dynamic process of **250a** in comparison to those of **252**. Based on such observations, it was suggested that the Fe-P_4 bond for the related complex **172** was kinetically more labile than for the Ru-P_4 and Os-P_4 analogues, **250a** and **252**, respectively.

3.2. Group 9 metals

Undoubtedly, in the period 2011–2020 for group 9 metals, the activation of white phosphorus by cobalt complexes have been the most prevalent. Such complexes have led not only to activated tetraphosphorus moieties, but even products of fragmentation/reaggregation and functionalization. Remarkable contributions have been made in this matter by the groups of Radius, Figueroa, Scheer, Driess and Wolf, among others. Least represented are the species derived from rhodium and iridium.

3.2.0.1. Cobalt

It is common for cobalt(I) complexes bearing labile ligands as potential vacant sites to be used in the activation of white phosphorus [232,233]. One such example was in 2012, when the stepwise degradation of the P_4 tetrahedron at a cobalt(I) center was achieved by the group of Radius [232]. Upon reacting the cobalt compound [Cp*Co(*i*Pr$_2$Im)(η^2-C_2H_4)] (**277**, Cp* = η^5-C_5Me_5, *i*Pr$_2$-Im = 1,3-di-isopropylimidazolin-2-ylidene) with white phosphorus, a [Cp*Co(*i*Pr$_2$Im)] fragment inserts into the P_4-cage promoting cleavage of a P-P bond (Scheme 76**a**). The product, [Cp*Co(*i*Pr$_2$Im)(κ^2-P_4)] (**278**) features a butterfly-P_4 ligand (Fig. 70**a** shows its molecular structure). Complex **278** reacts with another equivalent of **277** cleaving a second P-P bond to give the dinuclear compound, [{Cp*Co(*i*Pr$_2$Im)}$_2$(μ,κ^2:κ^2-P_4)] (**279**), bearing a bridging *cyclo*-P_4^{4-} ligand. Single-crystal XRD (Fig. 70**b**) revealed that the P_4 ring shows a puckered conformation. This intermediate complex **279** undergoes further transformations when heated in toluene solution at 80 °C. After dissociation of one NHC ligand and rearrangement/opening of the *cyclo*-P_4^{4-} unit, two products are obtained, one featuring a *catena*-P_4, and the other two bridging dumbbell ligands, P_2^{2-}, [Cp*Co(μ,η^4:κ^2-P_4)Co(*i*Pr$_2$Im)Cp*] (**280**) and the previously reported [234] [{Cp*Co(μ,η^2:η^2-P_2)}$_2$] (**281a**), respectively. Fig. 70**c** shows the molecular structure of complex **280**. Furthermore, by controlling either the [Co]:P_4 stoichiometry or the reaction conditions, compounds **278**-**281a** can be selectively obtained from **277**, in high yields. A complex multistep mechanism was proposed by the same group after studying the transformation with DFT methods [235]. It was found that the formation of the dinuclear complex **279**, as well as the loss of the different NHC co-ligands (or CO, given that the analogous system was also modelled), were key steps in the reaction. Such loss was considered necessary since the vacant sites facilitate the transformations of the P_4-cage in the coordination spheres of the different cobalt species. According to the calculations, the presence of the donor NHC ligand is better for the overall reaction than with the carbonyl analogue, since the release of the former has a larger entropic effect than for the latter. These calculations highlighted the importance of the nature of the co-ligands on the outcome of P_4-activation reactions.

Figueroa and co-workers described the synthesis of the notable two-legged piano stool Co(I) complex [Cp*Co(N_2)(CNAr^{dipp2})] (**282**), featuring a sterically encumbering isocyanide and a labile N_2 ligand [233]. Such dinitrogen ligands can be displaced by Lewis bases under ambient conditions therefore, **282** can be seen as a stabilized source for the unsaturated 16 VE fragment [Cp*Co(CNAr^{dipp2})]. Reacting **282** with white phosphorus (ratio Co:P_4 = 1:1, Scheme 76**b**) yielded the butterfly-P_4 complex [Cp*Co(κ^2-P_4)(CNAr^{dipp2})] (**283**). The elongated P-P bond distance (2.606 Å) between the two P-bounded atoms is indicative of the cleavage of one of the edges of the tetrahedron, giving rise to the butterfly-P_4 ligand (see Fig. 71**a**). If the Co:P_4 ratio is 1:0.5, or if **283** is treated with an additional equivalent of **282**, the dinuclear

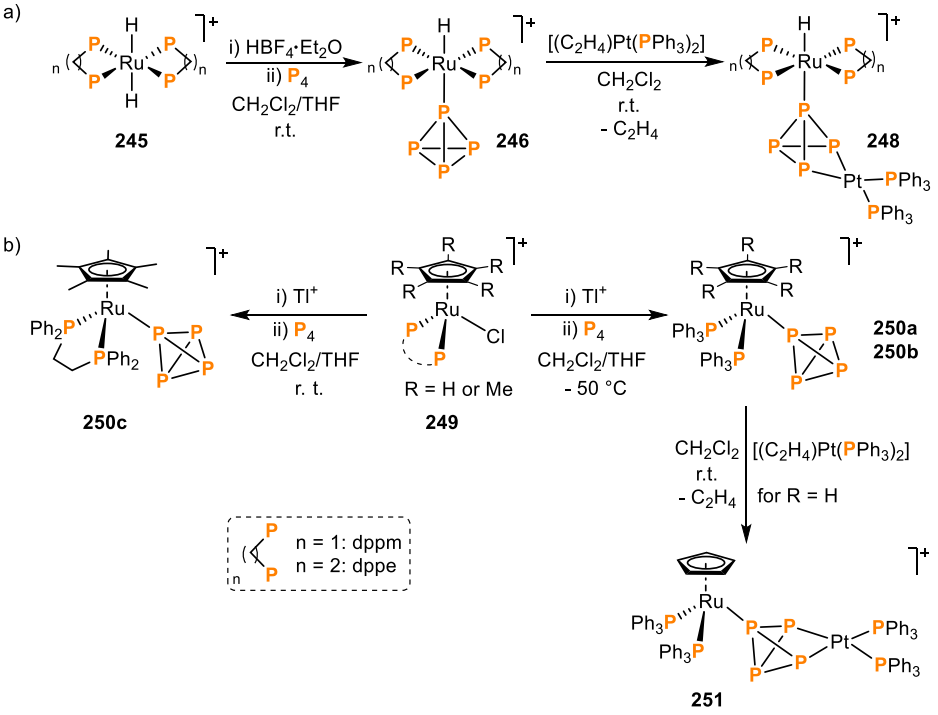

Scheme 71. Synthesis of Ru(η^1-P_4) and bimetallic Ru(μ,κ^1,κ^2-P_4)Pt complexes by Peruzzini and co-workers [178,222].

complex [{Cp*Co(CNAr^{dipp2})}$_2$(μ_2,κ^2:κ^2-P_4)] (**284**) is formed. In the latter, the mild activation of another P-P edge has occurred (Fig. 71**b** for the molecular structure) [233]. This behavior is analogous to the one observed in the activation of P_4 leading to complexes **278** and **279** [232].

Scheer and co-workers also reported on the activation of white phosphorus, through their investigations on the synthesis of the cobalt-*cyclo*-P_4 end-deck species [Cp‴Co(η^4-P_4)] (**285**), referred to as "missing homologue" of the series of first-row sandwich complexes Cp^{R}M(*cyclo*-P_n) [236]. **285** is obtained after reaction of the 14 valence electron Cp‴Co fragment source (**286**) with white phosphorus (Scheme 77**a**). The complex dimerizes irreversibly in solution to form two isomeric P_8 species [(Cp‴Co)$_2$(μ,κ^4:κ^2:κ^1-P_8)] (**287**). It should be noted that **287b** isomerizes to **287a**, thus suggesting a greater stability for the latter. Crystallographic analysis of **285** and **287** (Fig. 72) revealed that the *cyclo*-P_4 ligand in **285** is almost perfectly square planar and that the P_8 moiety in **287** is comprised by two bound P_5 and P_3 cycles. P-rich polyphosphorus complexes can be obtained by thermolytically promoted rearrangement of compound **285** and isomers **287** in solution. DFT calculations indicate that the solvent plays an important role on the synthesis of **285**, since it affects the degree of dissociation of the cobalt precursor to generate the 14 VE fragment. Moreover, these theoretical studies indicated that the key intermediate in the synthesis of the *cyclo*-P_4 complex is posited to be an intermediate η^3-tetrahedron P_4 species [236].

Recent investigations by the group of Scheer have also shown that complex **285** undergoes ring expansion [119] and ring contraction reactions (see Scheme 77**b**) [237]. By reacting complex **285** with the electrophilic pnictogenidene complexes [Cp*E{W(CO)$_5$}$_2$] the *cyclo*-P_4E ring (E = P, As) species resulting from the insertion of the phosphinidene or arsinidene atom into the *cyclo*-P_4 unit, are obtained [119]. Two isomers of [Cp‴Co(μ_3,η^4:η^1:η^1-P_5Cp*){W(CO)$_5$}$_2$] (**288**) and three isomers of the complex [Cp‴Co(μ_3,η^4:η^1:η^1-AsP$_4$Cp*){W(CO)$_5$}$_2$] (**289**) were isolated. Compounds **288** are the result of a ring-expansion reaction from a *cyclo*-P_4 to a substituted *cyclo*-P_5 motif coordinated in an η^4-mode to the cobalt center, with **288a** being the main product of reaction (ratio **288a**:**288b** = 1:0.19). The envelope conformation of the *cyclo*-P_5 ring was confirmed crystallographically, for both isomers (Fig. 73 shows the structure of **288a**), and is structurally reminiscent of the ferrate complexes **226** (see Scheme 68, above) [215]. A possible driving force for the reaction is the easing of the ring strain for the *cyclo*-P_4 moiety. Isomers **289** differ only on the position of the arsenic atom within the *cyclo*-P_4As ring (Fig. 73**b**). According to ^{1}H and ^{31}P NMR spectra, the three isomers are present in solution in the ratio **289a**:**289b**:**289c** = 0.48:0.42:0.10. DFT calculations revealed that the reaction proceeds similarly for the phosphinidine and the arsinidene reagents, *via* initial formation of an adduct between compound **285** and [Cp*E{W(CO)$_5$}$_2$], followed by a shift of a {W(CO)$_5$} fragment and the insertion of the pnictinidene into an unpolarized P-P bond of the *cyclo*-P_4 ligand to yield the ring-expanded products [119].

Ring contraction of the *cyclo*-P_4 ring occurs when compound **285** is treated with two equivalents of 1,3,4,5-tetramethylimidazo lin-2-ylidene (^{Me}NHC) to afford [(^{Me}NHC)$_2$P][Cp‴Co(η^3-*cyclo*-P_3)] (**290**, see Scheme 77 and Fig. 73**c**) under mild conditions [237]. The reaction proceeds *via* selective NHC-induced phosphorus cation extraction from the *cyclo*-P_4 ring in **285**, generating the ionic compound **290** containing an anionic [Co](*cyclo*-P_3)$^-$ ([Co] = Cp‴Co) complex and a bis(NHC)-coordinated P^I cation. It was not possible to either identify or isolate reaction intermediates to support a mechanistic proposal for the formation of **290** [237].

Further chemistry on the [Co]-*cyclo*-P_4 complex **285**, specifically its reduction or reaction with nucleophiles (Scheme 77**b**), was reported by the same group [238]. To avoid the previously reported [236] irreversible dimerization, the reactions were carried out at room temperature or lower. Reduction of **285** using K, KH or KC_8 (THF at r.t.) yields the known [Co](*cyclo*-P_3)$^-$ anionic complex, previously obtained from compound **290** [237], and a P_8-aggregate, [(Cp‴Co)$_2$(μ,η^3:η^3-P_8)]$^{2-}$ (**291**), which was structurally characterized (Fig. 73**d**). The P_8-ligand consists of a *cis*-bicyclo[3.3.0]octane

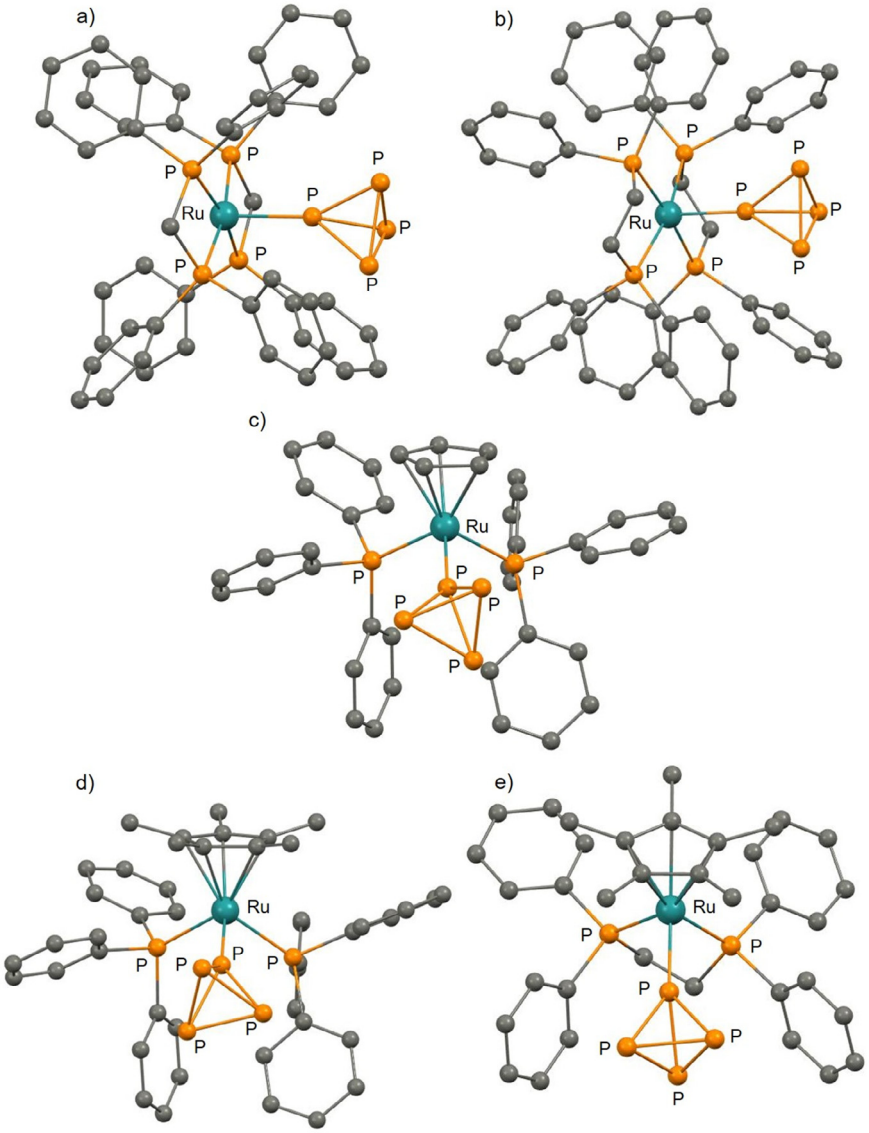

Fig. 65. X-ray structures of ruthenium(phosphine) cationic complexes featuring intact P_4-tetrahedron ligands: a) **246a**, b) **246b**, c) **250a**, d) **250b** and e) **250c**; adapted from Refs. [178,222].

core which serves as bridge between two {Cp‴Co} fragments. Alternatively, by treating **285** with nucleophiles such as organolithium reagents, substituted *cyclo*-P_4 complexes **292** can be selectively obtained at low temperatures. For **292b** (R = CH_2SiMe_3, Fig. 73**e**), both the equatorial and the axial-CH_2SiMe_3 isomers were identified. These compounds are metastable and upon warming to room temperature, the aggregation products **293**, featuring a P_8R ligand (R = *t*Bu, CH_2SiMe_3) similar to that in **291**, are obtained (see Fig. 73**f** for the structure of **293b**). For **292a** (R = *t*Bu), it was also possible to identify the novel diorgano-substituted *cyclo*-P_5R_2 species **294**, which is formed along with the known anion, **290** [237]. Likewise, the reaction of **285** with NaOH affords $[Cp'''Co(\eta^3\text{-}P_4(O)H)]^-$ (**295**) (Fig. 73**g**), which is presumably formed *via* attack of the OH^- group to a phosphorus atom, yielding a substituted P-OH moiety that undergoes tautomeric rearrangement to generate P=O and P-H bonds [238].

The use of low-valent transition metalates, including cobaltates, to activate P_4 has been investigated by the group of Wolf [207,214]. By reacting the cobaltate complex $[K(OEt_2)_2\{(^{dipp}BIAN)Co(\eta^4\text{-}1,5\text{-}cod)\}]$ (**296a**, ^{dipp}BIAN = 1,2-bis(2,6-diisopropylphenylimino)acenaphthene, 1,5-cod = 1,5-cyclooctadiene) with P_4, the dianion $[(^{dipp}BIAN)Co\}_2(\mu,\eta^4\text{:}\eta^4\text{-}P_4)]^{2-}$ (**297**, Scheme 78) is obtained [239]. The molecular structure of the dinuclear compound **297** was determined (see Fig. 74) indicating that, according to the P-P bond lengths, the P_4 motif can be described as a superposition of two mesomeric structures comprising two P_2^{2-} dianions and a P_4^{4-} unit. Cyclic voltammetry (CV) studies revealed that two reversible one-electron oxidation processes occur and therefore, preparative oxidation using $[Cp_2Fe]BAr^F_4$ allowed for the synthesis of species which are oxidized by one and two electrons. This led to a complete series of dinuclear cobalt tetraphosphido complexes $[(^{dipp}BIAN)Co\}_2(\mu,\eta^4\text{:}\eta^4\text{-}P_4)]^{n-}$ [n = 2 (**297**),n = 1 (**298**),n = 0 (**299**)]. Both **298a** and **299a** feature a cyclic P_4^{4-} motif, while the isomers **298b** and **299b** bear an open-chain P_4^{4-} ligand. However, the open-chain isomer **299b** was obtained only as a minor product in the single-crystal X-ray structure with approximately 9% occupancy. Additionally, the difference between **298a** and **298b** arises from the fact that these correspond to the ion-contact and the ion-separated structures of compound **298**, which does not affect the characterization in solution. The structures of this series of complexes demonstrate that

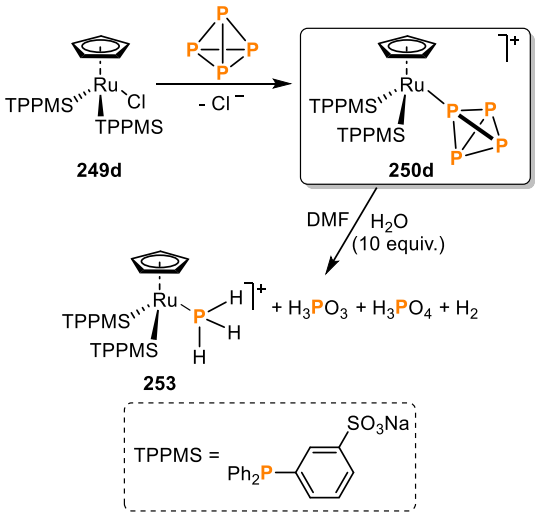

Scheme 72. Synthesis of a water-soluble tetraphosphorus complex and its reactivity towards hydrolysis.

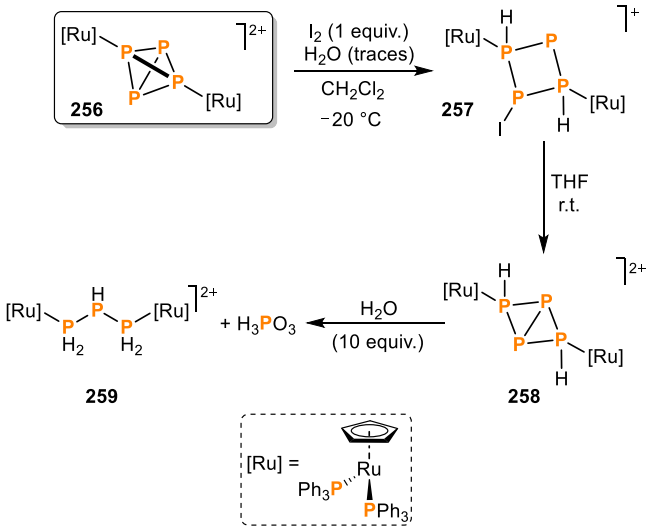

Scheme 73. Nucleophilic addition of iodine to the dinuclear complex [{CpRu(PPh$_3$)$_2$}$_2$(μ,η^1:η^1-P$_4$)](OTf)$_2$ (**256**) and subsequent hydrolysis of the coordinated P$_4$ ligand.

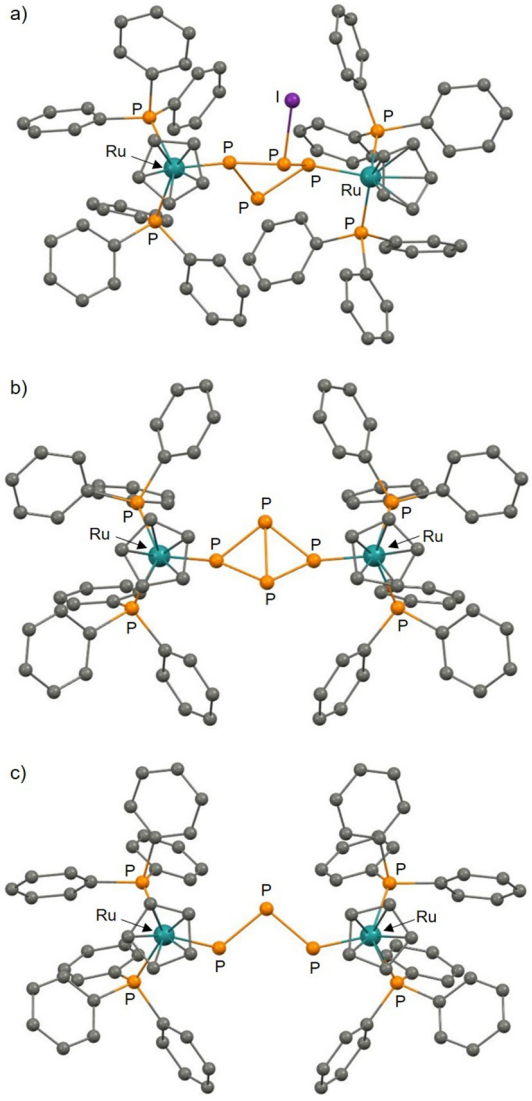

Fig. 66. X-ray structures of [{CpRu(PPh$_3$)$_2$}$_2$(μ$_1$:μ$_3$,η^1:η^1-P$_4$H$_2$I)]$^+$ (**257**) and its subsequent products of hydrolysis, [{CpRu(PPh$_3$)$_2$}$_2${μ$_1$:μ$_3$,η^1:η^1-P$_4$H$_2$}]$^+$ (**258**) and [{CpRu(PPh$_3$)$_2$}$_2${μ$_1$:μ$_3$,η^1:η^1-PH$_2$PHPH$_2$}]$^+$ (**259**). Hydrogen atoms have been omitted for clarity purposes; adapted from Ref. [224].

redox reactions on the complex do not affect the oxidation state of the P_4^{4-} ligand but effect changes in its structure (Fig. 74). It was highlighted that the presence of the redox-active ligand ^{dipp}BIAN was necessary to achieve such a degree of reduction of the P$_4$ molecule, due to its exceptional electron-releasing and -accepting properties.

Likewise, the synthesis of a *cyclo*-P$_4$ cobaltate anion [(PHDI)Co(η^4-P$_4$)]$^-$ (**300**, PHDI = bis(2,6-diisopropylphenyl)phenanthrene-9,10-diimine) was also reported by Wolf and co-workers [240]. Complex **300** was obtained after the reaction of [K(18c-6)(thf)$_{1.5}$][(PHDI)Co(η^4-1,5-cod)] (**301**, PHDI = bis(2,6-diisopropylphenyl)phenanthrene-9,10-diimine, see Scheme 79, bottom), analogous to **296a** [239], with white phosphorus. Interestingly, a contrasting behavior was observed between the reactivity of complex **300** and that of dinuclear **297**, for which only outer-sphere electron-transfer reactions were identified [239]. The *cyclo*-P$_4$ unit in complex **300** can either be further coordinated to other metallic fragments, as in complex **302** (Scheme 79**a**), or selectively functionalized with diorganochlorophosphanes (R$_2$PCl, R = Cy, *t*Bu, Ph, Mes, N(*i*Pr)$_2$), yielding the neutral ring-expansion η^4-*cyclo*-P$_5$R$_2$ products (**303**) quantitatively (Scheme 79**b**). Single-crystal X-ray diffraction analysis of **302** revealed that the *cyclo*-P$_4$ unit is almost perfectly square (see Fig. 75**a**), with bond distances (2.147(7) Å on average) in-between the values expected for P-P single and P=P double bonds, thus confirming the presence of a P_4^{2-} ligand. The envelope conformation of the *cyclo*-P$_5$R$_2$ products **303** (see Fig. 75**b-c** for the molecular structures of **303a** and **303c**) is structurally reminiscent of complexes **226** (Scheme 68, above) and **288** (Scheme 77, below) [119].

The reactivity of complexes **303** with cyanide salts differs depending on the nature of the substituent, R (Scheme 79**b**). For the bulky R = Mes, after reacting with cyanide (1 equivalent) a rearrangement of the *cyclo*-P$_5$R$_2$ moiety leads to the cyclotetraphosphido complex **304** (see Fig. 75**d** for the molecular structure). Addition of a second equivalent of cyanide does not promote further conversion of **304**. In contrast, for the other derivatives, treatment of **303** with 2 equivalents of the cyanide salt results in the remarkable fragmentation of the *cyclo*-P$_5$R$_2$ ligand into P$_3$ and P$_2$ units, forming the anionic cyclotriphosphido cobalt complex **305**

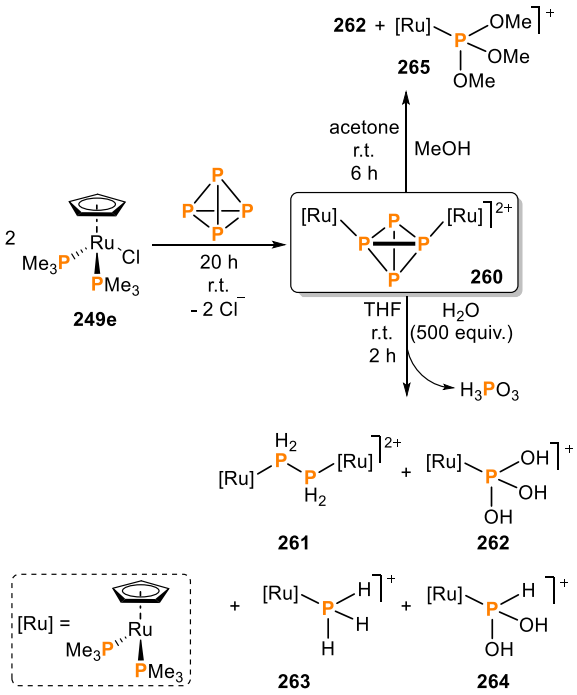

Scheme 74. Synthesis and reactivity towards H_2O and MeOH of the cationic complex $[\{CpRu(PMe_3)_2\}_2(\mu,\eta^1{:}\eta^1\text{-}P_4)]^{2+}$ (**260**) by the group of Caporali, Peruzzini and co-workers [227].

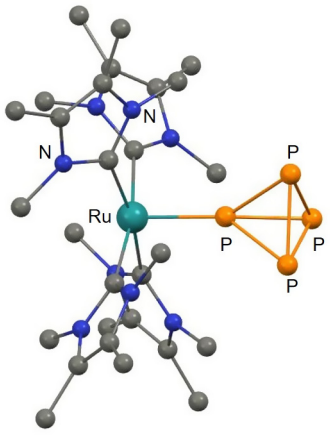

Fig. 67. X-ray structure of **267**. The counterion has been removed for clarity. Adapted from Ref. [228].

and releasing the corresponding 1-cyanodiphosphan-1-ide anions (**306**). Fig. 75**e-f** shows the molecular structures of complex **305** and the cyanodiphosphan-1-ide **306b**, respectively. The different outcome in reactivity between the *cyclo*-$P_5(Mes)_2$ complex and its analogues was attributed to steric shielding that hinders its [3 + 2] fragmentation. It was proposed that similar cyclotetraphosphido complexes could be key intermediates in the formation of species **305** and **306** [240].

Rectangular P_4 and *cyclo*-P_3 ligands coordinated to low-valent β-diketiminato cobalt complexes were also reported by the groups of Driess [82] and Scheer [241]. Driess and co-workers [82] described the synthesis (Scheme 80**a**) of the neutral *cyclo*-P_4 complexes $[(LCo)_2(\mu_2{:}\eta^4,\eta^4\text{-}P_4)]$ [L: L^0 = CH[CHN(2,6-*i*$Pr_2C_6H_3$)]$_2$ (**307a**); L^1 = CH[CMeN(2,6-$Et_2C_6H_3$)]$_2$ (**307b**)], which were obtained by treatment of either [L^0Co·toluene] (**220b**) or [(L^1Co)$_2$] (**308**) with 0.5/1 equivalents of white phosphorus at room temperature, respectively. The molecular structures of complexes **307a** and **307b** revealed that the cobalt centers reside in an octahedral geometry, and that the distances between both metal centers exclude any possible Co-Co interactions. Furthermore, the *cyclo*-P_4 ligand in such complexes can be described as rectangular with two long P-P bonds (2.289 Å for **307a** and 2.298 Å for **307b**) and two short P-P bonds (2.130 Å for **307a** and 2.124 Å for **307b**). Fig. 76**a** shows the molecular structure of **307b**. Broken-symmetry DFT calculations, along with bond order analysis, agreed well with the experimental characterization and supported the proposal that the ligand in such complexes corresponds to a tetraphosphacyclobutadiene motif. One-electron reduction of complexes **307** using KC_8 (1 equiv.), led to the anionic compounds $[(LCo)_2(\mu_2,\eta^4;\eta^4\text{-}P_4)]^-$ (**309**), which were isolated in good yields. Single-crystal X-ray diffraction showed that complexes **309a** and **309b** feature structural characteristics similar to **307**, except the P-P distances are approximately the same giving a square P_4 ring as opposed to the rectangular one found in the latter. Theoretical calculations and additional characterization evidenced that compounds **309** feature a delocalized six π-electrons *cyclo*-P_4^{2-} ligand, with mixed-valent cobalt(I,II) centers [82].

Similarly, the group of Scheer reported [241] the related monoanionic complex $[(L^3Co)_2(\mu_2,\eta^4;\eta^4\text{-}P_4)]^-$ [L^3 = CH[CMeN(2,6-*i*$Pr_2C_6H_3$)]$_2$ (**309c**)] and the P_3-containing compound $[(L^3Co)_2(\mu_2{:}\eta^3,\eta^3\text{-}P_3)]^-$ (**310**), which were obtained after the reaction of P_4 with the formal Co(0) precursor $[K_2(L^3Co)_2(\mu_2{:}\eta^1,\eta^1\text{-}N_2)]$ (**311**, Scheme 80**b**). Compound **310** is the result of P-atom abstraction from the P_4-middle deck in **309c**. Single-crystal analysis of **309c** revealed the characteristic features of a planar *cyclo*-P_4^{2-} motif (Fig. 76**b**). This evidence, together with the results from magnetic measurements (Evans method and SQUID) led to the conclusion that, as for complexes **309a** and **309b**, the *cyclo*-P_4 ligand bridges mixed-valent Co(I) and Co(II) centers. For compound **310** (see Fig. 76**c** for the X-ray structure), such characterization indicated that the *cyclo*-P_3^{3-} bridges two Co(II) sites. Interestingly, reacting the Co(I) precursors [LCo·toluene] (L = L^2 (**220a**), L^3 (**220c**) or L^4 (**220d**), see Scheme 80, bottom) with P_4 yields the corresponding neutral species under different conditions. At room temperature, the reaction afforded compound $[(L^3Co)_2(\mu_2{:}\eta^4,\eta^4\text{-}P_4)]$ (**307c**) selectively (see Fig. 76**d** for the molecular structure), and the approach can be reproduced for the analogues **307d** and **307e**. The *cyclo*-P_4 unit in such complexes was described as a neutral P_4^0 ligand, and would be analogous to the examples reported by Driess, **307a** and **307b** [82]. Upon refluxing in toluene, complex **307c** underwent a thermally induced elimination of a P-atom, forming $[(L^3Co)_2(\mu_2,\eta^3{:}\eta^3\text{-}P_3)]$ (**312**). One-electron reductions of the neutral compounds bearing ligand L^3 yielded the corresponding monoanionic complexes **309c** and **310** [241]. Altering the size of the β-diketiminato ligands in **220** does not affect the P_4 activation products [82,241], this behavior contrasts with that previously observed for the iron analogues **215** [212,213].

As mentioned above, the groups of Peruzzini and Scheer studied the reactivity of intact P_4-manganese or ruthenium complexes towards low-valent iron or cobalt compounds [81]. Besides the reactivity towards the β-diketiminato iron (**215c**) and cobalt (**220a**) compounds discussed in Section 3.1.1, the manganese complex **161** and the ruthenium complex **250a** were also reacted individually with the 14 VE cobalt fragment source **286** (Scheme 81). Such reactions afforded $[\{Cp^{BIG}Mn(CO)_2\}_2\{CoCp'''\}(\mu,\eta^1{:}\eta^1{:}\eta^4\text{-}P_4)]$ (**313**) or $[\{CpRu(PPh_3)_2\}\{CoCp'''\}(\mu,\eta^1{:}\eta^4\text{-}P_4)]OTf$ (**314**), which correspond to a $[Cp'''Co(\eta^4\text{-}P_4)]$ motif coordinating to 16 VE Mn- or Ru- complex fragments. Remarkably, compound **314**, with one substitution at the *cyclo*-P_4 moiety, or the doubly substituted **313**, do not undergo further degradation or reaggregation as previously observed with the metastable compound **285** (*cf.* Scheme 77, below) [236–238]. Hence, the intact P_4 ligand in complexes **161**

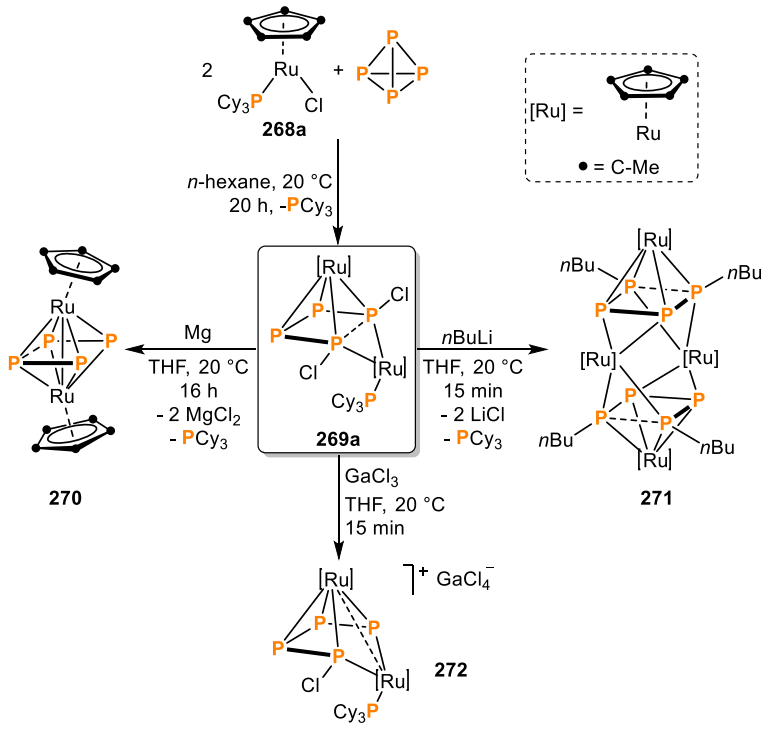

Scheme 75. Ruthenium-mediated halogenation of P_4 and subsequent functionalization of the resulting P_4Cl_2 complex.

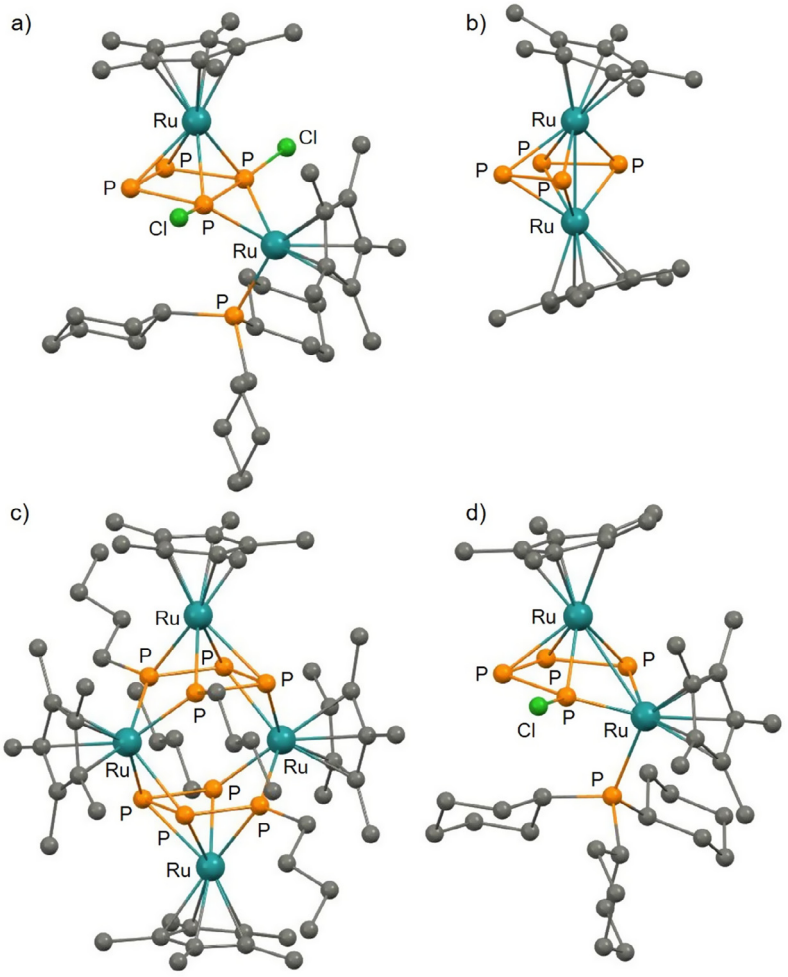

Fig. 68. X-ray structures of complexes a) **269a**, b) **270**, c) **271** and **272**; adapted from Ref. [229].

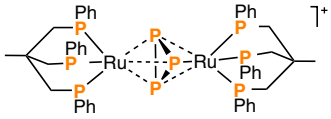

Fig. 69. Complex [(triphos)Ru(μ,η³:η³-P₃)Ru(triphos)]⁺ (**275**).

and **250a**, or the free P_4 molecule behaved in an analogous manner towards **286**, but the formation of the *cyclo*-P_4 motif using the intact-P_4 compounds becomes more advantageous. A similar behavior was also observed for the β-diketiminato iron (**215c**) and cobalt (**220a**) complexes discussed above. DFT calculations revealed that the formation of **314** proceeds through a potential intermediate in which a butterfly-shaped P_4 motif is bridging both the ruthenium and the cobalt centers, behaving as an η^3-coordinated ligand towards the latter while still η^1-coordinated to the former. This would be an example of a rare triphosphaallyl ligand. In such putative species, the P_4 ligand has one of the P-P bonds cleaved. These observations indicate that the P_4 tetrahedron is not released from the coordination sphere of the starting metal complexes during the reaction. The structure then rearranges to the final *cyclo*-P_4 moiety. The theoretical results are in good agreement with the characterization in the solid state *via* X-ray diffraction (Fig. 77) [81].

Recently, Power, Wolf and co-workers [242] reported on the isolation of the unusual Co_2Sn_2 heterobimetallic cluster $[Ar'SnCo]_2$ (**315**, Ar′ = C_6H_3-2,6(C_6H_3-2,6-*i*Pr_2)$_2$), and its reactivity towards white phosphorus (Scheme 82). Selective insertion of the P_4 tetrahedron into the Co_2Sn_2 cluster core of **315** results in opening of the white phosphorus molecule to obtain a *catena*-P_4 ligand, which has been functionalized after migration of a tin-bound terphenyl substituent to a P-atom. The product $[Ar'_2Sn_2Co_2P_4]$ (**316**), corresponds to the first molecular cluster compound containing phosphorus, cobalt and tin. Characterization through XRD (Fig. 78) revealed bond distances in the range of single P-P bonds (2.2005(8) to 2.1621(8) Å) for the P_4-chain ligand.

As previously mentioned, back in 1991 Barr and Dahl reported the synthesis of the complex $[\{Cp^*Co(\mu,\eta^2{:}\eta^2\text{-}P_2)\}_2]$ (**281a**) in low yield, *via* the photolytic reaction of $[Cp^*Co(\mu\text{-}CO)_2]$ with P_4 [234]. In 2010, Scheer and co-workers described [243] a procedure for the quantitative synthesis of $[\{Cp'''Co(\mu,\eta^2{:}\eta^2\text{-}P_2)\}_2]$ (**281b**, Cp‴ = 1,2,4-*t*$Bu_3C_5H_2$), using $[(Cp'''Co)_2(\mu,\eta^4{:}\eta^4\text{-}C_7H_8)]$ (**286**) as a starting material in the presence of white phosphorus, in toluene at room temperature. Several polyphosphorus frameworks (*e.g.* P_8, P_{12}, P_{16}, and P_{24}) were also accessed after treatment of **286** with white phosphorus and adjusting the stoichiometry and/or reaction conditions [243]. More recently, Roesky, Konchenko, Scheer, and co-workers synthesized [244] $[(Cp'''Co)_2(\mu_3,\kappa^3{:}\kappa^3{:}\kappa^2\text{-}P_4)SmCp^R_2]$ (**317**, Cp^R = Cp* (η^5-C_5Me_5) or η^5-C_5Me_4*i*Pr; Scheme 83), featuring

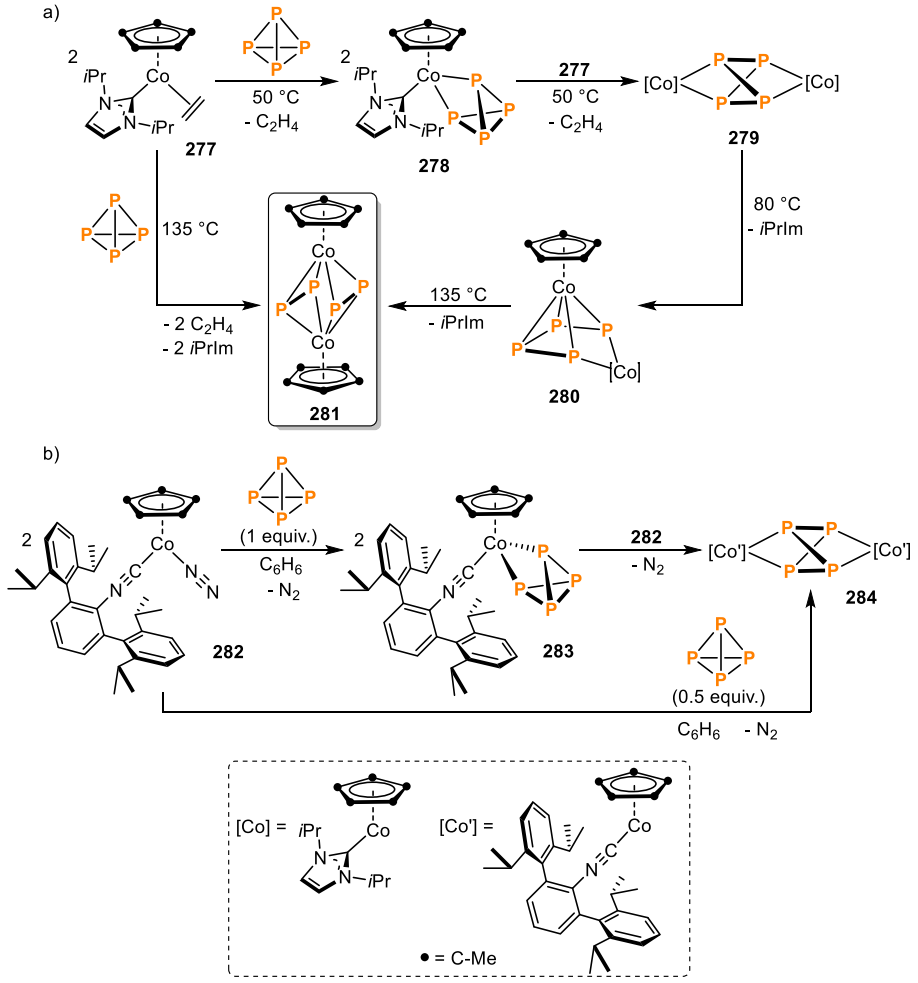

Scheme 76. Stepwise activation of P_4 at Co(I) by the groups of a) Radius [232] and b) Figueroa [233].

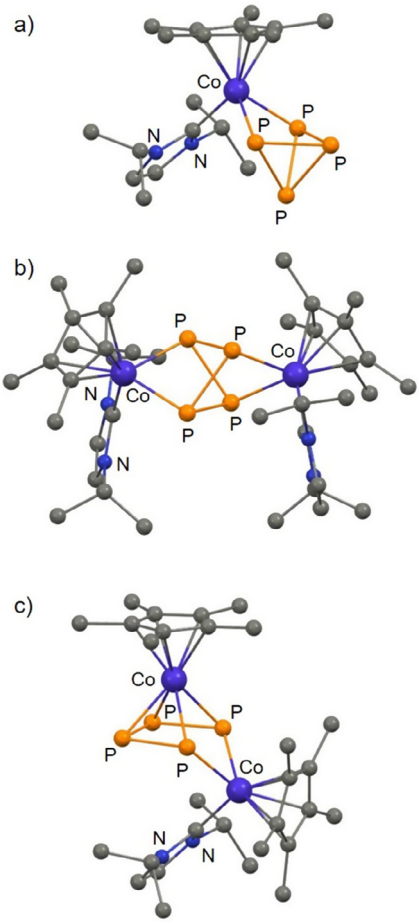

Fig. 70. X-ray structures of complexes **278**–**280**, intermediates in the stepwise activation of P_4 at cobalt; adapted from Ref. [232].

a *catena*-P_4 ligand, *via* an unusual intramolecular P–P coupling process starting from **281b**. Such polyphosphide complexes were obtained after reduction of the transition metal by the divalent samarocene $[Cp^R_2Sm(THF)_n]$ [Cp^R = Cp* (η^5-C_5Me_5) (**24a**) or η^5-C_5Me_4iPr (**24b**)]. DFT calculations and analysis of the bonding situation in **317** revealed that the coupling of the P_2^{2-} units in **281b** to form a new P-P bond is not the result of the direct reduction of the P-atoms, but a consequence of the rearrangement of the positive charges between the two metal atoms. Hence, the aggregation of the P_2^{2-} ligands led to the formation of an acyclic P_4^{4-} motif [244]. Fig. 79**a** shows the X-ray structure of **317a**.

Similar reactivity was reported in a subsequent contribution by Scheer [245], in which P-P bond formation is induced *via* redox reactions. By reacting **281b** with weakly coordinating anion salts of Ag(I) (Scheme 83), the formation of two new P-P bonds was observed resulting in the *cyclo*-P_4^{3-} cationic complex $[(Cp'''Co)_2(\mu,\eta^4{:}\eta^4\text{-}P_4)]X$ (**318**, X = BF_4, FAl [FAl{$OC_6F_{10}(C_6F_5)$}$_3$]). If the reaction is carried out in the presence of Ag[TEF] (2 equiv., [TEF] = [Al{$OC(CF_3)_3$}$_4$), another electron is abstracted from the P_4 moiety, giving rise to the planar *cyclo*-P_4^{2-} triple-decker compound $[(Cp'''Co)_2(\mu,\eta^4{:}\eta^4\text{-}P_4)][TEF]_2$ (**319**). The *cyclo*-P_4^{2-} in compound **319** has identical P-P bond distances [(2.236(2) and 2.239(2) Å], which suggest the presence of single bonds. The oxidations leading to **318** and **319** are fully reversible. Treating the oxidized products with KC_8 reforms complex **281b**, in accordance with the cyclic voltammetry results. The use of a small excess of KC_8 (>1 equiv.) led to the formation of a different product, namely the cyclobutadiene-like P_4 middle deck compound $[K(18\text{-c-}6)(dme)_2][(Cp'''Co)_2(\mu,\eta^4{:}\eta^4\text{-}P_4)]$ (**320**). However, when **281b** was reacted with two equivalents of KC_8, the anionic product $[K(18\text{-c-}6)(dme)_2][K(18\text{-c-}6][(Cp'''Co)_2(\mu,\eta^3{:}\eta^3\text{-}P_4)]$ (**321**) was isolated. The reduced compound features an open-chain P_4 ligand, which was described as butadiene-like, and was reminiscent of the trinuclear dicobalt-samarium complex **317**. Fig. 79**b-c** show the molecular structures of **320** and **321**, respectively.

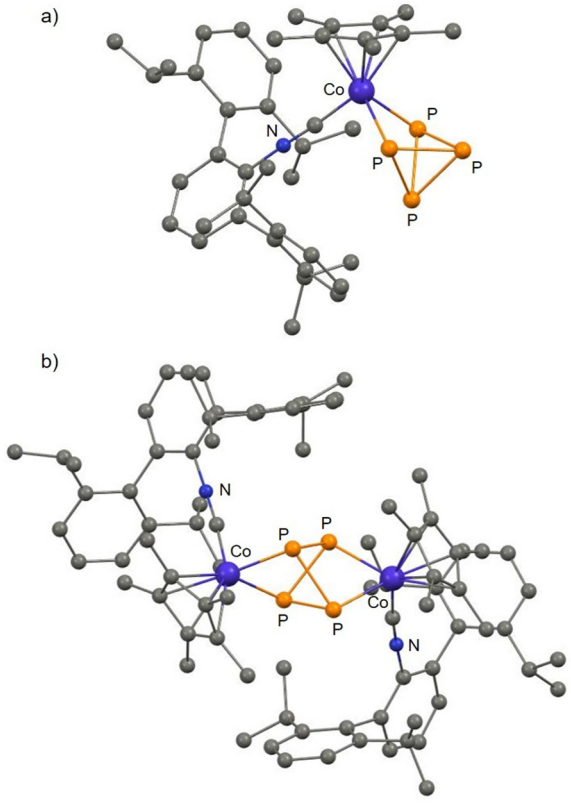

Fig. 71. X-ray structures of a) **283** and b) **284**; adapted from Ref. [233].

The chemistry of heterobimetallic complexes featuring a highly reduced P_4-chain (*catena*-P_4) ligand similar to the previously discussed iron complex **213** (Scheme 64, Section 3.1.1.) has been reported on by the collaboration between the Wolf and Weigand groups [207]. In contrast to the synthesis of the iron complex, monitoring of the reaction *via* $^{31}P\{^1H\}$ NMR spectroscopy revealed selective formation of the cobalt analogue $[K(dme)_2\{(\eta^4\text{-}C_{14}H_{10})Co(\mu,\eta^4{:}\eta^2\text{-}P_4)Ga(nacnac)\}]$ (**214**) (see Scheme 64). Dark-violet crystals of **214**, suitable for XRD, were analyzed, revealing the presence of a $Co(\mu,P_4)Ga$ core similar to that of the iron analogue (P-$P_{terminal}$ = 2.1095(9) Å and 2.1057(9) Å, P-$P_{internal}$ = 2.1825(9) Å). In this case, with respect to the iron complex **213**, an interaction was observed between the $K(dme)_2^+$ moiety, the anthracene ligand and one of the phosphorus atoms in the *catena*-P_4 ligand. NMR as well as UV–Vis data on this complex agree with the molecular structure determined by XRD. Complex **214** presents structural similarities with the samarium-cobalt complex **317** [244]. Reaction of the cobaltate precursor $[K(dme)_2][Co(\eta^4\text{-}C_{14}H_{10})_2]$ (**212**) [211,246,247] with an excess of [(nacnac)Ga(κ^2-P_4)] (**210**) did not result in the substitution of the second anthracene ligand, yielding again **214** as the sole product.

Related heterodinuclear cobalt-gallium compounds bearing a *catena*-P_4 ligand, namely $[K(dme)_2\{(^RBIAN)Co(\mu,\eta^4{:}\kappa^2\text{-}P_4)Ga(nacnac)\}]$ [^{R}BIAN = ^{dipp}BIAN, **322a**; ^{Mes}BIAN (bis(mesitylimino)acenaphthenediimine), **322b**; the molecular structure of **322b** is shown in Fig. 80**a**], were later reported [209]. Complexes **322** (Scheme 84**a**)

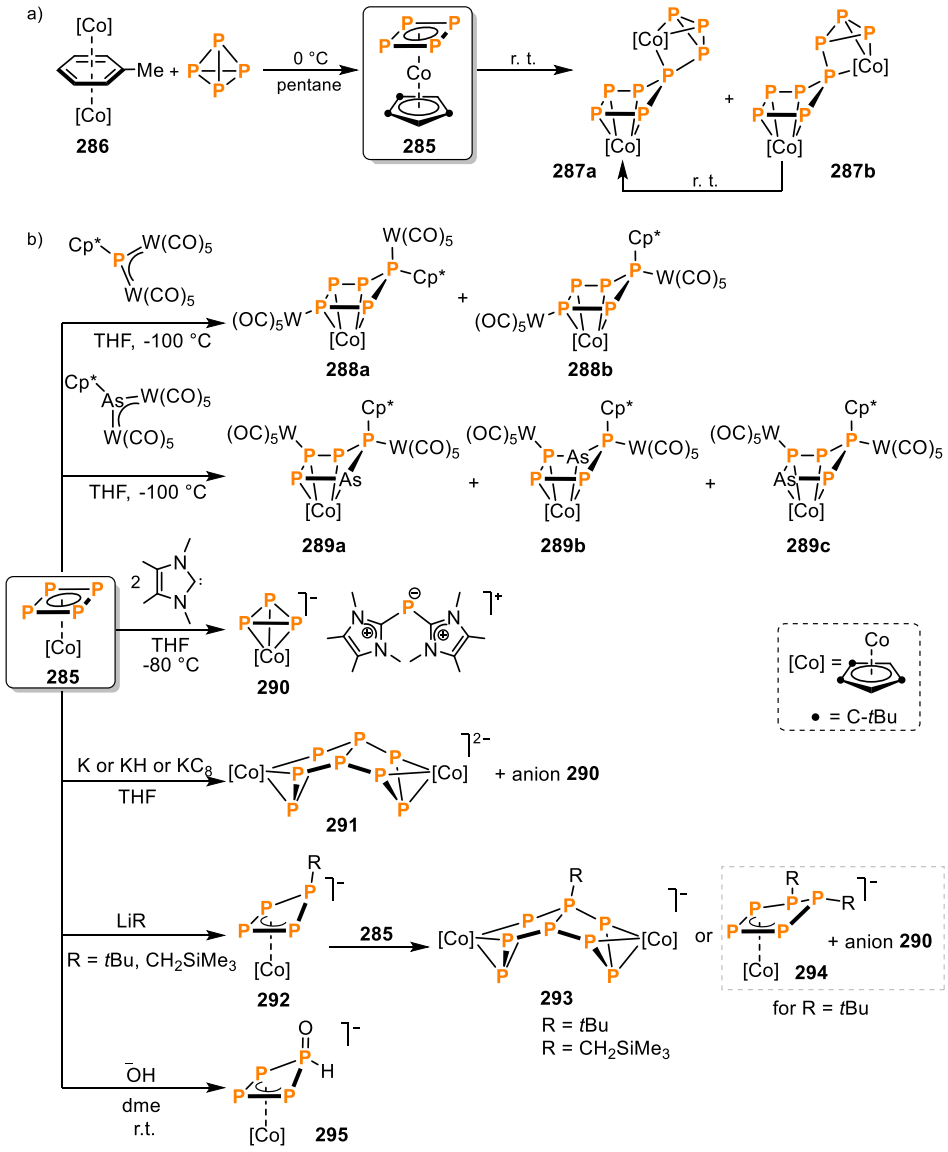

Scheme 77. Synthesis and functionalization of the *cyclo*-P_4 complex [Cp‴Co(η^4-P_4)] (**285**) by Scheer and co-workers.

were obtained by reaction between [K(Et_2O){(^{R}BIAN)Co(η^4-1,5-cod)}] [^{R}BIAN = ^{dipp}BIAN (**296a**), ^{Mes}BIAN (**296b**)] and [(nacnac)Ga (κ^2-P_4)] (**210**), through oxidative addition of a P-P bond at the cobalt center. **322b** can be used in the construction of organofunctionalized polyphosphorus *cyclo*-P_5R_2 ligands upon reaction with alkylchlorophosphanes (R_nPCl_{3-n}, Scheme 84**b**). Treatment of **322b** with dialkylchlorophosphanes (R_2PCl, R = *i*Pr, *t*Bu, Cy) selectively affords a series of η^4-coordinated *cyclo*-P_5R_2 complexes (**323**). Such complexes resemble species **303**, reported by Wolf and co-workers (see Scheme 79, below) [240], and have the same envelope conformation as in the iron complexes **226** and **227**, by the group of Scheer (Scheme 68, above; Fig. 80**b** shows the molecular structure of **323a**) [215]. During the course of the reaction the [Ga(nacnac)] fragment is released. A contrasting behavior was observed upon reacting **322b** with the alkyldichlorophosphane *t*$BuPCl_2$, in which a *cyclo*-P_5 ligand is formed (**324**), and the chloride shifts to the P-coordinated gallium fragment (Fig. 80**c**). Monitoring of the reaction on an NMR scale, $^{31}P\{^1H\}$ VT NMR studies, and DFT calculations gave insights into the mechanism of functionalization of the *catena*-P_4 motif by chlorophosphanes. Upon P-P condensation with *i*Pr_2PCl at low temperature, the two reaction intermediates were identified. Of these presumably isomeric species, the more abundant was characterized via XRD (Fig. 80**d**), and its molecular structure confirms that the neutral disubstituted P_5-chain complex **325** is formed. In solution (C_6D_6) at room temperature, such intermediate irreversibly affords **323**, after dissociation of [Ga(nacnac)] (Scheme 84) [209].

In 2019 [248] Figueroa and co-workers reported on the synthesis of the zero-valent tetraisocyanide complex Co($CNAr^{Mes2}$)$_4$ (**326**, Ar^{Mes2} = 2,6-(2,4,6-$Me_3C_6H_2$)$_2C_6H_3$), a sterically encumbered analogue of the binary cobalt carbonyl complex $Co(CO)_4$, which undergoes associative ligand substitution reactions. To assess on the possible one electron metalloradical behavior of **326**, its reactivity towards a variety of substrates was tested. Reaction towards elemental sulfur (S_8) or phosphorus (P_4), among other substrates, revealed that such cobalt(0) complex reacts in a multielectron manner to produce formal Co(III) centers. By treating **326** with P_4 (Scheme 85), the diamagnetic *cyclo*-P_3 complex (η^3-P_3)Co ($CNAr^{Mes2}$)$_3$ (**327**) was isolated. XRD (Fig. 81) and $^{31}P\{^1H\}$ NMR (singlet at δ = –278 ppm) confirm the presence of the *cyclo*-P_3 ligand. It was highlighted that, unlike the analogous (η^3-P_3)Co ($CO)_3$ (**328**), **327** shows remarkable thermal stability in solution

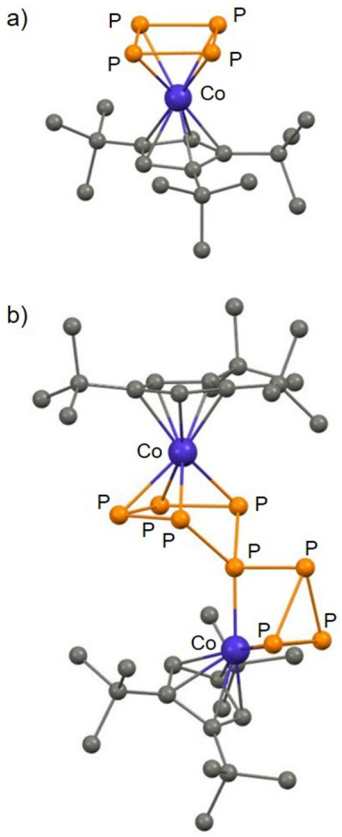

Fig. 72. X-ray structures of a) [Cp‴Co(η^4-P_4)] (**285**) and b) the dimeric [(Cp‴Co)$_2$(μ,κ^4:κ^2:κ^1-P_8)] (**287a**); adapted from Ref. [236].

at room temperature, and is even stable for days at 60 °C, attributed to its higher steric protection afforded by the bulky isocyanide ligands [248].

3.2.1. Rhodium

In 2006, Peruzzini, Midollini, Yakhvarov and co-workers investigated the interaction between the cationic species [M(dppm)$_2$]$^+$ [M = Rh (**329**), Ir (**330**); dppm = 1,1-bis(diphenylphosphino)methane ($Ph_2PCH_2PPh_2$)] and white phosphorus [249]. In 2011, Schoeller revisited the activation of P_4 at rhodium with such a system from a theoretical point of view through DFT calculations in the gas phase [250]. In particular, the formation of the inserted product [Rh(dppm)($Ph_2PCH_2PPh_2$PPPP)]OTf (**331**), in which a new P-P bond formed between a dppm ligand and the white phosphorus molecule, was evaluated. According to the calculations, due to a conformationally controlled philicity (the transition metal fragment can behave as either a nucleophile or an electrophile, after twisting the four-membered (PCP)Rh rings) the insertion reaction into P_4 would occur through a small energy barrier. Therefore, it was suggested that product **331** is obtained from an [M]-η^1-P_4 complex (**332**), which undergoes ligand dissociation and reaction through a series of intermediates (Scheme 86). Such a dissociation was identified as the rate-determining step. Furthermore, an equilibrium between **332** and the butterfly-P_4 complex [M]-(η^1:η^1-P_4)-[M] (**333**), stabilized by π-stacking with the phenyl rings of the dppm ligands, was proposed.

Caporali, Peruzzini and co-workers [251] investigated the activation of P_4 by the dimeric Rh(I) complex [RhCl(CO)(dppm)]$_2$ (**334**). Reaction of the dinuclear rhodium(I) compound with white phosphorus yielded the compound [Rh_2(CO)$_2$(μ,dppm)$_2$(μ,η^2-P_2)] (**335**, Scheme 87), which features a bridging P_2 unit. According to its molecular structure, the P_2 ligand is oriented perpendicularly to the intermetallic vector, forming a Rh_2P_2 tetrahedrane core. The solid state structure (Fig. 82) additionally revealed a Rh-Rh single bond (2.723 Å), and a remarkably short P-P bond (2.081 Å). It was suggested that the formation of the P_2 unit can be viewed as the oxidative addition of the P_4 molecule to the rhodium centers, which resulted in its symmetrical cleavage. VT NMR spectroscopic screening of the reaction revealed the formation of a species at −40 °C, which was proposed to be the hypothetical butterfly-P_4 intermediate complex **336**, according to its spectroscopic data. Computational and molecular orbital (MO) studies on the truncated model [Rh_2(CO)$_2${μ,P(CH_3)$_2$$CH_2$P($CH_3$)$_2$}$_2$($\mu$,$\eta^2$-$P_2$)] (**335′**) were in good agreement with the molecular structure determined for complex **335**. The MO qualitative analysis indicated that the HOMO of the complex has metal–metal bond character, in accordance with XRD findings. Comparison between the P_2 ligand and the isolobal units S_2^{2-} or C_2H_2, showed that the phosphorus motif behaved more like the disulfide anion, rather than like acetylene. Hence, the authors described the ligand as a P_2^{4-} ligand, which should be considered as an eight-electron donor, and the metal centers in the product are formally Rh(II) [251]. The complex is diamagnetic due to the formation of a Rh-Rh bond.

3.2.2. Iridium

During the period reviewed in this contribution, the chemistry of iridium complexes towards white phosphorus was scarcely explored.

However, in 2019 Wolf and co-workers [53], reported on the direct catalytic transformation of white phosphorus into arylphosphines and phosphonium salts, using the iridium complex, [Ir(dtbbpy)(ppy)$_2$]PF_6 ([**337**]PF_6; dtbbpy = 4,4′-di-*tert*-butyl-2,2′-bipyridine, ppy = 2-(2-pyridyl)phenyl) as a catalyst (see Scheme 88). The catalytic preparation of organophosphorus compounds was performed directly from P_4 and aryl iodides (C-P bond formation) using blue-LED visible light irradiation. Synthetically valuable triarylphosphines and tetraarylphosphonium salts were obtained in yields up to around 80%. Control experiments carried out in absence of iridium catalyst [**337**]PF_6, visible light irradiation (455 nm) or reductant (NEt_3), confirmed the role each one of them plays in the reaction. The type of product formed was strongly dependent on the steric nature of the aryl iodide used (Scheme 88, bottom). For *ortho*-substituted substrates, tertiary phosphines were the major products, whereas the phosphonium salts were mainly obtained with less encumbered substrates (*e.g. meta*- or *para*-substituted aryl iodides). Steric tuning of the aryl-iodides allowed for the selective formation of secondary or primary phosphines when mesityl (2,4,6-trimethylphenyl) and 2,6-dimesitylphenyl-iodide was used, respectively. Also, electron-withdrawing groups on the arene ring seemed to disfavor the formation of the quaternary phosphonium salt. Mechanistic experiments ($^{31}P\{^1H\}$ NMR scale) revealed the sequential formation of $PhPH_2$, Ph_2PH and Ph_3P as reaction intermediates for the model substrate phenyl iodide. The hydrogen atoms of the intermediate species are probably the result of hydrogen atom abstraction from the reductant, NEt_3. Redox potential measurements indicate that a reductive quenching mechanism, in which the excited state of the photocatalyst is reduced by NEt_3 to produce the neutral complex [**337**], is feasible. Individual experiments using the successive reaction intermediates instead of white phosphorus, afforded Ph_4P^+, with conversions similar or superior to the model reaction with P_4, and each reaction step appears to be photochemically mediated. Although such experiments gave significant insight into the reaction mechanism, the authors highlighted that further experiments are required to fully understand the initial activation path of the P_4 cage. This system represents a rare example of the direct catalytic carbofunctionalization of white phosphorus [252].

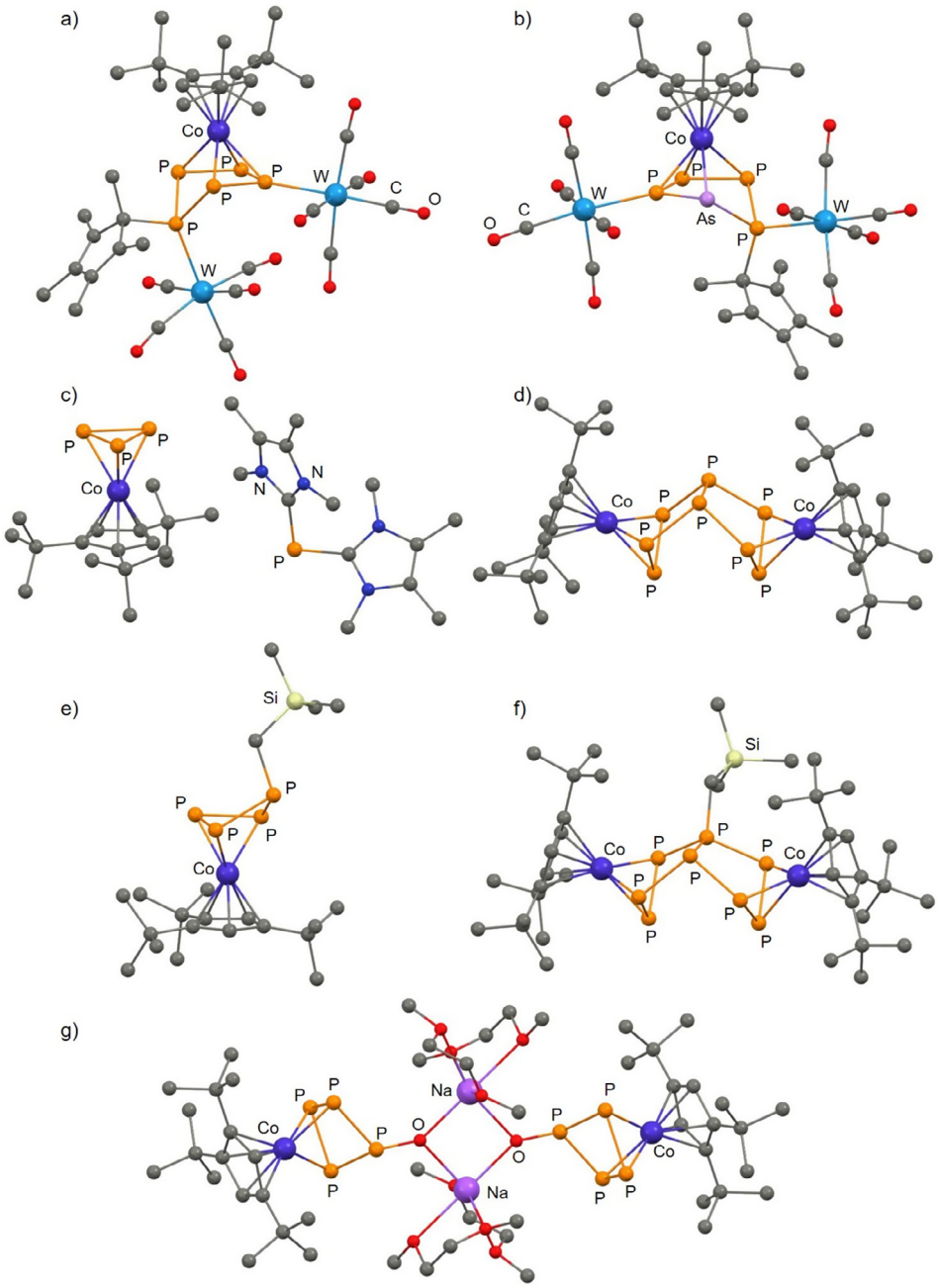

Fig. 73. X-ray structures of selected products of functionalization of [Cp‴Co(η^4-P_4)] (**285**): a) **288a**, b) **289**, c) **290**, d) **291**, e) **292b**, f) **293b**, g) **295**; adapted from Refs. [119,237,238].

3.3. Group 10 metals

The coordination chemistry or activation of white phosphorus with group 10 metals has been increasingly studied in recent years, with most of the investigations involving nickel complexes [253–263], while palladium is undoubtedly the least represented. The formation of nickel or palladium phosphide nanoparticles from white phosphorus has also been described.

3.3.1. Nickel

The 17 valence electron (VE) nickel radicals [CpNi(NHC)] (NHC = IDipp (1,3-bis(2,6-diisopropylphenyl)imidazolin-2-ylidene, **338a**), IMes [1,3-bis(2,4,6-trimethylphenyl)imidazolin-2-ylidene, **338b**)] activate white phosphorus to generate the bimetallic butterfly-P_4 (P_4^{2-}) complexes, {CpNi(NHC)}$_2$(μ,κ^1:κ^1-P_4)] (**339**) (Scheme 89**a**) [253,254]. The selective reaction of P_4 with **338a** occurs under mild conditions and quantitatively, and contrasts with the reactivity of the latter with sulfur or selenium, in which at least two products formed [253]. The bond distances of the butterfly-P_4 motif lie within the range of P-P single bonds (see Fig. 83**a**) for the molecular structure of **339b**), and its $^{31}P\{^1H\}$ NMR spectrum is similar to, *e.g.*, that of species **178** [190,193,195]. The P_4 scaffold in complex **339b** undergoes reversible insertion of the heteroallene phenyl isothiocyanate (Scheme 89**b**) [254]. The main products obtained are the two isomeric complexes **340a** and **340b**, featuring the unusual bicyclo [3.1.0]heterohexane framework. The analogous reaction between **339a** and a large excess of PhNCS resulted in a mixture containing

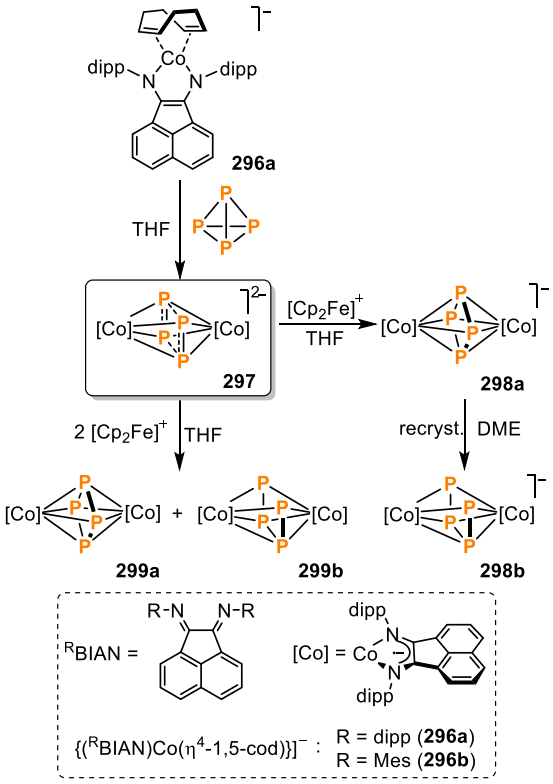

Scheme 78. Synthesis of dinuclear tetraphosphido complexes by activation of P_4 at $[K(OEt_2)_2\{Co(^{dipp}BIAN)(cod)\}]$ (**296a**).

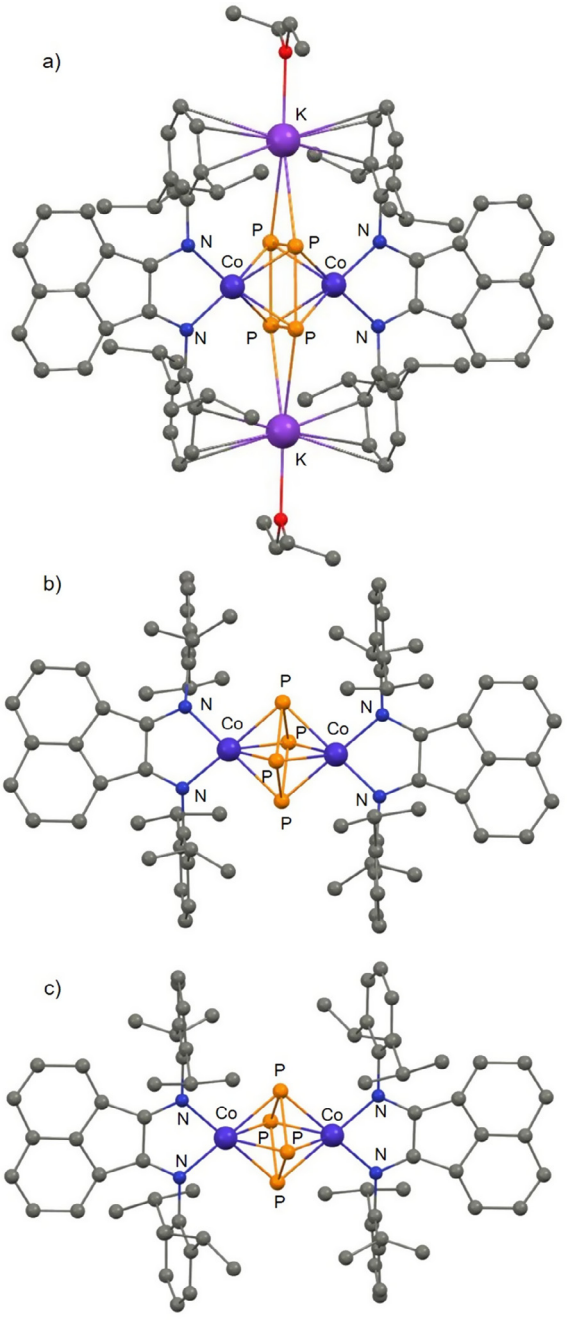

Fig. 74. X-ray structures of the dinuclear cobalt tetraphosphido complexes $[(^{dipp}BIAN)Co)_2(\mu,\eta^4{:}\eta^4\text{-}P_4)]^{n-}$ a) n = 2 (**297**), b) n = 1 (**298a**) and c) n = 0 (**299a**); adapted from Ref. [239].

mainly unreacted **339a** (50%), P_4 (35%) and a product similar to **340b** (15%), according to the $^{31}P\{^1H\}$ NMR spectroscopic monitoring. Both regioisomers **340** were characterized through XRD (Fig. 83**b-c**), and **340a** was isolated as an analytically pure solid. Products **340** equilibrate slowly with the starting materials **339b** and PhNCS in solution [254].

Driess and co-workers [255] showed that β-diketiminato nickel (I) complexes activate the P_4 tetrahedron affording the dinuclear Ni-complexes, $[(L^RNi)_2(\mu,\kappa^3{:}\kappa^3\text{-}P_4)]$ (L^R = HC[CMeN(2,6-$R_2C_6H_3$)]$_2$; R = *i*Pr (**341a**), Et (**341b**); Scheme 90) [256]. Compounds **341** feature a doubly κ^3–coordinated P_4 ligand, and were synthesized upon reacting P_4 with the corresponding β-diketiminate nickel(I) complexes $[(L^RNi)_2{\cdot}$toluene] (**342**) or, for **341a**, the dihydride $[(L^{iPr}\text{-}NiH)_2]$ (**343**) with subsequent dihydrogen release. The κ^3-coordination of the P_4 scaffold was confirmed via XRD (see Fig. 84 for the structure of **341a**). Moreover, two P-P bonds are considerably longer than typical single bonds (2.769 Å and 2.531 Å), but shorter than the sum of the van der Waals radii, suggesting activation of the P_4-cage. Dissolution of complex **341a** in toluene gave rise to a paramagnetic species, contrasting with the diamagnetic behavior observed in the solid state. It was proposed that **341a** underwent reversible dissociation in solution, to generate the paramagnetic complex $[L^{iPr}Ni(\eta^2\text{-}P_4)]$ (**344**), featuring an intact η^2-P_4 ligand, and **342**, by dimerization of the remaining $[L^{iPr}Ni^I]$ fragment. The presence of **344** in toluene solution was supported by high-resolution electrospray ionization mass spectrometry (HR ESI-MS) and DFT calculations. The same behavior was not observed for the less-hindered analogue **341b**. Furthermore, the calculations also indicate that the activation of the P_4 moiety occurs without reduction to P_4^{2-}, therefore featuring Ni(I) metal centers in the activated product.

The symmetric cleavage of P_4 at a Ni(0) center, to yield a butterfly-Ni_2P_2 complex, was described by the Radius group in 2013 [257]. The nickel(0) precursor $[Ni_2(i\text{Pr}_2\text{Im})_4(cod)]$ (**345**) ($i\text{Pr}_2$-Im = 1,3-diisopropylimidazolin-2-ylidene) reacts with P_4 to afford the butterfly-Ni_2P_2 complex $[\{Ni_2(i\text{Pr}_2\text{Im})_2\}_2(\mu,\eta^2{:}\eta^2\text{-}P_2)]$ (**346**, see Scheme 91**a**). The characterization of **346** in solution and in the solid state (Fig. 85), as well as optimization of its structure through DFT calculations, are all in good agreement with each other. Analysis of the frontier orbitals and comparison between the planarized and the bent Ni_2P_2 scaffold revealed that the latter is more stable, with an energy barrier of 99.93 kJ/mol. Such stabilization was assigned to a second order Jahn–Teller distortion [257]. The preparation of related Ni_2P_2 compound was later reported by Wolf, Goicoechea and co-workers, by reacting **338** with a 2-phosphaethynolate salt (Scheme 91**b**) [258]. The complex

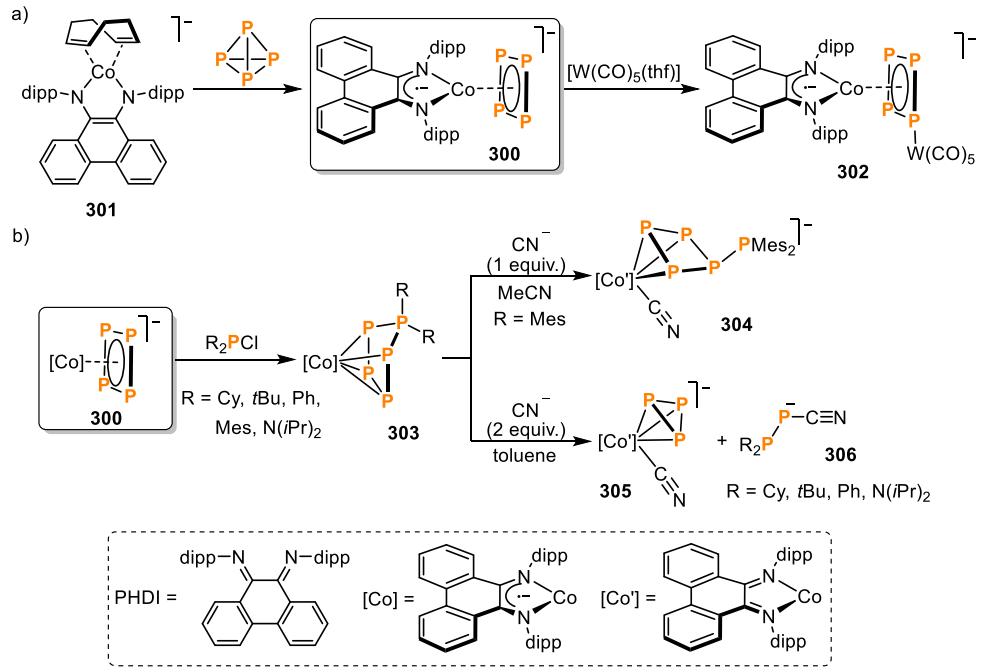

Scheme 79. a) Synthesis of the *cyclo*-P_4 cobaltate anion $[(PHDI)Co(\eta^4\text{-}P_4)]^-$ (**300**) by activation of P_4 and b) functionalization of the P_4 moiety with chlorophosphanes followed by fragmentation/rearrangement of the cyclic P_5 ligand.

$[\{Ni(NHC)(CO)\}_2(\mu,\eta^2\text{:}\eta^2\text{-}P_2)]$ (**347**, NHC = IMes; IDipp) shows a similar structure as **346**. While this complex was not prepared from P_4, its reaction with carbon monoxide (2 bar) yields P_4, presumably by dimerization of unsaturated P_2 units. The use of **346** as a transient P_2 source was demonstrated by trapping experiments with 3,4,8,9-tetramethyl-1,6-diphosphabicyclo(4.4.0)deca-3,8-diene (TMDPDD) and 2,3-dimethyl-1,3-butadiene (DMB).

Subsequently, Wolf and co-workers described the activation of white phosphorus at a Ni(0) center affording metal phosphide frameworks [259]. Following on from the reactivity of the Ni(I) complex **338** with P_4 they were able to synthesize [259] nickel-phosphido clusters and the first nickel pentaphosphacyclopentadienyl complexes by reaction of the Ni(0) precursors $[Ni(NHC)_2]$ (NHC = IMes (1,3-bis(2,4,6-trimethylphenyl)imidazolin-2-ylidene), **348a**; IDipp (1,3-bis(2,6-diisopropylphenyl)imidazolin-2-ylidene), **348b**) or $[(IDipp)Ni(\eta^6\text{-toluene})]$ (**349**) with P_4 (Scheme 92). The steric encumbrance of the NHC used had a profound effect on the product formed. Upon reaction between the smaller **348a** and P_4 (0.5 equiv.) in toluene, the electron-deficient trinuclear Ni_3P_4 (**350**, Scheme 92, top) was obtained, while in THF the reaction afforded the same cluster-core **350** along with Ni_3P_6 (**351**) and the dinuclear inverse sandwich Ni_2P_5 complex (**352a**, Scheme 92, middle). According to the Wade–Mingos rules, compounds **350** and **351** can be described as *superhypercloso* and *hypercloso* clusters. When utilizing the bulkier $[Ni(IDipp)_2]$ (**348b**, Scheme 92, bottom) as a metal precursor, the reaction afforded the Ni_3P_8 (**353**) *closo*-cluster with a novel homoquadricyclane-like P_8 framework as well as the IDipp analogue of the *cyclo*-P_5-Ni compound $[(IPh)_2Ni_2P_5]$ (**352b**) although separation of the products from the dissociated IDipp ligand proved to be difficult. The use of **349** as a starting material, in the presence of P_4 (0.5 equiv.) also afforded products **353** and **352b**. The molecular structures of compounds **350**–**353** (Fig. 86) showed the presence of monocarbene nickel moieties on the Ni-P framework in each case. Theoretical calculations on the truncated model $[(IPh)_2Ni_2P_5]$ (**352′**, IPh = 1,3-diphenylimidazolin-2-ylidene) were performed, and their agreement with the experimental EPR characterization revealed that the spin density in this species is evenly distributed between the Ni-atoms.

Similarly, Weigand, Wolf and co-workers described later [260] the preparation of $(NHC)Ni^0$ complexes, obtained by reacting the previously known compound $[(nacnac)Si(\kappa^2\text{-}P_4)]$ (**354**, nacnac = CH[C(Me)N(Dipp)][C(CH_2)N(Dipp)]) [261] with a suitable "$(NHC)Ni^0$" source. Treatment of the nickel(0) synthon $[(NHC)Ni(\eta^2\text{-vtms})_2]$ (**355**, NHC = IDipp, IMes; vtms = $Me_3SiCH{=}CH_2$) with **354** yielded different coordination compounds, depending on the stoichiometry used (ratio **355**:**354** = 1:1 or 1:2). The complexes $[(NHC)Ni\{(\mu,\kappa^2\text{:}\kappa^2\text{-}P_4)Si(nacnac)\}_2]$ (**356**) were obtained after reaction of the Ni(0) precursor with 2 equiv. of **354** (Scheme 93, left), while analogous reaction in 1:1 ratio afforded compound $[(IDipp)Ni(\mu,\kappa^2\text{:}\kappa^2\text{-}P_4)Si(nacnac)]$ (**357**, for NHC = IDipp). The structures of these complexes confirm the coordination of **354** to the (NHC)Ni(0) fragment (see Fig. 87**a-b**). In solution, compound **357** decomposes slowly (over a 3 weeks period), dimerizing to yield the unusual $Ni_2Si_2P_8$ cluster $[(IDipp)Ni_2P_8\{Si(nacnac)\}_2]$ (**358**) (see Scheme 93, right). An alternative pathway for the clean formation of **358** was found, in which precursor **355** was heated to 60 °C in the presence of **354**, thus circumventing the isolation of complex **357**. The unusual structure of the cluster was determined through X-ray crystallography (see Fig. 87**c**), and shows strongly varying P-P bond distances (range: 2.1702(8)–3.4219(8) Å). The two "(nacnac)Si" fragments stabilize the P_8 framework.

To investigate the potential of *cyclo*-P_3 complexes as phosphorus-based building blocks, Scheer and co-workers [262] studied the reactivity of the nickel complex $[Cp'''Ni(\eta^3\text{-}P_3)]$ (**359**, $Cp''' = \eta^5\text{-}1,2,4\text{-}tBu_3C_5H_2$) towards main group nucleophiles and reducing agents (Scheme 94). Upon reaction with potassium, the anionic dinuclear complex **360**, bearing a realgar-type P_8 ligand, was obtained (Fig. 88**a** for its X-ray structure). A similar P_8-motif was also identified for the dinuclear cobalt complex **291** (see Scheme 77, above), with the main difference being that, in the latter case an additional P-P bond has been cleaved [238].

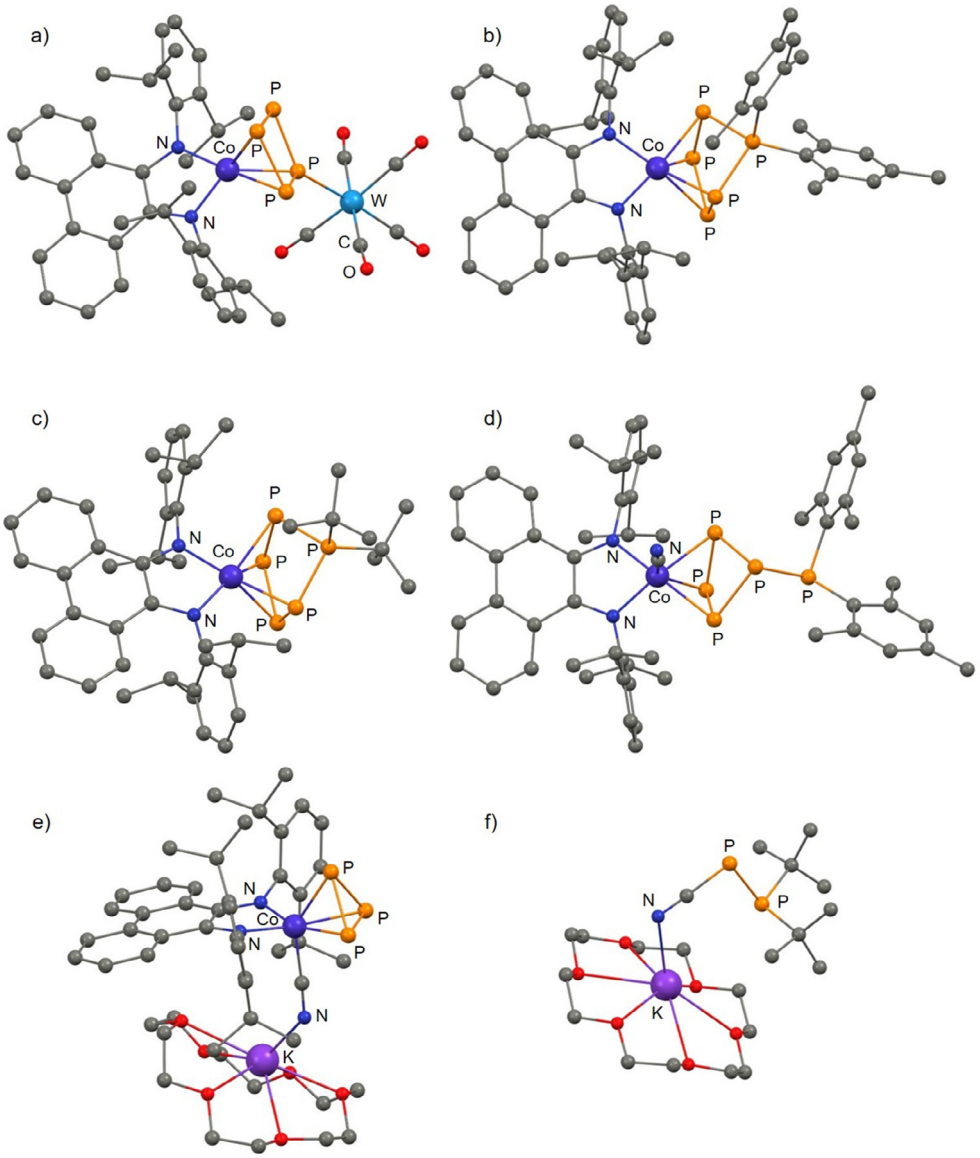

Fig. 75. Molecular structures of a) adduct **302** and selected products of functionalization of the *cyclo*-P_4 ligand in **300**: b) **303a**, c) **303c**, d) **304**, e) **305** and f) **306b**; adapted from Ref. [240].

Treatment of **359** with nucleophiles afforded an anionic triple-decker sandwich complex (**361**), a functionalized η^2-triphosphirene species (**362**) and a ring expansion product (**363**). The formation of **361** from the reaction of **359** and $NaNH_2$ contrasts with the behavior of pentaphosphaferrocene (**25**) towards the same nucleophile, which leads to dinuclear species **227** (*vide supra*). Based on the results from CV experiments, the oxidation of **361** with AgOTf (OTf = $CF_3SO_3^-$) led to the formation of the neutral triple-decker compound **364**. Crystallographic analysis of both triple-decker species reveals that the three-membered phosphorus ring is anionic for complex **361** and neutral for **364** and in the latter case, distorted (shown in Fig. 88**b**). When **359** was reacted with $LiNMe_2$ (Scheme 94, bottom), instead of forming a similar triple-decker complex, the highly sensitive η^2-triphosphirene **362** was obtained as the major product. The molecular structure reveals that the *cyclo*-P_3 unit is coordinated to the nickel center in an η^2 fashion, while the non-coordinated P-atom bears the NMe_2 substituent (see Fig. 88**c** for the molecular structure). Analogous reaction with $LiPPh_2$ led, by contrast, to the formation of the highly sensitive heptaphosphane compound $Li[(Cp'''Ni)_2(\mu,\kappa^2{:}\kappa^2\text{-}(P_6PPh_2)]$ (**363**), which could not be crystallized. The existence of the $P_6PPh_2^-$ ligand was confirmed after protonation of **363** with HBF_4, which afforded the more stable neutral species **365** (Fig. 88**d** shows its X-ray structure). Remarkably, the $P_6PPh_2^-$ ligand is formed by a P_6 bicyclic scaffold substituted by an exocyclic PPh_2 group and acts as a bridge between the two nickel centers in **365**. ^{31}P VT NMR studies revealed that when a reaction between the nickel *cyclo*-P_3 sandwich compound **359** and $LiPPh_2$ occurs, an intermediate analogous to the triphosphirene species **362** is formed, subsequently incorporating a second equivalent of **359** and rearranging to **363** on a rapid timescale. It was proposed that, similarly, in the reaction between **359** and NMe_2^- a reaggregation of the polyphosphorus ligand and addition of the nucleophile leads to the formation of an unstable $P_6NMe_2^-$-containing complex as a minor product [262].

Yakhvarov and co-workers [263] reported on the interaction between coordinatively unsaturated organonickel σ-complexes and white phosphorus leading to the formation of arylphosphinic

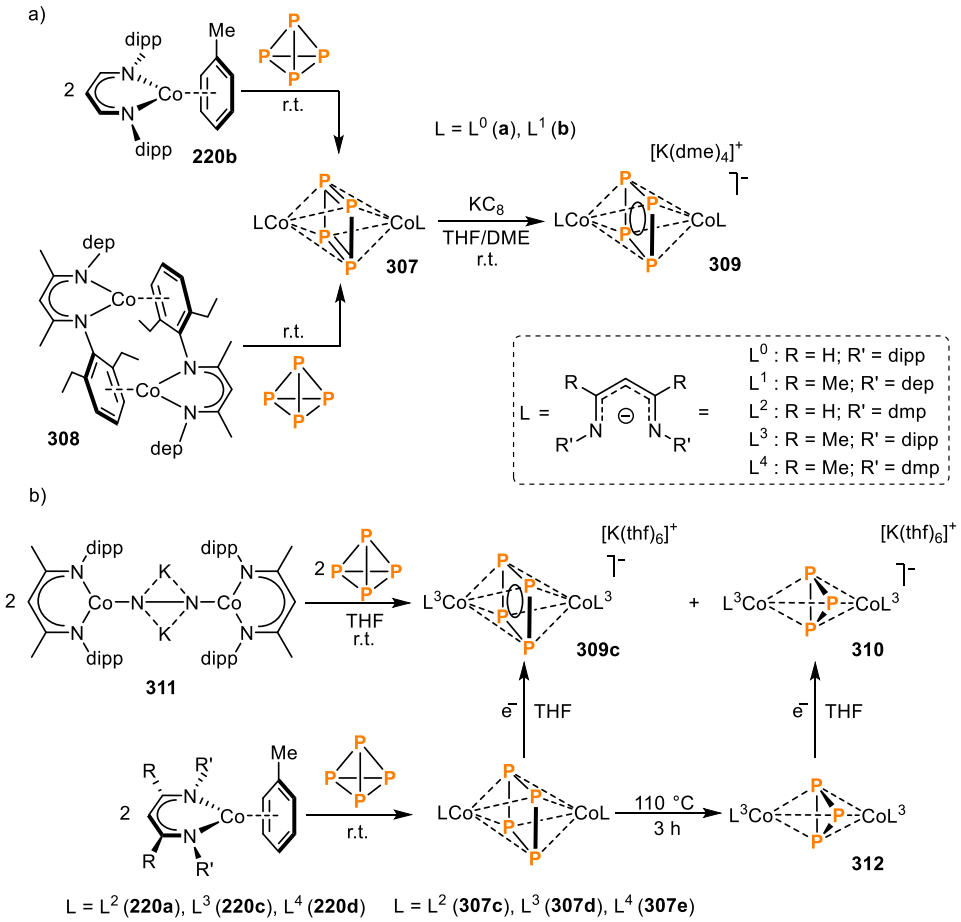

Scheme 80. Cobalt complexes featuring a) rectangular P_4 ligands, by the group of Driess [82] and b) *cyclo*-P_4 or *cyclo*-P_3 ligands, by the group of Scheer [241].

acids ArP(O)(OH)H. The complexes [(bpy)Ni(Ar)(Br)] [**366**; bpy = 2,2′-bipyridine, Ar = 2,4,6-trimethylphenyl (Mes) or 2,4,6-triisopropylphenyl (Tipp)] were activated either by reaction with a halide scavenger, such as $TlPF_6$, or electrochemically. Attempts to activate P_4 directly with **366** resulted to no reaction, evidencing that a vacant coordination at the nickel center site was needed. It was proposed that the P_4-cage should coordinate to the metal center, and the authors found evidence of formation of free Mes_2PH and coordinated $MesPH_2$ when complex **366a** was used. In the chemically activated system, addition of small amounts of water or concentrated HCl (37% w/w) did not alter the type of products obtained, after 6 h. However, prolonged reaction (stirring, 6 days) afforded the arylphosphinic acid MesP(O)(OH)H in moderate yields (32%). The analogous reaction with **366b** formed TippP(O)(OH)O (24% yield), without detecting $Tipp_2PH$, probably due to the higher steric demand of the substituents. Electrochemical activation of complexes **366**, followed by treatment with P_4, gave rise to the formation of a black precipitate, attributed to nickel phosphides, which after vigorous stirring and addition of HCl (2 M) returned better yields of the arylphosphinic acids ArP(O)(OH)H (Ar = Mes, 53%; Tipp = 42%).

The use of P_4 as a soluble and highly reactive "P" source to form nickel-phosphide and other metal-phosphide nanoparticles (M_xP_y) has been extensively documented by Mézailles and co-workers [221,264–267]. In Section 3.1.1, the synthesis of FeP nanoparticles from iron nanoparticles and white phosphorus, was described [221]. An early example of the investigations by this group, albeit previous to the period under review, is the synthesis of nickel phosphide nanoparticles from white phosphorus [264,265]. Ni_2P (**367**) was obtained by reaction of Ni(0) complexes (such as [Ni(cod)$_2$] (**368**), cod = 1,5-cyclooctadiene) or preformed (stabilized) Ni(0) nanoparticles with P_4 when used in a 2:1 ratio (Ni/P) [265]. Ni_2P-Ni core–shell monodispersed nanocomposites were also prepared by the same group, using mild reaction conditions and P_4 as phosphorus source [266]. By reacting well-defined monodisperse Ni nanoparticles with substoichiometric amounts of white phosphorus in solution at low temperatures (<220 °C), nanoparticles composed of two crystallized phases (Ni_2P and Ni fcc) were obtained. The crystallization of Ni_2P occurs after phosphorus insertion into the Ni fcc nanoparticles, hence yielding Ni_2P cores surrounded by magnetic Ni shells. The transformation of the nanoparticles into the core–shell structure proceeds without observing other Ni_xP_y crystallized intermediates. Fine-tuning of the magnetic properties of the core–shell Ni-P system was achieved through adjustment of the amount of P_4 used [266]. Later, by contrast, another investigation revealed an interplay between the P diffusion on the nanoparticles and the crystallization phase [221]. When substoichiometric amounts of white phosphorus were used in the Ni-P system (Ni/P <2) in this case, unreacted P_4 was identified (^{31}P NMR). Even by using a large excess of white phosphorus, hollow Ni_2P nanoparticles were preferentially obtained from monodispersed nickel nanoparticles in solution up to 320 °C.

Mézailles, Carenco and co-workers also described the synthesis of crystalline bimetallic phosphide Ni–Cu–P nanoparticles, which were obtained by reacting core–shell copper–nickel nanoparticles with white phosphorus [267]. The authors synthesized core–shell

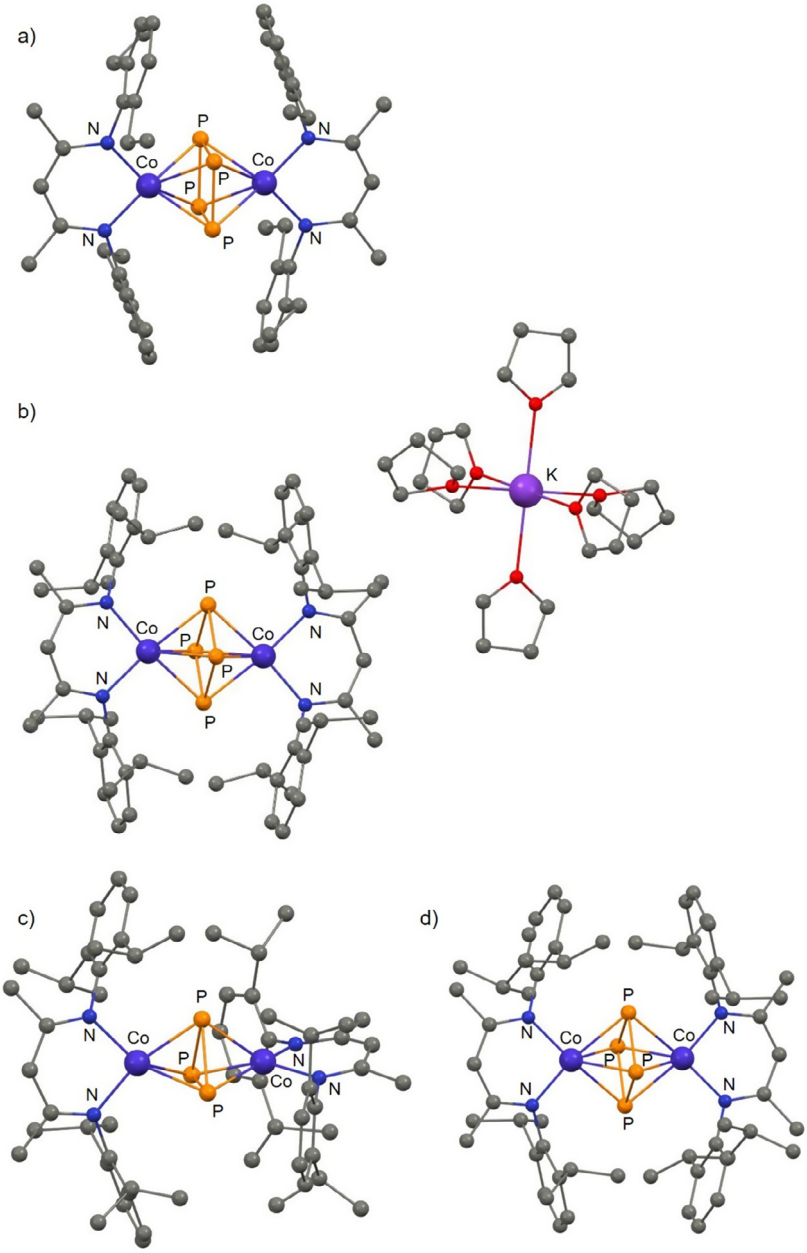

Fig. 76. X-ray structures of selected β-diketiminato cobalt(*cyclo*-P_n) complexes: a) **307b**, b) **309c**, c) **310** and **307c**; adapted from Refs. [82,241].

$Cu_{0.25}Ni_{0.75}$ nanoparticles and reacted them with P_4, yielding crystalline Ni–Cu–P nanoparticles. This investigation afforded hollow monocrystalline $(Ni,Cu)_2P$ nanoparticles together with Cu nanoparticles, which crystallized in a mixed phase isostructural to Ni_2P, using a stoichiometry aiming for full phosphidation of Ni into Ni_2P. For this system, it was possible to gain insights into the mechanism of formation of the nanoparticles. According to the proposal by this group, a metal preference of phosphorus towards nickel instead of copper was observed, yielding hollow Ni-rich phosphide nanoparticles and Cu nanoparticles. The insertion of phosphorus into the bimetallic nanoparticles triggered their amorphization and recrystallization, thus promoting an outward migration of copper to leave a void in the core. In the course of the copper migration, an amorphous intermediate of $(Ni,Cu)_2P$ could initially form, to crystallize later into mixed phosphide. Alternatively, the formation of pure Ni_2P with subsequent evolution towards $(Ni,Cu)_2P$ could also occur. Finally, the migrated copper crystallizes into Cu fcc nanoparticles [267].

3.3.2. Palladium

Very few reports on the chemistry of palladium towards white phosphorus were published in the period 2011–2020. The synthesis of Pd-secondary phosphine oxide compounds from P_4-derived H_3PO has been recently published in a collaboration between the groups of Yakhvarov and Hey-Hawkins [49]. However, the transformation of P_4 into H_3PO was carried out electrochemically. Subsequent reaction of the produced H_3PO with cyclic ketones afforded the secondary phosphine oxides, which were used as ligands towards palladium(II) [49].

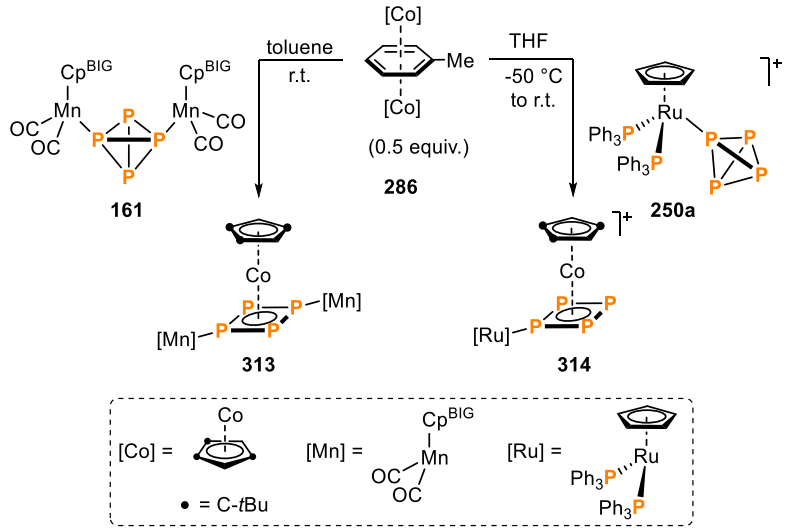

Scheme 81. Aromatic *cyclo*-P_4 ligands at cobalt obtained after activation of coordinated P_4-tetrahedra.

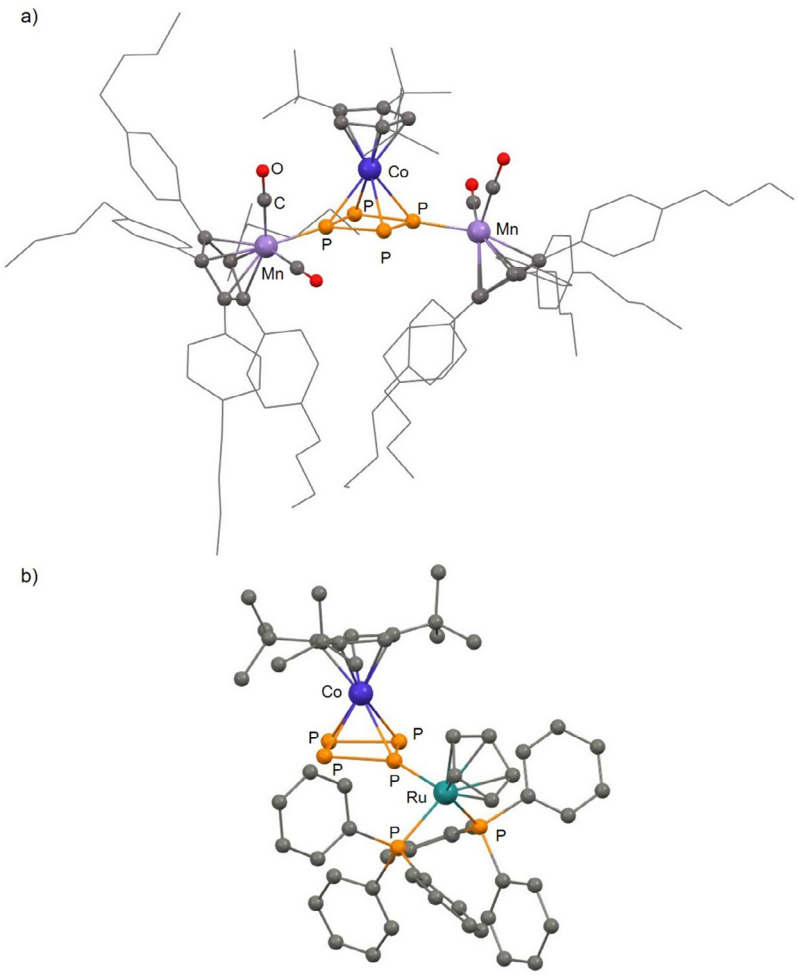

Fig. 77. X-ray structures of a) **313** and b) **314**; adapted from Ref. [81].

Nevertheless, and despite the fact that the contribution dates from 2010 and strictly speaking falls outside the scope of this review, it is worth mentioning that the group of Yakhvarov described a catalytic system for the transformation of P_4 into H_3PO_3 [268]. By reacting $[Pd(PPh_3)_2Br_2]$ (**369**) with P_4, in the presence of a stoichiometric amount of $NaBPh_4$ in THF/water, labile cationic Pd(II)-solvato complexes were generated, and phosphorous acid was obtained. The formation of H_3PO_3, along with the

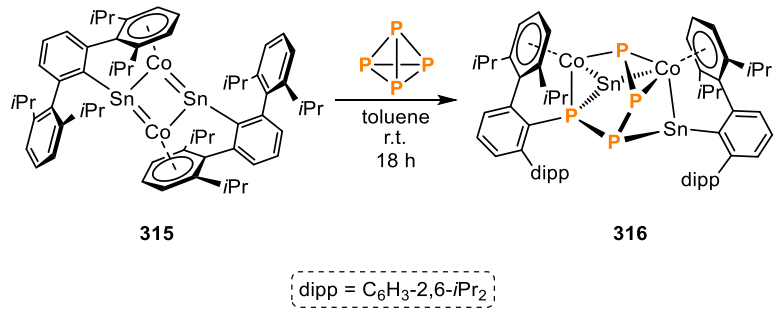

Scheme 82. Insertion of P_4 into the framework of a cobalt-tin (Co_2Sn_2) cluster.

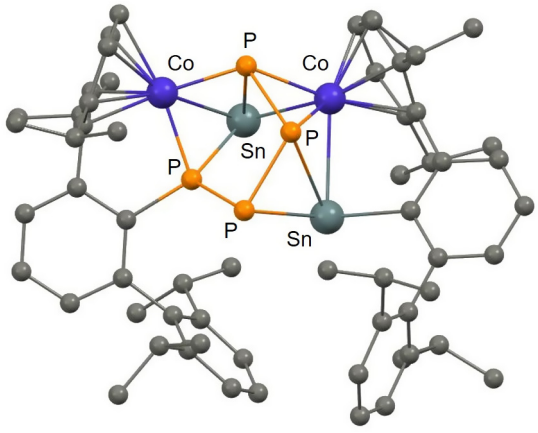

Fig. 78. Molecular structure of the cluster [Ar'$_2$Sn$_2$Co$_2$P$_4$] (**316**); adapted from Ref. [242].

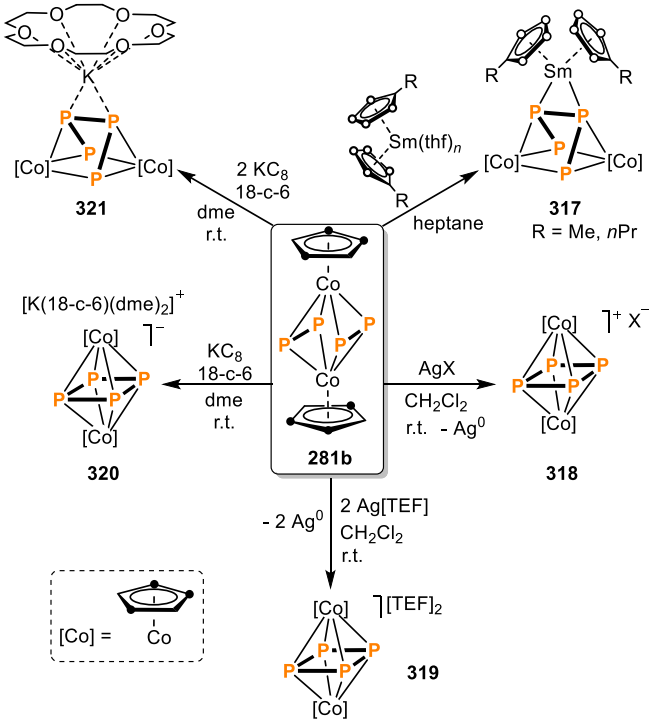

Scheme 83. Formation of P_4 ligands *via* coupling of P_2^{2-} ligands on **281b**.

minor products H_3PO_4 and $H_4P_2O_7$, was confirmed *via* NMR spectroscopy. The products were converted to H_3PO_4 after addition of small amounts of aqueous HCl (2 N). Mechanistic studies (NMR, MALDI-MAS) revealed that a ligand exchange of the phosphine ligands at Pd(II) by the P_4-cage (Scheme 95), followed by hydrolysis of the coordinated P_4 tetrahedron led to the major product H_3PO_3. Furthermore, spectroscopic evidence indicated that the species $[Pd(PPh_3)_3]^{2+}$ and $[Pd(PPh_3)_2]$ were present during the reaction. Consequently, it was proposed that the oxidation of white phosphorus occurs with partial reduction of Pd(II) → Pd(0), which is maintained in solution by recoordination of the PPh_3 ligands liberated at an earlier stage in the reaction. No further evidence for the mechanistic proposal was given.

The formation of palladium phosphide nanoparticles was described by Mézailles and co-workers [221,269]. By reacting Pd nanoparticles synthesized in oleylamine with exact amounts of P_4 (0.5 equiv. or 0.1 equiv. of P_4, respectively), both PdP_2 (**370**) and Pd_5P_2 (**371**) nanoparticles were selectively obtained [221]. For the crystallization of the two different phases, high temperatures were required. For nanoparticles with lower P-content, even at the high temperature used (310 °C), it was not possible to crystallize the amorphous Pd_3P (**372**) obtained. Hence, the authors described the amorphous plain Pd_3P nanoparticles as having a particularly high stability [221]. Further investigations revealed that the formation of crystallized palladium phosphide nanoparticles is a two-step process [269]. In a first step, amorphous Pd–P nanoparticles are formed at moderate temperatures, while crystallization occurs at higher temperatures (270–310 °C). Moreover, the crystallization temperature was found to be strongly dependent on the Pd/P ratio. The Pd-P system proved to be complex at the nanoscale, and only three crystalline phases were identified, as a result: PdP_2, Pd_5P_2, and Pd_3P. Quantitative phase-to-phase transformation from P-poor phosphides (Pd_3P and Pd_5P_2) to the P-rich PdP_2 was also demonstrated. The use of a defined molecular precursor such as P_4 resulted key for the study of a nanoscale phase diagram for this system, given that it reacts stoichiometrically to generate P (0) species under mild conditions [269].

3.3.3. Platinum

The platinum-promoted opening of a coordinated P_4-ligand was reported by Peruzzini and co-workers, as described in Section 3.1.2 (Scheme 71**a**, *vide supra*) [178,222]. The cationic complexes *trans*-$[Ru(PP)_2(H)(\eta^1\text{-}P_4)]^+$ (PP = dppm or dppe, **246**), featuring intact P_4 tetrahedra, were reacted with $[(C_2H_4)Pt(PPh_3)_2]$ (**247**) in CH_2Cl_2, to yield the heterobimetallic compounds $[\{Ru(PP)_2(H)\}(\mu,\kappa^1,\kappa^2\text{-}P_4)\{Pt(PPh_3)_2\}]BF_4$ (PP = dppm or dppe, **248**). Here the P_4 moiety has undergone activation of one P-P bond, with insertion of the platinum unit (Scheme 71**a**) [178,222]. Similar behavior was observed when the piano-stool complex was reacted with the Pt(0) precursor, yielding the P_4-butterfly compound $[\{CpRu(PPh_3)_2\}(\mu,\kappa^1,\kappa^2\text{-}$

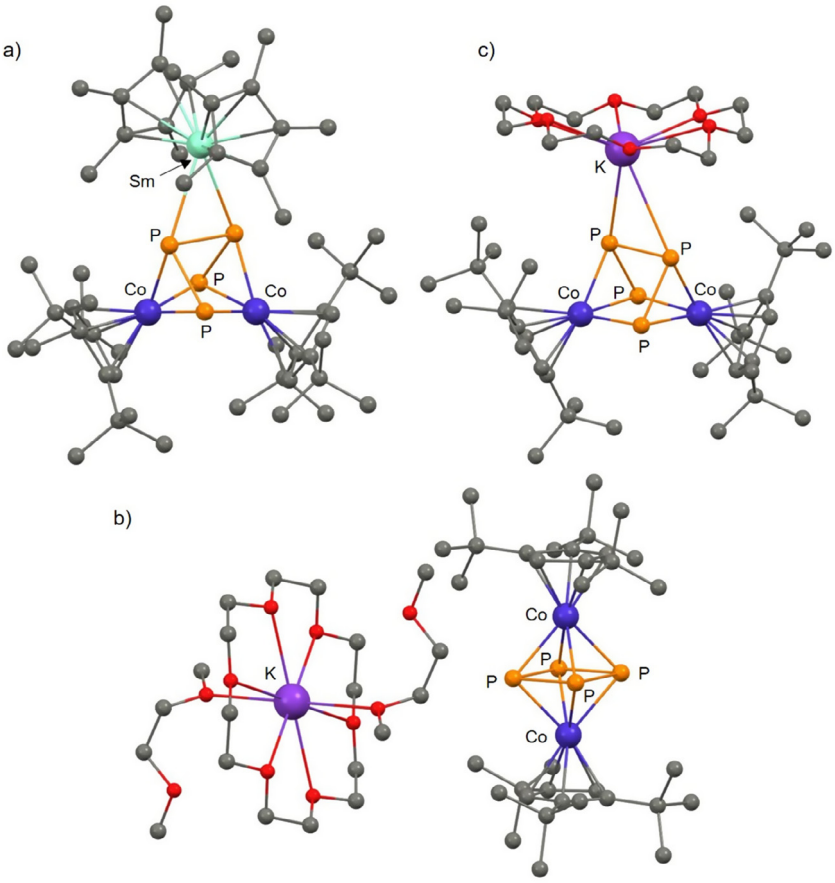

Fig. 79. X-ray structures of selected products of P-P coupling at cobalt: a) **317a**, b) **320** and c) **321**; adapted from Ref. [244,245].

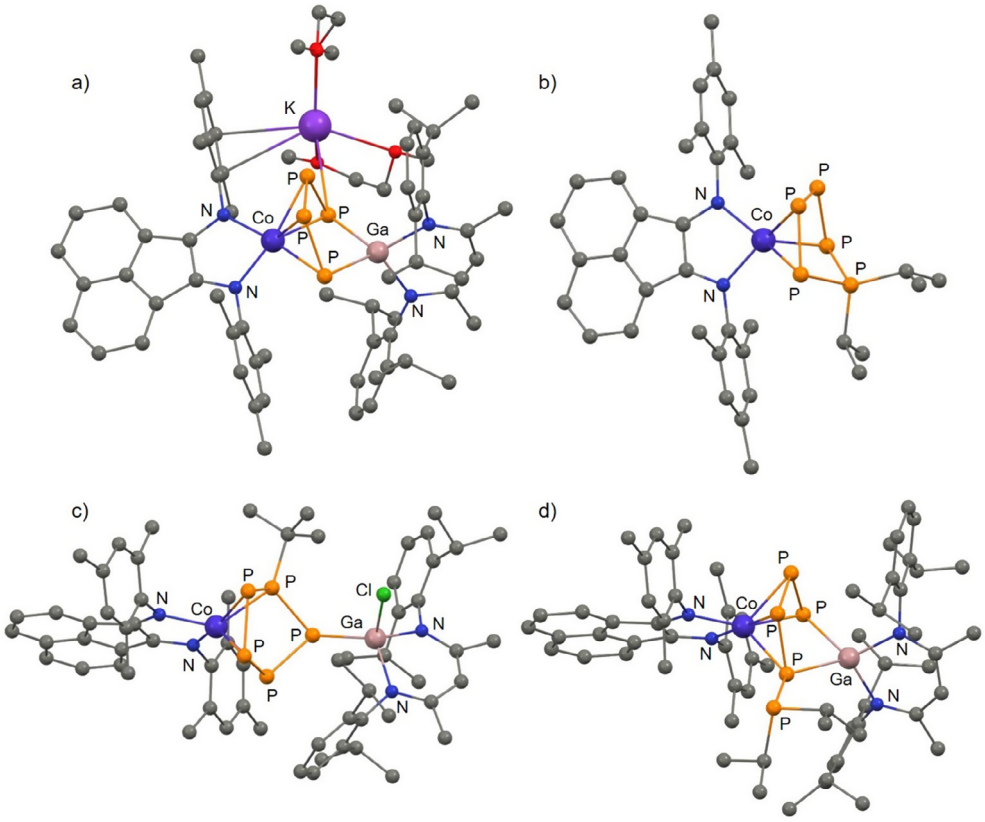

Fig. 80. X-ray structures of a) **322b**, b) **323a**, c) **324** and d) **325**; adapted from Ref. [209].

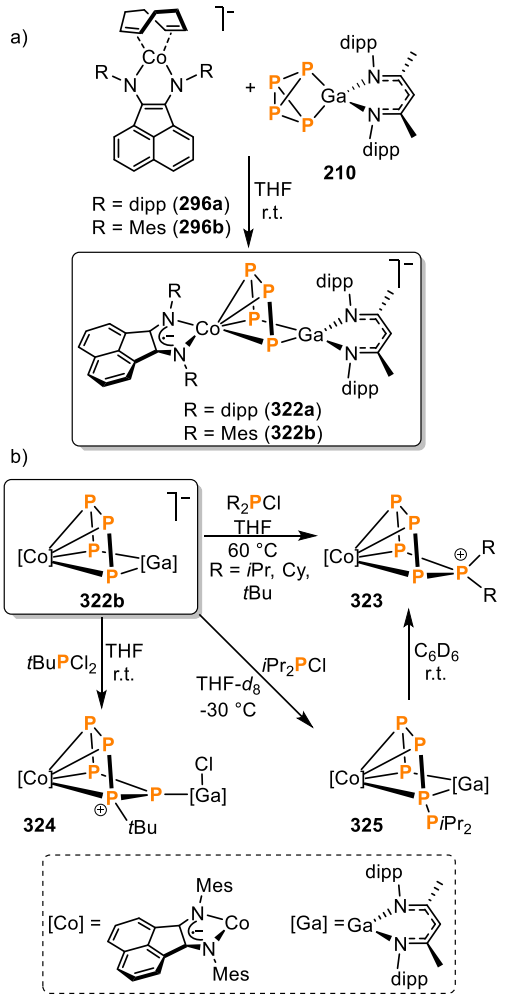

Scheme 84. Synthesis of the *catena*-P_4 heterodinuclear complex **322b** and functionalization of the P_4-ligand with chlorophosphanes.

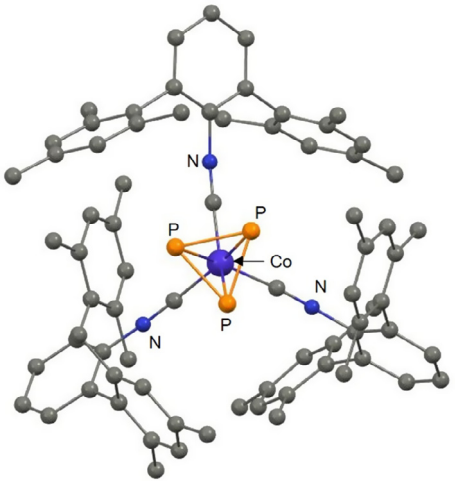

Fig. 81. X-ray structure of $(\eta^3\text{-}P_3)Co(CNAr^{Mes2})_3$ (**327**); adapted from Ref. [248].

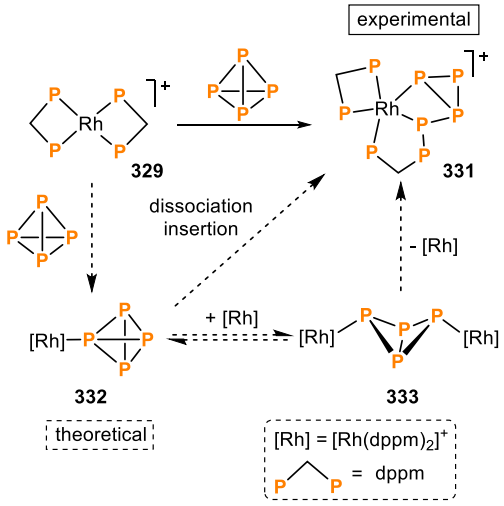

Scheme 86. Mechanism proposed by Schoeller for the activation of P_4 at $[Rh(dppm)_2]^+$ (**329**).

$P_4\{Pt(PPh_3)_2\}]^+$ (**251**; Scheme 71**b**, *vide supra*). For the three bimetallic species, dynamic processes in solution were identified [178,222] through variable temperature $^{31}P\{^1H\}$ NMR and $^{31}P\{^1H\}$ EXSY experiments. The fluxional process was described as a combination of two independent motions. Complete scrambling of all of the phosphorus atoms in the P_4-cage was observed as the result of chemical exchange at the Ru-center, specifically between the Ru-bonded and the free P atoms of the tetrahedron (swinging or pendulum-like), without rupture of the Ru-P bond, thus passing through an $\eta^2\text{-}P_4\{Pt(PPh_3)_2\}$ motif. In a second process, the platinum center exchanges between the three P-atoms not coordinated to ruthenium [178]. For **248a**, such a proposal was confirmed through DFT calculations on the model compound **248′**, featuring $H_2PCH_2PH_2$ instead of dppm [222]. The activation parameters for the dynamic processes, calculated from the VT NMR experiments, were reported [178,222].

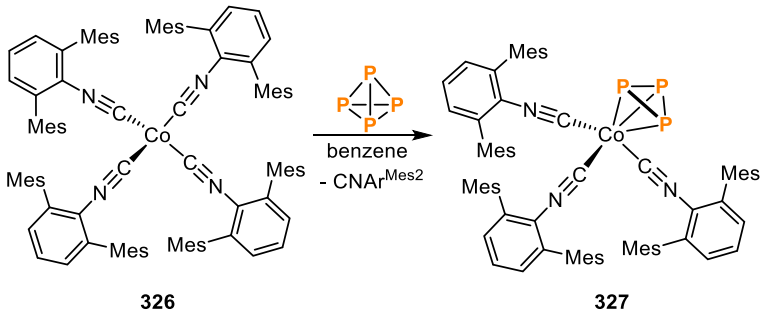

Scheme 85. Synthesis of a *cyclo*-P_3 cobalt complex by Figueroa and co-workers [248].

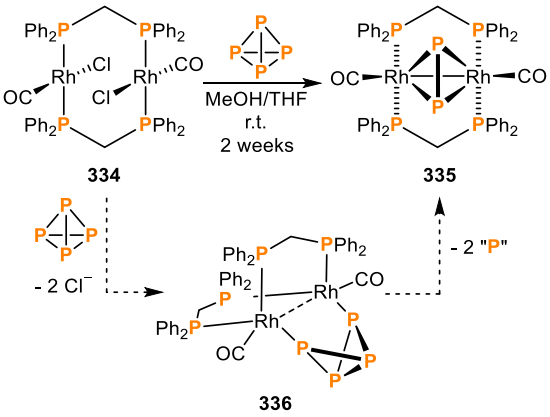

Scheme 87. Synthesis of the diphosphorus compound $[Rh_2(CO)_2(\mu\text{-dppm})_2(\mu,\eta^2\text{-}P_2)]$ (**335**) by Caporali, Peruzzini and co-workers [251].

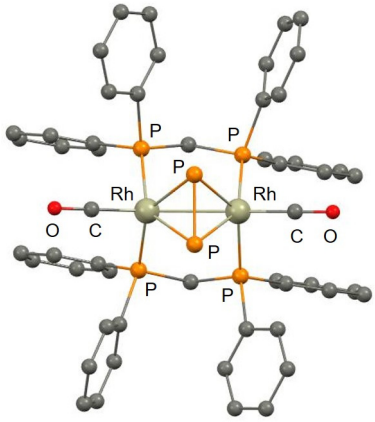

Fig. 82. X-ray structure of $[Rh_2(CO)_2(\mu\text{-dppm})_2(\mu,\eta^2\text{-}P_2)]$ (**335**), adapted from Ref. [251].

The dinuclear complex $[(\{(dppp)Pt\}_2)_2(\mu,\eta^2{:}\eta^2\text{-}P_2)]$ (dppp = 1, 3-bis(diphenylphosphanyl)propane, **373**) was reported in 2010 by Mézailles and co-workers [270]. The formation of **373** (Scheme 96) was achieved using the Pt(0) precursor, [(dppp)Pt(C_2Ph_2)] (**374**) in the presence of white phosphorus (0.5 equiv.). Fig. 89 shows the molecular structure of the complex, determined using X-ray diffraction. DFT calculations showed that the P_2 bridging scaffold in **373** can be considered as a P_2^{4-} ligand and, thus the metal centers have been oxidized to Pt(II). The observation of a red precipitate along with complex **373**, and the theoretical studies supported the proposal that a "P_2" fragment was eliminated from the P_4 cage as a highly reduced P_2^{4-} fragment [270]. In 2013, Radius and co-workers also concluded that the P_2 ligand in **373** corresponded to a P_2^{4-} unit, while revisiting such investigations in the frame of their own study on the related Ni_2P_2 complex $[\{Ni_2(i\text{Pr}_2\text{-Im})_2\}_2(\mu,\eta^2{:}\eta^2\text{-}P_2)]$ (**346**), discussed above [257]. Furthermore, this group performed calculations on the platinum analogue $[\{Pt_2(i\text{Pr}_2\text{-Im})_2\}_2(\mu,\eta^2{:}\eta^2\text{-}P_2)]$ (**375**) to determine the influence of the metal center (Ni vs. Pt) and of the ancillary ligand (NHC vs. diphosphine) on the nature of the P_2 bridge. The results indicated that the ligand does not exert a significant influence on the distribution of the frontier orbitals of the platinum complexes. Moreover, the structural features calculated for **375** are in good agreement with those found for **346**, with the main difference being a longer M–P distance, attributed to the increase in atomic radius for the platinum complex. Nevertheless, it was found that for the platinum analogue, the planarized structure would be significantly more destabilized than in the case of the nickel compound. The stronger destabilization would also be caused by a second-order Jahn-Teller distortion, and by unfavorable bonding interactions between the platinum atoms and the P_2 ligand [257].

3.4. Group 11 metals

The chemistry of white phosphorus towards coinage metals has been of interest in the period under review [181–187,195,271–279], with most of the examples involving either copper or gold species.

3.4.1. Copper

The coordination of white phosphorus towards coinage metal salts was investigated by the groups of Green, Russell, Slattery and co-workers [271]. Suitable cationic coinage metal precursors were generated from simple inorganic salts in the presence of Lewis acids, and then reacted with P_4. Equimolar amounts of MX (for M = Cu, Au, X = Cl; for M = Ag, X = OTf) and $GaCl_3$ in dichloromethane, followed by addition of P_4, led to the formation of ion-contacted coordination polymers for copper and silver, of the general formula $(P_4MGaCl_4)_n$ [M = Cu (**376**); M = Ag (**377**)]. The molecular structure of **376** (see Fig. 90) features chains of $CuGaCl_4$ units linked by P_4 molecules. Each P_4 tetrahedron is coordinated through P_2 edges to a different copper center, connecting two metal centers and aggregating to form the coordination polymer. The bond lengths on the coordinated edge of the P_4 molecule feature elongated distances (P-P bond = 2.3744 Å) with respect to the free P_4 tetrahedron (2.21 Å), while the distances of uncoordinated edges (2.1742–2.1787 Å) are in the range of the distances in the latter. The product is thermally unstable and sensitive to oxygen [271].

Russell and co-workers also investigated on the coordination of the intact P_4 tetrahedron towards coinage metal-phosphine/–NHC compounds (Scheme 97**a**) [272]. The series of complexes $[(Pt\text{Bu}_2\text{-Ar})M(\eta^2\text{-}P_4)]^+$ (M = Cu (**378**), Au (**379**); $Pt\text{Bu}_2\text{Ar}$ = JohnPhos [$Pt\text{Bu}_2$(*o*-biphenyl)], *t*BuXPhos [$Pt\text{Bu}_2$(2′,4′,6′-triisopropylbiphenyl)] were obtained upon treatment of a suitable $(Pt\text{Bu}_2\text{Ar})MX$ (MX = CuI, AuCl) precursor with a halide scavenger, followed by addition of one equivalent of white phosphorus. Both copper complexes present similar structural features, according to XRD (see Fig. 91 for the structure of $[(\text{JohnPhos})Cu(\eta^2\text{-}P_4)]^+$, **378a**). As previously observed for analogous compounds [271,273–275], a dynamic behavior was observed on the NMR timescale for the P_4 ligand, featuring a unique singlet on $^{31}P\{^1H\}$ for the tetrahedron in each example of the series of complexes.

In 2016, Lammertsma and co-workers reported on the coordination chemistry of P_4 towards coinage metal cations such as Cu^+ and Au^+ [276]. The commercially available *N*–heterocyclic carbene (NHC) complexes (IDipp)MCl ([M = Cu (**380**), Au (**381**); IDipp = 1,3-bis(diisopropylphenyl)imidazolin-2-ylidene)] were suitable precursors, in the presence of a chloride scavenger, for the synthesis of the M–P_4 cationic adducts, $[(IDipp)M(\eta^2\text{-}P_4)]^+$ (M = Cu (**382**), Au (**383**); Scheme 97**b**). Almost simultaneously, Russell and co-workers also reported on the synthesis of complex **383** by a different synthetic approach (see Scheme 97) [272]. $^{31}P\{^1H\}$ NMR spectra of the complexes revealed broad singlets (δ = –483.1 ppm for **382** and δ = –464.4 ppm for **383**) indicative of fluxional behavior, similar to other η^2-P_4 complexes. VT NMR measurements (−90 °C) confirmed the dynamic behavior in solution, for both complexes [271–273]. Computational calculations on the bonding situation for $[(IDipp)M(\eta^2\text{-}P_4)]^+$ agree with the spectroscopic observations, suggesting that the P_4 ligands remain intact, and that oxidative addition by P-P bond cleavage is disfavored. Additionally, the stability of the complexes is in agreement with the theoretical

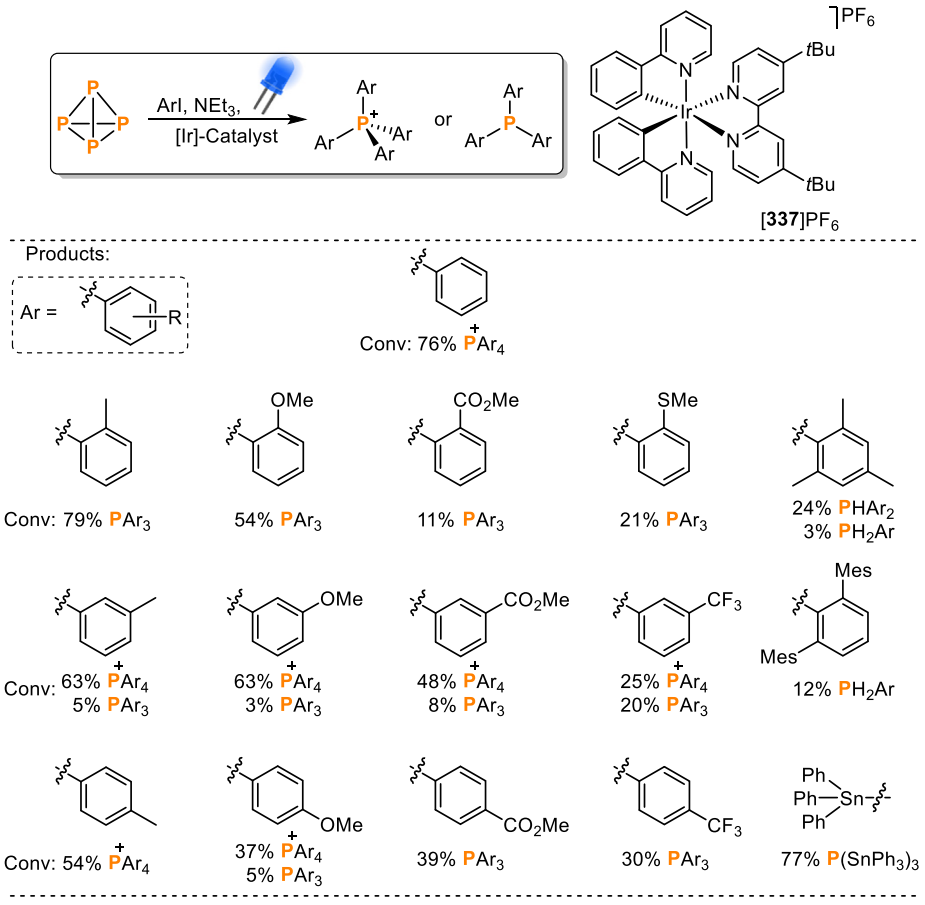

Scheme 88. Photocatalytic direct functionalization of white phosphorus with aryl iodides using [Ir(dtbbpy)(ppy)$_2$]PF$_6$ ([**337**]PF$_6$). Conversions were determined by quantitative ^{31}P NMR experiments using Ph$_3$P=O as an internal standard [53].

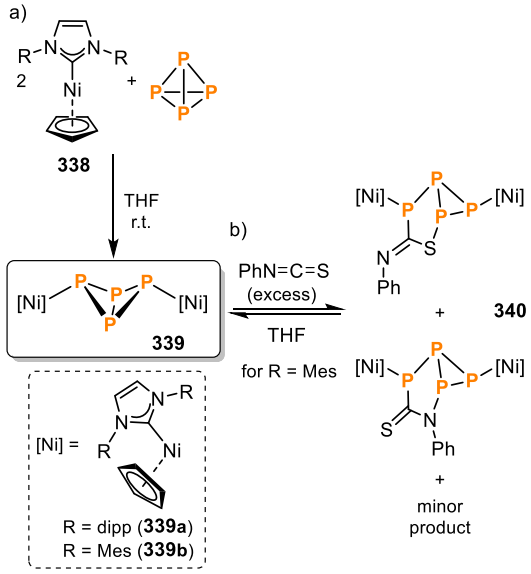

Scheme 89. a) Synthesis of {CpNi(NHC)}$_2$(μ,κ^1:κ^1-P$_4$)] (**339**, NHC = IDipp, IMes) and b) insertion of phenyl isothiocyanate into a P-P bond (NHC = IMes).

data, with the gold complex being more stable than the copper analogue [276].

Neutral copper complexes containing intact E$_4$ tetrahedra (E = P, As) as ligands were reported in 2015 by the group of Scheer [277]. The neutral dicopper compounds [{(nacnac)Cu}$_2$(μ,η^2:η^2-E$_4$)] [nacnac = [{N(C$_6$H$_3$*i*Pr$_2$-2,6)C(Me)}$_2$CH]$^-$; E = P (**384a**), As (**384b**)] featuring intact E$_4$ tetrahedra as bridging η^2:η^2-ligands were synthesized and fully characterized. **384a** is obtained upon reaction between [(nacnac)Cu(MeCN)] (**385**) and P$_4$ in a 2:1 ratio (Scheme 98, and Fig. 92 for the molecular structures). The complex is stable under argon in the solid state for long periods of time but decomposes slowly in solution and when exposed to light. The molecule features an almost square-planar copper center, while the P-P bonds within the tetrahedron are elongated with respect to the free white phosphorus, as revealed by crystallography. Moreover, reacting **384a** with a stronger Lewis base such as pyridine, leads to a displacement of the bridging η^2:η^2-P$_4$ ligand, releasing free P$_4$. By reacting **384a** with P$_4$, the mononuclear species [(nacnac)Cu(η^2-P$_4$)] (**386**), bearing an intact side-on coordinated P$_4$ tetrahedron, was obtained in solution. Such a mononuclear complex can also be obtained from the copper precursor **385** and an excess of P$_4$. In solution, a dynamic behavior on a NMR timescale was observed for complex **386**. VT ^{31}P{^{1}H} along with ^{31}P{^{1}H} EXSY NMR experiments indicated that, at low temperatures (up to 213 K), the main fluxional process is the tumbling (as previously mentioned, the η^1 → η^2 → η^1 walk down an edge of the tetrahedron) of the coordinated P$_4$. At higher temperatures, dissociation of the P$_4$ ligand takes place. Such release results in a shifted equilibrium between the mononuclear and dinuclear complexes, **386** and **384**, respectively (Scheme 98). For both complexes, DFT calculations confirm the coordination of the intact P$_4$ tetrahedron.

The chemistry of the chelating metalloligand [{Cp‴Fe(CO)$_2$}$_2$(μ,κ^1:κ^1-P$_4$)] (**178b**) towards copper precursors described by the

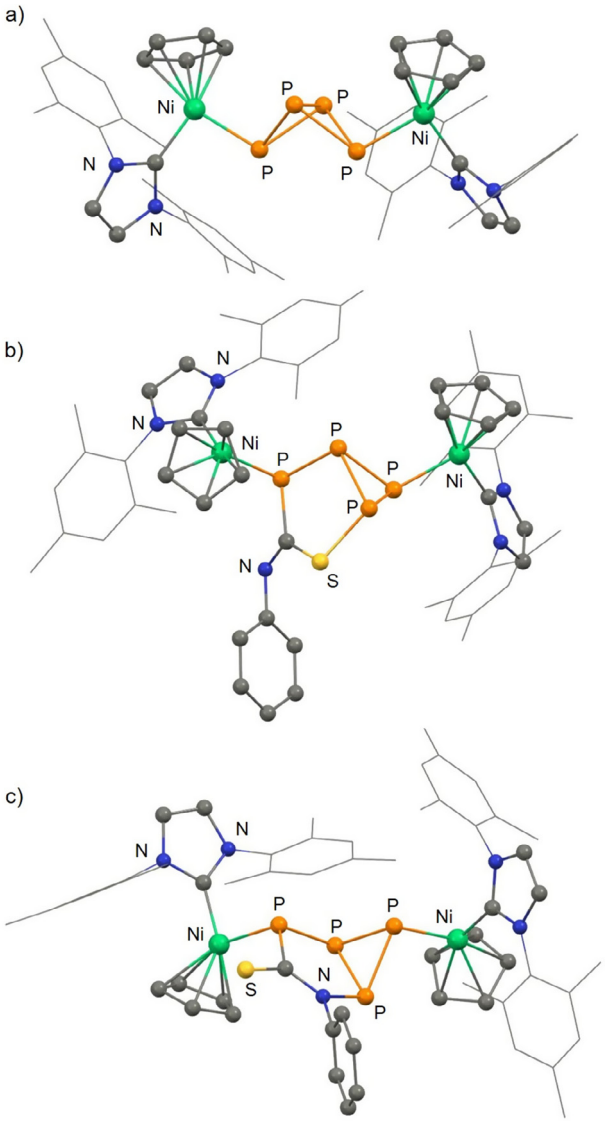

Fig. 83. X-ray structures of a) **339b** and b) and c) the bicyclo[3.1.0]heterohexane products (**340**) of insertion of phenyl isocyanate into the butterfly-P_4 motif; adapted from Ref. [254].

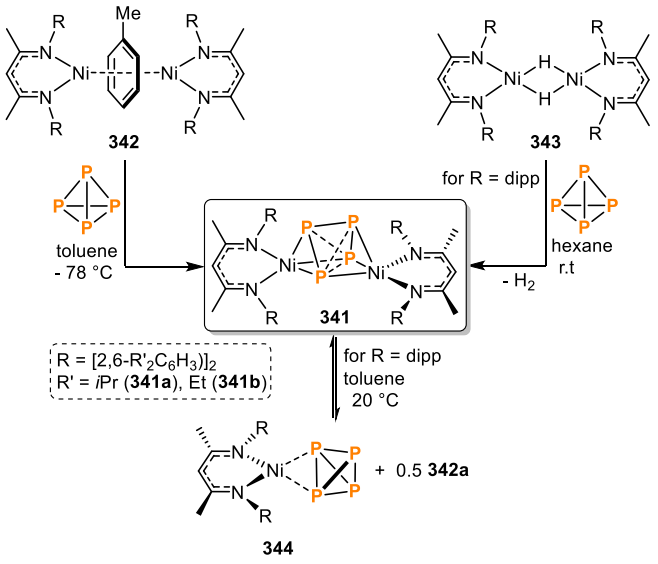

Scheme 90. Reversible activation of P_4 at Ni(I) by Driess and co-workers [256].

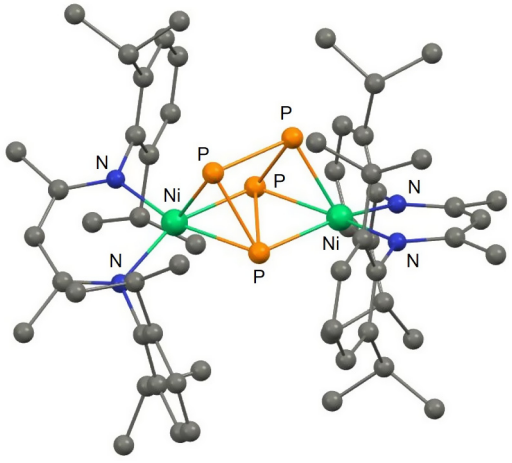

Fig. 84. X-ray structure of **341a**; adapted from Ref. [256].

group of Scheer (see Section 3.1.1), demonstrated the potential of such complexes to form heterometallic complexes containing P_n ligands [195]. The same group also studied the interaction between the mixed P_nAs_m ligand complex, $[\{Cp'''Fe\}_2(\mu,\eta^4{:}\eta^4\text{-}P_nAs_{4-n})]$ (**179c**, Section 3.1.1) and CuCl [192]. Upon reacting **179c** with CuCl in a 1:2 ratio, the 1D coordination polymer $[\{Cp'''Fe\}_2(\mu,\kappa^4{:}\kappa^4{:}\kappa^1{:}\kappa^1\text{-}E_4)\{Cu(\mu,Cl)\}_2(MeCN)]_\infty\cdot(CH_2Cl_2)_2$ (**387**, E_4 = P_nAs_{4-n}) was obtained. According to the occupancy pattern of the E_4 moiety and the XRD molecular structure (see Fig. 93), the undulated chain of the coordination polymer is formed through interaction of the phosphorus atoms with the copper centers.

Supramolecular Cu-(P_n) (n = 2) or Cu-*cyclo*-P_n (n = 3, 5, 6) structures have also been described by the group of Scheer [144,148,181–187,278] (see Section 2.4.2). The interaction between "naked" copper ions and chromium or molybdenum complexes featuring P_2 or *cyclo*-P_n ligands [148,278], or pentaphosphaferrocene (**25**) [181–187,278] proves the potential of such compounds to act as metalloligands towards Lewis acids, thus assembling supramolecular structures. "Inorganic fullerenes" have been obtained by interaction of **25** with Cu(I) halides [181–187]. Likewise, mononuclear or dinuclear Cu(I) complexes resulted from reacting P_2Mo_2 or *cyclo*-P_3 chromium or molybdenum metalloligands with "naked" copper cations, while the interaction with **25** afforded a one-dimensional coordination polymer featuring a paddle-wheel-shaped building block [144,278].

Mézailles and co-workers described the formation of copper phosphide nanoparticles from copper nanoparticles and white phosphorus [221]. The quantitative reduction of $Cu(acac)_2$ (acac = 2,4-pentanedionate) with oleylamine yielded copper nanoparticles which were reacted with P_4, using the stoichiometric amount required (1/12 equiv. of P_4) to yield Cu_3P (**388**) nanoparticles. Under very mild conditions (100 °C, 30 min), it was possible to crystallize the nanoparticles, yielding an original core–shell Cu–Cu_3P structure. No amorphous intermediate could be observed. The mild conditions used for the crystallization of the copper nanoparticles contrast with those required for the iron (Section 3.1.1), nickel (Section 3.3.1) or palladium (Section 3.3.2) nanoparticles.

3.4.2. Silver

As previously discussed (see Section 3.4.1), upon reacting P_4 with CuCl or AgOTf in the presence of $GaCl_3$, coordination polymers

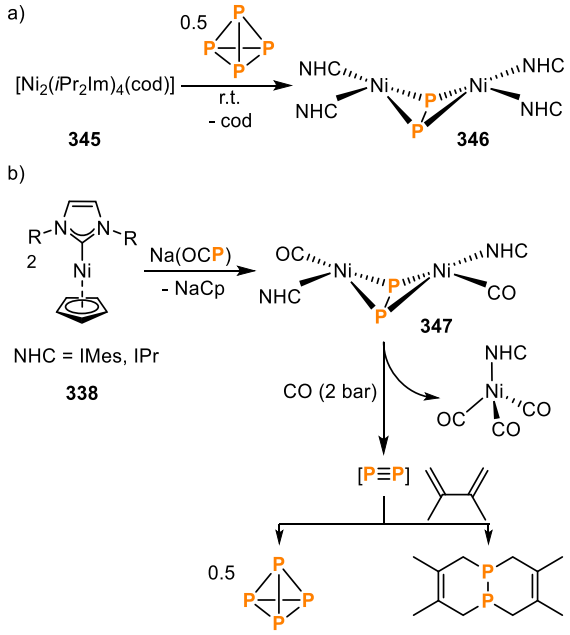

Scheme 91. Butterfly-Ni_2P_2 complexes by a) Radius and co-workers [257] and b) Wolf, Goicoechea and co-workers [258].

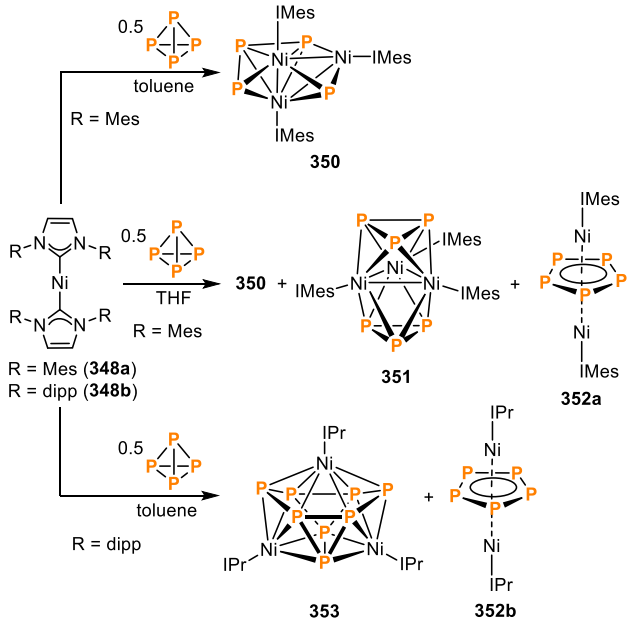

Scheme 92. Ni(0)-mediated degradation and aggregation of P_4 by Wolf and co-workers [259].

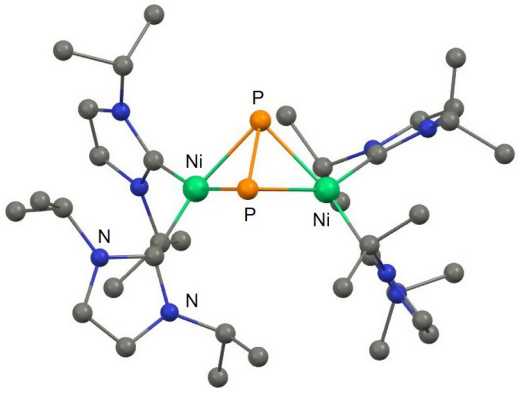

Fig. 85. X-ray structure of $[\{Ni_2(iPr_2Im)_2\}_2(\mu,\eta^2{:}\eta^2\text{-}P_2)]$ (**346**); adapted from Ref. [257].

of general formula $(P_4MGaCl_4)_n$ [M = Cu (**376**); M = Ag (**377**)] were obtained [271]. The silver polymer **377** (Fig. 94), however, presents structural differences with respect to the copper analogue **376**. In this case, the P_4 tetrahedron is not part of the polymer core skeleton but coordinates to the silver metal centers in an η^2-mode outside the main polymer net. The latter is composed of a $AgGaCl_4$ ladder. Coordination of the P_4 molecule in this polymer creates a distortion on the bond lengths within the tetrahedron, with the bond distance of the coordinated edge (2.3403 Å) being elongated in comparison to the rest of the P-P bonds (2.1670 to 2.2161 Å).

Scheer and co-workers have extensively studied the chemistry of P_n metalloligands towards Lewis acidic coinage metal cations, which leads to interesting supramolecular structures [144,148]. For example, organometallic-organic hybrid polymers were obtained by the interaction of $[Ag_2(\mathbf{110})_4]^{2+}$, [see Section 2.4.2, $[Cp_2Mo_2(CO)_4(\eta^2\text{-}P_2)]$ (**110**)], with the pyridine linker, di(pyridine-4-yl)ethene. Flexible coordination of the ligands, monomer–dimer equilibria, and dynamic behavior in solution were evidenced, giving rise to the formation of rectangular or 1D hybrid networks [144].

3.4.3. Gold

The interaction of P_4 with coinage metal salts in the presence of $GaCl_3$ afforded copper(I) and silver(I) coordination polymers **376** and **377**, as discussed in sections 3.4.1 and 3.4.2 [271]. By contrast, analogous reaction with AuCl yielded the until then unknown homoleptic cationic complex $[Au(\eta^2\text{-}P_4)_2]^+$ (**389**, Scheme 99) [273], which completed the series of coinage metal homoleptic complexes of the P_4 tetrahedron [273–275], $[M(\eta^2\text{-}P_4)_2]^+$ (M = Cu, Ag, Au). The molecular structure of **389** (Fig. 95**a**) reveals that, similar to the previously known examples [273–275], the cationic complex features two η^2-coordinated distorted P_4 tetrahedra, and is ion-separated. The bond distance of coordinated P-P edge is also elongated, as in the polymers **376** and **377**. Through gas-phase quantum chemical studies and a thermodynamic cycle it was possible to rationalize the differences in the formation of complex **389** in contrast with polymers **376** and **377**. Weak M–P_4 interactions were determined in all cases. However, the formation of $[M(\eta^2\text{-}P_4)_2]^+$ (M = Cu, Ag) is slightly endothermic, affording the coordination polymers **376** and **377**, which are built through M–Cl linkage.

In 2016, the selective functionalization of white phosphorus by addition of ArLi to a gold complex the *N*–heterocyclic carbene (NHC) gold(I) complex **383** was achieved by the group of Lammertsma [276]. The synthesis of **383** (Scheme 97, *vide supra*), featuring an intact η^2-coordinated P_4 tetrahedron, was already described in Section 3.4.1. above. The complex was characterized through X-ray diffraction (Fig. 95**b**). The Au(I) center resides in a distorted trigonal planar molecular geometry, with very similar Au-P bond lengths (2.4043 and 2.4286 Å) and an acute P1–Au1–P2 angle (57.79°). The stability of **383** allowed for additional studies regarding its reactivity. At low temperatures, **383** reacts with aryl lithium compounds (Scheme 100), yielding an asymmetrically substituted butterfly-P_4 ligand after P-C bond formation and cleavage of one P-P bond, as shown in intermediate **390**. ^{1}H NMR spectral analysis, as well as molecular structure determination through XRD, revealed that the reaction led to a doubly substituted RP_4 ligand. The latter coordinates two [(NHC)Au] fragments, the second of which formed after displacement of P_4 from a second equivalent

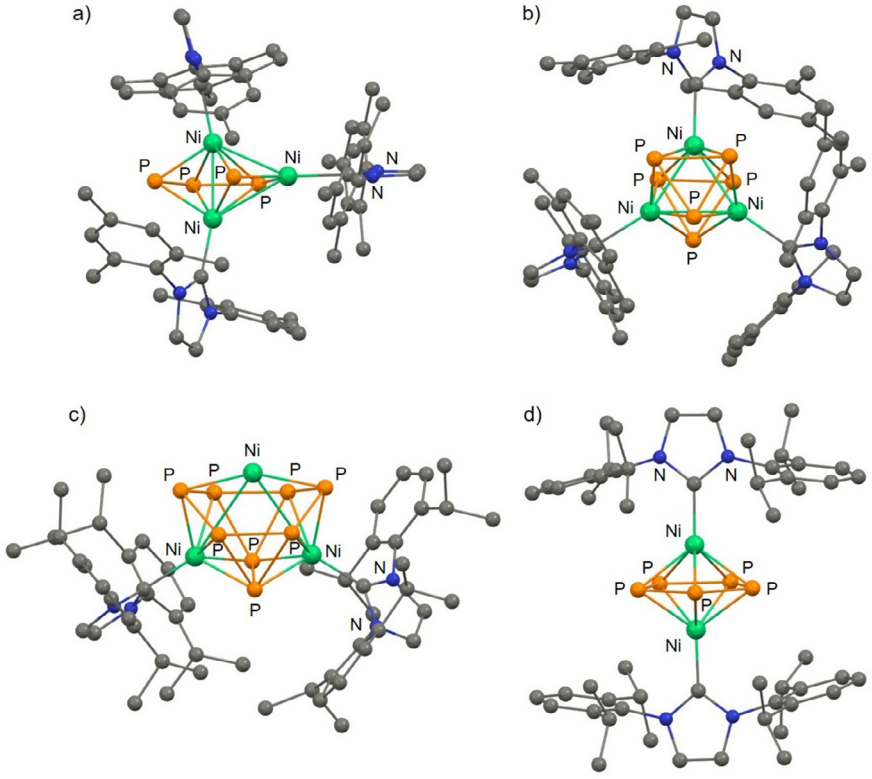

Fig. 86. Molecular structures of (NHC)Ni-phosphido clusters and inverse sandwich compound obtained by activation of P_4: a) **350**, b) **351**, c) **353** and d) **352b**; adapted from Ref. [259].

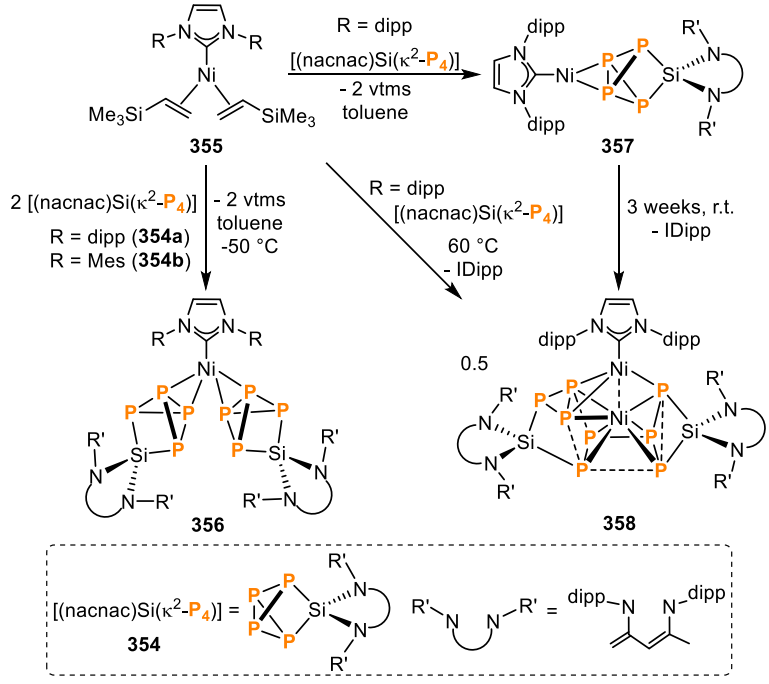

Scheme 93. Synthesis of Ni(0) complexes with bridging butterfly-P_4 ligands, and thermolysis to yield an unusual $Ni_2Si_2P_8$ cluster.

of **383**. The resulting bimetallic cationic complex **391** (see Fig. 96 for the molecular structure) was obtained in high yield. The ability of the butterfly-P_4 ligand to coordinate a second [(NHC)Au] fragment was found to be comparable with the reactivity observed with metalloligand **178b** upon interaction with Cu(I), yielding complexes **183** and **184** [195], described in Section 3.1.1. above. As mentioned before, compound **383** was reported, almost simultaneously, also by the group of Russell (see Scheme 97) [272].

Additionally, the formation of the complexes [(P*t*Bu$_2$Ar)Au(η^2-P_4)]$^+$ [P*t*Bu$_2$Ar = JohnPhos (**379a**), *t*BuXPhos (**379b**)] was described

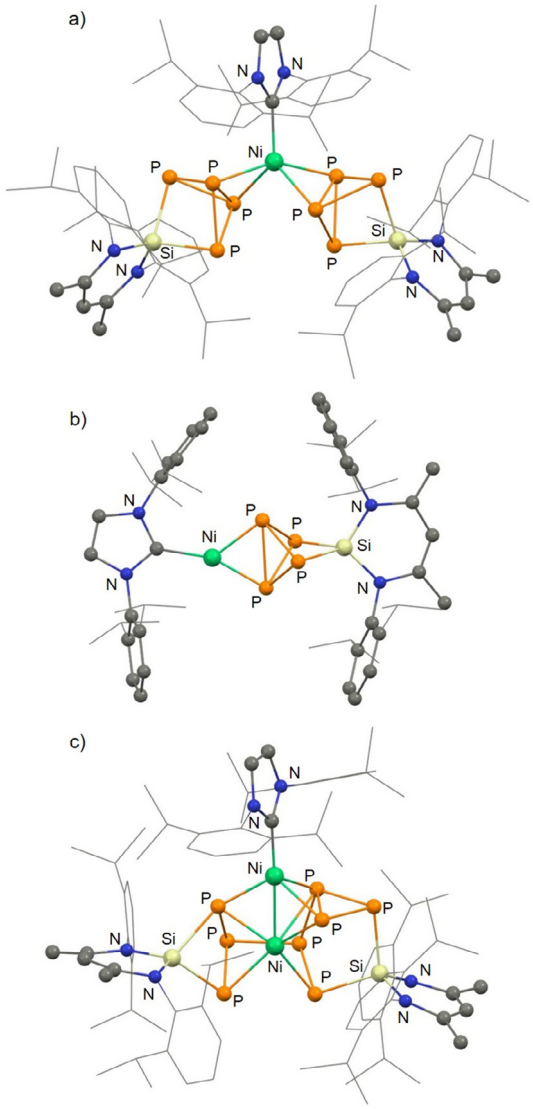

Fig. 87. X-ray structures of a) **356a**, b) **357** and c) the $Ni_2Si_2P_8$ cluster **358**; adapted from Ref. [260].

(Scheme 97**b**). Single-crystal characterization revealed that the coordination of the P_4 tetrahedron is affected by the steric hindrance on the phosphine co-ligand (see Fig. 95**c-d**). In complex **379b**, the more sterically encumbered *t*BuXPhos ligand causes a rotation of approximately 90° on the P_4 molecule with respect to **379a**, and that the P-P bond in **379a** is also shorter than in **379b** (2.341(3) Å *versus* 2.4182(8) Å, respectively). Thus, the geometry around the gold center in complex **379b** was initially described as T-shaped. However, DFT calculations, along with structural data, indicate that the differences observed might be attributed to a displacement in the binding of the P_4 tetrahedron between the limits of the $Au^{I}(\eta^2\text{-}P_4)$ and $Au^{III}(\eta^2\text{-}P_4)$ descriptions. In the latter case, a P_4^{2-} ligand would result from the oxidative addition of a P-P bond to the gold center. It was suggested that a marked shift towards Au^{III} character and a preference to adopt planar structures could be possible for the gold complexes with respect to the copper analogues **378**, which tend to be tetrahedral. In both cases the arene from the $PtBu_2Ar$ ligands would occupy a fourth coordination site. Such studies accounted also for the fluxionality observed on the NMR timescale, suggesting free rotation of the coordinated P_4 molecule, which should occur *via* an η^1-coordinated M^{I} intermediate with a deactivated P_4 unit.

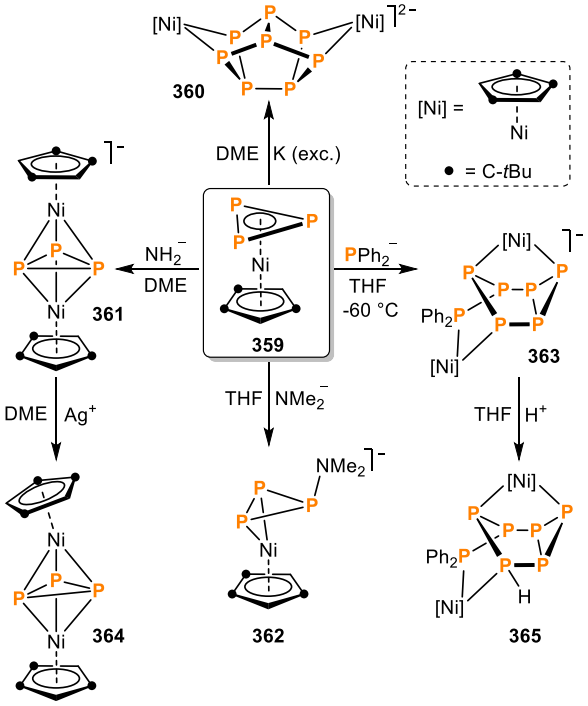

Scheme 94. Reactivity of the neutral *cyclo*-P_3 complex $[Cp'''Ni(\eta^3\text{-}P_3)]$ (**359**, $Cp''' = \eta^5\text{-}1,2,4\text{-}tBu_3C_5H_2$) with nucleophiles or potassium.

Ragogna and co-workers [279], described gold complexes of the previously reported P_4-derivatized low-valent germanium compound $[(2,6\text{-}Mes_2C_6H_3)_2Ge(\kappa^2\text{-}P_4)]$ (**392**) [280]. The metalation of **392** yielded either monosubstituted or disubstituted species, with the coordination occurring selectively at the wing-tip P-atoms (Scheme 101). The selective coordination at the P-atoms adjacent to germanium, was confirmed by DFT calculations and single-crystal X ray analysis for the monosubstituted complex $[\{(2,6\text{-}Mes_2C_6H_3)_2Ge(\kappa^2\text{:}\kappa^1\text{-}P_4)AuCl\}]$ (**393**, Fig. 97). Based on the theoretical analysis, the authors suggested [279] that the activation of P_4 at the germanium fragment results in a relative concentration of electron density at the wing-tip P-atoms rendering them better donors and explaining the selective coordination towards gold fragments. $^{31}P\{^1H\}$ VT NMR studies revealed that **393** is more stable than the related digold compound **394**.

Nanoscaled gold phosphides were also reported by the group of Mézailles and Sanchez, using white phosphorus as a soluble phosphorus donor [281]. By reacting gold nanoparticles with P_4, in an analogous manner as previously described for Ni_2P and Cu_3P (see sections 3.3.1 and 3.4.1) [221], instead of forming nanoparticles of the metastable gold phosphide (Au_2P_3, **395**), other nanostructures containing Au_2P_3, such as nanowires, were obtained. In a first attempt to produce such nanoparticles, moderate to intermediate temperatures (up to 250 °C) were used, observing that the reaction of gold nanoparticles with P_4 was limited to their surface. The authors concluded that gold nanoparticles do not convert into gold phosphide under such conditions. However, it was possible to prepare Au–P passivated gold nanoparticles by optimizing the initial reaction parameters. Furthermore, when harsher conditions (320 °C) were used, the formation of Au_2P_3 nanowires as well as aggregation into Au_2P_3–Au nanostructures, was observed. In the latter case, the gold phosphide domains were systematically larger than the unreacted gold nanoparticles.

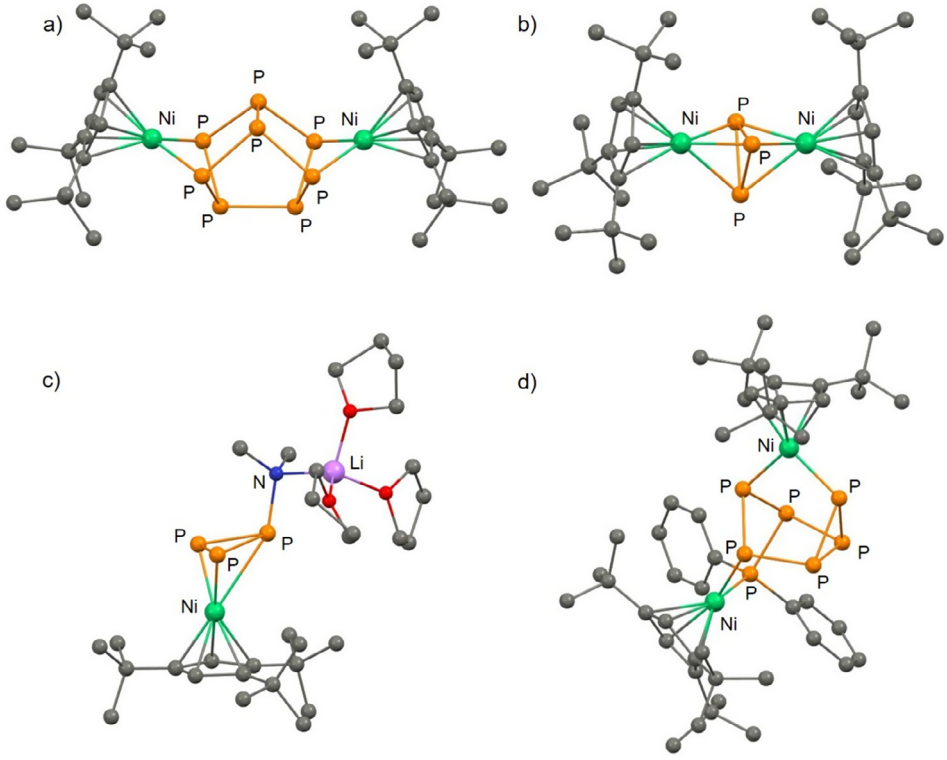

Fig. 88. X-ray structures of selected products of functionalization of [Cp‴Ni(η^3-P_3)] (**359**): a) dinuclear complex bearing a realgar-type P_8 ligand (**360**), b) neutral triple-decker **364**, c) η^2-triphosphirene compound **362** and d) dinuclear complex featuring a protonated $P_6PPh_2^-$ ligand **365** (hydrogen atoms omitted for clarity); adapted from Ref. [262].

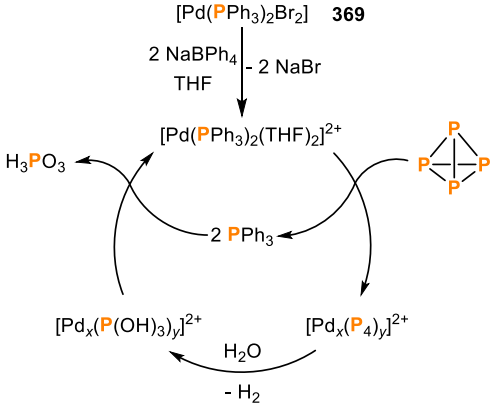

Scheme 95. Mechanistic proposal for the Pd(II) catalyzed hydrolysis of P_4 [268].

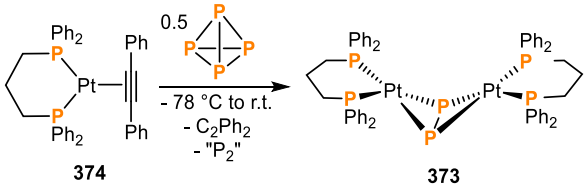

Scheme 96. Synthesis of [({(dppp)Pt}$_2$)$_2$(μ,η^2:η^2-P_2)] (**373**) by Mézailles and co-workers [270].

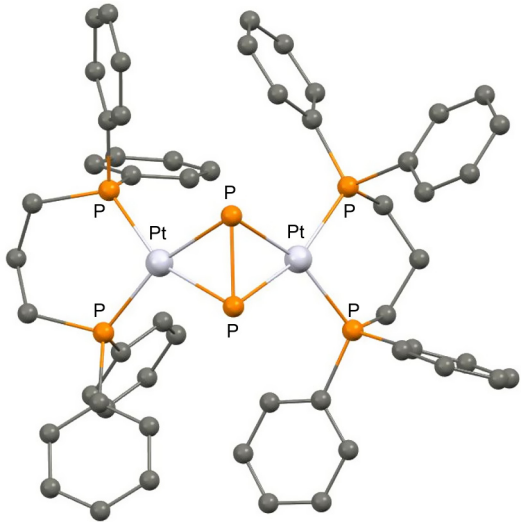

Fig. 89. X-ray structure of [({(dppp)Pt}$_2$)$_2$(μ,η^2:η^2-P_2)] (**373**); adapted from Ref. [270].

4. Surface coordination chemistry of exfoliated black phosphorus

The presence of a formal lone pair of electrons on each phosphorus atom in black phosphorus (BP) is reminiscent of the electronic structure of the white allotrope of phosphorus, P_4. This suggests the possibility of immobilizing metal fragments onto the BP surface. Recently, experimental studies have demonstrated that BP is able to form coordinative bonds of covalent character with the surface of metal nanoparticles grown *in situ* [282]. However, this has received limited attention both experimentally and theoretically. The very few examples reported testify that major difficulties must be overcome when converting P_4 into BP. Theoretical calculations [283] have shown that, like P_4, BP is a much weaker Lewis base than phosphines. This is mainly attributed to

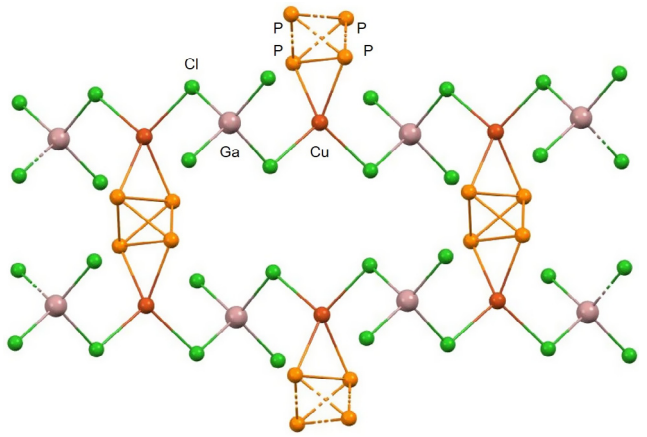

Fig. 90. X-ray crystal structure of the coordination polymer $(P_4CuGaCl_4)_n$ (**376**); adapted from Ref. [271].

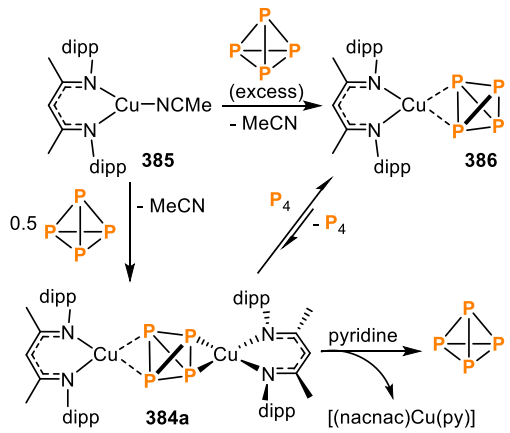

Scheme 98. Fixation and release of intact P_4 tetrahedra at copper(I), by Scheer and co-workers [277].

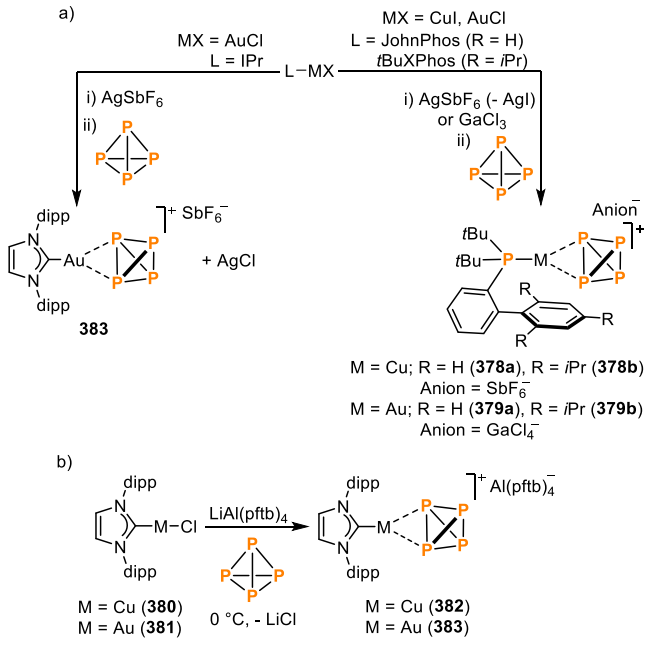

Scheme 97. Synthesis of coinage-metals adducts of white phosphorus (M = Cu, Au) by the groups of a) Russell [272] and b) Lammertsma [276].

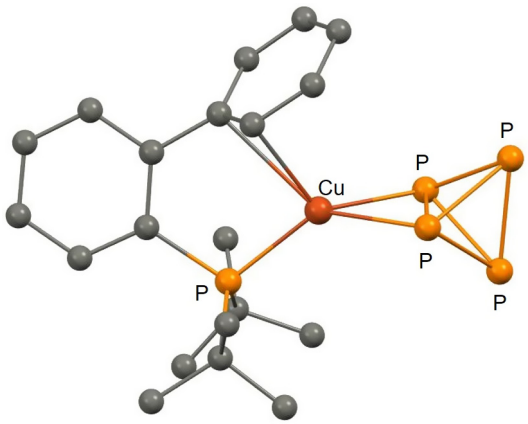

Fig. 91. X-ray structure of $[(JohnPhos)Cu(\eta^2\text{-}P_4)]^+$ (**378a**); adapted from Ref. [272].

the partial delocalization of the lone pairs of electrons on the phosphorus centers. Furthermore, the chair conformation of each P_6-unit in the skeleton of BP implies a tilting of the lone pairs at approximately 30° from the plane of the layer (see Fig. 98).

The η^1 coordination mode to a metal fragment limits the choice of ancillary ligands on the metal center, as larger substituents will quickly increase the steric repulsion from the neighboring P atoms. Besides η^1, η^2 and η^3-coordination modes were identified on the BP surface (see Fig. 99). However, as lone pairs on distinct P-atoms are not perfectly convergent, these geometries do not possess an optimal orbital overlap. This could be overcome at the cost of some local distortion of the BP surface. However, this is difficult due to its rigid structure.

Taking into account both the low donating ability and its steric requirements, the task of developing the coordination chemistry of BP seems very challenging. Only small and labile coordination complexes should be considered, to make the displacement of a co-ligand by BP in the coordination sphere of a metal more facile.

4.1. Black phosphorus functionalization with naked adsorbed metal atoms (adatoms)

One particular approach for metal surface decoration that avoids the need for ligands displacement is the use of naked metal atoms. One such technique is physical vapor deposition (PVD), whereby a metal is brought to the vapor phase and neutral atoms are deposited onto a target substrate (i.e. BP). If the interaction with the target material is strong enough to prevent aggregation, isolated atoms may be immobilized on its surface or can even diffuse into the lattice. The effect of adsorbed metal atoms (called *adatoms*) on the BP layers has been addressed theoretically and can span from the tuning of electronic and transport properties of BP to an increased affinity for selected gas molecules. Kulish and co-workers [284] carried out a first principle study on 20 different adatoms on monolayer BP. All the investigated metals preferred an η^3 coordination mode on BP with Ni, Co, Pd and Pt having the strongest adsorption energies, with Pt reaching a maximum value of − 4.71 eV. Notably, it has been shown experimentally (XAS, XPS) that M(0) systems, where M = Pd, Pt, in the form of nanoparticles, can interact strongly *via* a covalent bond with the BP surface [282,285]. Further studies on M_{adatom}/BP from other groups corroborated these trends [286–288]. S.P. Koenig *et al.* [289] used direct current sputtering to deposit Cu adatoms on a thin BP flake exfoliated mechanically. The latter was used to build a field effect transistor (FET). *Ab initio* calculations were carried out

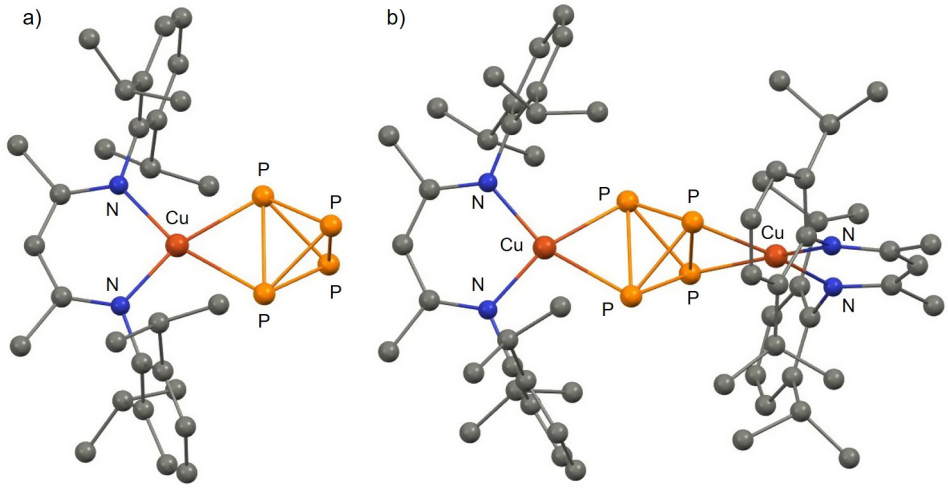

Fig. 92. X-ray structures of copper-diketiminato complexes featuring η^2-coordinated intact P_4 ligands; adapted from Ref. [277].

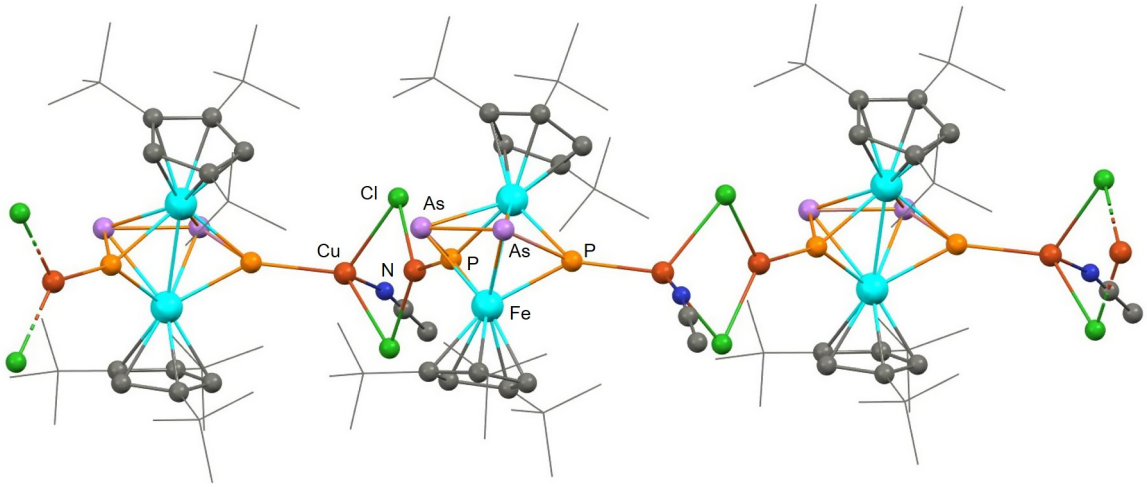

Fig. 93. Molecular structure of the 1D coordination polymer $[\{Cp'''Fe\}_2(\mu,\kappa^4{:}\kappa^4{:}k^1{:}k^1\text{-}E_4)\{Cu(\mu,Cl)\}_2(MeCN)]_\infty\cdot(CH_2Cl_2)_2$ (**387**, $E_4 = P_n\,As_{4-\ E4} = P_nAs_{4-n}$); adapted from Ref. [192].

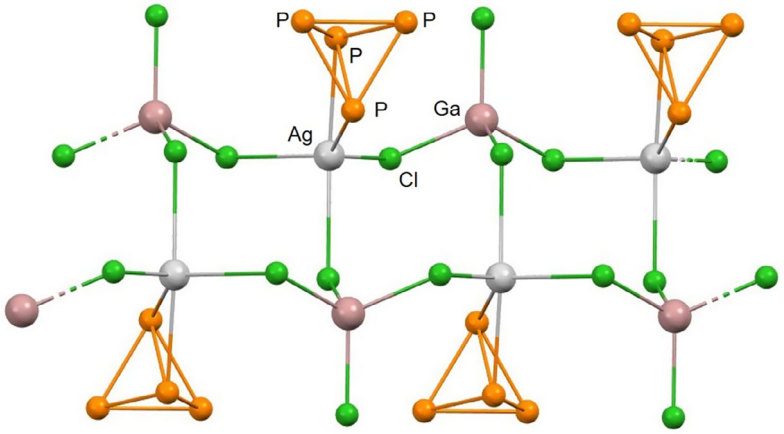

Fig. 94. X-ray crystal structure of the coordination polymer $(P_4AgGaCl_4)_n$ (**377**); adapted from Ref. [271].

on a Cu/four-layer-BP model system, considering both adsorbed (η^3) and intercalated Cu atoms (see Fig. 100).

In both these configurations, Cu behaves as an electron donor, transferring one electron to BP and leaving a stable closed shell Cu^+ cation. This turns BP into an n-type semiconductor, with a remarkable electron mobility of 2140 $cm^2V^{-1}s^{-1}$, measured at low temperature. Z. Guo and co-workers [290] tackled the limited durability of BP-based FETs, caused by surface oxidation, by func-

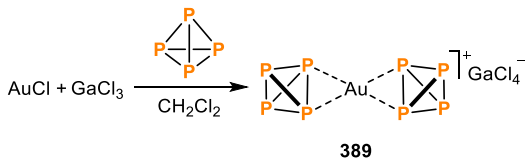

Scheme 99. Synthesis of the homoleptic complex $[Au(\eta^2\text{-}P_4)_2]GaCl_4$ (**389**).

tionalizing the BP surface with silver. However, instead of using Ag (0) atoms as with PVD, Ag^+ cations were anchored to the surface of BP by a chemical procedure. First, BP nanosheets (lateral dimension ~300 nm) were exfoliated mechanically and transferred onto a Si/SiO_2 wafer. Then, BP was exposed to Ag^+ ions by dipping the silicon wafer into a solution of $AgNO_3$ in NMP (N-Methyl-2-pyrrolidone). XPS measurement revealed that Ag^+ had been successfully immobilized on the BP surface (see Fig. 101**a**). The region around 133 eV in the P 2p XPS spectrum of BP is quite diagnostic for direct metal-phosphorus bonding (see also references [282] and [285]). Thus, a deshielded peak at 133.0 eV was assigned to the P-Ag bonds (Fig. 101**b**).

First principle calculations carried out on this system showed that Ag^+ adsorbs to the BP surface by the η^3 coordination mode, interacting with three distinct lone pairs of electrons (see Fig. 102), as was the case of isoelectronic Cu^+ described previously. However, Ag^+ ions behave as a p-type dopant for BP, drawing electron density away from the layer. The coordination of silver ions not only enhanced the transistor stability, leaving the flake morphology unaltered after several days of air exposure, but it also improved the transistor performance, doubling the hole mobility.

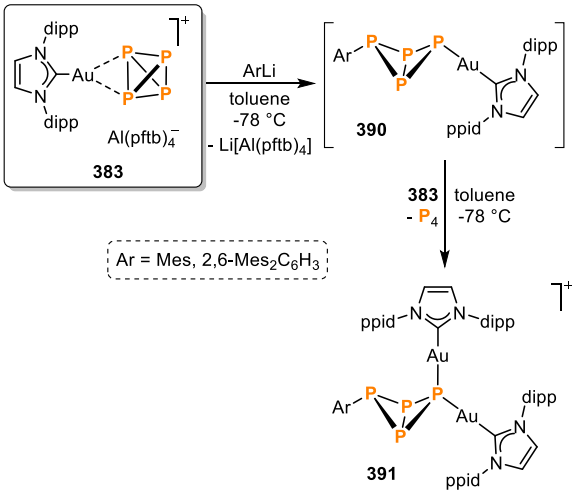

Scheme 100. Functionalization of P_4 by reaction of **383** with aryl lithium compounds.

4.2. Black phosphorus functionalization with a titanium complex

In 2016, Y. Zhao and co-workers [291] were the first to study the functionalization of exfoliated BP with a transition metal fragment, namely TiL_4 (L = *p*-toluenesulfonate). Ultrasmall BP nanosheets were prepared following a solvent-assisted procedure, carried out in NMP, previously described by the same group [292].

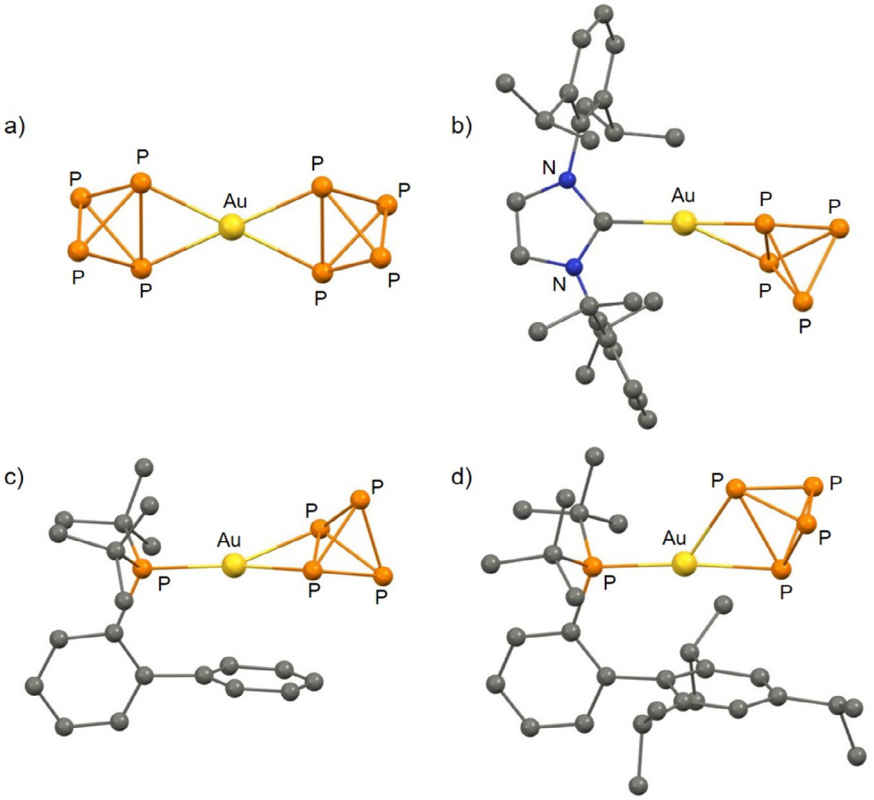

Fig. 95. X-ray crystal structures of cationic gold complexes featuring η^2-coordinated intact P_4 ligands: a) $[Au(\eta^2\text{-}P_4)_2]^+$ (**389**), b) [(IDipp)Au$(\eta^2\text{-}P_4)]^+$ (**383**), c) [(JohnPhos)Au$(\eta^2\text{-}P_4)]^+$ (**379a**) and d) [(*t*BuXPhos)Au$(\eta^2\text{-}P_4)]^+$ (**379b**); adapted from Refs. [271,272,276].

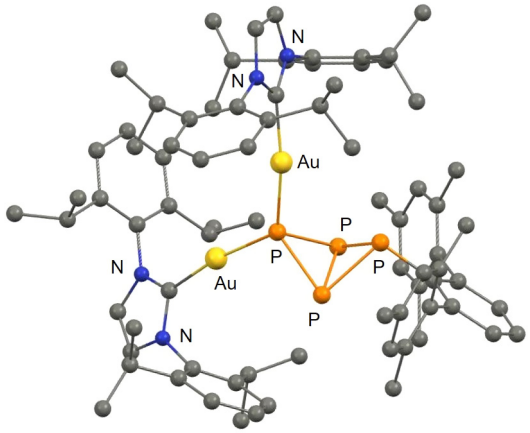

Fig. 96. X-ray crystal structure of the functionalized butterfly-P_4 gold complex **391**; adapted from Ref. [276].

By this method, BP quantum dots (BPQDs) with a lateral size of 2.6 ± 1.8 nm and a thickness of 1.5 ± 0.6 nm were obtained. The exfoliated material was then stirred with TiL_4 in NMP for 15 h to obtain TiL_4@BP. XPS measurements of the isolated material confirmed the presence of titanium and the broad peak at binding energy 132.4 eV in the P 2p XPS spectrum was assigned to direct P–Ti bonds (see Fig. 103**d**).

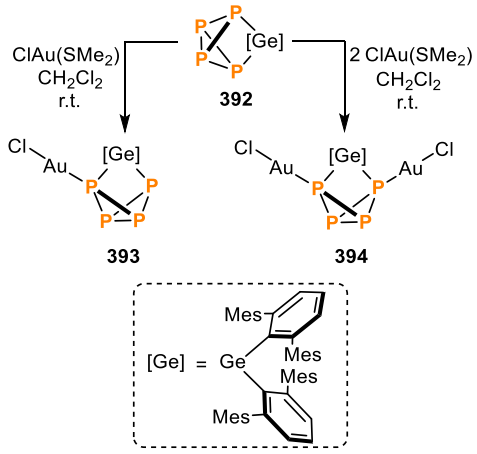

Scheme 101. Functionalization of an activated-P_4 germanium compound by coordination to Au(I).

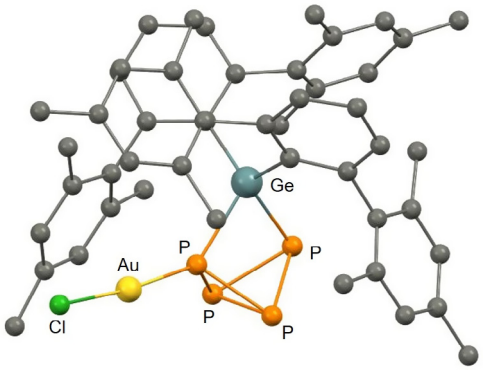

Fig. 97. X-ray crystal structure of [{(2,6-$Mes_2C_6H_3$)$_2$Ge(κ^2:κ^1-P_4)AuCl}] (**393**); adapted from Ref. [279].

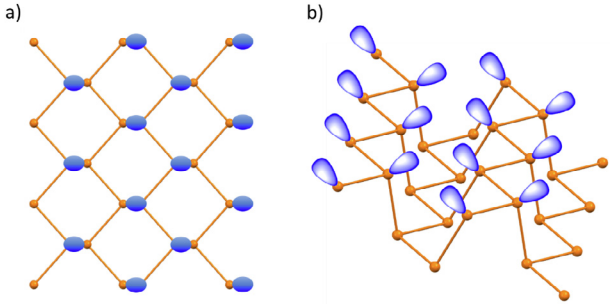

Fig. 98. a) Top and b) side view of the phosphorene lone pairs. Image b) clearly shows the tilting of the lone pairs with respect to the plane of the layer and the misalignment of two adjacent lone pairs due to P-P bond torsion of 60°; adapted from Ref. [283].

However, no further studies were carried out to shed light on the structure of this adduct and it is unclear how BP is interacting with the metal (i.e. if it has displaced one of the sulfonate ligand to give a charged L_3Ti^+–P adduct). NMR measurements performed on a TiL_4@BP suspension, although corroborating the persistency of sulfonate coligands in the collected material, did not help to clarify this point. A remarkable effect of the functionalization with TiL_4 was the increased stability of BPQDs towards ambient conditions. To compare the behavior of pristine BP with TiL_4@BP, dilute water suspension of the two were prepared. The suspensions were then exposed to air and their absorbance in the UV/VIS range was monitored over time. As shown in Fig. 104, the absorbance of bare BP at 450 nm decreased by 55% of the original value after 72 h, compared to the 5% for TiL_4@BP. It should be noted that when organic solvent solutions of BP and TiL_4@BP were exposed to air, they showed similar stability (see Fig. 104**d**).

A follow-up to this work [293] has been the biomedical application of TiL_4@BP, driven by the increasing attention devoted to BP in the life sciences. In 2015, M. Pumera and co-workers [294] demonstrated the low cytotoxicity of 2D BP and found it to be concentration-dependent and between that of graphene oxide and transition metals dichalcogenides. Moreover, BP is biodegradable, since in physiological medium, i.e. in presence of water and oxygen, it oxidizes forming phosphates [295,296], which are naturally present in the human body. Additionally, BP has been shown to be an efficient photosensitizer with superior quantum yields and a pronounced ability to generate singlet oxygen ($^1O_2$) [297], opening it up to applications in photothermal and photoacoustic (PA) therapy. TiL_4@BP has been used as a contrast agent for *in vivo* PA imaging of cancer. The method is based on the adsorption of near-IR light from a contrast agent to image a tumor location. Combining the enhanced stability imparted to BP by the functionalization with TiL_4 and its high near-IR extinction coefficient, TiL_4@BP outperformed previously reported nanostructured contrast agents such as bare Au nanorods [298]. *In vivo* experiments were performed with TiL_4@BP as a PA contrast agent to image tumor area in nude mice (Balb/C nude) previously inoculated with MCF-7 cancer cells. Remarkably, after injecting TiL_4@BP, the mice showed larger PA signals in the tumor than pre-injection, the maximum intensity being reached after 4 h (see Fig. 105). This further demonstrated the high potential of TiL_4@BP in clinical applications as a PA contrast agent, characterized by both a selective accumulation at tumor sites and a remarkable spatial resolution.

4.3. Black phosphorus functionalization with cisplatin derivatives

Since the seminal work of B. Rosenberg in 1965 [299], the cisplatin (*cis*-diamminedichloroplatinum, **396**) family has been lar-

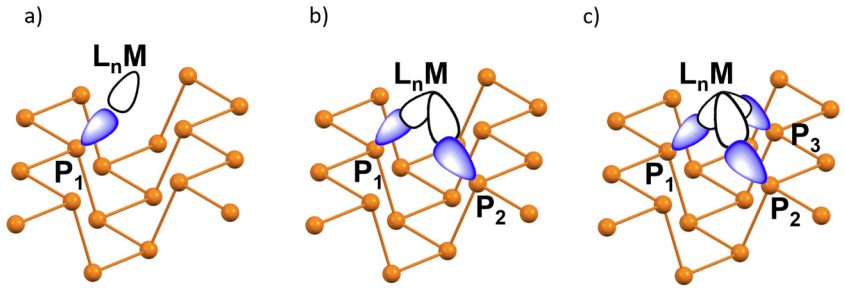

Fig. 99. The three potential bonding modes of BP towards a metal fragment. a) η^1 coordination with formation of single P-M bond, b) η^2 coordination and c) η^3 coordination; adapted from Ref. [283].

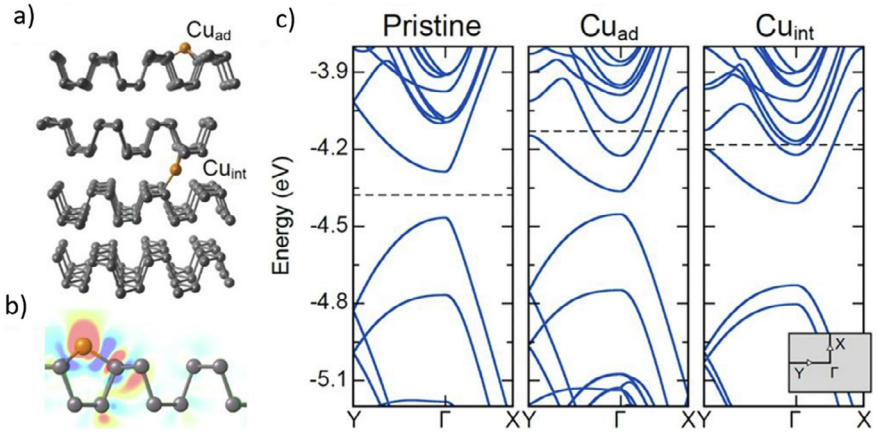

Fig. 100. a) Schematic drawing of the two possible location of Cu: adsorbed on the surface (Cu_{ad}) and interstitial (Cu_{int}). b) Charge density difference of the Cu_{ad}. The red and blue regions refer to electron depletion and accumulation, respectively. c) Calculated band structure of pristine four-layer BP, four-layer BP with adsorbed Cu (Cu_{ad}), and four-layer BP with interstitial Cu (Cu_{int}). The dashed line indicates the Femi level for each case. Reprinted with permission from Fig. 1 in Ref. [289]. Copyright 2016 American Chemical Society.

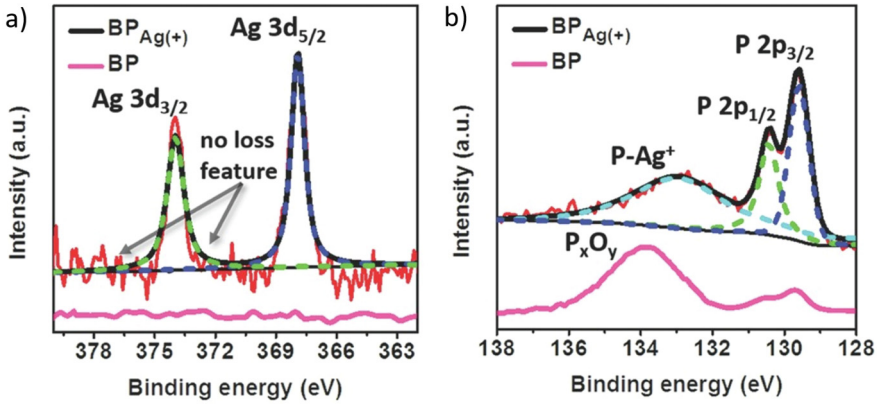

Fig. 101. a) P 2p and b) Ag 3d XPS spectra of bare BP and Ag^+/BP, recorded after 3 days of air exposure. Reprinted with permission from Fig. 1 in Ref. [290]. Copyright 2017 John Wiley and Sons.

gely studied for its antitumor activity and it is still used today to treat several cancers, including testicular, ovarian, cervical and lung cancer, either alone or in combination with other antitumor agents.

Searching for a metal fragment with powerful anticancer activity, M. Fojtů *et al.* [300] used cisplatin (CP, **396**) and oxaliplatin (OP, **397**; see Fig. 106) to modify BP and use it for drug delivery.

A well-characterized human ovarian cell line A2780, derived from tumor tissue of an untreated patient, was used as a target in *in vitro* studies. As both **396** and **397** are known to be effective towards this type of cancer, the goal was to highlight a potential enhancement in cytotoxicity induced by the 2D BP carrier. BP nanosheets were prepared by liquid exfoliation in NMP. The exfoliated material, having lateral dimensions in the range 100–500 nm and a thickness of few tenths of nm, was afterwards dispersed in water, **396** or **397** were added, and the mixture was incubated for 24 h. The functionalized BP nanosheets, BPCP (BP modified with **396**) and BPOP (BP modified with **397**), were isolated and characterized. The P 2p XPS spectra, beside the characteristic signal of pristine BP, displayed a smaller broad peak slightly above

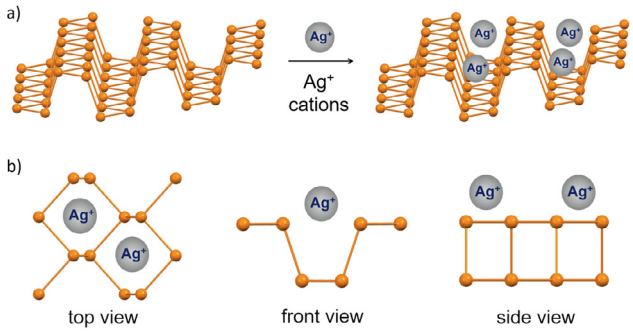

Fig. 102. a) Scheme illustrating adsorption of Ag^+ on BP. b) Three different views of the BP/Ag^+ structure. Adapted from Ref. [290].

~133.5 eV possibly due to Pt–P bonds. Both BPCP and BPOP featured a double contribution in their Pt 4f spectra, suggesting the presence of two distinct Pt(II) species, the minor component being slightly more electron-depleted (see Fig. 107**b**). In the case of BPOP, this contribution amounted to 30% of total Pt in the sample. The nature of these species however was not further investigated.

In vitro studies revealed that while cisplatin activity was almost unaffected by the presence of BP, the cytotoxicity of oxaliplatin towards ovarian cells was significantly increased, reaching a maximum enhancement of 21% when the BPOP concentration used was 30 μg mL^{-1}. As in all the experiments performed the total concentration of **397** was the same, only the amount of BP being varied, the superior suppression of cancer cell growth is ascribed solely to the BP. Though no detailed investigations of the mechanism were carried out, the authors attributed the cytotoxicity enhancement to a major cellular uptake of **397** once bound to the BP shuttle and the different behavior of **396** is due to its supposed weaker interaction with BP.

J. Zhang *et al.* [301], in disagreement with the findings from M. Fojtů and co-workers described above [300], also tried to immobilize cisplatin on 2D BP but no Pt incorporation could be detected by XPS. Thus they switched to a cisplatin derivative, namely [Pt$(NH_3)_2(NO_3)_2$] (**398**). Given the non-coordinating behavior of NO_3^-, the charged moiety $[Pt(NH_3)_2]^{2+}$, being highly electrophilic, should then interact better with the surface of the BP nanosheets. BP was reacted with Pt-NO_3 in water/NMP under an inert atmosphere for 18 h. High resolution Pt 4f XPS confirmed the successful incorporation of platinum, featuring Pt $4f_{7/2}$ and $4f_{5/2}$ peaks at 73.0 and 76.3 eV respectively. However, no shifts in peak positions were observed compared to the precursor **398**. Since d^8 Pt^{2+} favors a square planar coordination, an η^2 coordination of BP would be expected with the two NO_3^- as counteranions. Remarkably, alongside an increased environmental stability compared to pristine BP, BP nanosheets functionalized with **398** showed a significantly greater cytotoxicity and apoptotic-promoting capability towards cisplatin resistant cell-lines A2780 and HepG2. This was proposed to be the synergetic effect of BP, which previous works demonstrated to be efficient in damaging cancer even when it is unfunctionalized [302].

4.4. Black phosphorus functionalization with lanthanide complexes

Following the approach outlined for surface modification of BP with TiL_4 (see Section 4.2), L. Wu *et al.* [303] attempted the metal functionalization of BP nanosheets using lanthanide complexes. Lanthanides have large atomic radii, which should allow for an easier interaction with the lone pairs of electrons of the phosphorus atoms. As in the case of TiL_4, a sulfonate anion was chosen as an ancillary ligand, since it was thought suitable to enhance the electrophilicity of the metal, promoting the coordination to BP. A variety of LnL_3 species (with L = trifluoromethanesulfonate and Ln = Gd, Y, La, Nd, Sm, Eu, Tb, Er, see Fig. 108) were tested in the surface functionalization of BPQDs [292] having lateral dimension 2.6 ± 1.8 nm and thickness 1.5 ± 0.6 nm. A suspension of BPQDs in NMP was stirred at room temperature under an inert atmosphere with an excess of LnL_3. By this method it was possible to decorate the BP surface with lanthanide pendants, as confirmed by EDS analysis of the isolated LnL_3@BPQDs (see Fig. 108**b**).

Although theoretical investigations were not carried out on the system, the authors propose that LnL_3 species will coordinate to three phosphorus atoms on the BP surface (η^3-BP), as shown in Fig. 109. This sounds reasonable considering the large atomic radius of lanthanide metals, which favors a larger hapticity of BP. Such coordination has been shown with Lu^{3+} [67] and Y^{3+} [63] complexes bearing a trihapto coordinated *cyclo*-P_3 ligand, derived

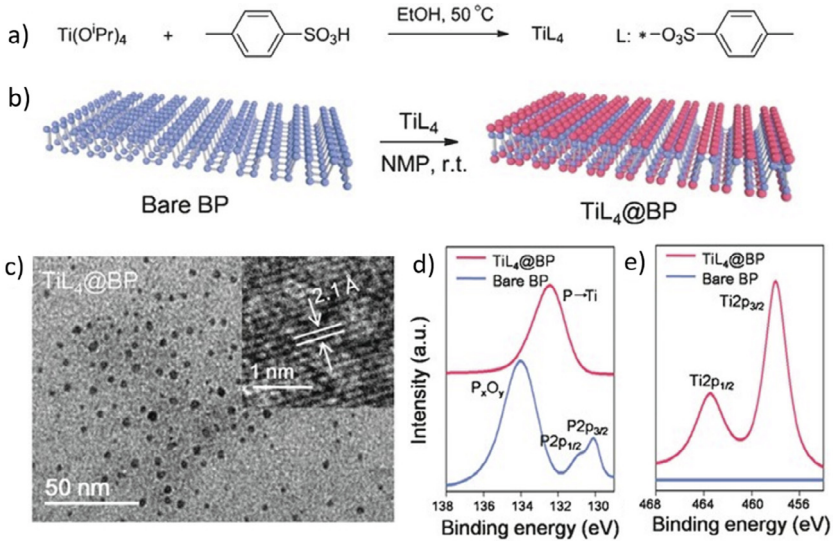

Fig. 103. Fabrication and characterization of TiL_4-decorated BPQDs (named TiL_4@BP). a) Synthesis and structural formula of TiL_4; b) surface coordination of TiL_4 to BP; c) TEM image with inset HRTEM image of TiL_4@BP; d) P 2p and e) Ti 2p XPS spectra of TiL_4@BP, acquired after 3 days of air exposure. Reprinted with permission from Fig. 1 in Ref. [291]. Copyright 2016 John Wiley and Sons.

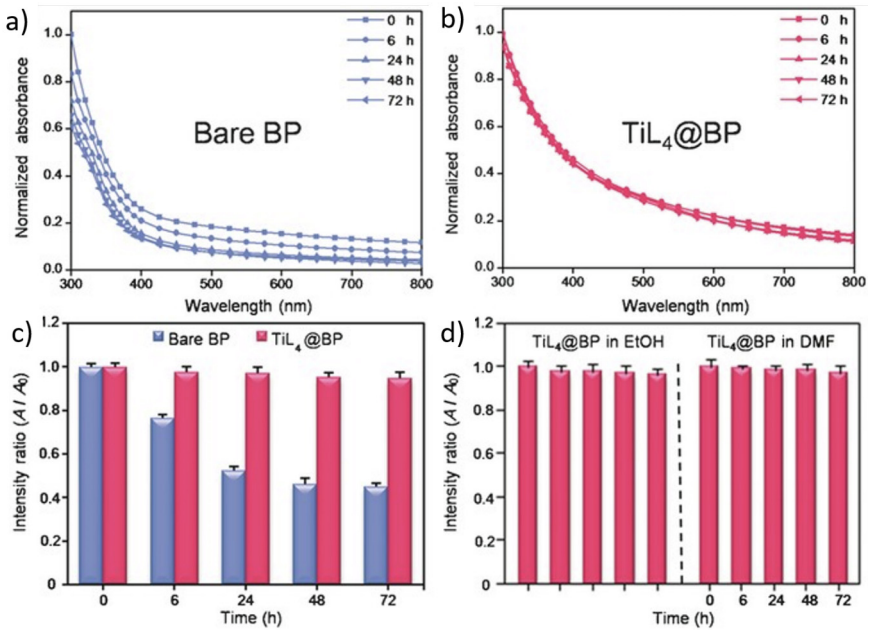

Fig. 104. Stability of bare BP and TiL_4@BP in water. a) Absorption spectra of bare BP and b) TiL_4@BP dispersed in water after exposure to air for 0, 6, 24, 48, and 72 h; c) variation of the absorption ratios (A/A_0) at 450 nm of BP and TiL_4@BP over time, in water; d) A/A_0 of TiL_4@BP over time in EtOH and DMF. Reproduced with permission from Fig. 2 in Ref. [291]. Copyright 2016 John Wiley and Sons.

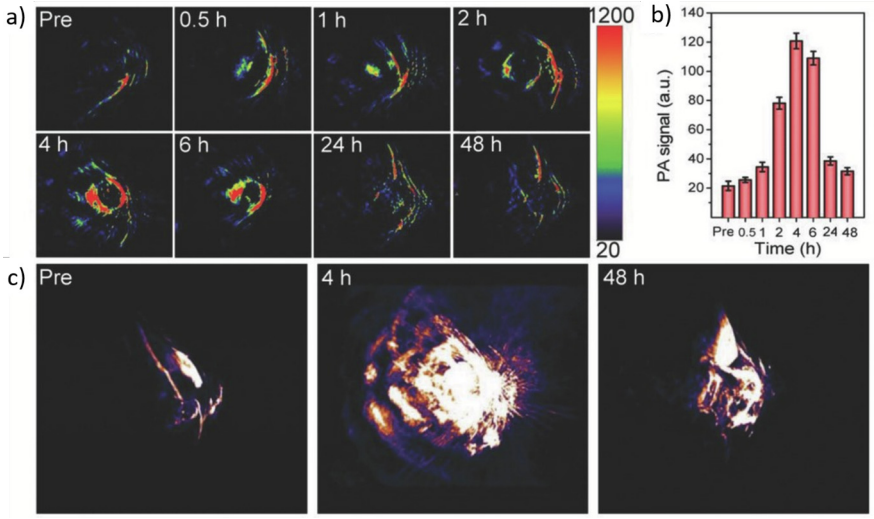

Fig. 105. *In vivo* PA performances of TiL_4@BP. a) Time-dependent PA images of the MCF-7 cells in the xenografted tumor in the BALB/c nude mice after intravenous injection of TiL_4@BP. The signal intensity bar is shown on the right side. b) Quantitative analysis of each ROI signal in a). Maximum intensity is recorded after 4 h. c) Typical 3D PA images of the tumor taken at different times pre- and post-injection of TiL_4@BP. Reproduced with permission from Fig. 6 in Ref. [293]. Copyright 2017 John Wiley and Sons.

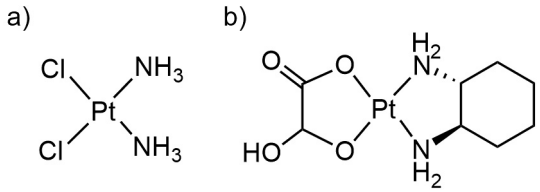

Fig. 106. Molecular structures of a) cisplatin (**396**) and b) oxaliplatin (**397**).

from their interaction with white phosphorus. XPS studies of GdL_3/BPQDs at the P 2p core level highlighted the presence of an electron-depleted phosphorus species at 132.9 eV, assigned to the P-atoms bonded to the electrophilic GdL_3 fragment (Fig. 108**d**). Furthermore, an appreciable red-shift is observed in the Gd 3d XPS spectrum compared to free GdL_3 (Fig. 108**c**), in accordance with the donation of electron density from the σ orbitals of BP to Gd. As with the TiL_4 functionalization, LnL_3@BPQDs showed an enhanced stability towards air and water with respect to bare BPQDs, as revealed by UV–Vis absorption measurements carried out on aqueous suspensions aged over 8 days.

This functionalization strategy was extended from BPQDs to BP nanosheets having an average size of 300 nm. The environmental stability of the obtained LnL_3@BP was evaluated *via* TEM. As reported in Fig. 110, while bare BP nanosheets were fully degraded after 8 days of exposure, GdL_3@BP kept its morphology. Accordingly, recording UV/Vis absorption measurements in aqueous sus-

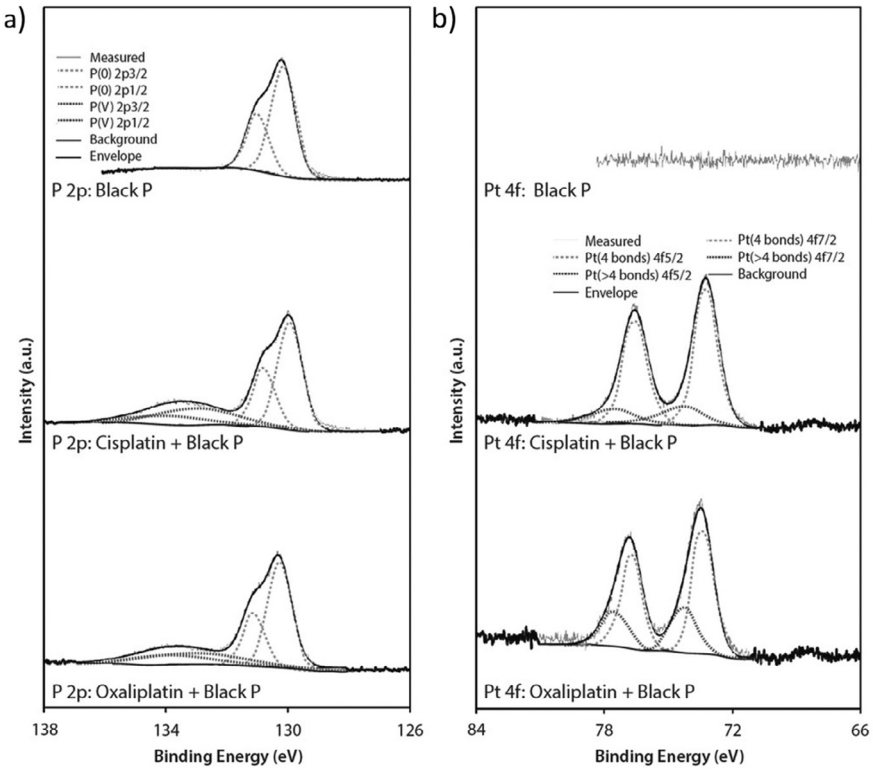

Fig. 107. a) Core level P 2p XPS spectra of pristine BP, BPCP and BPOP and b) relative Pt 4f core-level. All scans were referenced to adventitious C 1s peak at 284.5 eV. Reproduced with permission from Fig. 6 in Ref. [300]. Copyright 2017 John Wiley and Sons.

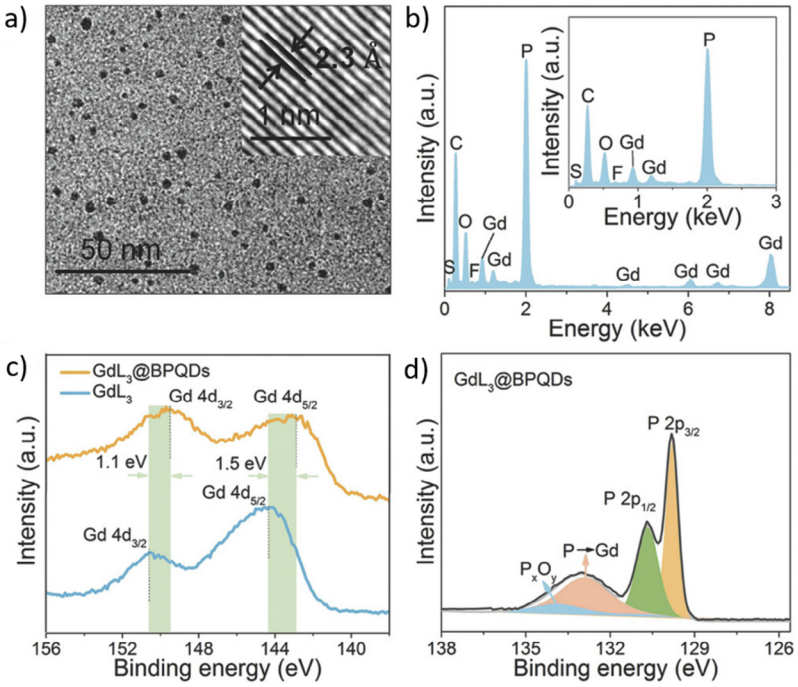

Fig. 108. Characterization of GdL_3-coordinated BPQDs (named GdL_3@BPQDs). a) TEM image and HRTEM inset; b) EDS spectra; c) Gd 4d XPS spectra of GdL_3@BPQDs and free GdL_3; d) P 2p XPS spectrum of GdL_3@BPQDs. Reproduced with permission from Fig. 1 in Ref. [303]. Copyright 2018 John Wiley and Sons.

pensions of LnL_3@BP over time, only a minimal loss in absorbance was observed, meaning the stabilization effect is not related to flake dimensions (BPQDs or BP nanosheets). Furthermore, this remarkable stabilizing effect was common to all the lanthanides under study.

Depending on the lanthanide selected, the series LnL_3@BPQDs exhibited different physicochemical properties: samples containing Eu^{3+}, Nd^{3+} and Tb^{3+} possessed fluorescence, while Gd@BPQDs showed magnetic resonance responsiveness. The fluorescence spectra of the free LnL_3 species were almost superimposable to

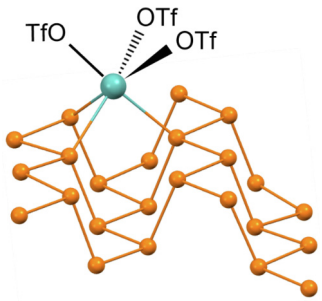

Fig. 109. Atomistic model of the adduct between BP and LnL_3 fragment, L = OTf = Trifluoromethanesulphonate; adapted from Ref. [303].

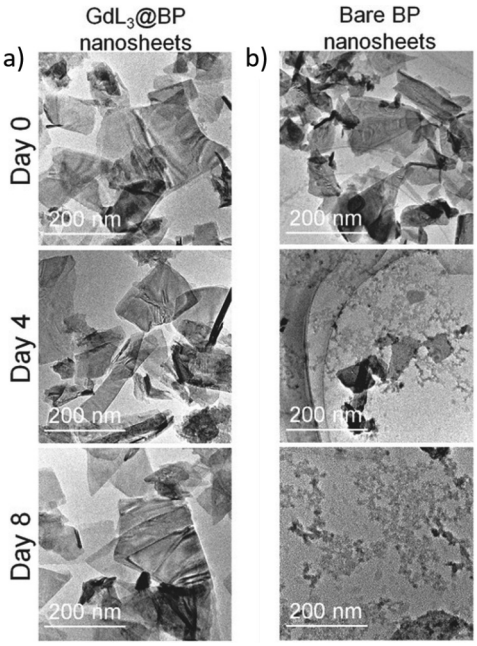

Fig. 110. Stability evaluation of bare BP nanosheets and GdL_3@BP. TEM images of a) GdL_3@BP nanosheets and b) bare BP nanosheets exposed to air for 0, 4, and 8 days. Reproduced with permission from Fig. 3 in Ref. [303]. Copyright 2018 John Wiley and Sons.

those recorded for LnL_3@BPQDs. The absence of any shift upon coordination was proposed to be due to the electronic transitions responsible for fluorescence only concerning the 4f levels of the metal, whereas the coordination to BP is expected to involve only 4d orbitals. Paramagnetic Gd^{3+} is commonly employed as an MRI contrast agent in commercial solutions, such as Magnevist, Dotarem and Primovist. All these formulations contain Gd^{3+} chelates. As they are paramagnetic, when in a physiological medium the Gd^{3+} species interacts with the protons of water molecules, reducing their T_1 NMR relaxation times. Image contrast in MRI is based on differences in the (average) relaxation times of tissues, thus contrast agents enhance resolution. Considering the properties of Gd^{3+} and the biocompatibility of BP, preliminary studies were carried out on aqueous suspensions of GdL_3@BPQDs, highlighting a linear increase in $1/T_1$ intensities with concentration. Further studies are needed to fully exploit the potential of GdL_3@-BPQDs in this field.

5. Conclusion and perspectives

The present survey on the coordination chemistry of elemental phosphorus towards transition metals summarized the impressive results achieved in the last decade in the activation of P_4 at a metal center and gives an initial review of the surface coordination of exfoliated black phosphorus (BP). Sections 2 and 3 described a rich variety of phosphorus-containing structural motifs, such as P_4 activation, degradation, aggregation products, functionalized compounds, and nanostructured phosphides. Stabilization of such structures is achieved through an array of spectator ligands which include cyclopentadienyl derivatives, the extended family of β-diketiminato ligands, bulky isocyanides, amides, (chelating) phosphines and N-heterocyclic carbenes (NHCs). In metal complexes, the nuclearity of the polyphosphido ligand obtained from P_4 is generally dictated by the electron count of the metal center. Nevertheless, the electronic and steric properties of the ancillary ligands can play an important role in guiding structure and reactivity (see for example the differently substituted cyclopentadienyl iron complexes in Section 3.1.1. and the substitution of trimethylphosphine with trimethylphosphine as a ligand in ruthenium complexes described in Section 3.1.2). Furthermore, while the coordination and initial activation of P_4 at TMs can already be considered an established and mature field, the functionalization of the activated phosphorus motifs has been much less explored and the release of the resulting P_n moieties remains a highly desirable research objective. This is especially relevant for the further development of phosphorus-based synthesis on an industrial level. Nevertheless, the chemistry presented in these sections provides further, although still rather limited, details into the mechanisms of activation of white phosphorus by transition metals. In recent work, the long-envisioned target of a catalytic functionalization of white phosphorus has been achieved.

Finally, the rediscovery of the black allotrope, whose surface behaves as a polydentate phosphine ligand, brings the reader briefly to the world of materials science. Section 4 summarizes its promising reactivity towards unsaturated transition metal complexes, which represents the starting point not only for new heterogeneous catalysts but also for new 2D phosphorus-based materials endowed with unique properties.

Declaration of Competing Interest

The authors declare that they have no known competing financial interests or personal relationships that could have appeared to influence the work reported in this paper.

Acknowledgments

M.C. thanks the Italian Ministry for University and Research (MUR) for funding the project PRIN 2017 KFY7XF FERMAT “Fast ElectRon dynamics in novel hybrid-2D MATerials”. Thanks are also expressed to Italmatch Chemicals (Arese, Italy) for financing a doctoral grant to L.G. R.W. would like to thank a number of dedicated former and present co-workers for their vital contributions to the group’s research in the field. Their names are in the references. In addition, generous financial support by the European Research Council (CoG 772299) is gratefully acknowledged.

References

[1] J. Emsley, The 13th Element: The Sordid Tale of Murder, Fire, and Phosphorus, John Wiley & Sons Inc, New York, 2000.
[2] D.E.C. Corbridge, Phosphorus: Chemistry, Biochemistry and Technology, sixth ed., CRC Press, Boca Raton, FL, 2013.
[3] D.C.B. Whittet, J.E. Chiar, Cosmic evolution of the biogenic elements and compounds, Astron. Astrophys. Rev. 5 (1993) 1–35, https://doi.org/10.1007/BF00872922.
[4] B. Elvers, U. Fritz, Phosphorus Compounds, Inorganic to Plastics, Additives, Wiley-VCH, Weinheim, Germany, 2011.
[5] see ref. [2], p. 95..

[6] B.M. Cossairt, N.A. Piro, C.C. Cummins, Early-transition-metal-mediated activation and transformation of white phosphorus, Chem. Rev. 110 (2010) 4164–4177, https://doi.org/10.1021/cr9003709.

[7] M. Caporali, L. Gonsalvi, A. Rossin, M. Peruzzini, P_4 activation by late-transition metal complexes, Chem. Rev. 110 (2010) 4178–4235, https://doi.org/10.1021/cr900349u.

[8] M. Caporali, M. Serrano-Ruiz, M. Peruzzini, Benign chlorine-free approaches to organophosphorus compounds, in: P. Tundo, L.-N. He, E. Lokteva, C. Mota (Eds.), Chemistry Beyond Chlorine, Springer Int, Switzerland, 2016, pp. 97–136, https://doi.org/10.1007/978-3-319-30073-3_3.

[9] J.E. Borger, A.W. Ehlers, J.C. Slootweg, K. Lammertsma, Functionalization of P_4 through direct P–C bond formation, Chem. Eur. J. 23 (2017) 11738–11746, https://doi.org/10.1002/chem.201702067.

[10] S. Du, J. Yang, J. Hu, Z. Chai, G. Luo, Y. Luo, W.-X. Zhang, Z. Xi, Direct functionalization of white phosphorus to cyclotetraphosphanes: selective formation of four P–C bonds, J. Am. Chem. Soc. 141 (2019) 6843–6847, https://doi.org/10.1021/jacs.9b02628.

[11] D. Scheschkewitz, A convenient P^- source, Nat. Chem. 12 (2020) 785–787, https://doi.org/10.1038/s41557-020-0534-0.

[12] M. Scheer, G. Balázs, A. Seitz, P_4 Activation by main group elements and compounds, Chem. Rev. 110 (2010) 4236–4256, https://doi.org/10.1021/cr100010e.

[13] N.A. Giffin, J.D. Masuda, Reactivity of white phosphorus with compounds of the *p*-block, Coord. Chem. Rev. 255 (2011) 1342–1359, https://doi.org/10.1016/j.ccr.2010.12.016.

[14] S. Khan, S.S. Sen, H.W. Roesky, Activation of phosphorus by group 14 elements in low oxidation states, Chem. Comm. 48 (2012) 2169–2179, https://doi.org/10.1039/C2CC17449A.

[15] Alternative synthesis of P1 products directly from phosphates have been recently proposed: M.B. Geeson, C.C. Cummins, Let's Make White Phosphorus Obsolete, ACS Cent. Sci. 6 (2020) 848–860, https://doi.org/10.1021/acscentsci.0c00332.

[16] M.B. Geeson, P. Ríos, W.J. Transue, C.C. Cummins, Orthophosphate and sulfate utilization for C-E (E = P, S) bond formation via trichlorosilyl phosphide and sulfide anions, J. Am. Chem. Soc. 141 (2019) 6375–6384, https://doi.org/10.1021/jacs.9b01475.

[17] M.B. Geeson, C.C. Cummins, Phosphoric acid as a precursor to chemicals traditionally synthesized from white phosphorus, Science 359 (2018) 1383–1385, https://doi.org/10.1126/science.aar6620.

[18] W. Schipper, Phosphorus: too big to fail, Eur. J. Inorg. Chem. (2014) 1567–1571, https://doi.org/10.1002/ejic.201400115.

[19] H.-G. von Schnering, W. Hönle, Chemistry and structural chemistry of phosphides and polyphosphides. 48. Bridging chasms with polyphosphides, Chem. Rev. 88 (1988) 243–273, https://doi.org/10.1021/cr00083a012.

[20] S. Carenco, D. Portehault, C. Boissière, N. Mézailles, C. Sanchez, Nanoscaled metal borides and phosphides: recent developments and perspectives, Chem. Rev. 113 (2013) 7981–8065, https://doi.org/10.1021/cr400020d.

[21] Y. Shi, B. Zhang, Recent advances in transition metal phosphide nanomaterials: synthesis and applications in hydrogen evolution reaction, Chem. Soc. Rev. 45 (2016) 1529–1541, https://doi.org/10.1039/C5CS00434A.

[22] M.H. Holthausen, J.J. Weigand, The chemistry of cationic polyphosphorus cages – syntheses, structure and reactivity, Chem. Soc. Rev. 43 (2014) 6639–6657, https://doi.org/10.1039/C4CS00019F.

[23] A.K. Adhikari, C.G.P. Ziegler, K. Schwedtmann, C. Taube, J.J. Weigand, R. Wolf, Functionalization of Pentaphosphorus Cations by Complexation, Angew. Chem. Int. Ed. 58 (2019) 18584–18590, https://doi.org/10.1002/anie.201908998.

[24] E. Peresypkina, A. Virovets, M. Scheer, Supramolecular synthons: will giant rigid superspheres do?, Cryst. Growth Des. 16 (2016) 2335–2341, https://doi.org/10.1021/acs.cgd.6b00136.

[25] H.-F. Ji, Fundamentals and applications of phosphorus nanomaterials, ACS Sympos. Ser. 1333 (2019) ix–x, https://doi.org/10.1021/bk-2019-1333.ch002.

[26] H. Huang, L. Zhang, B. Xiao, Y. Cheng, J. Zhang, The structure and electronic properties of crimson phosphorus, Appl. Phys. Lett. 115 (2019), https://doi.org/10.1063/1.5118860 163101.

[27] R.H. Jeon, D.I. Kim, J.W. Lee, J.-H. Yu, B.G. Jeong, H.M. Oh, M.S. Jeong, J.-H. Boo, Ultra fast metal-free reduction catalyst of partial oxidized violet phosphorus synthesized via controlled mechanical energy, 2D Mater. 6 (2019), https://doi.org/10.1088/2053-1583/ab39c6 045039.

[28] P.E.M. Amaral, D.C. Hall Jr., Rahul Pai, J.E. Król, V. Kalra, G.D. Ehrlich, H.-F. Ji, Fibrous phosphorus quantum dots for cell imaging, ACS Appl. Nano Mater. 3 (2020) 752–759, https://doi.org/10.1021/acsanm.9b01786.

[29] R. Gusmão, Z. Sofer, M. Pumera, Black phosphorus rediscovered: from bulk material to monolayers, Angew. Chem. Int. Ed. 56 (2017) 8052–8072.

[30] Y. Liu, D. Cui, M. Chen, Z. Li, C. Zhou, Synthesis of red and black phosphorus nanomaterials, Chapter 1, in: H.-F. Ji (Ed.), Fundamentals and Applications of Phosphorus Nanomaterials, ACS Symposium Series, 2019, pp. 1–25.

[31] S. Lange, P. Schmidt, T. Nilges, Au_3SnP_7@Black phosphorus: an easy access to black phosphorus, Inorg. Chem. 46 (2007) 4028–4035, https://doi.org/10.1021/ic062192q.

[32] T. Nilges, M. Kersting, T. Pfeifer, A fast low-pressure transport route to large black phosphorus single crystals, J. Solid State Chem. 181 (2008) 1707–1711, https://doi.org/10.1016/j.jssc.2008.03.008.

[33] H. Du, X. Lin, Z. Xu, D. Chu, Recent developments in black phosphorus transistors, J. Mater. Chem. C 3 (2015) 8760–8775, https://doi.org/10.1039/C5TC01484K.

[34] G. Qu, T. Xia, W. Zhou, X. Zhang, H. Zhang, L. Hu, J. Shi, X.-F. Yu, G. Jiang, Property–activity relationship of black phosphorus at the nano–bio interface: from molecules to organisms, Chem. Rev. 120 (2020) 2288–2346, https://doi.org/10.1021/acs.chemrev.9b00445.

[35] L. Li, Y. Yu, G.J. Ye, Q. Ge, X. Ou, H. Wu, D. Feng, X.H. Chen, Y. Zhang, Black phosphorus field-effect transistors, Nat. Nanotechnol. 9 (2014) 372–377, https://doi.org/10.1038/nnano.2014.35.

[36] H. Liu, A.T. Neal, Z. Zhu, D. Tomanek, P.D. Ye, Phosphorene: an unexplored 2D semiconductor with a high hole mobility, ACS Nano 8 (2014) 4033–4041, https://doi.org/10.1021/nn501226z.

[37] X. Ling, H. Wang, S. Huang, F. Xia, M.S. Dresselhaus, The renaissance of black phosphorus, Proc. Natl. Acad. Sci. U.S.A. 112 (2015) 4523–4530, https://doi.org/10.1073/pnas.1416581112.

[38] M. Peruzzini, R. Bini, M. Bolognesi, M. Caporali, M. Ceppatelli, F. Cicogna, S. Coiai, S. Heun, A. Ienco, I. Iglesias Benito, A. Kumar, G. Manca, E. Passaglia, D. Scelta, M. Serrano-Ruiz, F. Telesio, S. Toffanin, M. Vanni, A perspective on recent advances in phosphorene functionalization and its applications in devices, Eur. J. Inorg. Chem. (2019) 1476–1494, https://doi.org/10.1002/ejic.201801219.

[39] S. Wu, K. San Hui, K.N. Hui, 2D black phosphorus: from preparation to applications for electrochemical energy storage, Adv. Sci. 5 (2018) 1700491, https://doi.org/10.1002/advs.201700491.

[40] E.S. Reich, Phosphorene excites materials scientists, Nature 506 (2014) 19, https://doi.org/10.1038/506019a.

[41] A. Castellanos-Gomez, L. Vicarelli, E. Prada, J.O. Island, K.L. Narasimha-Acharya, S.I. Blanter, D.J. Groenendijk, M. Buscema, G.A. Steele, J.V. Alvarez, H. W. Zandbergen, J.J. Palacios, H.S.J. van der Zant, Isolation and characterization of few-layer black phosphorus, 2D Mater 1 (2014), https://doi.org/10.1088/2053-1583/1/2/025001, 025001.

[42] F. Scalambra, M. Peruzzini, A. Romerosa, Chapter Four - Recent advances in transition metal-mediated transformations of white phosphorus, Adv. Organomet. Chem. 72 (2019) 173–222, https://doi.org/10.1016/bs.adomc.2019.06.001.

[43] C.M. Hoidn, D.J. Scott, R. Wolf, Transition metal-mediated functionalization of white phosphorus, Chem. Eur. J. 27 (2021) 1886–1902, https://doi.org/10.1002/chem.202001854.

[44] M. Di Vaira, M. Peruzzini, P. Stoppioni, d^6 metal systems for white phosphorus activation, C. R. Chim. 13 (2010) 935–942, https://doi.org/10.1016/j.crci.2010.07.004.

[45] M. Peruzzini, L. Gonsalvi, A. Romerosa, Coordination chemistry and functionalization of white phosphorus *via* transition metal complexes, Chem. Soc. Rev. 34 (2005) 1038–1047, https://doi.org/10.1039/B510917E.

[46] L.-P. Wang, D. Tofan, J. Chen, T. Van Voorhisa, C.C. Cummins, A pathway to diphosphorus from the dissociation of photoexcited tetraphosphorus, RSC Adv. 3 (2013) 23166–23171, https://doi.org/10.1039/C3RA43940B.

[47] M. Serrano-Ruiz, A. Romerosa, P. Lorenzo-Luis, Elemental phosphorus and electromagnetic radiation, Eur. J. Inorg. Chem. (2014) 1587–1598, https://doi.org/10.1002/ejic.201301361.

[48] Z.N. Gafurov, A.A. Kagilev, A.O. Kantyukov, O.G. Sinyashin, D.G. Yakhvarov, Hydrogenation reaction pathways in chemistry of white phosphorus, Pure Appl. Chem. 91 (2019) 797–810, https://doi.org/10.1515/pac-2018-1007.

[49] E. Gorbachuk, E. Badeeva, A. Gubaidullin, A. Samigullina, A. Voloshina, A. Sapunova, E. Hey-Hawkins, O. Sinyashin, D. Yakhvarov, Bis(α-hydroxycycloalkyl)phosphine oxides obtained from white phosphorus via phosphine oxide H_3PO: synthesis molecular structure, coordination properties and biological activity, ChemPlusChem 85 (2020) 958–962, https://doi.org/10.1002/cplu.202000220.

[50] D.G. Yakhvarov, E.V. Gorbachuk, O.G. Sinyashin, Electrode reactions of elemental (white) phosphorus and phosphane PH_3, Eur. J. Inorg. Chem. (2013) 4709–4726, https://doi.org/10.1002/ejic.201300845.

[51] Yu. G. Budnikova, S.A. Krasnov, Electrochemical transformation of white phosphorus to compounds with phosphorus-hydrogen and phosphorus-carbon bonds, Chapter 5, in: Jang Ho Chun (Ed.), Developments in Electrochemistry, IntechOpen, 2012, pp. 101–124.

[52] D. Yakhvarov, M. Caporali, L. Gonsalvi, S. Latypov, V. Mirabello, I. Rizvanov, O. Sinyashin, P. Stoppioni, W. Schipper, M. Peruzzini, Experimental evidence of phosphine oxide generation in solution and trapping by ruthenium complexes, Angew. Chem. Int. Ed. 50 (2011) 5370–5373, https://doi.org/10.1002/anie.201100822.

[53] U. Lennert, P.B. Arockiam, V. Streitferdt, D.J. Scott, C. Rödl, R.M. Gschwind, R. Wolf, Direct catalytic transformation of white phosphorus into arylphosphines and phosphonium salts, Nat. Catal. 2 (2019) 1101–1106, https://doi.org/10.1038/s41929-019-0378-4.

[54] K.M. Armstrong, P. Kilian, Catalytic synthesis of triaryl phosphates from white phosphorus, Eur. J. Inorg. Chem. (2011) 2138–2147, https://doi.org/10.1002/ejic.201100046.

[55] F. Dielmann, E.V. Peresypkina, B. Kramer, F. Hastreiter, B.P. Johnson, M. Zabel, C. Heindl, M. Scheer, cyclo-P_4 building blocks: achieving non-classical fullerene topology and beyond, Angew. Chem. Int. Ed. 55 (2016) 14833–14837, https://doi.org/10.1002/anie.201606074.

[56] T. Li, S. Kaercher, P.W. Roesky, Synthesis, structure and reactivity of rare-earth metal complexes containing anionic phosphorus ligands, Chem. Soc. Rev. 43 (2014) 42–57, https://doi.org/10.1039/c3cs60163c.

[57] W. Huang, S.I. Khan, P.L. Diaconescu, Scandium arene inverted-sandwich complexes supported by a ferrocene diamide ligand, J. Am. Chem. Soc. 133 (2011) 10410–10413, https://doi.org/10.1021/ja204304f.

[58] W. Huang, P.L. Diaconescu, P_4 activation by group 3 metal arene complexes, Chem. Commun. 48 (2012) 2216–2218, https://doi.org/10.1039/c2cc17638f.

[59] M. Baudler, K. Glinka, Monocyclic and polycyclic phosphanes, Chem. Rev. 93 (1993) 1623–1667, https://doi.org/10.1021/cr00020a010.

[60] D.E.C. Corbridge, E.J. Lowe, Structure of white phosphorus: single crystal X-ray examination, Nature (1952) 629, https://doi.org/10.1038/170629a0.

[61] A.S. Nizovtsev, A.S. Ivanov, A.I. Boldyrev, S.N. Konchenko, Li_4E_8 (E = P, As, Sb, Bi) clusters: the quest for realgar-type $[E_8]^{4-}$ zintl anions, Eur. J. Inorg. Chem. (2015) 5801–5807, https://doi.org/10.1002/ejic.201500931.

[62] W. Huang, P.L. Diaconescu, P_4 activation by lanthanum and lutetium naphthalene complexes supported by a ferrocene diamide ligand, Eur. J. Inorg. Chem. (2013) 4090–4096, https://doi.org/10.1002/ejic.201300225.

[63] F. Zhang, J. Zhang, Z. Chen, L. Weng, X. Zhou, An yttrium organic *cyclo*-P_4 complex and its selective conversions, Inorg. Chem. 58 (2019) 8451–8459, https://doi.org/10.1021/acs.inorgchem.9b00589.

[64] M. Scheer, U. Becker, M.H. Chisholm, J.C. Huffman, F. Lemoigno, O. Eisenstein, [Cp″Co(P_4){(Cp″Co)$_2$(μ-CO)}] (Cp″ = η^5-$C_5H_3tBu_2$): a complex with a P_4 unit on the way to a P_1 and a P_3 ligand, Inorg. Chem. 34 (1995) 3117–3119, https://doi.org/10.1021/ic00115a049.

[65] M. Scheer, U. Becker, J. Magull, The reaction of P_4 with [Cp'Mo(CO)$_3$], (Cp' = η^5-C_5H_4tBu)-the structure of lCp'Mo(CO)$_2$<(η^3-P_4){Cr(CO)$_5$}$_4$(H)>], Polyhedron 17 (1998) 1983–1989, https://doi.org/10.1016/S0277-5387(97)00480-4.

[66] M. Scheer, U. Becker, Zur Transformation des P_4-Tetraeders durch Ni-Komplexe, Chem. Ber. 129 (1996) 1307–1310, https://doi.org/10.1002/cber.19961291026.

[67] S. Du, J. Yin, Y. Chi, L. Xu, W.-X. Zhang, Dual functionalization of white phosphorus: formation, characterization, and reactivity of rare-earth-metal *Cyclo*-P_3 complexes, Angew. Chem. Int. Ed. 56 (2017) 15886–15890, https://doi.org/10.1002/anie.201708897.

[68] L. Xu, Y. Chi, S. Du, W. Zhang, Z. Xi, Direct synthesis of phospholyl lithium from white phosphorus, Angew. Chem. Int. Ed. 55 (2016) 9187–9190, https://doi.org/10.1002/anie.201602790.

[69] M. Di Vaira, C.A. Ghilardi, S. Midollini, L. Sacconi, cyclo-Triphosphorus (δ-P3) as a ligand in cobalt and nickel complexes with 1,1,1-tris (diphenylphosphinomethyl)ethane. Formation and structures, J. Am. Chem. Soc. 100 (1978) 2550–2551, https://doi.org/10.1021/ja00476a049.

[70] C. Bianchini, C. Mealli, A. Meli, L. Sacconi, Synthesis and crystal structure of two isomorphus rhodium and iridium complexes with cyclo-triphosphorus and 1,1,1-tris(diphenylphosphinomethyl)-ethane, Inorg. Chim. Acta. 37 (1979) L543–L544, https://doi.org/10.1016/S0020-1693(00)95502-6.

[71] M. Di Vaira, L. Sacconi, P. Stoppioni, Structural correlations and NMR properties of mononuclear cyclic triphosphorus complexes, J. Organomet. Chem. 250 (1983) 183–195, https://doi.org/10.1016/0022-328X(83)85049-9.

[72] F. Dapporto, P. Sacconi, L. Stoppioni, P. Zanobini, Palladium and platinum complexes with cyclo-triphosphorus and tetrahedro-tetraphosphorus as ligands, Inorg. Chem. 20 (1981) 3834–3839, https://doi.org/10.1021/ic50225a047.

[73] L. Midollini, S. Orlandini, A. Sacconi, [(triphos)Co(δ-P_3)Cr$_2$(CO)$_{10}$]: a trinuclear hetero- metal complex containing cyclo-triphosphorus as μ^3-ligand, Angew. Chem. Int. Ed. 18 (1979) 81–82, https://doi.org/10.1002/anie.197900811.

[74] M. Di Vaira, M.P. Ehses, P. Stoppioni, M. Peruzzini, Cyclotriphosphorus complexes: solid state structures and dynamic behavior of monoadducts with carbonyl fragments, Inorg. Chem. 39 (2000) 2199–2205, https://doi.org/10.1021/ic991380w.

[75] S.N. Konchenko, N.A. Pushkarevsky, M.T. Gamer, R. Köppe, H. Schnöckel, P.W. Roesky, [{(η^5-C_5Me_5)$_2$Sm}$_4$$P_8$]: a molecular polyphosphide of the rare-earth elements, J. Am. Chem. Soc. 131 (2009) 5740–5741, https://doi.org/10.1021/ja901045m.

[76] C. Schoo, S. Bestgen, R. Köppe, S.N. Konchenko, P.W. Roesky, Reactivity of bulky Ln(II) amidinates towards P_4, As_4, and As_4S_4, Chem. Commun. 54 (2018) 4770–4773, https://doi.org/10.1039/c8cc01519h.

[77] F. Kraus, J.C. Aschenbrenner, N. Korber, P_4^{2-}: a 6π aromatic polyphosphide in dicesium cyclotetraphosphide-ammonia (1/2), Angew. Chem. Int. Ed. 42 (2003) 4030–4033, https://doi.org/10.1002/anie.200351776.

[78] W.W. Seidel, O.T. Summerscales, B.O. Patrick, M.D. Fryzuk, Activation of white phosphorus by reduction in the presence of a zirconium diamidodiphosphine macrocycle: formation of a bridging square-planar cyclo-P_4 unit, Angew. Chem. Int. Ed. 48 (2009) 115–117, https://doi.org/10.1002/anie.200803739.

[79] O.J. Scherer, J. Vondung, G. Wolmershäuser, Tetraphosphacyclobutadiene as complex ligand, Angew. Chem. Int. Ed. Engl. 28 (1989) 1355–1357, https://doi.org/10.1002/anie.198913551.

[80] O.J. Scherer, R. Winter, G. Wolmershäuser, Niob- und Tantalkomplexe mit P_2- und P_4-Liganden, Z. Anorg. Allg. Chem. 619 (1993) 827–835, https://doi.org/10.1002/zaac.19936190504.

[81] M. Modl, S. Heinl, G. Balázs, F. Delgado Calvo, M. Caporali, G. Manca, M. Keilwerth, K. Meyer, M. Peruzzini, M. Scheer, Metal-assisted opening of intact P_4 Tetrahedra, Chem. Eur. J. 25 (2019) 6300–6305, https://doi.org/10.1002/chem.201900778.

[82] N. Yao, Y. Lindenmaier, S. Xiong, T. Inoue, M. Szilvási, J. Adelhardt, K. Sutter, M. Driess, K. Meyer, A Neutral Tetraphosphacyclobutadiene Ligand in Cobalt (I) Complexes, Angew. Chem. Int. Ed. 54 (2015) 1250–1254, https://doi.org/10.1002/anie.201409469.

[83] T. Li, M.T. Gamer, M. Scheer, S.N. Konchenko, P.W. Roesky, P-P bond formation via reductive dimerization of [Cp*Fe(η^5-P_5)] by divalent samarocenes, Chem. Commun. 49 (2013) 2183–2185, https://doi.org/10.1039/c3cc38841g.

[84] O.J. Scherer, B. Hobel, Double open-edged P_{10} dihydrofulvalene as a 16-electron donor ligand, Angew. Chem. Int. Ed. 31 (1992) 1027–1028, https://doi.org/10.1002/anie.199210271.

[85] A.N. Selikhov, T.V. Mahrova, A.V. Cherkasov, G.K. Fukin, J. Larionova, J. Long, A. A. Trifonov, Base-free lanthanoidocenes(II) coordinated by bulky pentabenzylcyclopentadienyl ligands, Organometallics 34 (2015) 1991–1998, https://doi.org/10.1021/acs.organomet.5b00243.

[86] A.N. Selikhov, T.V. Mahrova, A.V. Cherkasov, G.K. Fukin, E. Kirillov, C. Alvarez Lamsfus, L. Maron, A.A. Trifonov, Yb(II) Triple-Decker Complex with the μ-bridging naphthalene dianion [Cp^{Bn5}Yb(DME)]$_2$(μ-η^4:η^4-$C_{10}H_8$). Oxidative substitution of $[C_{10}H_8]^{2-}$ by 1,4-diphenylbuta-1,3-diene and P_4 and protonolysis of the Yb-$C_{10}H_8$ bond by $PhPH_2$, Organometallics 35 (2016) 2401–2409, https://doi.org/10.1021/acs.organomet.6b00428.

[87] A. Formanuik, F. Ortu, R. Beekmeyer, A. Kerridge, R.W. Adams, D.P. Mills, White phosphorus activation by a Th(III) complex, Dalton Trans. 45 (2016) 2390–2393, https://doi.org/10.1039/c5dt04528b.

[88] P. Pyykkö, M. Atsumi, Molecular double-bond covalent radii for elements Li-E112, Chem. Eur. J. 15 (2009) 12770–12779, https://doi.org/10.1002/chem.200901472.

[89] P.C. Blake, M.A. Edelman, P.B. Hitchcock, J. Hu, M.F. Lappert, S. Tian, G. Müller, J.L. Atwood, H. Zhang, Organometallic chemistry of the actinides: Part 4 The chemistry of some tris(cyclopentadienyl)actinide complexes, J. Organomet. Chem. 551 (1998) 261–270, https://doi.org/10.1016/S0022-328X(97)00477-4.

[90] O.J. Scherer, B. Werner, G. Heckmann, G. Wolmershäuser, Bicyclic P_6 as complex ligand, Angew. Chem. Int. Ed. 30 (1991) 553–555, https://doi.org/10.1002/anie.199105531.

[91] A.S.P. Frey, F.G.N. Cloke, P.B. Hitchcock, I.J. Day, J.C. Green, G. Aitken, Mechanistic studies on the reductive cyclooligomerisation of CO by U(III) mixed sandwich complexes; the molecular structure of [U(η-C_8H_6{Si*i*Pr$_3$-1,4}$_2$)(η-Cp*)]$_2$(μ-η^1:η^1-C_2O_2), J. Am. Chem. Soc. 130 (2008) 13816–13817, https://doi.org/10.1021/ja8059792.

[92] A.S.P. Frey, F.G.N. Cloke, P.B. Hitchcock, J.C. Green, Activation of P_4 by U(η^5-C_5Me_5)(η^8-C_8H_6(Si*i*Pr$_3$)$_2$-1,4)(THF); The X-ray structure of [U(η^5-C_5Me_5)(η^8-C_8H_6(Si*i*Pr$_3$)$_2$-1,4)]$_2$(μ-η^2:η^2-P_4), New J. Chem. 35 (2011) 2022–2026, https://doi.org/10.1039/c1nj20163h.

[93] B.M. Gardner, F. Tuna, E.J.L. McInnes, J. McMaster, W. Lewis, A.J. Blake, S.T. Liddle, An inverted-sandwich diuranium μ-η^5:η^5-cyclo-P_5 complex supported by U-P_5 δ-bonding, Angew. Chem. Int. Ed. 54 (2015) 7068–7072, https://doi.org/10.1002/anie.201501728.

[94] T. Li, J. Wiecko, N.A. Pushkarevsky, M.T. Gamer, R. Köppe, S.N. Konchenko, M. Scheer, P.W. Roesky, Mixed-metal lanthanide-iron triple-decker complexes with a cyclo-P_5 building block, Angew. Chem. Int. Ed. 50 (2011) 9491–9495, https://doi.org/10.1002/anie.201102748.

[95] D. Patel, F. Tuna, E.J.L. McInnes, W. Lewis, A.J. Blake, S.T. Liddle, An actinide Zintl cluster: a Tris(triamidouranium)μ^3-η^2:η^2:η^2-heptaphosphanortricyclane and its diverse synthetic utility, Angew. Chem. Int. Ed. 52 (2013) 13334–13337, https://doi.org/10.1002/anie.201306492.

[96] P.L. Diaconescu, P.L. Arnold, T.A. Baker, D.J. Mindiola, C.C. Cummins, Arene-bridged diuranium complexes: Inverted sandwiches supported by δ backbonding, J. Am. Chem. Soc. 122 (2000) 6108–6109, https://doi.org/10.1021/ja994484e.

[97] D. Patel, F. Moro, J. McMaster, W. Lewis, A.J. Blake, S.T. Liddle, A formal high oxidation state inverse-sandwich diuranium complex: a new route to f-block-metal bonds, Angew. Chem. Int. Ed. 50 (2011) 10388–10392, https://doi.org/10.1002/anie.201104110.

[98] S. Scharfe, F. Kraus, S. Stegmaier, A. Schier, T.F. Fässler, Zintl ions, cage compounds, and intermetalloid clusters of group 14 and group 15 elements, Angew. Chem. Int. Ed. 50 (2011) 3630–3670, https://doi.org/10.1002/anie.201001630.

[99] K.G. Weinberg, Synthesis of arylphosphonous dichlorides, diarylphosphinous chlorides, and 1,6-diphosphatriptycene from elemental phosphorus, J. Org. Chem. 40 (1975) 3586–3589, https://doi.org/10.1021/jo00912a027.

[100] B.M. Cossairt, C.C. Cummins, Radical synthesis of trialkyl, triaryl, trisilyl and tristannyl phosphines from P_4, New J. Chem. 34 (2010) 1533–1536, https://doi.org/10.1039/c0nj00124d.

[101] T. Agapie, P.L. Diaconescu, C.C. Cummins, Methine (CH) transfer via a chlorine atom abstraction/benzene-elimination strategy: molybdenum methylidyne synthesis and elaboration to a phosphaisocyanide complex, J. Am. Chem. Soc. 124 (2002) 2412–2413, https://doi.org/10.1021/ja017278r.

[102] T. Agapie, P.L. Diaconescu, D.J. Mindiola, C.C. Cummins, Radical scission of symmetrical 1,4-dicarbonyl compounds: C-C bond cleavage with Titanium (IV) enolate formation and related reactions, Organometallics 21 (2002) 1329–1340, https://doi.org/10.1021/om0107284.

[103] J.O. Scherer, M. Swarowsky, H. Swarowsky, G. Wolmershauser, P_4 Isomers as Complex Ligands, Angew. Chem. Int. Ed. 27 (1988) 694–695, https://doi.org/10.1002/anie.198806941.

[104] U. Vogel, M. Eberl, M. Eckhardt, A. Seitz, E.M. Rummel, A.Y. Timoshkin, E.V. Peresypkina, M. Scheer, Access to phosphorus-rich zirconium complexes, Angew. Chem. Int. Ed. 50 (2011) 8982–8985, https://doi.org/10.1002/anie.201103634.

[105] D.W. Bullet, Valence band structures of phosphorus allotropes II, Solid State Commun. 55 (1985) 257–260, https://doi.org/10.1016/0038-1098(85)90728-8.

[106] A.E. Seitz, U. Vogel, M. Eberl, M. Eckhardt, G. Balázs, E.V. Peresypkina, M. Bodensteiner, M. Zabel, M. Scheer, Coordination behavior of [Cp″$_2$Zr($\eta^{1:1}$–

P_4)] towards different Lewis acids, Chem. Eur. J. 23 (2017) 10319–10327, https://doi.org/10.1002/chem.201701380.
[107] Y. Nakanishi, Y. Ishida, H. Kawaguchi, Zirconium hydride complex supported by a tetradentate carbon-centered tripodal tris(aryloxide) ligand: synthesis, structure, and reactivity, Inorg. Chem. 55 (2016) 3967–3973, https://doi.org/10.1021/acs.inorgchem.6b00233.
[108] M.A. Lockwood, P.E. Fanwick, I.P. Rothwell, Conversion of arene groups to η^2-cyclohexene rings at tungsten metal centers, Polyhedron 14 (1995) 3363–3366, https://doi.org/10.1016/0277-5387(95)85015-5.
[109] M.A. Lockwood, P.E. Fanwick, I.P. Rothwell, Reactivity of a tungsten(II) aryloxide with imines, ketones and aldehydes, Chem. Commun. 17 (1996) 2013–2014, https://doi.org/10.1039/CC9960002013.
[110] B.L. Tran, M. Pink, X. Gao, H. Park, D.J. Mindiola, Low-coordinate and neutral nitrido complexes of vanadium, J. Am. Chem. Soc. 132 (2010) 1458–1459, https://doi.org/10.1021/ja908303k.
[111] B.L. Tran, M. Singhal, H. Park, O.P. Lam, M. Pink, J. Krzystek, A. Ozarowski, J. Telser, K. Meyer, D.J. Mindiola, Reactivity studies of a masked three-coordinate vanadium(II) complex, Angew. Chem. Int. Ed. 49 (2010) 9871–9875, https://doi.org/10.1002/anie.201005029.
[112] B. Pinter, K.T. Smith, M. Kamitani, E.M. Zolnhofer, B.L. Tran, S. Fortier, M. Pink, G. Wu, B.C. Manor, K. Meyer, M.H. Baik, D.J. Mindiola, Cyclo-P_3 complexes of vanadium: redox properties and origin of the ^{31}P NMR chemical shift, J. Am. Chem. Soc. 137 (2015) 15247–15261, https://doi.org/10.1021/jacs.5b10074.
[113] M. Di Vaira, P. Stoppioni, Formation of the novel P_6 chain ligand from two P_3 rings bound to metal ligand systems, Polyhedron 13 (1994) 3045–3051, https://doi.org/10.1016/S0277-5387(00)83669-4.
[114] M. Di Vaira, P. Stoppioni, M. Peruzzini, Synthesis and characterization of gold adducts of [M(tppme)(P_3)] [M = Co, Rh, or Ir; tppme = 1,1,1-tris (diphenylphosphinomethyl)ethane]. X-ray crystal structures of [Au{M (tppme)(P_3)}$_2$]PF_6 (M = Co, Rh, or Ir), J. Chem. Soc. Dalton Trans. (1990) 109–113, https://doi.org/10.1039/DT9900000109.
[115] B.M. Cossairt, M.C. Diawara, C.C. Cummins, Facile synthesis of AsP_3, Science 323 (2009) 602, https://doi.org/10.1126/science.1168260.
[116] B.M. Cossairt, C.C. Cummins, Shuttling P_3 from niobium to rhodium: The synthesis and use of $Ph_3SnP_3(C_6H_8)$ as a P_3-synthon, Angew. Chem. Int. Ed. 49 (2010) 1595–1598, https://doi.org/10.1002/anie.200906633.
[117] G.R. Morello, T.R. Cundari, Density functional study of oxygen insertion into niobium-phosphorus bonds: novel mechanism for liberating P_3-synthons, Organometallics 35 (2016) 3624–3634, https://doi.org/10.1021/acs.organomet.6b00679.
[118] M. Di Vaira, L. Sacconi, Transition Metal complexes with cyclo-triphosphorus (η^3-P_3) and tetrahedro-tetraphosphorus (η^1-P_4) ligands, Angew. Chem. Int. Ed. 21 (1982) 330–342, https://doi.org/10.1002/anie.198203301.
[119] M. Piesch, M. Seidl, M. Stubenhofer, M. Scheer, Ring expansions of nonpolar polyphosphorus rings, Chem. Eur. J. 25 (2019) 6311–6316, https://doi.org/10.1002/chem.201901149.
[120] A. Velian, C.C. Cummins, Synthesis of a diniobium tetraphosphorus complex by a 2(3–1) process, Chem. Sci. 3 (2012) 1003–1006, https://doi.org/10.1039/c2sc00931e.
[121] C.E. Laplaza, W.M. Davis, C.C. Cummins, A Molybdenum-phosphorus triple bond: synthesis, structure, and reactivity of the terminal phosphido (P^{3-}) complex [Mo(P)(NRAr)$_3$], Angew. Chem. Int. Ed. Engl. 34 (1995) 2042–2044, https://doi.org/10.1002/anie.199520421.
[122] D. Tofan, B.M. Cossairt, C.C. Cummins, White phosphorus activation at a metal-phosphorus triple bond: a new route to cyclo-triphosphorus or cyclo-pentaphosphorus complexes of niobium, Inorg. Chem. 50 (2011) 12349–12358, https://doi.org/10.1021/ic2014607.
[123] I. Krummenacher, C.C. Cummins, Carbon-Phosphorus triple bond formation through multiple bond metathesis of an anionic niobium phosphide with carbon dioxide, Polyhedron 32 (2012) 10–13, https://doi.org/10.1016/j.poly.2011.07.016.
[124] D.W. Stephan, Room temperature reduction of CO_2 to methanol by Al-based frustrated lewis pairs and ammonia borane, J. Am. Chem. Soc. 132 (2010) 1796–1797, https://doi.org/10.1021/ja9104792.
[125] J.S. Figueroa, C.C. Cummins, Phosphaalkynes from acid chlorides via P for O (Cl) metathesis: a recyclable niobium phosphide (P^{3-}) reagent that effects C - P triple-bond formation, J. Am. Chem. Soc. 126 (2004) 13916–13917, https://doi.org/10.1021/ja0461522.
[126] C. Camp, L. Maron, R.G. Bergman, J. Arnold, Activation of white phosphorus by low-valent group 5 complexes: formation and reactivity of cyclo-P_4 inverted sandwich compounds, J. Am. Chem. Soc. 136 (2014) 17652–17661, https://doi.org/10.1021/ja5107282.
[127] J.D. Masuda, W.W. Schoeller, B. Donnadieu, G. Bertrand, NHC-mediated aggregation of P_4: isolation of a P_{12} cluster, J. Am. Chem. Soc. 129 (2007) 14180–14181, https://doi.org/10.1021/ja077296u.
[128] O.J. Scherer, G. Berg, G. Wolmershäuser, P_8 and P_{12} as complex ligands, Chem. Ber. 129 (1996) 53–58, https://doi.org/10.1002/cber.19961290112.
[129] J. Bai, A.V. Virovets, M. Scheer, Synthesis of inorganic fullerene-like molecules, Science 300 (2003) 781–784, https://doi.org/10.1126/science.1081119.
[130] B.P. Johnson, F. Dielmann, G. Balázs, M. Sierka, M. Scheer, Spherical cluster comprising a four- and six- membered-ring motif, Angew. Chem. Int. Ed. 45 (2006) 2473–2475, https://doi.org/10.1002/anie.200503511.
[131] T. Nguyen, A.D. Sutton, M. Brynda, J.C. Fettinger, G.J. Long, P.P. Power, Synthesis of a stable compound with fivefold bonding between two chromium(I) centers, Science 310 (2005) 844–848, https://doi.org/10.1126/science.1116789.
[132] M. Kaupp, S. Demeshko, R. Kempe, A. Noor, G. Glatz, R. Mu, Carboalumination of a chromium-chromium quintuple bond, Nat. Chem. 1 (2009) 322–325, https://doi.org/10.1038/NCHEM.255.
[133] C. Schwarzmaier, A. Noor, G. Glatz, M. Zabel, A.Y. Timoshkin, B.M. Cossairt, C. C. Cummins, R. Kempe, M. Scheer, Formation of cyclo-P_4 units (E_4 = P_4, As_4, AsP_3) by a complex with a Cr- Cr quintuple bond, Angew. Chem. Int. Ed. 50 (2011) 7283–7286, https://doi.org/10.1002/anie.201102361.
[134] T. Arnold, H. Braunschweig, J.O.C. Jimenez-Halla, K. Radacki, S.S. Sen, Simultaneous fragmentation and activation of white phosphorus, Chem. Eur. J. 19 (2013) 9114–9117, https://doi.org/10.1002/chem.201300895.
[135] M. Driess, A.D. Fanta, D.R. Powell, R. West, Synthesis, characterization, and complexation of an unusual P_2Si_2 bicyclobutane with butterfly-structure: 2,2,4,4-Tetramesityl-1,3-diphospha-2,4-disilabicyclo[1.1.0]butane, Angew. Chem. Int. Ed. 28 (1989) 1038–1040, https://doi.org/10.1002/anie.198910381.
[136] M. Yoshifuji, I. Shima, N. Inamoto, K. Hirotsu, T. Higuchi, Synthesis and structure of bis(2,4,6-tri-*tert*-butylphenyl)diphosphene: isolation of a true "phosphobenzene", J. Am. Chem. Soc. 103 (1981) 4587–4589, https://doi.org/10.1021/ja00405a054.
[137] D. Yang, J. Zhao, L. Yu, X. Lin, W. Zhang, H. Ma, A. Gogoll, Z. Zhang, Y. Wang, X.-J. Yang, B. Wu, Air- and light-stable P_4 and As_4 within an anion-coordination-based tetrahedral cage, J. Am. Chem. Soc. 139 (2017) 5946–5951, https://doi.org/10.1021/jacs.7b01890.
[138] A.E. Seitz, F. Hippauf, W. Kremer, S. Kaskel, M. Scheer, Facile storage and release of white phosphorus and yellow arsenic, Nat. Commun. 9 (2018) 361, https://doi.org/10.1038/s41467-017-02735-2.
[139] K.A. Mandla, C.E. Moore, A.L. Rheingold, J.S. Figueroa, Photolytic reductive elimination of white phosphorus from a mononuclear cyclo-P_4 transition metal complex, Angew. Chem. Int. Ed. 58 (2019) 1779–1783, https://doi.org/10.1002/anie.201809042.
[140] G. Rathenau, Optische und photochemische Versuche mit Phosphor, Physica. 4 (1937) 503–514, https://doi.org/10.1016/S0031-8914(37)80084-1.
[141] D. Tofan, C.C. Cummins, Photochemical incorporation of diphosphorus units into organic molecules, Angew. Chem. Int. Ed. 49 (2010) 7516–7518, https://doi.org/10.1002/anie.201004385.
[142] K.A. Mandla, M.L. Neville, C.E. Moore, A.L. Rheingold, J.S. Figueroa, Dianionic mononuclear cyclo-P_4 complexes of zero-valent molybdenum: coordination of the cyclo-P_4 dianion in the absence of intramolecular charge transfer, Angew. Chem. Int. Ed. 58 (2019) 15329–15333, https://doi.org/10.1002/anie.201908885.
[143] M. Scheer, L.J. Gregoriades, M. Zabel, J. Bai, I. Krossing, G. Brunklaus, H. Eckert, Self-assemblies based on [$Cp_2Mo_2(CO)_4(\mu,\eta^2$-$P_2)$]—solid state structure and dynamic behaviour in solution, Chem. Eur. J. 2 (2008) 282–295, https://doi.org/10.1002/chem.200700715.
[144] B. Attenberger, S. Welsch, M. Zabel, E. Peresypkina, M. Scheer, Diphosphorus complexes as building blocks for the design of phosphorus-containing organometallic-organic hybrid materials, Angew. Chem. Int. Ed. 50 (2011) 11516–11519, https://doi.org/10.1002/anie.201103046.
[145] Y. Yao, W. Shen, B. Nohra, C. Lescop, R. Réau, Coordination-driven hierarchical organization of π-conjugated systems: from molecular to supramolecular π-stacked assemblies, Chem. Eur. J. 16 (2010) 7143–7163, https://doi.org/10.1002/chem.201000621.
[146] M. Elsayed Moussa, B. Attenberger, E.V. Peresypkina, M. Fleischmann, G. Balázs, M. Scheer, Facile synthesis of one-dimensional organometallic-organic hybrid polymers based on a diphosphorus complex and flexible bipyridyl linkers, Chem. Commun. 52 (2016) 10004–10007, https://doi.org/10.1039/c6cc05224j.
[147] O.J. Scherer, H. Sitzmann, G. Wolmershäuser, Hexaphosphabenzene as complex ligand, Angew. Chem. Int. Ed. 24 (1985) 351–353, https://doi.org/10.1002/anie.198503511.
[148] M. Fleischmann, F. Dielmann, L.J. Gregoriades, E.V. Peresypkina, A.V. Virovets, S. Huber, A.Y. Timoshkin, G. Balázs, M. Scheer, Redox and coordination behavior of the hexaphosphabenzene ligand in [($Cp^*Mo)_2(\mu,\eta^6$:η^6-$P_6)$] towards the "Naked" Cations Cu^+, Ag^+, and Tl^+, Angew. Chem. Int. Ed. 54 (2015) 13110–13115, https://doi.org/10.1002/anie.201506362.
[149] C. Heindl, E.V. Peresypkina, D. Lüdeker, G. Brunklaus, A.V. Virovets, M. Scheer, A cyclo-P_6 ligand complex for the formation of planar 2D layers, Chem. Eur. J. 22 (2016) 2599–2604, https://doi.org/10.1002/chem.201504644.
[150] M.A. Alvarez, M.E. García, D. García-Vivó, A. Ramos, M.A. Ruiz, Mild P_4 activation to give an anionic diphosphorus complex with a dual binding ability at a single P site, Inorg. Chem. 50 (2011) 2064–2066, https://doi.org/10.1021/ic102407s.
[151] M.A. Alvarez, M.E. García, D. García-Vivó, A. Ramos, M.A. Ruiz, Reactivity of the Anionic diphosphorus complex [$Mo_2Cp_2(\mu,PCy_2)(CO)_2(\mu,\kappa^2$:$\kappa^2$-$P_2)$]$^-$, toward ER3X electrophiles (E = C to Pb): insights into the multisite donor ability and dynamics of the P_2 ligand, Inorg. Chem. 51 (2012) 11061–11075, https://doi.org/10.1021/ic301612g.
[152] M.A. Alvarez, M.E. García, D. García-Vivó, R. Lozano, A. Ramos, M.A. Ruiz, Reactivity of the anionic diphosphorus complex [$Mo_2Cp_2(\mu$-$PCy_2)(\mu$-κ^2:κ^2-$P_2)(CO)_2$]$^-$ toward phosphorus- and transition metal-based electrophiles, Inorg. Chem. 52 (2013) 9005–9018, https://doi.org/10.1021/ic401204j.
[153] M.A. Alvarez, M.E. García, D. García-Vivó, R. Lozano, A. Ramos, M.A. Ruiz, Diphosphorus-bridged heterometallic anions and hydrides derived from reactions of complex [$Mo_2Cp_2(\mu$-$PCy_2)(\mu$-κ^2:κ^2-$P_2)(CO)_2$]$^-$ with precursors of

16-electron metal carbonyl fragments, J. Organomet. Chem. 791 (2015) 279–288, https://doi.org/10.1016/j.jorganchem.2015.06.016.
[154] M.A. Alvarez, M.E. García, D. García-Vivó, R. Lozano, A. Ramos, M.A. Ruiz, Mild P-P bond cleavage in the methyldiphosphenyl complex $[Mo_2Cp_2(\mu\text{-}PCy_2)(\mu\text{-}\kappa^2\text{:}\kappa^2\text{-}P_2Me)(CO)_2]$ to give novel phosphide-bridged trinuclear derivatives, inorg. chem. 53 (2014) 11261–11273, https://doi.org/10.1021/ic501857f.
[155] M.A. Alvarez, M.E. García, R. Lozano, A. Ramos, M.A. Ruiz, Tetranuclear phosphide- and phosphinidene-bridged derivatives of the diphosphenyl complex $[Mo_2Cp_2(\mu\text{-}PCy_2)(\mu\text{-}\kappa^2\text{:}\kappa^2\text{-}P_2Me)(CO)_2]$, Inorg. Chem. 54 (2015) 2455–2466, https://doi.org/10.1021/ic503076x.
[156] M.A. Alvarez, M. Casado-Ruano, M.E. García, D. García-Vivó, M.A. Ruiz, Dehydrogenation, methyl elimination and insertion reaction of the agostic methyl-bridged complex $[Mo_2Cp_2(\mu,\kappa^1\text{:}\eta^2\text{-}CH_3)(\mu,P^tBu_2)(\mu,CO)]$, Chem. Eur. J. 24 (2018) 9504–9507, https://doi.org/10.1002/chem.201801944.
[157] N. Arleth, M.T. Gamer, R. Köppe, N.A. Pushkarevsky, S.N. Konchenko, M. Fleischmann, M. Bodensteiner, M. Scheer, P.W. Roesky, The approach to 4d/4f-polyphosphides, Chem. Sci. 6 (2015) 7179–7184, https://doi.org/10.1039/c5sc02252e.
[158] O.J. Scherer, H. Sitzmann, G. Wolmershäuser, Umsetzung von P_4 mit $(\eta^5\text{-}C_5H_5)(CO)_2Mo{\equiv}Mo(CO)_2(\eta^5\text{-}C_5H_5)$ zu den Tetraedrischen molybdankomplexen $P_n[Mo(CO)_2(\eta^5\text{-}C_5H_5)]_{4\text{-}n}$ (n= 2, 3), J. Organomet. Chem. 268 (1984) C9–C12, https://doi.org/10.1016/0022-328X(84)85105-0.
[159] M.A. Alvarez, M.E. García, D. García-Vivó, M.A. Ruiz, M.F. Vega, Reactions of the unsaturated ditungsten anion $[W_2Cp_2(\mu\text{-}PCy_2)(\mu\text{-}\kappa^2\text{:}\kappa^2\text{-}P_2)(CO)_2]^-$ with C- and P-based electrophiles, Organometallics. 34 (2015) 870–878, https://doi.org/10.1021/om501202j.
[160] L. Weber, The chemistry of diphosphenes and their heavy congeners: synthesis, structure, and reactivity, Chem. Rev. 92 (1992) 1839–1906, https://doi.org/10.1021/cr00016a008.
[161] J.M. Breunig, D. Tofan, C.C. Cummins, Contrasting cyclo-P_3 ligand transfer reactivity of valence-isoelectronic aryloxide complexes $[(P_3)Nb(ODipp)_3]^-$ and $[(P_3)W(ODipp)_3]$, Eur. J. Inorg. Chem. (2014) 1605–1609, https://doi.org/10.1002/ejic.201301140.
[162] S. Heinl, E.V. Peresypkina, A.Y. Timoshkin, P. Mastrorilli, V. Gallo, M. Scheer, Intact P_4 Tetrahedra as terminal and bridging ligands in neutral complexes of manganese, Angew. Chem. Int. Ed. 52 (2013) 10887–10891, https://doi.org/10.1002/anie.201305315.
[163] T. Gröer, G. Baum, M. Scheer, Complexes with a monohapto bound phosphorus tetrahedron and phosphaalkyne, Organometallics 17 (1998) 5916–5919, https://doi.org/10.1021/om9806794.
[164] I. de los Ríos, J.-R. Hamon, P. Hamon, C. Lapinte, L. Toupet, A. Romerosa, M. Peruzzini, Synthesis of exceptionally stable iron and ruthenium η^1-tetrahedro-tetraphosphorus complexes: evidence for a strong temperature dependence of M−P_4 π-back donation, Angew. Chem. Int. Ed. 40 (2001) 3910–3912, https://doi.org/10.1002/1521-3773(20011015)40:20<3910::AID-ANIE3910>3.0.CO;2-2.
[165] M. Di Vaira, P. Frediani, S. Costantini, Easy hydrolysis of white phosphorus coordinated to ruthenium, Dalton Trans. 13 (2005) 2234–2236, https://doi.org/10.1039/B504795A.
[166] M. Di Vaira, M. Peruzzini, S. Seniori, P. Stoppioni, Hydrolytic disproportionation of coordinated white phosphorus in $[CpRu(dppe)(\eta^1\text{-}P_4)]PF_6$ [dppe = 1,2-bis(diphenylphosphino)ethane], J. Organomet. Chem. 691 (2006) 3931–3937, https://doi.org/10.1016/j.jorganchem.2006.05.049.
[167] P. Barbaro, M. Di Vaira, M. Peruzzini, S. Seniori Costantini, Stoppioni, Hydrolysis of dinuclear ruthenium complexes $[\{CpRu(PPh_3)_2\}_2(\mu,\eta^{1:1}\text{-}L)][CF_3SO_3]_2$ (L= P_4, P_4S_3): simple access to metal complexes of P_2H_4 and PH_2SH, Chem. Eur. J. 13 (2007) 6682–6690, https://doi.org/10.1002/chem.200601846.
[168] M. Caporali, M. Di Vaira, M. Peruzzini, S. Costantini, P. Stoppioni, F. Zanobini, Synthesis, characterization and hydrolysis of osmium tetraphosphorus complexes, Eur. J. Inorg. Chem. 1 (2010) 152–158, https://doi.org/10.1002/ejic.200900884.
[169] M. Di Vaira, M. Peruzzini, S. Seniori Costantini, P. Stoppioni, Coordination and reactivity of white phosphorus and tetraphosphorus trisulphide in the presence of the fragment CpFe(dppe) [dppe = 1,2-bis(diphenylphosphino) ethane], J. Organomet. Chem. 695 (2010) 816–820, https://doi.org/10.1016/j.jorganchem.2009.12.022.
[170] S. Heinl, K. Kiefer, G. Balázs, C. Wickleder, M. Scheer, The synthesis of the heterocubane cluster $[\{CpMn\}_4(\mu^3\text{-}P)_4]$ as a tetrahedral shaped starting material for the formation of polymeric coordination compounds, Chem. Commun. 51 (2015) 13474–13477, https://doi.org/10.1039/c5cc04800a.
[171] S. Heinl, G. Balázs, M. Bodensteiner, M. Scheer, Synthesis and characterization of manganese triple-decker complexes, Dalton Trans. 45 (2016) 1962–1966, https://doi.org/10.1039/c5dt01750e.
[172] A.R. Kudinov, D.A. Loginov, Z.A. Starikova, P.V. Petrovskii, M. Corsini, P. Zanello, Iron- and Ruthenium-containing triple-Decker Complexes with a central pentaphospholyl ligand - X-ray structures of $[(\eta\text{-}C_5H_5)Fe(\mu\text{-}\eta\text{:}\eta\text{-}P_5)Ru(\eta\text{-}C_5Me_5)]PF_6$ and $[(\eta\text{-}C_5Me_5)Ru(\mu\text{-}\eta\text{:}\eta\text{-}P_5)Ru(\eta\text{-}C_5Me_5)]PF_6$, Eur. J. Inorg. Chem. (2002) 3018–3027, https://doi.org/10.1002/1099-0682(200211)2002:11<3018::AID-EJIC3018>3.0.CO;2-A.
[173] T.D. Lohrey, L. Maron, R.G. Bergman, J. Arnold, Heterotetrametallic Re−Zn−Zn−Re complex Generated by an anionic Rhenium(I) β-diketiminate, J. Am. Chem. Soc. 141 (2019) 800–804, https://doi.org/10.1021/jacs.8b12494.
[174] T.D. Lohrey, G. Rao, R.D. Britt, R.G. Bergman, J. Arnold, H_2 activation and direct access to terminal nitride and cyclo-P_3 complexes by an acceptor-free Rhenium(II) β-diketiminate, Inorg. Chem. 58 (2019) 13492–13501, https://doi.org/10.1021/acs.inorgchem.9b02556.
[175] A.P. Ginsberg, W.E. Lindsell, W.E. Silverthorn, Reactions of carbon subsulfide and of elementary phosphorus, sulfur, and selenium with complexes of the platinum metals, Trans. Acad. Sci. N. Y. 33 (1971) 303–312, https://doi.org/10.1111/j.2164-0947.1971.tb02597.x.
[176] A.P. Ginsberg, W.E. Lindsell, Rhodium complexes with the molecular unit P_4 as a ligand, J. Am. Chem. Soc. 93 (1971) 2082–2084, https://doi.org/10.1021/ja00737a059.
[177] P. Dapporto, S. Midollini, L. Sacconi, tetrahedro-Tetraphosphorus as Monodentate Ligand in a Nickel(0) Complex, Angew. Chem., Int. Ed. Engl. 18 (1979) 469, https://doi.org/10.1002/anie.197904691.
[178] V. Mirabello, M. Caporali, V. Gallo, L. Gonsalvi, D. Gudat, W. Frey, A. Ienco, M. Latronico, P. Mastrorilli, M. Peruzzini, Solution and solid-state dynamics of metal-coordinated white phosphorus, Chem. Eur. J. 18 (2012) 11238–11250, https://doi.org/10.1002/chem.201201330.
[179] I.M. Riddlestone, P. Weis, A. Martens, M. Schorpp, H. Scherer, I. Krossing, From phosphidic to phosphonium? Umpolung of the P_4-bonding situation in $[CpFe(CO)(L)(\eta^1\text{-}P_4)]+$ cations (L=CO or PPh_3), Chem. Eur. J. 25 (2019) 10546–10551, https://doi.org/10.1002/chem.201902075.
[180] M. Peruzzini, L. Marvelli, A. Romerosa, A. Rossi, F. Vizza, F. Zanobini, Synthesis and characterization of tetrahedro-tetraphosphorus complexes of Rhenium – evidence for the first bridging complex of white phosphorus, Eur. J. Inorg. Chem. (1999) 931–933, https://doi.org/10.1002/(SICI)1099-0682(199906)1999:6<931::AID-EJIC931>3.0.CO;2-1.
[181] C. Heindl, E.V. Peresypkina, A.V. Virovets, W. Kremer, M. Scheer, Giant Rugby Ball $[\{Cp^{Bn}Fe(\eta^5\text{-}P_5)\}_{24}Cu_{96}Br_{96}]$ derived from pentaphosphaferrocene and CuB_r2, J. Am. Chem. Soc. 137 (2015) 10938–10941, https://doi.org/10.1021/jacs.5b06835.
[182] S. Heinl, E. Peresypkina, J. Sutter, M. Scheer, Giant spherical cluster with I-C_{140} fullerene topology, Angew. Chem. Int. Ed. 54 (2015) 13431–13435, https://doi.org/10.1002/anie.201505516.
[183] M. Fleischmann, J.S. Jones, F.P. Gabbaï, M. Scheer, A comparative study of the coordination behavior of *cyclo*-P_5 and *cyclo*-As_5 ligand complexes towards the trinuclear Lewis acid complex (perfluoro-*ortho*-phenylene)mercury, Chem. Sci. 6 (2015) 132–139, https://doi.org/10.1039/C4SC02353F.
[184] F. Dielmann, M. Fleischmann, C. Heindl, E.V. Peresypkina, A.V. Virovets, R.M. Gschwind, M. Scheer, Tunable porosities and shapes of fullerene-like spheres, Chem. Eur. J. 21 (2015) 6208–6214, https://doi.org/10.1002/chem.201500692.
[185] F. Dielmann, C. Heindl, F. Hastreiter, E.V. Peresypkina, A.V. Virovets, R.M. Gschwind, M. Scheer, A nano-sized supramolecule beyond the fullerene topology, Angew. Chem. Int. Ed. 53 (2014) 13605–13608, https://doi.org/10.1002/anie.201407120.
[186] A. Schindler, C. Heindl, G. Balázs, C. Gröger, A.V. Virovets, E.V. Peresypkina, M. Scheer, Size-determining dependencies in supramolecular organometallic host-guest chemistry, Chem. Eur. J. 18 (2012) 829–835, https://doi.org/10.1002/chem.201103141.
[187] S. Welsch, C. Gröger, M. Sierka, M. Scheer, An organometallic nanosized capsule consisting of cyclo-P_5 units and copper(I) ions, Angew. Chem. Int. Ed. 50 (2011) 1435–1438, https://doi.org/10.1002/anie.201005910.
[188] O.J. Scherer, T. Hilt, G. Wolmershäuser, P_4 Activation with $[\{Cp'''(OC)_2Fe\}_2]$ (Cp''' = $C_5H_2tBu_3$-1,2,4): Exclusive formation of the exo/ exo-butterfly complex $[\{Cp'''(OC)_2Fe\}_2(\mu\text{-}\eta^1\text{:}\eta^1\text{-}P_4)]$, Organometallics 17 (1998) 4110–4112, https://doi.org/10.1021/om9801148, and references cited therein.
[189] O.J. Scherer, G. Schwarz, G. Wolmershäuser, Eisen-Zweikernkomplexe mit unterschiedlichen P_4-Liganden, Z. Anorg. Allg. Chem. 622 (1996) 951–957, https://doi.org/10.1002/zaac.19966220606, and references cited therein.
[190] S. Heinl, M. Scheer, Activation of group 15 based cage compounds by $[Cp^{BIG}Fe(CO)_2]$ radicals, Chem. Sci. 5 (2014) 3221–3225, https://doi.org/10.1039/C4SC01213E.
[191] S. Heinl, G. Balázs, M. Scheer, The superbulky P_n ligand complexes $[Cp^{BIG}Fe(\eta^5\text{−}P_5)]$ and $[(Cp^{BIG}Fe)_2(\mu,\eta^{4:4}\text{–}P_4)]$—synthesis and characterization, phosphorus, Sulfur Silicon Relat. Elem. 189 (2014) 924–932, https://doi.org/10.1080/10426507.2014.903489.
[192] C. Schwarzmaier, M. Bodensteiner, A.Y. Timoshkin, M. Scheer, An approach to mixed pnasm ligand complexes, Angew. Chem. Int. Ed. 53 (2014) 290–293, https://doi.org/10.1002/anie.201308239.
[193] C. Schwarzmaier, A.Y. Timoshkin, G. Balázs, M. Scheer, Selective formation and unusual reactivity of tetraarsabicyclo[1.1.0]butane complexes, Angew. Chem. Int. Ed. 53 (2014) 9077–9081, https://doi.org/10.1002/anie.201404653.
[194] S. Heinl, A.Y. Timoshkin, J. Müller, M. Scheer, Unexpected differences in the reactivity between the phosphorus and arsenic derivatives $[(Cp^{BIG}Fe)_2(\mu,\eta^{4:4}\text{–}E_4)]$ (E = P and As), Chem. Commun. 54 (2018) 2244–2247, https://doi.org/10.1039/C7CC09730A.
[195] C. Schwarzmaier, S. Heinl, G. Balázs, M. Scheer, E_4 butterfly complexes (E=P, As) as chelating ligands, Angew. Chem. Int. Ed. 54 (2015) 13116–13121, https://doi.org/10.1002/anie.201506784.
[196] P. Comba, C. Katsichtis, B. Nuber, H. Pritzkow, Solid-state and solution structural properties of copper(I) compounds with bidentate phosphane ligands, Eur. J. Inorg. Chem. (1999) 777–783, https://doi.org/10.1002/(SICI)1099-0682(199905)1999:5<777::AID-EJIC777>3.0.CO;2-A.
[197] J. Müller, S. Heinl, C. Schwarzmaier, G. Balázs, M. Keilwerth, K. Meyer, M. Scheer, Rearrangement of a P_4 butterfly complex—the formation of a

homoleptic phosphorus-iron sandwich complex, Angew. Chem. Int. Ed. 56 (2017) 7312–7317, https://doi.org/10.1002/anie.201703175.
[198] E. Urnėžius, W.W. Brennessel, C.J. Cramer, J.E. Ellis, P. von Ragué Schleyer, A carbon-free sandwich complex $[(P_5)_2Ti]^{2-}$, Science 295 (2002) 832–834, https://doi.org/10.1126/science.1067325.
[199] M.D. Walter, J. Grunenberg, P.S. White, Reactivity studies on $[Cp'FeI]_2$: from iron hydrides to P_4-activation, Chem. Sci. 2 (2011) 2120–2130, https://doi.org/10.1039/C1SC00413A.
[200] S. Heinl, S. Reisinger, C. Schwarzmaier, M. Bodensteiner, M. Scheer, Selective functionalization of P4 by metal-mediated C-P bond formation, Angew. Chem. Int. Ed. 53 (2014) 7639–7642, https://doi.org/10.1002/anie.201403295.
[201] D.N. Akbayeva, O.J. Scherer, $[(\eta^5\text{-}C_5HR_4)CuCO]$ (R = $CHMe_2$) – a remarkably stable copper carbonyl complex and its reaction with P_4, Z. Anorg. Allg. Chem. 627 (2001) 1429–1430, https://doi.org/10.1002/1521-3749(200107)627:7<1429::AID-ZAAC1429>3.0.CO;2-K.
[202] J.E. Borger, M.K. Jongkind, A.W. Ehlers, M. Lutz, J.C. Slootweg, K. Lammertsma, Metalate-mediated functionalization of P_4 by trapping anionic $[Cp^*Fe(CO)_2(\eta^1\text{-}P_4)]^-$ with Lewis acids, Chem. Open 6 (2017) 350–353, https://doi.org/10.1002/open.201700027.
[203] J.E. Borger, A.W. Ehlers, M. Lutz, J.C. Slootweg, K. Lammertsma, Functionalization of P4 using a lewis acid stabilized bicyclo[1.1.0] tetraphosphabutane anion, Angew. Chem. Int. Ed. 53 (2014) 12836–12839, https://doi.org/10.1002/anie.201405879.
[204] M.J. Drance, S. Wang, M. Gembicky, A.L. Rheingold, J.S. Figueroa, Probing for four-coordinate zerovalent iron in a π-acidic ligand field: a functional source of FeL_4 enabled by labile dinitrogen binding, Organometallics 39 (2020) 3394–3402, https://doi.org/10.1021/acs.organomet.0c00487.
[205] A. Cavaillé, N. Saffon-Merceron, N. Nebra, M. Fustier-Boutignon, N. Mézailles, Synthesis and reactivity of an end-deck cyclo-P4 iron complex, Angew. Chem. Int. Ed. 57 (2018) 1874–1878, https://doi.org/10.1002/anie.201711130.
[206] U. Chakraborty, J. Leitl, B. Mühldorf, M. Bodensteiner, S. Pelties, R. Wolf, Mono- and dinuclear tetraphosphabutadiene ferrate anions, Dalton Trans. 47 (2018) 3693–3697, https://doi.org/10.1039/C7DT04641C.
[207] C.G.P. Ziegler, F. Hennersdorf, J.J. Weigand, R. Wolf, Iron-gallium and cobalt-gallium tetraphosphido complexes, Z. Anorg. Allg. Chem. 646 (2020) 552–557, https://doi.org/10.1002/zaac.201900351.
[208] G. Prabusankar, A. Doddi, C. Gemel, M. Winter, R.A. Fischer, P−P bond activation of P_4 tetrahedron by group 13 carbenoid and its bis molybdenum pentacarbonyl adduct, Inorg. Chem. 49 (2010) 7976–7980, https://doi.org/10.1021/ic1010743.
[209] C.G.P. Ziegler, T.M. Maier, S. Pelties, C. Taube, F. Hennersdorf, A.W. Ehlers, J.J. Weigand, R. Wolf, Construction of alkyl-substituted pentaphosphido ligands in the coordination sphere of cobalt, Chem. Sci. 10 (2019) 1302–1308, https://doi.org/10.1039/C8SC04745F.
[210] W.W. Brennessel, R.E. Jilek, J.E. Ellis, Bis(1,2,3,4-η^4-anthracene)ferrate(1−): a paramagnetic homoleptic polyarene transition-metal anion, Angew. Chem. Int. Ed. 46 (2007) 6132–6136, https://doi.org/10.1002/anie.200701353.
[211] W. W. Brennessel, J.E. Ellis, Sterically crowded σ- and π-bonded metal aryl complexes, Chapter Four. In: P. P. Power (Ed.) Inorganic Syntheses, vol. 37, Wiley, pp. 76–84..
[212] S. Yao, T. Szilvási, N. Lindenmaier, Y. Xiong, S. Inoue, M. Adelhardt, J. Sutter, K. Meyer, M. Driess, Reductive cleavage of P_4 by iron(i) centres: synthesis and structural characterisation of $Fe_2(P_2)_2$ complexes with two bridging P_2^{2-} ligands, Chem. Commun. 51 (2015) 6153–6156, https://doi.org/10.1039/C5CC00147A.
[213] F. Spitzer, C. Graßl, G. Balázs, E.M. Zolnhofer, K. Meyer, M. Scheer, Influence of the nacnac ligand in iron(I)-mediated P_4 transformations, Angew. Chem. Int. Ed. 55 (2016) 4340–4344, https://doi.org/10.1002/anie.201510716.
[214] E.-M. Schnöckelborg, J.J. Weigand, R. Wolf, Synthesis of anionic iron polyphosphides by reaction of white phosphorus with "Cp*Fe⁻", Angew. Chem. Int. Ed. 50 (2011) 6657–6660, https://doi.org/10.1002/anie.201101038.
[215] M.V. Butovskii, G. Balázs, E.V. Peresypkina, A.V. Virovets, M. Seidl, M. Scheer, Functionalization of a cyclo-P_5 ligand by main-group element nucleophiles, Angew. Chem. Int. Ed. 53 (2014) 7643–7646, https://doi.org/10.1002/anie.201403581.
[216] R. Yadav, T. Simler, S. Reichl, B. Goswami, C. Schoo, R. Köppe, M. Scheer, P.W. Roesky, Highly selective substitution and insertion reactions of silylenes in a metal-coordinated polyphosphide, J. Am. Chem. Soc. 142 (2020) 1190–1195, https://doi.org/10.1021/jacs.9b12151.
[217] A.E. Seitz, M. Eckhardt, A. Erlebach, E.V. Peresypkina, M. Sierka, M. Scheer, Pnictogen-silicon analogues of benzene, J. Am. Chem. Soc. 138 (2016) 10433–10436, https://doi.org/10.1021/jacs.6b07389.
[218] H. Brake, E. Peresypkina, A.V. Virovets, M. Piesch, W. Kremer, L. Zimmermann, C. Klimas, M. Scheer, Iodination of cyclo-E_5-complexes (E=P, As), Angew. Chem. Int. Ed. 59 (2020) 16241–16246, https://doi.org/10.1002/anie.202004812.
[219] M.V. Butovskiy, G. Balázs, M. Bodensteiner, E.V. Peresypkina, A.V. Virovets, J. Sutter, M. Scheer, Ferrocene and pentaphosphaferrocene: a comparative study regarding redox chemistry, Angew. Chem. Int. Ed. 52 (2013) 2972–2976, https://doi.org/10.1002/anie.201209329.
[220] H. Krauss, G. Balázs, M. Bodensteiner, M. Scheer, The potential of a *cyclo*-As_5 ligand complex in coordination chemistry, Chem. Sci. 1 (2010) 337–342, https://doi.org/10.1039/C0SC00254B.
[221] S. Carenco, Y. Hu, I. Florea, O. Ersen, C. Boissière, N. Mézailles, C. Sanchez, Metal-Dependent Interplay between Crystallization and Phosphorus Diffusion during the Synthesis of Metal Phosphide Nanoparticles, Chem. Mater. 24 (2012) 4134–4145, https://doi.org/10.1021/cm3022243.
[222] V. Mirabello, M. Caporali, V. Gallo, L. Gonsalvi, A. Ienco, M. Latronico, P. Mastrorilli, M. Peruzzini, Dynamic behaviour of Ru and Ru–Pt complexes containing *tetrahedro*-P_4 ligand, Dalton Trans. 40 (2011) 9668–9671, https://doi.org/10.1039/C1DT10572H.
[223] M. Caporali, L. Gonsalvi, R. Kagirov, V. Mirabello, M. Peruzzini, O. Sinyashin, P. Stoppioni, D. Yakhvarov, The first water-soluble tetraphosphorus ruthenium complex. Synthesis, characterization and kinetic study of its hydrolysis, J. Organomet. Chem. 714 (2012) 67–73, https://doi.org/10.1016/j.jorganchem.2012.03.019.
[224] P. Barbaro, C. Bazzicalupi, M. Peruzzini, S. Seniori Costantini, P. Stoppioni, Iodine activation of coordinated white phosphorus: formation and transformation of 1,3-dihydride-2-iodidecyclotetraphosphane, Angew. Chem. Int. Ed. 51 (2012) 8628–8631, https://doi.org/10.1002/anie.201203908.
[225] M. Baudler, Chain and Ring phosphorus compounds—analogies between phosphorus and carbon chemistry, Angew. Chem. Int. Ed. 21 (1982) 492–512, https://doi.org/10.1002/anie.198204921.
[226] P. Junkes, M. Baudler, J. Dobbers, D. Rackwitz, Kernresonanzuntersuchungen an Phosphanen, Z. Naturforsch. B 27 (1972) 1451–1456.
[227] M. Caporali, F. Delgado Calvo, C. Bazzicalupi, S. Seniori Costantini, M. Peruzzini, Influence of highly basic phosphine ligand on the reactivity and hydrolysis of P_4 and P_4S_3 supported by ruthenium fragments, J. Organomet. Chem. 859 (2018) 68–74, https://doi.org/10.1016/j.jorganchem.2018.01.005.
[228] L.J.L. Häller, E. Mas-Marzá, M.K. Cybulski, R.A. Sanguramath, S.A. Macgregor, M.F. Mahon, C. Raynaud, C.A. Russell, M.K. Whittlesey, Computation provides chemical insight into the diverse hydride NMR chemical shifts of $[Ru(NHC)_4(L)H]^{0/+}$ species (NHC = N-heterocyclic carbene; L = vacant, H_2, N_2, CO, MeCN, O_2, P_4, SO_2, H^-, F^- and Cl^-) and their $[Ru(R_2PCH_2CH_2PR_2)_2(L)H]^+$ congeners, Dalton Trans. 46 (2017) 2861–2873, https://doi.org/10.1039/C7DT00117G.
[229] M. Bispinghoff, Z. Benkő, H. Grützmacher, F. Delgado Calvo, M. Caporali, M. Peruzzini, Ruthenium mediated halogenation of white phosphorus: synthesis and reactivity of the unprecedented P_4Cl_2 moiety, Dalton Trans. 48 (2019) 3593–3600, https://doi.org/10.1039/C8DT01840E.
[230] F. Fabrizi de Biani, M. Corsini, A. Ienco, M. Peruzzini, F. Zanobini, More about the redox behavior of late transition metal triple-decker complexes with cyclo-triphosphorus, Inorg. Chim. Acta 470 (2018) 428–432, https://doi.org/10.1016/j.ica.2017.07.014.
[231] C.A. Ghilardi, S. Midollini, A. Orlandini, L. Sacconi, Single- and mixed-metal complexes with cyclo-triphosphorus and 1,1,1-tris((diphenylphosphino) methyl)ethane, triphos. Synthesis and structural characterization of $[(triphos)Co(\eta^3\text{-}P_3)]$ and $[(triphos)Co(\mu,(\eta^3\text{-}P_3))\{Cr_2(CO)_{10}\}]$, Inorg. Chem. 19 (1980) 301–306, https://doi.org/10.1021/ic50204a005.
[232] S. Dürr, D. Ertler, U. Radius, Symmetrical P_4 Cleavage at Cobalt: Characterization of Intermediates on the Way from P_4 to Coordinated P_2 Units, Inorg. Chem. 51 (2012) 3904–3909, https://doi.org/10.1021/ic300219w.
[233] C.C. Mokhtarzadeh, A.L. Rheingold, J.S. Figueroa, Dinitrogen binding, P_4-activation and aza-Büchner ring expansions mediated by an isocyano analogue of the CpCo(CO) fragment, Dalton Trans. 45 (2016) 14561–14569, https://doi.org/10.1039/C6DT02789J.
[234] M.E. Barr, L.F. Dahl, Synthesis, stereophysical bonding features, and chemical-electrochemical reactivity of two dimetal-bridging diphosphide cobalt and iron complexes: $Co_2(\eta^5\text{-}C_5Me_5)2(\mu_2,\eta^2\text{-}P_2)_2$ and $Fe_2(\eta^5\text{-}C_5Me_5)_2(\mu_2,\eta^2\text{-}P_2)_2$, Organometallics 10 (1991) 3991–3996, https://doi.org/10.1021/om00058a013.
[235] B. Zarzycki, F.M. Bickelhaupt, U. Radius, Symmetrical P_4 cleavage at cobalt half sandwich complexes $[(\eta^5\text{-}C_5H_5)Co(L)]$ (L = CO, NHC) – a computational case study on the mechanism of symmetrical P_4 degradation to P_2 ligands, Dalton Trans. 42 (2013) 7468–7481, https://doi.org/10.1039/C3DT50267H.
[236] F. Dielmann, A. Timoshkin, M. Piesch, G. Balázs, M. Scheer, The cobalt *cyclo*-P_4 sandwich complex and its role in the formation of polyphosphorus compounds, Angew. Chem. Int. Ed. 56 (2017) 1671–1675, https://doi.org/10.1002/anie.201610967.
[237] M. Piesch, S. Reichl, Michael Seidl, M Balázs, G. Scheer, Ring contraction by NHC-induced pnictogen abstraction, Angew. Chem. Int. Ed. 58 (2019) 16563–16568, https://doi.org/10.1002/anie.201908397.
[238] M. Piesch, M. Seidl, M. Scheer, Transformations of the *cyclo*-P_4 ligand in $[Cp'''Co(\eta^4\text{-}P_4)]$, Chem. Sci. 11 (2020) 6745–6751, https://doi.org/10.1039/D0SC01740J.
[239] S. Pelties, T. Maier, D. Herrmann, B. de Bruin, C. Rebreyend, S. Gärtner, I.G. Shenderovich, R. Wolf, Selective P_4 activation by a highly reduced cobaltate: synthesis of dicobalt tetraphosphido complexes, Chem. Eur. J. 23 (2017) 6094–6102, https://doi.org/10.1002/chem.201603296.
[240] C.M. Hoidn, T.M. Maier, K. Trabitsch, J.J. Weigand, R. Wolf, [3+2] Fragmentation of a Pentaphosphido ligand by cyanide, Angew. Chem. Int. Ed. 58 (2019) 18931–18936.
[241] F. Spitzer, C. Graßl, G. Balázs, E. Mädl, M. Keilwerth, E.M. Zolnhofer, K. Meyer, M. Scheer, Nacnac-Cobalt-mediated P_4 transformations, Chem. Eur. J. 23 (2017) 2716–2721, https://doi.org/10.1002/chem.201605451.
[242] C.M. Hoidn, C. Rödl, M.L. McCrea-Hendrick, T. Block, R. Pöttgen, A.W. Ehlers, P. P. Power, R. Wolf, Synthesis of a cyclic Co_2Sn_2 cluster using a Co^- synthon, J.

Am. Chem. Soc. 140 (2018) 13195–13199, https://doi.org/10.1021/jacs.8b08517.
[243] F. Dielmann, M. Sierka, A.V. Virovets, M. Scheer, Access to extended polyphosphorus frameworks, Angew. Chem. Int. Ed. 49 (2010) 6860–6864, https://doi.org/10.1002/anie.201001000.
[244] T. Li, N. Arleth, M.T. Gamer, R. Köppe, T. Augenstein, F. Dielmann, M. Scheer, S. N. Konchenko, P.W. Roesky, Intramolecular phosphorus-phosphorus bond formation within a Co_2P_4 core, Inorg. Chem. 52 (2013) 14231–14236, https://doi.org/10.1021/ic402159y.
[245] M. Piesch, C. Graßl, M. Scheer, Element-element bond formation upon oxidation and reduction, Angew. Chem. Int. Ed. 59 (2020) 7154–7160, https://doi.org/10.1002/anie.201916622.
[246] W.W. Brennessel, J.V.G. Young, J.E. Ellis, Bis(1,2,3,4-η^4-anthracene)cobaltate (1−), Angew. Chem. Int. Ed. 41 (2002) 1211–1215.
[247] W.W. Brennessel, J.E. Ellis, Naphthalene and anthracene cobaltates(1−): useful storable sources of an atomic cobalt anion, Inorg. Chem. 51 (2012) 9076–9094, https://doi.org/10.1021/ic301240u.
[248] C. Chan, A.E. Carpenter, M. Gembicky, C.E. Moore, A.L. Rheingold, J.S. Figueroa, Associative ligand exchange and substrate activation reactions by a zero-valent cobalt tetraisocyanide complex, Organometallics 38 (2019) 1436–1444, https://doi.org/10.1021/acs.organomet.8b00777.
[249] D. Yakhvarov, P. Barbaro, L. Gonsalvi, S. Mañas Carpio, S. Midollini, A. Orlandini, M. Peruzzini, O. Sinyashin, F. Zanobini, A Snapshot of P_4 tetrahedron opening: Rh- and Ir-mediated activation of white phosphorus, Angew. Chem. Int. Ed. 45 (2006) 4182–4185, https://doi.org/10.1002/anie.200601048.
[250] W.W. Schoeller, Computational insight into the Rh-mediated activation of white phosphorus, Inorg. Chem. 50 (2011) 22–29, https://doi.org/10.1021/ic100803m.
[251] M. Caporali, L. Gonsalvi, V. Mirabello, A. Ienco, G. Manca, F. Zanobini, M. Peruzzini, The bimetallic activation of white phosphorus by *trans*-[RhCl(CO)(dppm)]$_2$ results in a tetrahedro-Rh_2P_2 moiety, Eur. J. Inorg. Chem. (2014) 1652–1659, https://doi.org/10.1002/ejic.201400046.
[252] P.B. Arockiam, U. Lennert, C. Graf, R. Rothfelder, D.J. Scott, T.G. Fischer, K. Zeitler, R. Wolf, Versatile visible-light-driven synthesis of unsymmetrical phosphines and phosphonium salts, Chem. Eur. J. 26 (2020) 16374–16382, https://doi.org/10.1002/chem.202002646.
[253] S. Pelties, D. Herrmann, B. de Bruin, F. Hartl, R. Wolf, Selective P_4 activation by an organometallic nickel(I) radical: formation of a dinuclear nickel(II) tetraphosphide and related di- and trichalcogenides, Chem. Commun. 50 (2014) 7014–7016, https://doi.org/10.1039/C4CC02601B.
[254] S. Pelties, A.W. Ehlers, R. Wolf, Insertion of phenyl isothiocyanate into a P-P bond of a nickel-substituted bicyclo[1.1.0]tetraphosphabutane, Chem. Commun. 52 (2016) 6601–6604, https://doi.org/10.1039/C6CC01572G.
[255] S. Yao, M. Driess, Lessons from isolable nickel(I) precursor complexes for small molecule activation, Acc. Chem. Res. 45 (2012) 276–287, https://doi.org/10.1021/ar200156r.
[256] S. Yao, Y. Xiong, C. Milsmann, E. Bill, S. Pfirrmann, C. Limberg, M. Driess, Reversible P_4 activation with Nickel(I) and an η^3-coordinated tetraphosphorus ligand between Two Ni^I centers, Chem. Eur. J. 16 (2010) 436–439, https://doi.org/10.1002/chem.200902820.
[257] B. Zarzycki, T. Zell, D. Schmidt, U. Radius, P_4 Activation at Ni^0: selective formation of an NHC-stabilized, dinuclear nickel complex [Ni_2(*i*Pr_2Im)$_4$(μ, $\eta^{2:2}$–P_2)], Eur. J. Inorg. Chem. (2013) 2051–2058, https://doi.org/10.1002/ejic.201201368.
[258] G. Hierlmeier, A. Hinz, R. Wolf, J.M. Goicoechea, Synthesis and reactivity of nickel-stabilised μ^2:η^2,η^2-P_2, As_2 and PAs units, Angew. Chem. Int. Ed. 57 (2018) 431–436, https://doi.org/10.1002/anie.201710582.
[259] G. Hierlmeier, P. Coburger, N.P. van Leest, B. de Bruin, R. Wolf, Aggregation and degradation of white phosphorus mediated by N-heterocyclic carbene Nickel(0) complexes, Angew. Chem. Int. Ed. 59 (2020) 14148–14153, https://doi.org/10.1002/anie.202004020.
[260] C.G.P. Ziegler, C. Taube, J.A. Kelly, G. Hierlmeier, M. Uttendorfer, J.J. Weigand, R. Wolf, An unusual $Ni_2Si_2P_8$ cluster formed by complexation and thermolysis, Chem. Comm. 56 (2020) 14071–14074, https://doi.org/10.1039/D0CC05365A.
[261] Y. Xiong, S. Yao, M. Brym, M. Driess, Consecutive insertion of a silylene into the P_4 Tetrahedron: facile access to strained SiP_4 and Si_2P_4 cage compounds, Angew. Chem. Int. Ed. 46 (2007) 4511–4513, https://doi.org/10.1002/anie.200701203.
[262] E. Mädl, G. Balázs, E.V. Peresypkina, M. Scheer, Unexpected reactivity of [(η^5-1,2,4-*t*$Bu_3C_5H_2$)Ni(η^3-P_3)] towards main group nucleophiles and by reduction, Angew. Chem. Int. Ed. 55 (2016) 7702–7707, https://doi.org/10.1002/anie.201601775.
[263] D.G. Yakhvarov, S.V. Kvashennikova, O.G. Sinyashin, Reactions of activated organonickel σ-complexes with elemental (white) phosphorus, Russ. Chem. Bull. 62 (2013) 2472–2476, https://doi.org/10.1007/s11172-013-0358-9.
[264] S. Carenco, M. Demange, C. Boissière, C. Sanchez, N. Mézailles, Metal phosphides: from chemist's oddities to designed functional materials, Chapter 6 in B, in: Pignataro (Ed.), Molecules at Work. Selfassembly, Nanomaterials, Molecular Machinery, Wiley-VCH Verlag, Weinheim, 2012, pp. 113–120.
[265] S. Carenco, I. Resa, X. Le Goff, P. Le Floch, N. Mézailles, White phosphorus as single source of "P" in the synthesis of nickel phosphide, Chem. Commun. (2008) 2568–2570, https://doi.org/10.1039/B802454E.
[266] S. Carenco, X.F. Le Goff, J. Shi, L. Roiban, O. Ersen, C. Boissière, C. Sanchez, N. Mézailles, Magnetic core−shell nanoparticles from nanoscale-induced phase segregation, Chem. Mater. 23 (2011) 2270–2277, https://doi.org/10.1021/cm200575g.
[267] A.-M. Nguyen, M. Bahri, S. Dreyfuss, S. Moldovan, A. Miche, C. Méthivier, O. Ersen, N. Mézailles, S. Carenco, Bimetallic phosphide (Ni,Cu)$_2$P nanoparticles by inward phosphorus migration and outward copper migration, Chem. Mater. 31 (2019) 6124–6134, https://doi.org/10.1021/acs.chemmater.9b01505.
[268] R.M. Kagirov, A.V. Voloshin, I.Kh. Rizvanov, O.G. Sinyashin, D.G. Yakhvarov, Activation and transformation of white phosphorus by palladium(II) complexes, Russ. Chem. Bull. 59 (2010) 1116–1118, https://doi.org/10.1007/s11172-010-0213-1.
[269] S. Carenco, Y. Hu, I. Florea, O. Ersen, C. Boissière, C. Sanchez, N. Mézailles, Structural transitions at the nanoscale: the example of palladium phosphides synthesized from white phosphorus, Dalton Trans. 42 (2013) 12667–12674, https://doi.org/10.1039/C3DT50686J.
[270] M. Demange, X.-F. Le Goff, P. Le Floch, N. Mézailles, P_4 Activation with Pt^0 metal centers: selective formation of a dinuclear Pt_2(μ,$\eta^{2:2}$–P_2) complex, Chem. Eur. J. 16 (2010) 12064–12068, https://doi.org/10.1002/chem.201000894.
[271] L.C. Forfar, T.J. Clark, M. Green, S.M. Mansell, C.A. Russell, R.A. Sanguramath, J. M. Slattery, White phosphorus as a ligand for the coinage metals, Chem. Commun. 48 (2012) 1970–1972, https://doi.org/10.1039/C2CC15291F.
[272] L.C. Forfar, D. Zeng, M. Green, J.E. McGrady, C.A. Russell, Probing the structure, dynamics, and bonding of coinage metal complexes of white phosphorus, Chem. Eur. J. 22 (2016) 5397–5403, https://doi.org/10.1002/chem.201505031.
[273] G. Santiso-Quiñones, A. Reisinger, J. Slattery, I. Krossing, Homoleptic Cu–phosphorus and Cu–ethene complexes, Chem. Commun. (2007) 5046–5048, https://doi.org/10.1039/B710899K.
[274] I. Krossing, L. van Wüllen, Superweak complexes of tetrahedral P_4 molecules with the silver cation of weakly coordinating anions, Chem. Eur. J. 8 (2002) 700–711, https://doi.org/10.1002/1521-3765(20020201)8:3<700::AID-CHEM700>3.0.CO;2-C.
[275] I. Krossing, Ag(P_4)$_2^+$: the first homoleptic metal−phosphorus cation, J. Am. Chem. Soc. 123 (2001) 4603–4604, https://doi.org/10.1021/ja002007m.
[276] J.E. Borger, M.S. Bakker, A.W. Ehlers, M. Lutz, J.C. Slootweg, K. Lammertsma, Functionalization of P_4 in the coordination sphere of coinage metal cations, Chem. Commun. 52 (2016) 3284–3287, https://doi.org/10.1039/C5CC10037B.
[277] F. Spitzer, M. Sierka, M. Latronico, P. Mastrorilli, A.V. Virovets, M. Scheer, Fixation and Release of Intact E4 Tetrahedra (E=P, As), Angew. Chem. Int. Ed. 54 (2015) 4392–4396, https://doi.org/10.1002/anie.201411451.
[278] M. Fleischmann, S. Welsch, E.V. Peresypkina, A.V. Virovets, M. Scheer, Highly Dynamic Coordination Behavior of P_n Ligand Complexes towards "Naked" Cu^+ Cations, Chem. Eur. J. 21 (2015) 14332–14336, https://doi.org/10.1002/chem.201502775.
[279] C.M.E. Graham, C.L.B. Macdonald, P.P. Power, Z.D. Brown, P.J. Ragogna, Transition metal functionalization of P_4 using a diarylgermylene anchor, Inorg. Chem. 56 (2017) 9111–9119, https://doi.org/10.1021/acs.inorgchem.7b01138.
[280] J.W. Dube, C.M.E. Graham, C.L.B. Macdonald, Z.D. Brown, P.P. Power, P.J. Ragogna, Reversible, photoinduced activation of P_4 by low-coordinate main group compounds, Chem. Eur. J. 20 (2014) 6739–6744, https://doi.org/10.1002/chem.201402031.
[281] S. Carenco, I. Florea, O. Ersen, C. Boissière, N. Mézailles, C. Sanchez, Towards nanoscaled gold phosphides: surface passivation and growth of composite nanostructures, New J. Chem. 37 (2013) 1231–1237, https://doi.org/10.1039/C3NJ41037D.
[282] M. Vanni, M. Serrano-Ruiz, F. Telesio, S. Heun, M. Banchelli, P. Matteini, A.M. Mio, G. Nicotra, C. Spinella, S. Caporali, A. Giaccherini, F. D'Acapito, M. Caporali, M. Peruzzini, Black phosphorus/palladium nanohybrid: unraveling the nature of P-Pd interaction and application in selective hydrogenation, Chem. Mater. 31 (2019) 5075–5080, https://doi.org/10.1021/acs.chemmater.9b00851.
[283] A. Ienco, G. Manca, M. Peruzzini, C. Mealli, Modelling strategies for the covalent functionalization of 2D phosphorene, Dalton Trans. 47 (2018) 17243–17256, https://doi.org/10.1039/C8DT03628D.
[284] V.V. Kulish, O.I. Maliy, C. Persson, P. Wu, Adsorption of metal adatoms on single layer phosphorene, Phys. Chem. Chem. Phys. 17 (2015) 992–1000, https://doi.org/10.1039/C4CP03890H.
[285] L. Bai, X. Wang, S. Tang, Y. Kang, J. Wang, Y. Yu, Z.-K. Zhou, C. Ma, X. Zhang, J. Jiang, P.K. Chu, X.-F. Yu, Black phosphorus/platinum heterostructure: a highly efficient photocatalyst for solar-driven chemical reactions, Adv. Mater. 30 (2018) 1803641, https://doi.org/10.1002/adma.201803641.
[286] N. Suvansinpan, F. Hussain, G. Zhang, C.H. Chiu, Y. Cai, Y.-W. Zhang, Substitutionally doped phosphorene: electronic properties and gas sensing, Nanotechnology 27 (2016), https://doi.org/10.1088/0957-4484/27/6/065708 065708.
[287] Q.H. Yu, Y. Jiang, W. Zhang, B.-Z. Wu, J.-R. Yin, P. Zhang, Y.-H. Ding, Noble metal atoms doped phosphorene: electronic properties and gas adsorption ability, Mater. Res. Express 4 (2017), https://doi.org/10.1088/2053-1591/aa6c12 045703.
[288] Y. Luo, C. Ren, S. Wang, S. Li, P. Zhang, J. Yu, M. Sun, Z. Sun, W. Tang, Adsorption of transition metals on black phosphorene: a first-principles

study, Nanoscale Res. Lett. 13 (2018) 282, https://doi.org/10.1186/s11671-018-2696-x.
[289] S.P. Koenig, R.A. Doganov, L. Seixas, A. Carvalho, J.Y. Tan, K. Watanabe, T. Taniguchi, N. Yakovlev, A.H. Castro Neto, B. Özyilmaz, Electron doping of ultrathin black phosphorus with Cu adatoms, Nano Lett. 16 (2016) 2145–2151, https://doi.org/10.1021/acs.nanolett.5b03278.
[290] Z. Guo, S. Chen, Z. Wang, Z. Yang, F. Liu, Y. Xu, J. Wang, Y. Yi, H. Zhang, L. Liao, P.K. Chu, X.-F. Yu, Metal-ion-modified black phosphorus with enhanced stability and transistor performance, Adv. Mater. 29 (2017) 1703811, https://doi.org/10.1002/adma.201703811.
[291] Y. Zhao, H. Wang, H. Huang, Q. Xiao, Y. Xu, Z. Guo, H. Xie, J. Shao, Z. Sun, W. Han, X.-F. Yu, P. Li, P.K. Chu, Improved biocompatibility of black phosphorus nanosheets by chemical modification, Angew. Chem. Int. Ed. 55 (2016) 5003–5007, https://doi.org/10.1002/anie.201706228.
[292] Z. Sun, H. Xie, S.Y. Tang, X.-F. Yu, Z. Guo, J. Shao, H. Zhang, H. Huang, H. Wang, P.K. Chu, Ultrasmall black phosphorus quantum dots: synthesis and use as photothermal agents, Angew. Chem. Int. Ed. 54 (2015) 11526–11530, https://doi.org/10.1002/anie.201506154.
[293] Z. Sun, Y. Zhao, Z. Li, H. Cui, Y. Zhou, W. Li, W. Tao, H. Zhang, H. Wang, P.K. Chu, X.-F. Yu, TiL_4-coordinated black phosphorus quantum dots as an efficient contrast agent for *In Vivo* photoacoustic imaging of cancer, Small 13 (2017) 1602896, https://doi.org/10.1002/smll.201602896.
[294] N.M. Latiff, W.Z. Teo, Z. Sofer, A.C. Fisher, M. Pumera, The cytotoxicity of layered black phosphorus, Chem. Eur. J. 21 (2015) 13991–13995, https://doi.org/10.1002/chem.201502006.
[295] Q. Li, Q. Zhou, L. Shi, Q. Chen, J. Wang, Recent advances in oxidation and degradation mechanisms of ultrathin 2D materials under ambient conditions and their passivation strategies, J. Mater. Chem. A 7 (2019) 4291–4312, https://doi.org/10.1039/C8TA10306B.
[296] M. Caporali, M. Serrano-Ruiz, F. Telesio, S. Heun, A. Verdini, A. Cossaro, M. Dalmiglio, A. Goldoni, M. Peruzzini, Enhanced ambient stability of exfoliated black phosphorus by passivation with nickel nanoparticles, Nanotechnology 31 (2020), https://doi.org/10.1088/1361-6528/ab851e 275708.
[297] H. Wang, X.Z. Yang, W. Shao, S.C. Chen, J.F. Xie, X.D. Zhang, J. Wang, Y. Xie, Ultrathin black phosphorus nanosheets for efficient singlet oxygen generation, J. Am. Chem. Soc. 137 (2015) 11376–11382, https://doi.org/10.1021/jacs.5b06025.
[298] J.V. Jokerst, A.J. Cole, D. Van de Sompel, S.S. Gambhir, Gold nanorods for ovarian cancer detection with photoacoustic imaging and resection guidance *via* raman imaging in living Mice, ACS Nano 6 (2012) 10366–10377, https://doi.org/10.1021/nn304347g.
[299] B. Rosenberg, L. VanCamp, J.E. Trosko, V.H. Mansour, Platinum compounds: a new class of potent antitumour agents, Nature 222 (1969) 385–386, https://doi.org/10.1038/222385a0.
[300] M. Fojtů, X. Chia, Z. Sofer, M. Masařík, M. Pumera, Black phosphorus nanoparticles potentiate the anticancer effect of oxaliplatin in ovarian cancer cell line, Adv. Funct. Mater. 27 (2017) 1701955, https://doi.org/10.1002/adfm.201701955.
[301] J. Zhang, Y. Ma, K. Hu, Y. Feng, S. Chen, X. Yang, J.F.-C. Loo, H. Zhang, F. Yin, Z. Li, Surface coordination of black phosphorus with modified cisplatin, Bioconjugate Chem. 30 (2019) 1658–1664, https://doi.org/10.1021/acs.bioconjchem.9b00128.
[302] M.G. Raucci, I. Fasolino, M. Caporali, M. Serrano-Ruiz, M. Peruzzini, L. Ambrosio, Exfoliated Black phosphorus promotes *in vitro* bone regeneration and suppresses osteosarcoma progression through cancer-related inflammation inhibition, ACS Appl. Mater. Interfaces 11 (2019) 9333–9342, https://doi.org/10.1021/acsami.8b21592.
[303] L. Wu, J. Wang, J. Lu, D. Liu, N. Yang, H. Huang, P.K. Chu, X.-F. Yu, Lanthanide-coordinated black phosphorus, Small 14 (2018) 1801405, https://doi.org/10.1002/smll.201801405.